The nature of the chemically enriched components of the Iceland mantle plume

Alice Josiane Williams

Thesis submitted as partial fulfilment of the requirements for the degree of Doctor of Philosophy (Ph. D) in Geology

University of Edinburgh, 2005

Declaration

I declare that this thesis is solely my own work except where otherwise acknowledged.

Acknowledgements

I would like to take the opportunity to thank a number of people for their support over the past few years. First and foremost are my supervisors Fin Stuart, Godfrey Fitton and Rob Ellam whose patience, encouragement and advice were unremitting. For assistance in the laboratories at SUERC and for general light-relief I would like to thank Anne, Vinnie, Kathy, Maria, Valerie and Jim, not to mention the many other characters at SUERC. In Edinburgh thanks go to Dodie James for XRF training and assistance, and Bjorn Hardarson for his hospitality and expertise in Iceland. In addition, Yvonne Smit, Lucy Bunce, Kaj Hoernle, Reidar Trønnes and John Faithfull were all kind enough to donate sample material. From the bright beginning to those last few (many) manic hours no-one could have been more supportive than my friends Solveigh Lass-Evans and Chris McCormick. Finally, it goes without saying that the past few years would have been so much more difficult without the understanding and unrelenting support of John and my family. I hope I've done them proud.

This research was funded by a PhD studentship from the Natural Environment Research Council (NER/S/A/2001/63150)

Abstract

Postglacial basalts in the three Icelandic flank-zones (the Snæfellsnes Peninsula, the Southern Flank Zone, and the Eastern Flank Zone) are mildly alkaline and are highly enriched in incompatible elements compared to both tholeiitic basalt erupted in the Icelandic rift-zones and to normal mid-ocean ridge basalt (N-MORB) from the Mid-Atlantic Ridge to the north and south of Iceland. A relatively limited number of isotopic studies of individual flank-zones and volcanic centres indicate that there may be more than one enriched component present in the plume; however their origins and relationships are uncertain. Previously recognised similarities between the enriched mantle supplying volcanism the Snæfellsnes Peninsula and that present beneath volcanic centres elsewhere in the North Atlantic region might suggest that enriched mantle domains sampled in the flank-zones are not necessarily intrinsic to the plume, but exist as heterogeneities in the shallow asthenospheric mantle. The main intentions of this research are to identify and characterise enriched components in the sub-Icelandic mantle and to determine their origins and relationships with other mantle components.

Helium, strontium, neodymium and lead isotope data, in conjunction with major and trace element data, allow the characterisation of enriched mantle sources in the flank-zones. Postglacial olivine- and pyroxene-bearing basalt samples have been collected from each of three flank-zones. Olivine and pyroxene $^{3}He/^{4}He$ do not appear to have been affected by pre- or post-eruptive addition of radiogenic ^{4}He, and therefore $^{3}He/^{4}He$ are considered to represent the time-integrated $^{3}He/(U+Th)$ of the mantle source. Published oxygen isotope data indicate that the flank-zone basalts have not been affected by crustal contamination.

Coherent trends in He-Sr-Nd-Pb isotope co-variation diagrams allow the identification of three distinct enriched components in the North Atlantic mantle. Each enriched component is characterised by lower $^{143}Nd/^{144}Nd$ and more radiogenic Pb and Sr isotope ratios than the depleted mantle components sampled in the rift-zones and along the MAR. One enriched component, EI_1, is most prevalent in the mantle beneath the SFZ. It is distinguished from the other enriched components by its high $^{3}He/^{4}He$ (>19 R_a) extreme Pb isotope composition ($^{206}Pb/^{204}Pb > 19.4$) and lower ΔNb (0.2). It is probably derived from recycled oceanic crust (a young-HIMU-like component). The second enriched component, EI_2, is only sampled at Öræfajökull (EFZ), and is distinguished by its extreme $^{87}Sr/^{86}Sr$ (> 0.7037) and positive Δ7/4. Its isotopic composition most likely has its origins in recycled pelagic or terrigenous sediments.

The third enriched component, EI_3, dominates the Jan Mayen (North Atlantic) and Snæfell (EFZ) mantle sources. It has similar Sr and Nd isotopic compositions to EI_1, but is characterised by less-radiogenic Pb isotope ratios ($^{206}Pb/^{204}Pb$ ~18.6), higher ΔNb (~0.6) and lower $^{3}He/^{4}He$ (<5.5 R_a). It is also most likely derived from young recycled oceanic crust. Enriched mantle beneath Snæfellsnes appears to be derived from mixing of EI_1 and EI_3. Either two depleted components (DI_1 and DI_2) or a single, variably degassed depleted component (DI_1), are required to explain trends in He-Sr, He-Nd or He-Pb co-variation diagrams. DI_1 is assumed to represent the depleted Iceland plume component and DI_2 the N-MORB mantle.

A mixing model is presented which enables plume-derived enriched components to be distinguished from those present in the shallow asthenospheric mantle. Only EI_1 appears to be intrinsic to the plume, whereas EI_2 and EI_3 are upper-mantle heterogeneities. Mixing relationships between enriched and depleted components indicate that the Iceland mantle plume may be zoned, with pure plume-derived mantle only present at the very core of the plume in south-eastern Iceland. If so, the lateral extent of both the outflow of plume-derived material and the sheath surrounding the plume, appears to be asymmetric, extending farther to the south of Iceland than to the north.

CONTENTS

Chapter 1 1
Introduction, aims and objectives

1.1 Introduction 2
1.2 The geology and geodynamics of Iceland 7
1.2.1 The geological history of Iceland and the North Atlantic 7
1.2.2 The Iceland mantle plume 12
1.2.3 Alternative models for melt generation in Iceland 13
1.3 Aims and objectives 15

Chapter 2 17
Characterisation of chemically enriched basalts from the Snaefellsnes Peninsula, western Iceland

2.1 Introduction 18
2.2 Geology and tectonics of the Snæfellsnes Peninsula 19
2.2.1 Tertiary (>2.5 Ma) 19
2.2.2 Plio-Pleistocene (2.5 Ma – 10 ka) and Recent formations (<10 ka) 20
2.3 Sampling strategy 23
2.4 Analytical Results 24
2.4.1 Major elements 24
2.4.2 Trace elements 30
2.4.3 Helium isotopes 34
2.4.3.1 Effect of He abundance and blank corrections on $^3He/^4He$ 36
2.4.3.2 Variation in $^3He/^4He$ between olivine and pyroxene phenocrysts 38
2.4.3.3 Regional variation in $^3He/^4He$ 39
2.4.4 Sr-Nd-Pb isotopes 40
2.5 Discussion 46
2.5.1 Introduction 46
2.5.2 Integrity of He isotope data 47
2.5.2.1 Ingrowth of radiogenic ^4He in phenocrysts 47
2.5.2.2 Post-eruptive production of cosmogenic ^3He 49
2.5.3 Crustal contamination 51
2.5.4 Fractional crystallisation 52
2.5.5 Partial melting 53
2.5.6 Source-characterisation: constraints from isotope ratios and major and trace element geochemistry 56
2.5.7 Previous conclusions regarding melting *vs.* source 61
2.6 Summary and conclusions 64

Chapter 3 66
Characterisation of chemically enriched basalts from the Eastern Flank Zone

3.1 Introduction 67
3.2 Geology of the Eastern Flank-zone 67
3.3 Sample descriptions 70
3.4. Results 71
3.4.1 Major elements 71
3.4.2 Trace elements 75
3.4.3 Helium isotopes 78
3.4.4 Sr, Nd and Pb isotopes 80
3.5 Discussion 82
3.5.1.1 Assimilation of old Icelandic crust 82
3.5.1.2 Involvement of continental crust 83
3.5.1.3 Fractional crystallisation 84
3.5.1.4 Melting processes 85
3.5.2 Source characterisation 86
3.6 Summary 89

Chapter 4 90
Characterisation of chemically enriched basalts from Southern Flank Zone

4.1 Introduction 91
4.2 Geology of the Southern Flank Zone 91
4.3 Sample descriptions 93
4.4 Results 95
4.4.1 Major elements 95
4.4.2 Trace elements 101
4.4.3 Helium isotopes 106
4.4.4 Sr, Nd and Pb isotopes 107
4.5 Discussion 110
4.5.1.1 Assimilation of Icelandic crust 110
4.5.1.2 Fractional crystallisation 112
4.5.1.3 Melting processes 113
4.5.2 Source characterisation 114
4.6 Summary 119

Chapter 5 120
The nature, origins, distribution and inter-relationships between enriched components in the sub-Icelandic mantle

5.1 Introduction 121
5.2 Characterisation of enriched mantle components 122
5.2.1 Defining "enriched" mantle: evidence from trace elements 122
5.2.2. Isotopes as source discriminants 123

5.2.3 Number and compositions of enriched mantle end-members: isotopic co-variations 128
5.2.4 Origins of mantle enrichment 134
5.2.4.1 EI_1 134
5.2.4.2 EI_2 135
5.2.4.3 EI_3 136
5.3 Origins of source heterogeneity in flank-zones and off-axis regions: mixing between mantle components. 137
5.3.1 Mixing models 137
5.3.2 Mixing parameters 141
5.3.3 Results of mixing model 142
5.3.3.1 Snæfellsnes Peninsula 143
5.3.3.2 Eastern Flank Zone 144
5.3.3.3 Southern Flank Zone 144
5.3.3.4 Jan Mayen and Vesteris seamount 144
5.4 The influence of enriched components in the North Atlantic region 150
5.4.1 The Northern Rift-Zone and the adjacent Kolbeinsey Ridge 151
5.4.2 The Eastern Rift-Zone 154
5.4.3 The Western Rift-Zone and the Reykjanes Ridge 154
5.4.4 The Mohns Ridge 155
5.4.5 Summary 156
5.4.6 Comparison with previous models 157
5.5 Possible implications for the structure and dynamics of the Iceland mantle plume 158
5.5.1 Interpretations of the spatial distribution of components in the North Atlantic mantle 159
5.5.2 The role of melting processes in sampling source heterogeneity 163
5.5.3 Is there an alternative to the Iceland plume model? 165

Chapter 6 168
Summary and conclusions

6.1 Introduction 169
6.2 The Snæfellsnes Peninsula 169
6.3 The Eastern Flank Zone 171
6.4 The Southern Flank Zone 172
6.5 The nature, number and origins of enriched components 172

References 176

Appendix 204

A1 Sample details 204
A1.1 Sampling constraints 204
A1.2 Sample descriptions 205
A2 Analytical techniques 208

A2.1 Helium isotope analyses 208
A2.1.1 Sample preparation 209
A2.1.2 Crushing procedure 209
A2.1.3 Fusion procedure 210
A2.1.4 Mass spectrometry 210
A2.1.5 Blank analyses 210
A2.1.6 Determining helium isotope concentrations and ratios 211
A2.2 Strontium and neodymium isotope analyses 211
A2.2.1 Sample preparation and chemical separation 212
A2.2.2 Mass spectrometry 212
A2.3 Lead isotope analyses 212
A2.3.1 Sample preparation, Pb separation and mass spectrometry 213
A2.3.2 Eliminating environmental contamination in Pb analyses 213
A2.4. Major element and trace element analyses 214

Figures

Page

Chapter 1
Introduction, aims and objectives

Fig. 1.1	Simplified map of Iceland illustrating the locations of the active rift-zones and flank zones	3
Fig. 1.2	Subaerial exposure of the plate boundary at the Reykjanes Peninsula, WRZ	4
Fig. 1.3	Log(Nb/Y)-log(Zr/Y) diagram of Icelandic basalts and MORB.	4
Fig. 1.4 (a)	Map of the tectonic location of Iceland in the North Atlantic	8
Fig. 1.4 (b)	Geological map of Iceland	9
Fig. 1.5	Relocation and propagation of the Icelandic rift-zones through time	9
Fig. 1.6	(a) Exposed section through a pillow basalt formation located at the tip of the Reykjanes Peninsula. (b) Hyaloclastite ridges along the Reykjanes Peninsula, WRZ	11 12
Fig. 1.7	Crustal thickness variations across Iceland and the adjacent parts of the Greenland-Faroe Ridge	15

Chapter 2
Characterisation of chemically enriched basalts from the Snaefellsnes Peninsula, western Iceland

Fig. 2.1	Tertiary volcanic centres and location of the Snæfellsnes syncline on the Snæfellsnes Peninsula	20
Fig. 2.2	The distribution of postglacial lava flows along the Snæfellsnes Peninsula and the location of the three volcanic systems	22

Fig. 2.3	Plot of total alkalis vs. silica concentrations for basalts from Snæfellsjökull , Lýsuskarð and Ljósufjöll	24
Fig. 2.4	Major oxide concentrations of Snæfellsnes basalts as a function of MgO	27
Fig. 2.5	Major oxide ratios of Snæfellsnes basalts as a function of MgO	28
Fig. 2.6	Regional variation in major element oxide (a) concentrations and (b) ratios	29
Fig. 2.7	Trace element concentrations (ppm) vs. MgO (wt. %)	32
Fig. 2.8	Incompatible trace element abundances of Snæfellsnes basalts	33
Fig. 2.9	Ce/Y vs. Nb/Zr	33
Fig. 2.10	Regional variation in VICE/MICE	34
Fig. 2.11	(a) Total He (cc STP) extracted by crushing olivine and pyroxene phenocrysts and (b) Total He (log scale) against $^{3}He/^{4}He$ (R/R_a)	37
Fig. 2.12	Plot of % blank correction against $^{3}He/^{4}He(R/R_a)$.	38
Fig. 2.13	Comparison of $^{3}He/^{4}He$ in co-existing olivines and pyroxenes	39
Fig. 2.14	Variation in $^{3}He/^{4}He$ of olivines with distance east (a) (0-150 km) and (b) (0-80 km) along the Peninsula	40
Fig. 2.15	$^{87}Sr/^{86}Sr$ vs. $^{143}Nd/^{144}Nd$	42
Fig. 2.16	Regional variations in (a) $^{87}Sr/^{86}Sr$ and (b) $^{143}Nd/^{144}Nd$	43
Fig. 2.17	(a) $^{206}Pb/^{204}Pb$ vs. $^{207}Pb/^{204}Pb$ and (b) $^{206}Pb/^{204}Pb$ vs. $^{208}Pb/^{204}Pb$	44

Fig. 2.18	Regional variations in (a) $^{206}Pb/^{204}Pb$; (b) $^{207}Pb/^{204}Pb$ and (c) $^{208}Pb/^{204}Pb$	45
Fig. 2.19	$^{206}Pb/^{204}Pb$ vs. (a) $^{87}Sr/^{86}Sr$ and (b) $^{143}Nd/^{144}Nd$	46
Fig. 2.20	$^{3}He/^{4}He$ vs. Mg# of Snæfellsnes basalts	49
Fig. 2.21	$^{3}He/^{4}He$ against ^{4}He measured by crush extraction of He from olivines	50
Fig. 2.22	Plots of mobile elements (K_2O, Rb) against the immobile element Nb	51
Fig. 2.23	Plots of incompatible major element concentrations against CaO/Al_2O_3	54
Fig. 2.24	Ce/Y vs. Zr/Nb	55
Fig. 2.25	CaO/Al_2O_3 vs. Ce/Y and Nb/Zr	55
Fig. 2.26	$^{3}He/^{4}He$ vs. (a) Ce/Y (b) Nb/Zr (c) TiO_2 and (d) P_2O_5	58
Fig. 2.27	$^{87}Sr/^{86}Sr$ vs. (a) Nb/Zr (b) Ce/Y (c) TiO_2 and (d) P_2O_5	58
Fig. 2.28	$^{143}Nd/^{144}Nd$ vs. (a) Nb/Zr (b) Ce/Y (c) TiO_2 and (d) P_2O_5	59
Fig. 2.29	$^{206}Pb/^{204}Pb$ vs. (a) Nb/Zr (b) Ce/Y (c) TiO_2 and (d) P_2O_5	59
Fig. 2.30	$^{3}He/^{4}He$ vs. (a) $^{87}Sr/^{86}Sr$; (b) $^{143}Nd/^{144}Nd$ and (c) $^{206}Pb/^{204}Pb$	60
Fig 2.31	Schematic cross-section illustrating the distribution of mantle sources and controls on melting processes and preferential source-tapping in Snæfellsnes	63

Chapter 3

Characterisation of chemically enriched basalts from the Eastern Flank Zone

Fig. 3.1	Simplified map of the EFZ and showing locations of Öræfajökull, Esjufjöll and Snæfell volcanoes and sample localities	70
Fig. 3.2	Total alkalis-silica (TAS) diagram of Snæfell and Öræfajökull basalts	72
Fig. 3.3	Major element oxide concentrations vs. MgO concentrations for samples from Öræfajökull and Snæfell	74
Fig. 3.4	Major element oxide ratios vs. MgO concentrations (>5 wt. %)	75
Fig. 3.5	Trace element concentrations vs. MgO concentration of samples from Snæfell and Öræfajökull	76
Fig. 3.6	Primitive-mantle normalised diagrams of Öræfajökull and Snæfell trace element abundances	77
Fig. 3.7	Ce/Y vs Nb/Zr of EFZ basalts (MgO > 5 wt. %)	78
Fig. 3.8	$^{3}He/^{4}He$ and total He released by crushing of olivine and pyroxene phenocrysts	79
Fig. 3.9	(a) $^{87}Sr/^{86}Sr$ vs. $^{143}Nd/^{144}Nd$, (b) $^{206}Pb/^{204}Pb$ vs. $^{207}Pb/^{204}Pb$, (c) $^{206}Pb/^{204}Pb$ vs. $^{208}Pb/^{204}Pb$, (d) $^{206}Pb/^{204}Pb$ vs. $^{87}Sr/^{86}Sr$ and (e) $^{206}Pb/^{204}Pb$ vs. $^{143}Nd/^{144}Nd$, for samples from Snæfell and Öræfajökull	81
Fig. 3.10	Ce/Y- Zr/Nb diagram of EFZ basalts with modelled partial melting curves of garnet- and spinel-lherzolites	85
Fig. 3.11	$^{3}He/^{4}He$ vs. (a) $^{87}Sr/^{86}Sr$, (b) $^{143}Nd/^{144}Nd$ and (c) $^{206}Pb/^{204}Pb$ of samples from Snæfell and Öræfajökull	88

Chapter 4

Characterisation of chemically enriched basalts from the Southern Flank Zone

Fig. 4.1	Simplified map of the SFZ	94

Fig. 4.2	Total alkalis vs. silica diagram of SFZ samples	96
Fig. 4.3	MgO (wt. %) vs. major element oxide concentrations (wt. %)	97
Fig. 4.4	MgO vs. major oxide ratios of SFZ basalts (MgO > 5 wt. %)	100
Fig. 4.5	Trace element concentrations (ppm) vs. MgO (wt. %)	102
Fig. 4.6	Ce/Y vs. Nb/Zr for SFZ basalts (MgO > 5 wt. %)	106
Fig. 4.7	Total ^{4}He concentrations vs. $^{3}He/^{4}He$ for SFZ olivines and pyroxenes	107
Fig. 4.8	$^{87}Sr/^{86}Sr$ vs. $^{143}Nd/^{144}Nd$	109
Fig. 4.9	$^{206}Pb/^{204}Pb$ vs. (a) $^{207}Pb/^{204}Pb$ and (b) $^{208}Pb/^{204}Pb$	109
Fig. 4.10	Plots of mobile elements (K_2O, Rb) against the immobile element Nb	112
Fig. 4.11	Incompatible major oxide concentrations vs. CaO/Al_2O_3	116
Fig. 4.12	$^{206}Pb/^{204}Pb$ vs. $^{87}Sr/^{86}Sr$ and $^{143}Nd/^{144}Nd$	117
Fig. 4.13	$^{3}He/^{4}He$ vs. $^{87}Sr/^{86}Sr$, $^{143}Nd/^{144}Nd$ and $^{206}Pb/^{204}Pb$	118

Chapter 5

The nature, origins, distribution and inter-relationships between enriched components in the sub-Icelandic mantle

Fig. 5.1	Log(Nb/Y)-log(Zr/Y) diagram showing all Icelandic data	123
Fig. 5.2	$^{87}Sr/^{86}Sr$ vs. $^{143}Nd/^{144}Nd$	125
Fig. 5.3	$^{206}Pb/^{204}Pb$ against (a) $^{207}Pb/^{204}Pb$ and (b) $^{208}Pb/^{204}Pb$	126

Fig. 5.4	$^{3}He/^{4}He$ released by in vacuo crushing of olivines from rift-zone and flank-zone basalts.	128
Fig. 5.5	$^{3}He/^{4}He$ vs. (a) Nb/Zr, (b) $^{87}Sr/^{86}Sr$, (c) $^{143}Nd/^{144}Nd$ and (d) $^{206}Pb/^{204}Pb$	130
Fig. 5.6	$^{206}Pb/^{204}Pb$ vs. (a) $^{87}Sr/^{86}Sr$ and (b) $^{143}Nd/^{144}Nd$	132
Fig. 5.7	Sketch diagrams demonstrating possible mixing systematics in Iceland. (a) Mixing between two depleted components and (b) mixing-trends between a single depleted component and an enriched component	139
Fig. 5.8	Results of mixing model calculations for (a) He-Sr, (b) He-Nd, (c) He-Pb, (d) Pb-Sr and (e) Pb-Nd	146
Fig. 5.9	Isotope variations along the MAR in the North Atlantic	152
Fig. 5.10	Results of mixing-model calculations based on two enriched – two depleted components, for (a) He-Sr and (b) Pb-Sr.	153
Fig. 5.11	Map of Iceland and the North Atlantic illustrating the different contributions of Icelandic end-members and mantle components to local source compositions	156
Fig. 5.12	Schematic diagram of the Iceland mantle plume	162
Fig. 5.13	Ce/Y vs. Zr/Nb	164

Chapter 6
Summary and Conclusions

Fig. 6.1	(a) Dynamics and structure of the Iceland plume as interpreted from the results of this study. (b) The role of melting in sampling enriched and depleted mantle in Snæfellsnes	174

Tables Page

Table 2.1	Sample details	23
Table 2.2	Major element oxide concentrations of Snæfellsnes basalts	25
Table 2.3	Trace element concentrations of Snaefellsnes basalts	31
Table 2.4	Helium isotope data from crush extractions of He from olivine and pyroxene phenocrysts	35
Table 2.5	Sr, Nd and Pb isotope compositions of Snæfellsnes basalts	41
Table 2.6	Production of radiogenic ^{4}He in olivines and pyroxenes	48
Table 2.7	Helium isotope data for furnace and crush extractions of helium from $SNS201_{olivine}$	50
Table 3.1	Sample details	71
Table 3.2	Major element oxide concentrations of EFZ samples	73
Table 3.3	Trace element concentrations of EFZ samples	76
Table 3.4	Helium isotope data from crush extractions of olivine and pyroxene phenocrysts	79
Table 3.5	Sr, Nd and Pb isotope compositions of EFZ samples	81
Table 4.1	Sample details	94
Table 4.2	Major element oxide concentrations of EFZ samples	96
Table 4.3	Trace element concentrations of EFZ samples	101
Table 4.4	Helium isotope data from crush extractions of olivine and pyroxene phenocrysts	107
Table 4.5	Sr, Nd and Pb isotope compositions of EFZ samples	108

Table 5.1 Compositions of enriched end-members identified in the Icelandic flank-zones and Jan Mayen. 133

Table 5.2 Isotope ratios and element concentrations of mantle components used in mixing calculations 142

Chapter 1

INTRODUCTION, AIMS AND OBJECTIVES

1.1 Introduction

Iceland is a volcanic island located in the northern Atlantic Ocean and situated along the Mid-Atlantic Ridge (MAR) spreading-ridge system. Although there has been some recent discussion (see Section 1.2.3, below), mantle melting at Iceland is widely regarded as being a result of adiabatic decompression (associated with sea-floor spreading) combined with the thermal influence of a mantle plume (e.g., Schilling, 1979, 1991; McKenzie and O'Nions, 1995; Fitton *et al.*, 1997; Hanan and Schilling, 1997; Darbyshire *et al*, 2000). The plate boundary on Iceland is marked by three active rift zones: the western rift-zone (WRZ), the northern rift-zone (NRZ) and the eastern rift-zone (ERZ), which converge over the head of the inferred mantle plume where the lithosphere is thinnest (Figures 1.1, 1.2). Volcanic activity outside the rift zones occurs in three regions known as flank-zones: the Snæfellsnes Peninsula (SNP), located at the site of an extinct rift-zone (e.g., Hardarson, 1993); the southern flank zone (SFZ), at the tip of the propagating ERZ (e.g., Furman *et al.*, 1991, 1995); and the eastern flank zone (EFZ), where no rifting has occurred (e.g., Hards *et al.*, 1995; Prestvik *et al.*, 2001). Basalt erupted in the rift zones is dominantly tholeiitic and has higher concentrations of incompatible elements than normal mid-ocean ridge basalt (N-MORB; Sun & McDonough, 1989) (e.g., Fitton *et al.*, 1997). In contrast, flank-zone basalts are transitional to mildly alkaline and are highly enriched in incompatible elements compared to both rift-zone basalt and N-MORB (e.g., Hardarson and Fitton, 1991; Furman *et al.*, 1991, 1995; Sigmarsson *et al.*, 1992; Hardarson, 1993; Hards *et al.*, 1995).

Despite the wealth of geochemical data from the region, there is some controversy as to the mantle origins of Icelandic and North Atlantic basalts. The chemical and isotopic data indicate that the sub-North Atlantic mantle is heterogeneous and are consistent with the presence of a depleted component derived from the shallow asthenospheric mantle and a more enriched component that is dominant in the Icelandic mantle and likely originates from recycled material stored in the lower mantle at the source of a plume (e.g., Schilling, 1973; 1982; Hanan and Schilling, 1997; Hanan *et al.*, 2000). ('Depleted' and 'enriched' hereafter refer to both isotopic and incompatible element composition.) There is abundant geochemical evidence that the most depleted Icelandic mantle, that supplies along

the active rift zones, is distinct from the N-MORB source and is intrinsic to the mantle plume (e.g., Hards *et al.*, 1995; Thirlwall, 1995; Kerr *et al.*, 1995; Fitton *et al.*, 1997, 2003; Kempton *et al.*, 2000; Thirlwall *et al.*, 2004). On a plot of log Nb/Y against log Zr/Y, for example, Icelandic basalts form an array parallel to, but displaced to higher Nb/Y than the global N-MORB field, reflecting Nb enrichment in the Icelandic mantle source (Fitton *et al.*, 1997) (Figure 1.3). The array is defined by two parallel lines. Enrichment or depletion in Nb, relative to the lower line, is expressed as the function ΔNb (ΔNb = 1.74 + log(Nb/Y) - 1.92 log(Zr/Y)), such that Icelandic basalt has positive ΔNb and N-MORB has negative ΔNb (Fitton *et al.*, 1997).

Figure 1.1 Simplified map of Iceland illustrating the locations of the rift zones and flank zones.

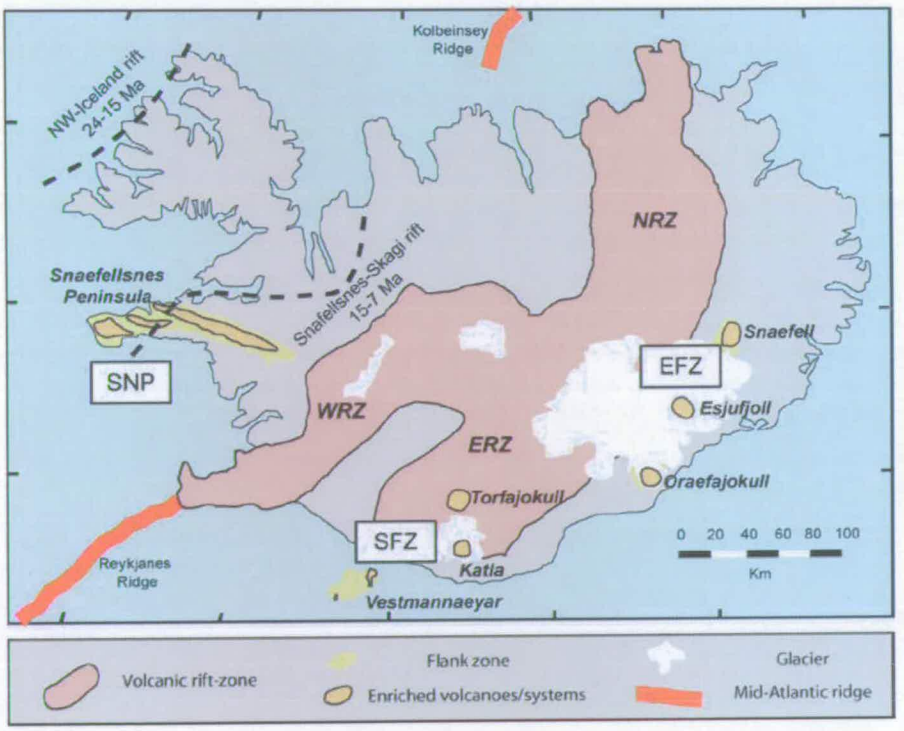

Figure 1.2 Subaerial exposure of the plate boundary at the Reykjanes Peninsula, WRZ.

Figure 1.3 Log(Nb/Y)-log(Zr/Y) diagram of Icelandic basalts and MORB. The Iceland array is defined by two parallel lines; the lower line defining the boundary between negative and positive ΔNb.

Data sources - Rift-zone basalts: Hemond *et al.*, 1993; Gee *et al.*, 1998; Kempton *et al.*, 2000; Hanan *et al.*, 2000; Fitton, *et al.*, 2003; Flank-zone basalts: McGarvie, 1984; McGarvie *et al.*, 1990; Furman *et al.*, 1991; Hardarson, 1993; Prestvik *et al.*, 2001; Hards *et al.*, 1995; MORB field: Fitton *et al.*, 1997. Average N-MORB from (H) Hofmann, 1988 and (SM) Sun and McDonough, 1989; Jan Mayen basalts: Stuart *et al.*, *in prep.*

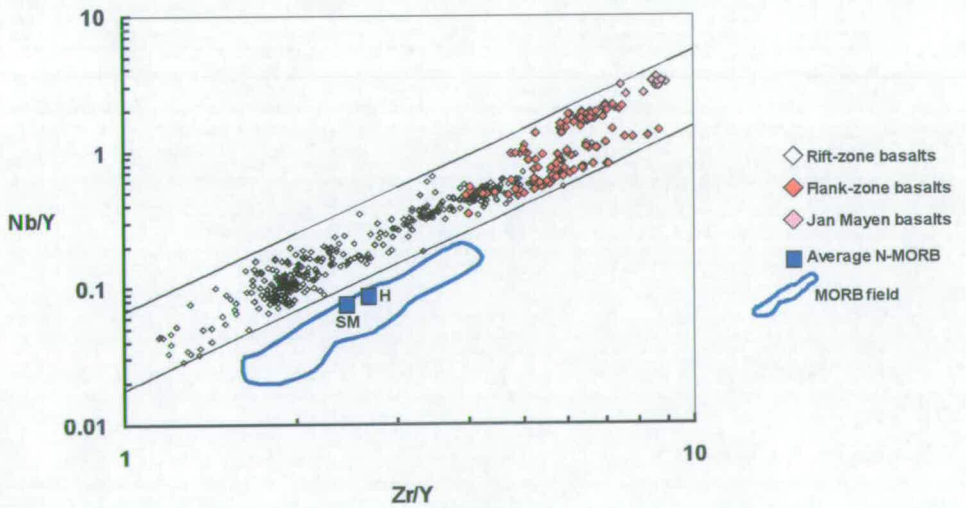

Isotope data also support the presence of a distinct depleted mantle source in Iceland (e.g., Thirlwall, 1995; Hards *et al.*, 1995, Kerr *et al.*, 1995; Kempton *et al.*, 2001; Thirlwall *et al.*, 2004). For example, Δ7/4 is used to define deviation of $^{207}Pb/^{204}Pb$ from the Northern Hemisphere Reference Line (NHRL: Hart *et al.*, (1984)) in a plot of $^{207}Pb/^{204}Pb$ against $^{206}Pb/^{204}Pb$. N-MORB is characterised by positive Δ7/4 and Icelandic basalt is characterised by negative Δ7/4 (Thirlwall *et al.*, 1995). Negative Δ7/4 has been suggested to represent U enrichment in the mantle source of Icelandic basalt (Thirlwall, 1997; Thirlwall *et al.*, 2004).

While numerous studies have focused on the nature and origin of the more-depleted Icelandic component(s), less attention has been paid to the origins of the isotopically and chemically enriched basalts. On the log Nb/Y-log Zr/Y diagram (Figure 1.3) the flank-zone basalts comprise the high Zr/Y - high Nb-Y end of the Iceland array; Snæfellsnes and SFZ basalts representing the most enriched compositions. These incompatible-element-enriched basalts also comprise the radiogenic ends of the Iceland fields in isotope space.

Studies of individual volcanic centres suggest there may be more than one enriched component in the sub-Icelandic mantle (e.g., Hardarson, 1993; Hards *et al.*, 1995; Furman *et al.*, 1991, 1995; Stecher *et al.*, 1999; Prestvik *et al.*, 2001), but the number, nature and origins of these have not been extensively explored. The similarities of enriched Icelandic basalts to those erupted outside the influence of the inferred mantle plume, for example at Jan Mayen some 650 km north of Iceland (e.g., Trønnes *et al.*, 1999), may indicate that the enriched components in the Icelandic mantle are not intrinsic to the mantle plume but exist as heterogeneities within the shallow asthenospheric mantle (Stuart *et al.*, *in prep.*). Alternatively, Jan Mayen basalts could be derived from enriched material from the ancestral mantle plume that has been trapped in the shallow mantle (Trønnes *et al.*, 1999).

The present research aims to resolve the number, nature, distribution and origins of enriched components in the North Atlantic mantle. Sr, Nd and Pb isotopes have previously been used to investigate the mantle sources of enriched basalts erupted in the individual flank-zones (see references above), but the published data-set have not generally allowed enriched components to be distinguished from one another, nor their origins and relationships to be constrained. Thirlwall *et al.*, (2004) have recently

investigated the number and origin of mantle components in Iceland based on new high-precision Pb isotope data in conjunction with Sr- and Nd-isotopes and trace element data, and two enriched (as defined solely on the basis of Nb/Zr) end-members were identified. However, only basalts from the SFZ were used in addition to the rift-zone basalts, and thus a significant proportion of the enriched basalts found in Iceland were ignored in their study. As a result, basalts from the SNP and EFZ cannot be accommodated in their model.

The aforementioned studies of individual flank-zones have alluded to the compositional diversity of enriched basalts, however, the use of Sr, Nd and Pb isotopes alone does not appear to be capable of distinguishing between enriched components or constraining their origins. Helium isotope ratios have been demonstrated in numerous studies to be effective source-discriminants and provide valuable information on the origins of mantle components (e.g. Farley and Neroda, 1998, Graham, 2002). High helium isotope ratios measured in primary basalt (up to 49.5 R_a; Stuart *et al.*, 2003; where R_a is the atmospheric $^3He/^4He = 1.39 \times 10^{-6}$) are regarded as unambiguous tracers of deep, plume-derived mantle (e.g., Lupton and Craig, 1975; Kurz *et al.*, 1982a,b; Allègre *et al.*, 1985; Farley and Neroda, 1998; Moreira and Allégre, 1998). Whereas the relatively degassed upper-mantle N-MORB source is characterised by uniform $^3He/^4He$ of ~8 R_a (e.g., see Graham, 2002), plume-derived mantle is often characterised by a high concentration of primordial ^3He, from an undegassed reservoir generally regarded to be located at depth in the mantle (e.g., Kellog and Wasserburg, 1990, Kurz *et al.*, 1982a, Macpherson *et al.*, 1998). Oceanic crust is degassed at the Earth's surface and recycled back into the mantle at subduction zones. Addition of U and Th during the recycling process increases the ^4He concentration in the recycled material through radioactive decay during mantle storage. As a result, volcanoes which sample mantle domains derived from recycled material, for example HIMU islands (high-μ or increased $^{238}U/Pb$ relative to the N-MORB-source) are often characterised by $^3He/^4He$ that are lower than the N-MORB ratio (e.g., Kurz *et al.*, 1982a, Graham *et al.*, 1992; Hanyu and Kaneoka, 1997). Jan Mayen basalts are characterised by $^3He/^4He$ of 5 - 6 R_a (Kurz *et al.*, 1982b; Stuart *et al.*, in prep), which are lower than both N-MORB and Quaternary Icelandic basalt ratios (up to 34.3 R_a; Macpherson *et al.*, 2005). This

suggests that the Jan Mayen mantle source has higher time-integrated ^{4}He, derived for example from recycled sediments or crust. He isotope data from flank-zone basalts can therefore be used in conjunction with Sr, Nd and Pb isotopes to distinguish between N-MORB source, recycled, and plume-derived origins for the enriched components in the sub-Icelandic mantle.

1.2 The geology and geodynamics of Iceland

1.2.1 The geological history of Iceland and the North Atlantic

The presence of a mantle plume in the North Atlantic region can be traced back to approximately 61 Ma and the initiation of continental rifting and flood-basalt volcanism in central Greenland (e.g., White and McKenzie, 1989; Holm *et al.*, 1993; Lawver and Müller, 1994; Thirlwall *et al.*, 1994; Saunders *et al.*, 1997; Storey *et al.*, 1998; Pederson *et al.*, 2002). In the early stages of the North Atlantic Igneous Province (NAIP) the plume head may have been up to 2000 km in diameter (e.g., Stuart *et al.*, 2000). Plate separation and the formation of oceanic crust began at around 56 – 52.5 Ma (e.g., Vogt and Avery, 1974; Saunders *et al.*, 1997).

The Iceland plume track through time is marked by the anomalously thick crust which forms the Greenland-Færöe ridge (e.g., Lawver and Müller, 1994) (Figure 1.4a). The MAR spreading-axes centred themselves over the head of the Iceland plume at approximately 24 Ma (Vink, 1984) and over the past 20 Myr have drifted north-westwards. As a result, the rift zones have repeatedly 'jumped' south-eastwards in order to maintain their position above the thin lithosphere at the centre of the Iceland plume, currently inferred to be beneath Vatnajökull (Figure 1.5). Rift relocation occurs by propagation through the older oceanic crust (e.g., Jóhannesson *et al.*, 1980; Steinþórsson *et al.*, 1987), and the active ERZ represents the most recent propagation of a new rift zone, which will eventually connect with the Reykjanes Ridge to the south of Iceland (e.g., Oskarsson *et al.*, 1982, 1985; Meyer *et al.*, 1985).

The oldest exposed volcanic rocks in Iceland are basaltic flows found in the NE and NW peripheries of the island (Figure 1.4b). These were erupted during the Tertiary era at 16 - 13 Ma (e.g., Hardarson *et al.*, 1997) and are thought to have been

produced in axial rift zones similar to those of the present-day. Two major palaeorifts have been identified in Iceland: the Snæfellsnes-Skagi rift and the NW-Iceland rift (Figure 1.1), which were active until approximately 5 Ma and 15 Ma respectively (Hardarson *et al.*, 1997; Kristjansson and Jóhannesson, 1999).

The exposed Tertiary basalts are dominantly tholeiitic and have similar chemical and isotopic compositions to those erupted in the active rift-zones (e.g., Jakobsson, 1979; Hardarson and Fitton, 1991; Hardarson *et al.*, 1997; Hanan and Schilling; 1997; Bunce, 2002). However, more isotopically depleted compositions appear to characterise the oldest basalts from the northwest rift, suggesting involvement of depleted N-MORB mantle in the rift-zone source at this time (Hardarson *et al.*, 1997).

Figure 1.4 (a) Map of the tectonic location of Iceland in the North Atlantic and **(b)** geological map of Iceland (reproduced from Jóhannesson and Sæmundsson, 1989).

(a)

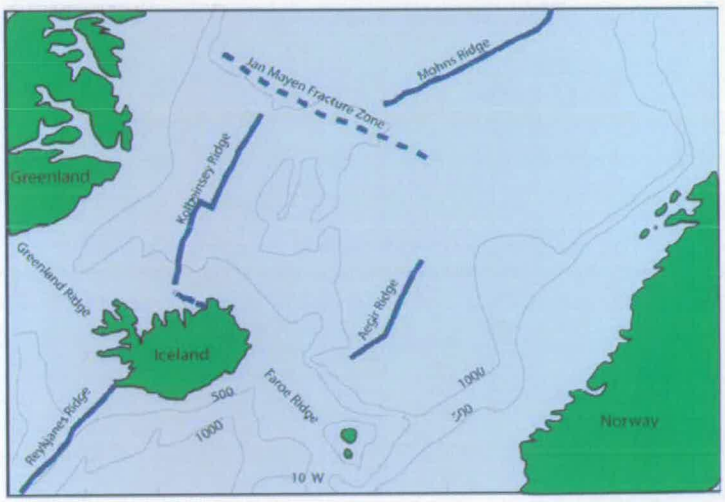

(b)

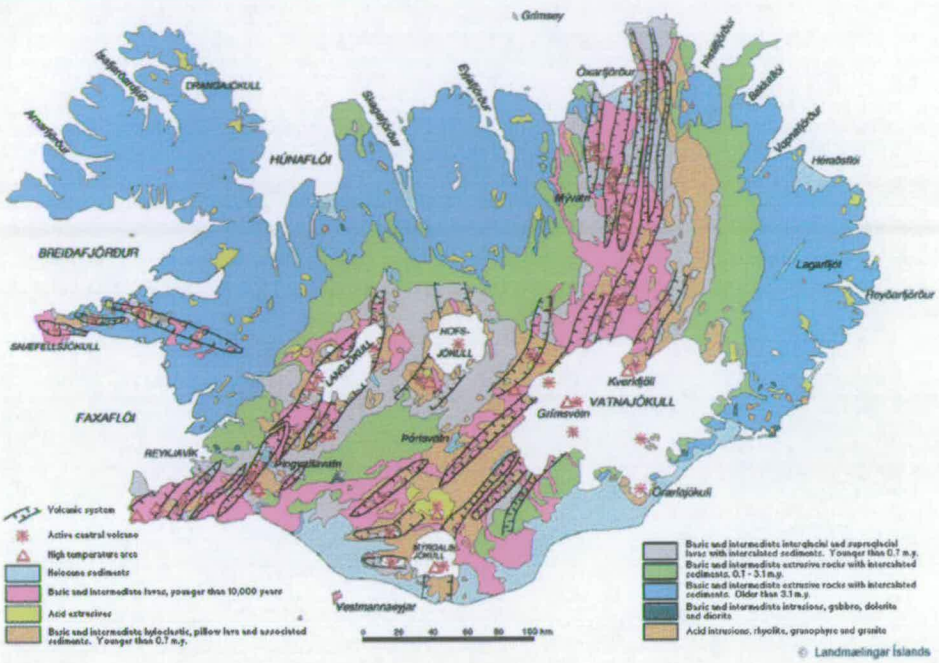

Figure 1.5: Relocation and propagation of the Icelandic rift-zones through time. In the schematic sections, open arrows indicate extinct rift-zones and filled arrows represent the position of active rift-zones. (From Stecher *et al.*, 1999 (redrawn from Ivarson *et al.*, 1992).)

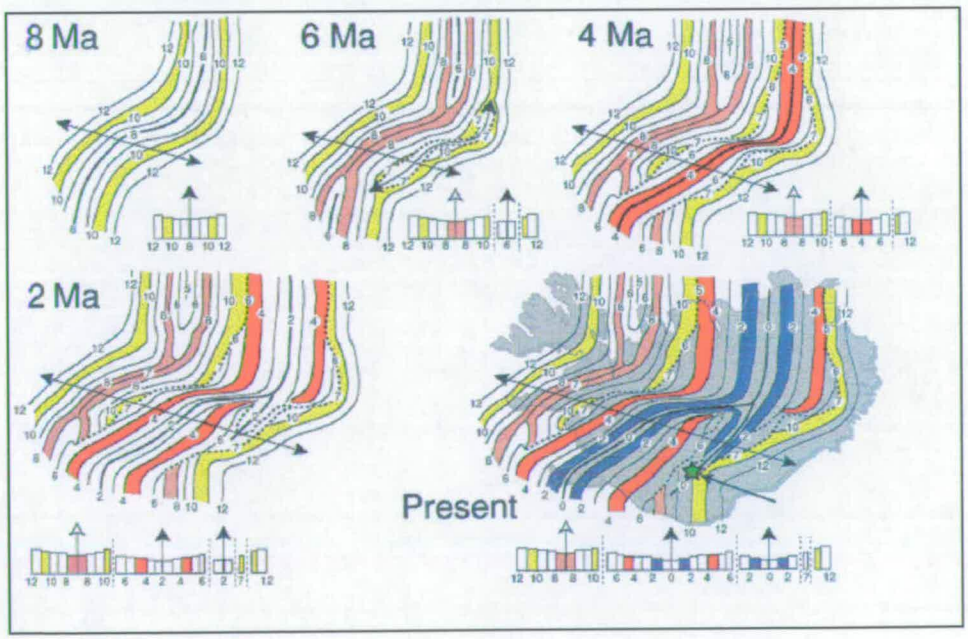

Spreading in the present-day rift-zones was initiated at approximately 6 Ma, after the propagation and the development of the WRZ and NRZ (Figure 1.5), and has continued uninterrupted in these regions until the present day. Propagation of the ERZ began at approximately 2 Ma and the tip of the propagating rift is currently located beneath the SFZ at Vestmannaeyjar (Sæmundsson, 1978). Volcanic activity in the rift-zones occurs along fissure swarms that are 5-10 km wide and up to 100 km long (e.g., Jakobsson, 1979) (Figure 1.4). Each rift-zone comprises around 4 to 5 subparallel swarms. Volcanism in the rift zones is initially tholeiitic, but over time more chemically evolved magmas are formed leading to the development of a silicic central volcanic complex (Figure 1.4).

The chemical and isotopic compositions of rift-zone basalts are consistent with derivation from a relatively depleted component that is intrinsic to the Iceland plume (e.g., Thirlwall, 1995; Fitton *et al.*, 1997; Thirlwall *et al.*, 2004). The range of incompatible element enrichment in Icelandic basalts is thought to result from variable degrees of melting, such that small-degree melting will preferentially sample more enriched material in the source (e.g., Fitton *et al.*, 2003)). During decompression melting, initial small-degree melts of more fusible enriched material will become increasingly diluted by depleted melt-fractions as the melt ascends (Elliott *et al.*, 1991). High mantle temperatures and long melt-columns (due to thin lithosphere) in the rift-zones therefore give rise to an abundance of depleted basalt flows in these regions. Small-volume flows composed of strongly depleted picrites, which represent melts formed during the most advanced stages of melting, are very occasionally found in the rift zones, but only in the older NRZ and WRZ where mantle upwelling is most vigorous (Fitton *et al.*, 2003).

Enriched alkaline and transitional basalts constitute only around 15% of Icelandic basaltic rocks formed in the Quaternary (Jakobsson *et al.*, 1972) and are confined to the non-rifting flank-zones, where the lithosphere is thicker, mantle temperatures are lower and mantle upwelling is less-vigorous than beneath the rift zones (e.g., Palmason, 1981; Kokfelt *et al.*, 2003) (Figure 1.1).

The inter-play between climate and volcanism in Iceland is well documented. The beginning of the Quaternary period in Iceland is fixed at the base of the Mammoth magnetic event at 3.1 Ma, at which the first signs of the onset of the ice-

age are found (Sæmundsson, 1980). There are known to have been at least 20 glacial cycles since that time, and the last glacial period in Iceland (the Weichsel period) started about 70 kyrs ago and continued until around 10 kyrs ago. Lavas erupted during glacial periods form ridges and table-mountains composed of hyaloclastite, tuff, pillow breccia and pillow basalt (Figures 1.4 and 1.6). In contrast, interglacial and postglacial lavas form extensive flat-lying flows of consolidated basalt (e.g., Jakobsson, 1980) (Figure 1.4). Interglacial flows can be distinguished from postglacial (Recent) flows by their striated and eroded surfaces and the presence of glacial drift. During the late-glacial periods magma eruption rates and degrees of melting were considerably higher than during the early glacial and postglacial periods (e.g., Hardarson and Fitton, 1991). These have been attributed to the release of ponded magma through tectonic movements in response to glacial unloading (e.g., Sigvaldason *et al.*, 1992) or to increased decompression melting due to rapid rebound of the crust during deglaciation (Hardarson and Fitton 1991; Jull and McKenzie, 1996; Slater *et al.*, 2001; Maclennan *et al.*, 2002).

Subglacial volcanism still occurs in the present-day beneath the ice-sheets which have developed over high central volcanoes in southern and eastern Iceland, and the most recent eruption in Iceland was the subglacial Grimsvötn eruption of November 2004.

Figure 1.6 (a) Exposed section through a pillow basalt formation located at the tip of the Reykjanes Peninsula and **(b)** hyaloclastite ridges along the Reykjanes Peninsula, WRZ.

(a)

(b)

1.2.2 The Iceland mantle plume

Mantle plumes were initially proposed by Morgan (1971, 1972) in order to explain occurrence of intraplate volcanic islands. There are undoubtedly different types of mantle plume which have a diversity of sources. Primary mantle plumes are those long-lived, high-temperature plumes which are thought to originate at depth in the mantle (e.g., Morgan, 1971; Richards *et al.*, 1989; Campbell and Griffiths, 1990; Schilling, 1991; White, 1995; Hoffmann, 1998; Courtillot *et al.*, 2003). Five criteria have been proposed by Courtillot *et al.*, (2003) for distinguishing between primary and secondary mantle plumes:

(1) The presence of a linear chain of volcanoes with monotonous age progression;

(2) The presence of flood basalt (i.e., a large igneous province) at the origin of the plume track;

(3) A large buoyancy flux (i.e., flow of material from the deep mantle);

(4) $^{3}He/^{4}He$ consistently higher than 10 R_a;

(5) A significant low shear wave velocity in the underlying mantle.

Iceland satisfies four or possibly five of these criteria and is thus considered to be a primary plume. The Greenland-Færöe ridge (Figures 1.5, 1.7) is inferred to represent the plume trail in the North Atlantic (criterion #1) which has its origins in the flood-basalt provinces in central Greenland and in the British Isles (criterion #2).

$^3He/^4He$ are higher than 8 R_a in the Icelandic rift-zone basalts, ranging up to ~34 R_a in central Iceland (Kurz *et al.*, 1985; Condomines *et al.*, 1983; Breddam *et al.*, 2000; 2002; Macpherson *et al.*, 2005). The $^3He/^4He$ of Tertiary Icelandic basalts range up to 37 R_a (Hilton *et al.*, 1999; Ellam and Stuart, 2004), and uncontaminated NAIP basalts are characterised by $^3He/^4He$ greater than 8 R_a and up to ~49 R_a (e.g., Graham *et al.*, 1998; Kirstein and Timmerman, 2000; Marty *et al.*, 1998; Stuart *et al.*, 2000; Stuart *et al.*, 2003; Ellam and Stuart, 2004). Thus, although $^3He/^4He$ can be variable, the occurrence of high ratios in the rift-zones suggests that helium isotopes support the presence of a mantle plume (criterion #4). Finally, P- and S-wave tomographic models show that a cylindrical velocity low extends from a depth of 100 km to greater than 400 km beneath Iceland (e.g., Tryggvason *et al.*, 1983; Bijwaard and Spakman, 1992; Wolfe *et al.*, 1997; Helmberger *et al.*, 1998; Shen *et al.*, 1998) (criterion #5).

Additional evidence for the presence of a mantle plume beneath Iceland includes: the eastward off-set of rift zones relative to the MAR (Sæmundsson, 1974); geochemical variations along the Reykjanes and Kolbeinsey Ridges to the south and north of Iceland (e.g., Taylor *et al.*, 1997; Mertz and Haase, 1997); the production of anomalously thick oceanic crust (up to 40km) beneath south-eastern Iceland at the inferred centre of the Iceland plume (e.g., Bjarnason *et al*, 1993; Darbyshire *et al.*, 2000; Kaban *et al.*, 2002) (Figure 1.8); and elevated mantle upwelling rates in south-east Iceland and along the rift zones (e.g., Ito *et al.*, 1999; Maclennan *et al.*, 2001).

1.2.3 Alternative models for melt generation in Iceland

Melting in the mantle can be induced by one or a combination of three main processes: decompression and thinning of the lithosphere (e.g., McKenzie and Bickle, 1988); temperature increase (e.g., White and McKenzie, 1995); and through volatile release (for example, water) (e.g., Thompson, 1992). While most models of melt generation at Iceland have focused on the interplay between decompression- and thermal-induced melting, recent controversy regarding the existence of mantle plumes has led to consideration of alternatives to, and modifications of, the high-temperature plume model. (e.g., Foulger *et al.*, 2000, 2003; Anderson, 1998, 2001; Nichols, 2003).

G. Foulger has considered in detail the possibility that deep-rooted, high-temperature mantle plumes do not exist (see www.mantleplumes.org for further information). An alternative hypothesis proposed for Iceland by Foulger *et al.*, 2005 is the remelting of subducted Iapetus crust, which may have been recyled back into the asthenosphere by lithospheric delamination during the opening of the North Atlantic. Remelting of abyssal gabbros is invoked to explain the chemistry of Icelandic basalts, and the high $^{3}He/^{4}He$ that characterise Icelandic basalts are explained by preservation of old He in either (U+Th)-poor Caledonian mantle lithosphere (after Anderson, 1998) or olivine cumulates in the lower crustal sections (after Natland, 2003). The presence of enhanced melt production along the Greenland-Faroe ridge is explained by storage of the Iapetus crust beneath the frontal thrust of the ancient Caledonian collision zone, which is inferred to be colinear to the Greenland-Faroe ridge.

The role of water in initiating melt anomalies in the asthenospheric mantle has been extensively investigated in studies of ridge-centred and off-axis volcanism (e.g., Bonatti, 1990; Asimow and Langmuir, 2003). The influence of water in generating melting in Iceland has been recently examined by Nichols *et al.*, (2002), who consider the possibility suggested by Schilling *et al.*, (1980), that the Iceland 'hotspot' might also be a 'wetspot'. The northerly increasing H_2O concentrations measured in basalts from along the Reykjanes Ridge and Iceland result in increasing melt fractions at a given melting temperature. A temperature increase of 100°C would be required to produce the equivalent increase in degree of melting in the absence of water, demonstrating that water plays a significant role in the generation of Icelandic basalt compositions.

Figure 1.7 Crustal thickness variations across Iceland and the adjacent parts of the Greenland-Faroe Ridge (from R.G Trønnes (www.norvol.hi.is), simplified from Kaban *et al.*, (2002))

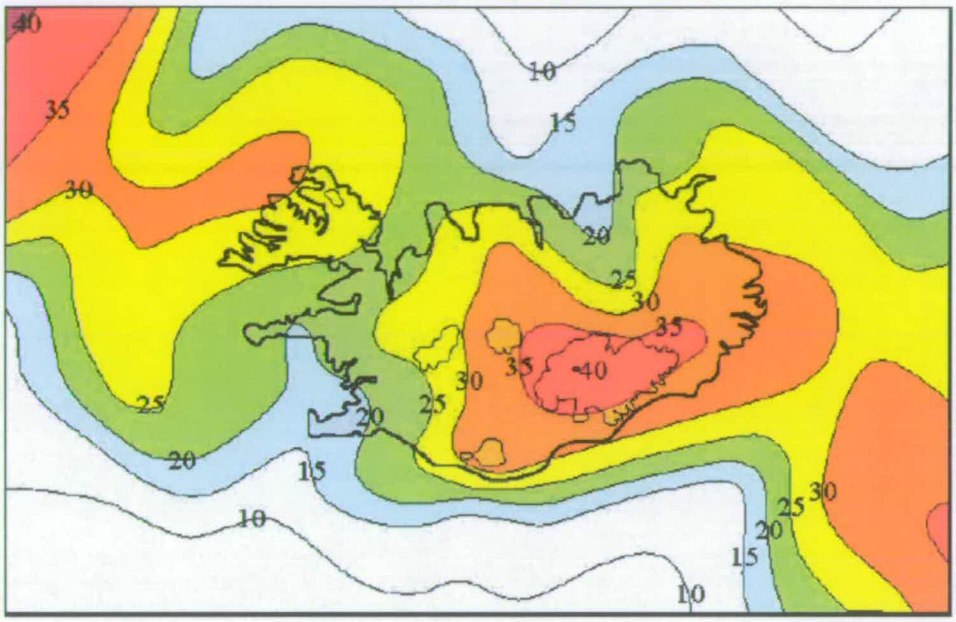

1.3 Aims and objectives

The principal aims of this research are to:

(i) provide a characterisation of enriched mantle in Iceland, as sampled by volcanism in the three Icelandic flank-zones;

(ii) determine the number of enriched components and their distribution;

(iii) investigate the origins of enriched components;

(iv) examine the interplay between enriched and depleted components in the North Atlantic mantle.

In order to characterise and compare the mantle sources of each of the three flank-zones, a comprehensive series of isotope and chemical analyses have been performed on samples collected from each of the three flank-zones. Trace element and major element compositions were determined by x-ray fluorescence to enable the effects of partial melting and fractional crystallisation to be distinguished from source composition, and to examine the role of partial melting in the sampling of

mantle sources. Source characterisation can be achieved using He, Sr, Nd and Pb isotope ratio determinations in addition to trace element data. By comparing the source compositions of each flank-zone, enriched mantle components can then be identified and characterised, enabling subsequent constraints to be made on the role of component-mixing in generating the compositions of sources. The origins of the enriched components will be constrained by comparing their isotopic and chemical characteristics to those of recognised mantle components.

Chapter 2

CHARACTERISATION OF CHEMICALLY ENRICHED BASALTS FROM THE SNÆFELLSNES PENINSULA, WESTERN ICELAND

2.1 Introduction

The alkalic, incompatible element-enriched basalts of the Snæfellsnes Peninsula and other off-axis volcanic zones in Iceland are derived from enriched mantle domains that are distinct from both the "depleted" plume component erupted in the rift zones and from the upper mantle source of basalts erupted along adjacent portions of the Mid-Atlantic Ridge (e.g., Hart *et al.*, 1973; O'Nions *et al.*, 1973; O'Nions and Gronvold, 1973; Furman *et al.*, 1991, 1995; Sigmarsson *et al.*, 1992; Hémond *et al.*, 1993; Hards *et al.*, 1995). The distribution, nature and origin of this component is controversial and a small number of studies have shown that the lavas from each flank zone may each represent isotopically distinct components (Furman *et al.*, 1991; Sigmarsson *et al.*, 1992; Hards *et al.*, 1995; Smit *et al.*, 1999; Stecher *et al.*, 1999; Prestvik *et al.*, 2001). That the enriched, alkalic basalts are restricted to off-axis regions reveals something about the processes governing the locations and origins of enriched mantle components. Does this imply that the enriched domains are restricted to the peripheral regions of the mantle plume? Not necessarily. The more fusible nature of the enriched domains means they may be preferentially tapped by small-degree melting. Therefore, the prevalent melting conditions may determine the degree of enrichment of basalts erupted at a particular location. The major and trace element composition of basalts provide valuable information about the melting regimes prevalent in Iceland's volcanic zones and can be used in conjunction with He-Sr-Nd-Pb isotope data to provide robust constraints on sources and their origin (see Chapter 1).

In this chapter, I report the geochemical characteristics of enriched basalts from the Snæfellsnes Peninsula, western Iceland. The peninsula has been selected for an in-depth investigation for the following reasons:

(1) Previous studies have identified the Quaternary Snæfellsnes Peninsula basalts to be amongst the most incompatible-element enriched on Iceland (e.g. Hardarson, 1993; Fitton *et al.*, 1997, 2003; Kokfelt *et al.*, 2003).

(2) Strontium and neodymium isotope geochemistry and the degree of incompatible trace element enrichment (Sigmarsson *et al.*, 1992; Hardarson, 1993; Bunce, 2002) indicate that the Snæfellsnes source is similar to that of Jan Mayen, located 350 km north of Iceland (Trønnes

et al., 1999, Stuart *et al.*, *in prep.*). This presents the possibility that the enriched component is not confined to the Iceland plume and may be present in the shallow upper mantle.

(3) The peninsula provides a geographical transect along which to study variation in source and the degree or depth of partial melting with increasing proximity to the plume-head (and therefore, increasing temperature, decreasing lithospheric thickness and "availability" of plume-source components).

The principal research problems to be addressed in this chapter include: (i) constraining the trace element and He-Sr-Nd-Pb isotope composition of the enriched component(s) in the Snæfellsnes source and (ii) identifying the dominant controls on their distribution, e.g., partial melting processes. Previous studies have shown significant geochemical variation along the peninsula which has variably been interpreted to be a result of source-mixing (increasing dilution of an enriched component with depleted plume material nearer to the plume head), the manifestation of melting processes (preferential melting of more fusible material at greater depths in the melt column) or a combination of both (Sigmarsson *et al.*, 1992; Hardarson, 1993; Smit *et al.*, 1999; Kokfelt *at al.*, 2003; in press). The main objective is to expand on these hypotheses using a comprehensive multi-isotopic approach. The current published data set include major and trace element data, Sr and Nd isotopes, oxygen isotopes, Re-Os isotopes and U-Th disequilibria (Sigmarsson *et al.*, 1992; Smit *et al*; 1999; Kokfelt *et al.*, 2003, in press). However, previous studies have highlighted the importance of Pb isotopes and He isotopes in identifying source components in Iceland and other ocean islands (see Chapter 1).

2.2 Geology and tectonics of the Snæfellsnes Peninsula

2.2.1 Tertiary (>2.5 Ma)

The earliest rocks in the Snæfellsnes Peninsula are Tertiary basalts erupted in the Snæfellsnes-Skagi rift zone, which was active from at least 16 Ma to around 5.2 Ma (Sæmundsson , 1974; Johannesson, 1980; Kristjansson and Jóhannesson, 1999) (see Chapter 1). The position of the extinct rift zone is marked by a SW-NE-trending

synclinal structure extending across the western and central parts of the peninsula (Johannesson, 1982a) (Figure 2.1). Tertiary volcanic rocks are dominantly tholeiitic basalts of similar composition to basalts erupted in the present-day rift zones. Silicic and intermediate lavas are also found and are mainly associated with central volcanoes, the largest of which are the Setberg 1 and Ellidi volcanoes that formed towards the end of Tertiary activity in the rift zone (Sigurdsson, 1970, Johannesson, 1982a) (Figure 2.1). The eastward relocation of the rift zone around 5.2 Ma resulted in a significant reduction in volcanic activity, but around 2.5 Ma, volcanism was renewed in the now non-rifting flank zone and has continued into the Holocene.

Figure 2.1: Tertiary volcanic centres and location of the Snæfellsnes syncline on the Snæfellsnes Peninsula (after Johannesson, 1982)

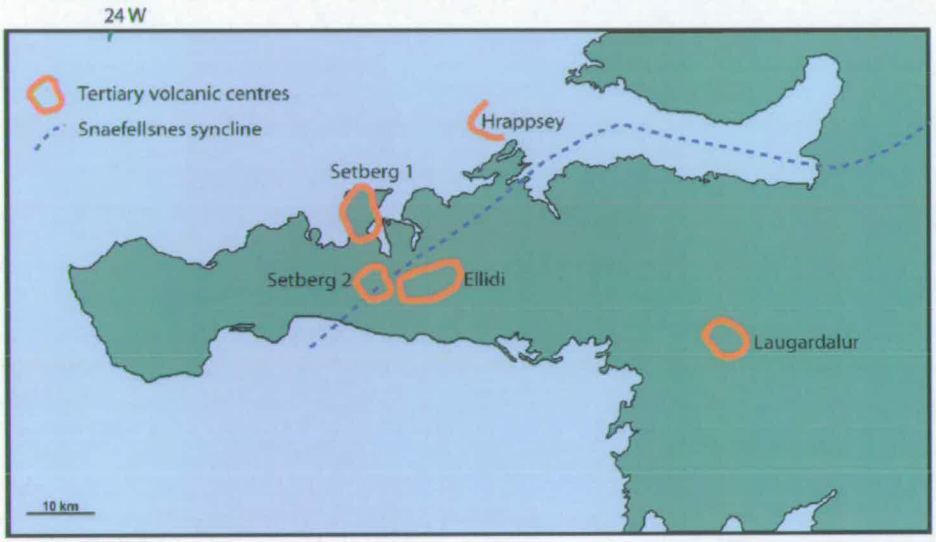

2.2.2 Plio-Pleistocene (2.5 Ma – 10 ka) and Recent formations (<10 ka)

The change from on-axis to off-axis volcanism is marked geochemically by a change from tholeiitic to alkaline basalt compositions and, as such, from depleted to increasingly enriched signatures (Hardarson, 1993; Bunce, 2002). The change in composition has been related to the an increase in depth of melting following the cessation of rifting, leaving enriched melts trapped at the base of the melting column (Bunce, 2002). The cause of the post-2.5 Ma volcanism and consequent tapping of enriched melts is uncertain and a number of possibilities have been considered. For

example, the build-up of stresses resulting from spreading along the new Northern and Western rift zones is thought to have resulted in the development of transcurrent faults and SE-trending en echelon cracks, through which melts can escape (e.g., Sigurdsson, 1970). Alternatively, Steinþórsson and Jacoby (1985) proposed that cooling of the crust, associated with the drift of the North American plate, would result in the development of cracks through which melts could escape. Jancin *et al* (1985) preferred the suggestion that the axes of old rift zones are simply sites of crustal weakness.

The start of the Quaternary period in Iceland is fixed by the Mammoth magnetic anomaly at 3.1 Ma, at which the first signs of the onset of the ice age in Iceland are found (Sæmundsson, 1980). The remains of around ten glaciations have been identified in Snæfellsnes (Jóhannesson, 1982a), and volcanic activity along the peninsula occurred from the onset of renewed volcanism around 2.5 Ma, throughout the glacial and interglacial periods and into the Holocene. Significant erosion took place at the end of Tertiary (up to 1000m of the Tertiary volcanic pile being removed), so the Quaternary lavas often lie unconformably on the Tertiary formations (Sigurdsson, 1970; Johannesson, 1982a). In addition, significant subsidence during the Early Pleistocene is indicated by the presence of submarine deposits covering the Tertiary volcanics in some localities, but this appears to have been followed by later uplift as the deposits are now found high above the present-day sea-level.

Quaternary volcanic rocks in Snæfellsnes (Figure 2.2) are divided into two main groups. The Plio-Pleistocene formations erupted during the glacial and interglacial periods (3.1 Ma – 10 ka), and Recent formations erupted after the retreat of the last ice-sheet (10 ka – present). Volcanic rocks erupted during glacial periods consist of hyaloclastite (often altered to palagonite), breccias, pillow lavas and columnar jointed basalts. In interglacial periods the eruptive units consist of thick basaltic lava flows, often separated from the subglacial formations by unconformities resulting from erosion. The postglacial volcanic rocks consist of mildly-alkaline basaltic flows, the most recent of which formed around 2 ka.

The Plio-Pleistocene and Recent volcanic rocks form a 120 km-long belt along the peninsula, from Grábrók in the east to the tip of the peninsula in the west. The

eruption sites have been grouped into three main volcanic systems, arranged en echelon within the W-E-trending belt. West to east, these are the Snæfellsjökull system, the Lýsuskarð system and the Ljósufjöll system (Jóhannesson, 1980) (Figure 2.2). The en echelon arrangement of the systems may be due to the accommodation of stresses in the Icelandic crust resulting from the initiation of spreading in the WRZ (Sigurdsson, 1970). Previous studies of Snæfellsnes Quaternary off-axis volcanism demonstrate that the Plio-Pleistocene and Recent formations are incompatible trace element enriched, typical of off-axis volcanism in the North Atlantic (Sigmarsson *et al* 1992; Hardarson, 1993; Bunce, 2002; Smit *et al*, 1999; 2002, Kokfelt *et al.*, *in press*). Regional variation points towards increasingly depleted compositions in an eastwards direction, corresponding to increasing degrees and decreasing depths of melting. However, volcanic productivity in the Quaternary increases in the opposite direction with the majority of postglacial volcanism associated with the Snæfellsjökull central volcano in westernmost Snæfellsnes (Figure 2.2). Furthermore, Sr and Nd isotopic data imply significant source-heterogeneity. Mantle upwelling rates have been shown to increase eastwards corresponding to the increased thermal gradient with proximity to the plume-head (Kokfelt *et al.*, 2003).

Figure 2.2: The distribution of postglacial lava flows along the Snæfellsnes Peninsula and the location of the three volcanic systems (based on Johansson, 1984)

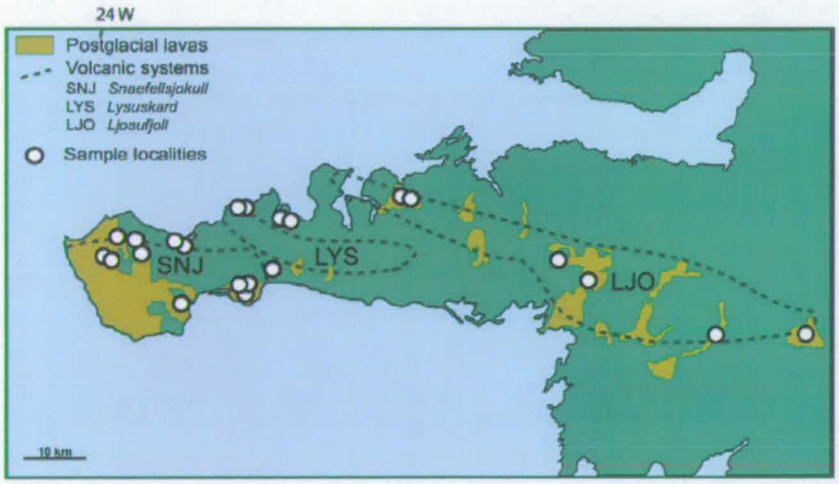

2.3 Sampling strategy

Samples were collected from each of the three Quaternary volcanic systems in order to span the entire peninsula. The use of helium isotopes imposes strict limitations on sampling material (for example, require olivine and pyroxene phenocrysts) and field settings (e.g. collecting from outcrops shielded from cosmic rays) (see Appendix 1). Suitable sampling localities were identified from the available literature. Localities in Snæfellsjökull were selected from the petrographic descriptions of Hardarson (1993). The availability of Quaternary samples from further east in the Peninsula, from the sample collection at the University of Edinburgh (Bunce, 2002) enabled a preliminary investigation into the regional variation in He-Sr-Nd-Pb isotope compositions. The recognition of regional geochemical variation prompted the collection of samples from the Ljósufjöll volcanic system in the east of the peninsula and samples were provided by Reidar Trønnes (Norvol, Iceland), Björn Hardarson (University of Edinburgh) and Kaj Hoernle (Geomar, Kiel). Sample locations and details are summarised in Figure 2.2 and Table 2.1, and petrological descriptions can be found in Appendix 1.2.

Table 2.1: Sample details

Volcanic system	Sample Name	Location	Approximate Age	Distance E of 24°W (km)
Snæfellsjökull	PSN1	NW of Kliffhraun	Glacial	17
	PSN7	Prestahraun	Glacial	4
	PSN8	E of Midhfell	Glacial	27
	PSN11	1 km E of PSN8	Post-glacial	30
	PSN13	SE of Olafsik	Post-glacial	15
	PSN14	Bekkjahraun	Post-glacial	2
	GSN9	Burfell	Glacial	8
	GSN11	N of Frodhurkotmuli	Glacial	21
	SNB40	Budahraun	Post-glacial	27.3
	SNS224	Budahraun	Post-glacial	27.3
	SNS219	Rauðholarhraun	Post-glacial	12.4
	SNS215	Sandhraun	Post-glacial	6.5
	SNS214	Olafsvikurenni	Post-glacial	12.2
Lýsuskarð	LB298	Myrarhyrna	c. 0.4 Ma[1]	31
	LB296	Myrarhyrna	c. 0.4 Ma[1]	31
	LB295	Myrarhyrna	c. 0.4 Ma[1]	31
	LB294	Myrarhyrna	c. 0.4 Ma[1]	31
	LB232	Bulandshöfdi	c. 1.2 Ma[1]	25
	LB231	Bulandshöfdi	1.2 Ma[1]	25
	LB230	Bulandshöfdi	1.2 Ma[1]	25
	LB229	Bulandshöfdi	c.1.2 Ma[1]	25

Ljósufjöll	IC7	Grabrokarhraun	< 3600 yrs[2]	120
	YS98-008	Horgsholtshraun	Post-glacial	60
	H105	?	Post-glacial	55.1
	SNS-211	Berserkjahraun	c. 4000[3,4]	51.5
	SNS-209	Berserkjahraun	c. 4000[3,4]	53.5
	SNS-206	Nykuhraun	Post-glacial	75.6
	SNS-201	Hraundalshraun	Post-glacial	101

[1] ^{40}Ar-^{39}Ar ages of Bunce (2002) for Bulandshöfdi (LB230, LB231) and Myrarhyrna (LB299)

[2] Schwarzbach and Munnich, (1956) in Hardarson (1993).

[3]Johannesson *et al*, (1981) in Hardarson (1993).

[4]Johannesson, (1982b) in Hardarson (1993).

2.4 Analytical Results

Major and trace element, and He, Sr, Nd, and Pb isotopic compositions were determined following the procedures detailed in Appendix 2. Major element concentrations for samples donated by R. Tronnes (prefixed SNS-) were determined at NORVOL and major and trace elements and radiogenic isotope ratios of the sample from K.Hoernle (H105) were determined at GEOMAR following procedures detailed in Kokfelt *et al* (*in press*). The results are tabulated in Tables 2.2 to 2.5 and in the following sections are examined and grouped according to volcanic system.

2.4.1 Major elements

Major element oxide concentration data are presented in Table 2.2. In Figure 2.3, a total alkali-silica (TAS) diagram, the narrow range of primitive compositions is demonstrated.

Figure 2.3: Plot of total alkalis *vs.* silica concentrations for basalts from Snæfellsjökull (blue circles), Lýsuskarð (red circles) and Ljósufjöll (green circles). The diagonal line marks the boundary between alkaline and subalkaline basalts, based on the divisions of Macdonald and Katsura, 1964.

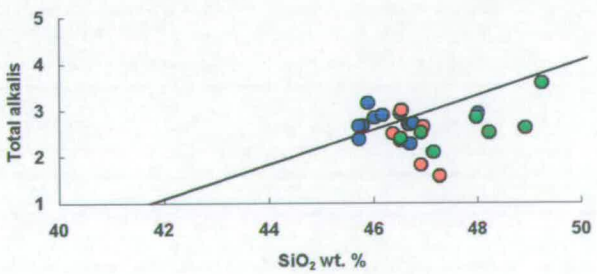

All samples are basalts (according to the nomenclature of Le Maitre, 1989) with the exception of two samples each from Snæfellsjökull and Lýsuskarð, which might be classified as picritic basalts. Using the divisions of Macdonald and Katsura (1964), the basalts from Snæfellsjökull are dominantly alkaline, whereas samples from Lýsuskarð and Ljósufjöll are mildly alkaline to tholeiitic.

The overall range in MgO is 8.5-14.7 wt%, and the range in Mg#, a function of MgO and $Fe_2O_3^t$, is 60-75. There is little variation in major oxide concentrations with MgO concentration. Only Al_2O_3, Na_2O and TiO_2 show slight correlation (Figure 2.4). Compositional differences between the three volcanic systems can be observed. Samples from Snæfellsjökull have lower Al_2O_3 and SiO_2, and higher TiO_2, MnO, Fe_2O_3 and P_2O_5 than samples from Ljósufjöll for any given MgO. With the exception of two samples with MgO concentrations greater than 12 wt. %, lavas from the Lýsuskarð system are generally similar to lavas from Snæfellsjökull (Figures 2.4, 2.5). Regional variation in major element compositions – notably, the enrichment of Snæfellsjökull and Lýsuskarð basalts in incompatible elements such as P_2O_5, and TiO_2 – is observed when major element oxide concentrations are plotted against sample locality (in distance (km) east along the peninsula) (Figure 2.6).

Table 2.2 Major element oxide concentrations of Snæfellsnes basalts

Sample	SiO_2 wt. %	TiO_2 wt. %	Al_2O_3 wt. %	Fe_2O_3 wt. %	MnO wt. %	MgO wt. %	CaO wt. %	Na_2O wt. %	K_2O wt. %	P_2O_5 wt. %	$Mg^{\#}$
Snaefellsjokull											
PSN1	46.01	2.75	14.97	12.27	0.19	9.06	11.06	2.37	0.47	0.86	61.92
PSN7	45.78	2.41	14.70	11.95	0.20	9.76	11.82	2.18	0.49	0.72	64.25
PSN8	46.50	2.13	14.86	11.68	0.19	9.02	12.68	2.04	0.31	0.60	62.95
PSN11	45.70	2.47	14.05	12.27	0.19	10.48	11.43	2.24	0.41	0.75	65.27
PSN13	45.88	2.66	13.47	12.86	0.22	10.16	10.70	2.46	0.70	0.87	63.49
PSN14	45.71	2.16	14.45	11.70	0.18	11.01	11.77	1.95	0.43	0.64	67.43
GSN9	46.69	2.01	14.48	10.95	0.18	10.95	11.75	1.97	0.30	0.71	68.76
GSN11	46.16	2.36	15.96	11.54	0.18	8.53	11.50	2.44	0.45	0.87	61.93
SNS214	48.01	2.47	13.31	10.76	0.19	11.46	10.61	2.11	0.83	0.25	67.68
SNS215	46.67	2.25	13.67	10.85	0.19	12.00	11.40	2.04	0.65	0.27	68.51
SNS219	46.75	2.34	14.39	10.99	0.19	10.70	11.55	2.06	0.65	0.37	65.69
SNS224	46.50	2.70	13.74	11.87	0.21	11.15	10.60	2.25	0.69	0.30	64.87
Lysuskard											
LB296	46.95	1.99	14.97	11.52	0.19	9.41	11.98	1.95	0.69	0.33	64.25
LB295	46.36	2.62	12.73	13.98	0.20	9.47	11.48	2.01	0.49	0.65	59.85
LB294	47.26	1.26	11.50	10.13	0.17	14.29	13.37	1.41	0.17	0.44	75.63
LB232	46.52	2.85	12.65	13.69	0.22	9.93	10.47	2.30	0.71	0.66	61.49
LB229	46.90	1.96	11.07	12.08	0.19	14.32	11.20	1.52	0.30	0.46	72.30

Sample	SiO_2	TiO_2	Al_2O_3	Fe_2O_3	MnO	MgO	CaO	Na_2O	K_2O	P_2O_5	$Mg^{\#}$
	wt. %	wt. %	wt. %	wt. %	wt. %	wt. %	wt. %	wt. %	wt. %	wt. %	
Ljosufjoll											
SNS201	48.92	1.56	15.28	10.44	0.18	9.38	11.54	2.24	0.38	0.08	63.86
SNS206	47.98	2.21	13.68	10.41	0.19	11.44	11.06	2.32	0.53	0.19	68.37
SNS209	48.23	1.68	12.14	9.76	0.18	14.71	10.65	1.88	0.64	0.14	74.77
SNS211	49.24	1.94	14.20	9.76	0.19	10.46	10.32	2.67	0.92	0.30	67.83
IC7	46.90	1.59	15.24	11.98	0.19	9.89	11.50	2.02	0.49	0.19	64.50
SNB130	46.51	1.52	13.96	11.36	0.19	11.97	11.90	2.11	0.29	0.20	69.86
H105	47.15	1.49	14.40	11.10	0.17	11.23	12.20	1.82	0.28	0.17	70.77

Note: All data corrected for loss on ignition. Range 0.62 to -0.41

Mg# = 100MgO/(MgO+FeO) (mol.); $FeO = 0.9Fe_2O_3{}^{t}$

Figure 2.4 Major oxide concentrations of Snæfellsnes basalts as a function of MgO. Symbols as in Figure 2.3

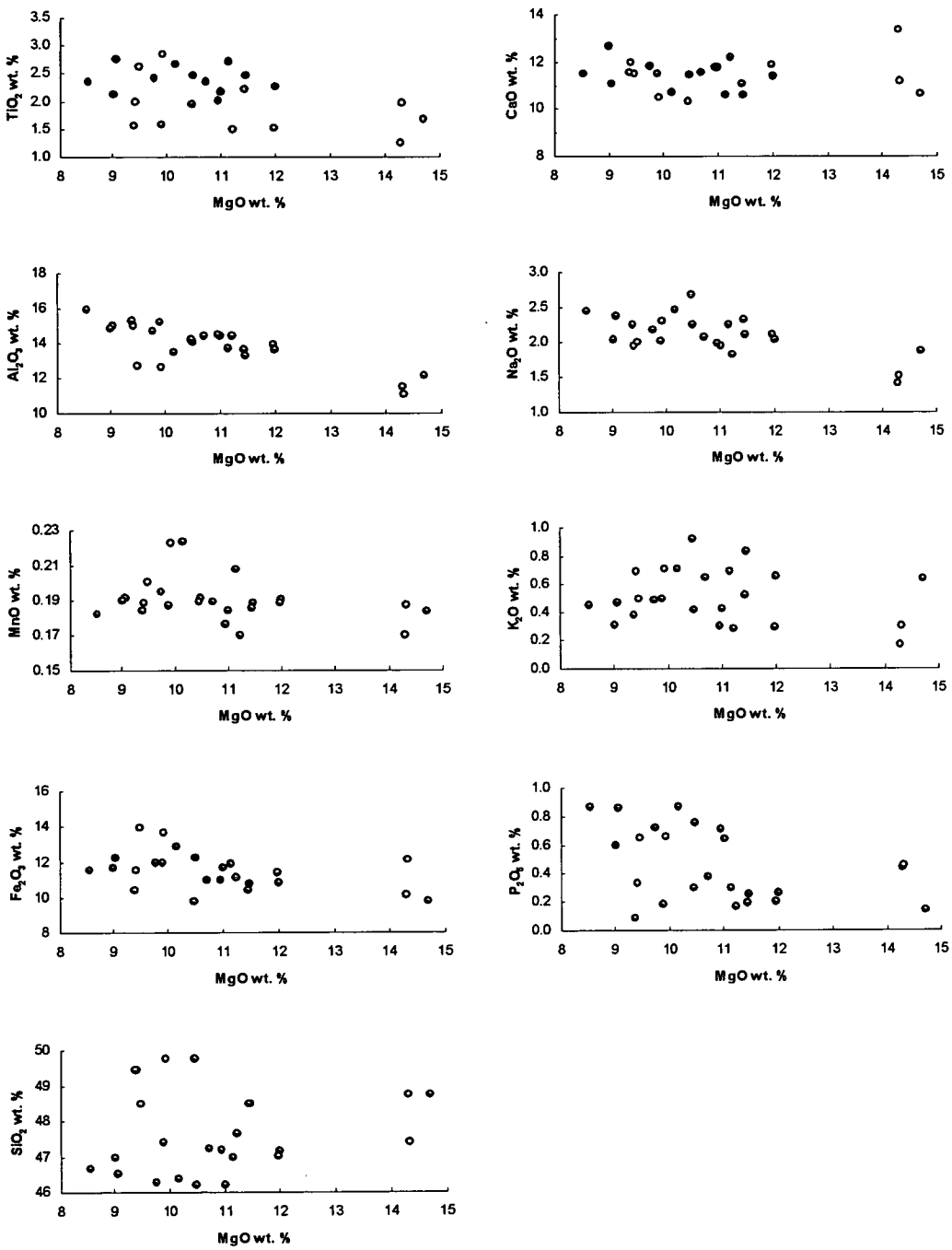

Figure 2.5 Major oxide ratios of Snæfellsnes basalts as a function of MgO. Symbols as in Figure 2.3

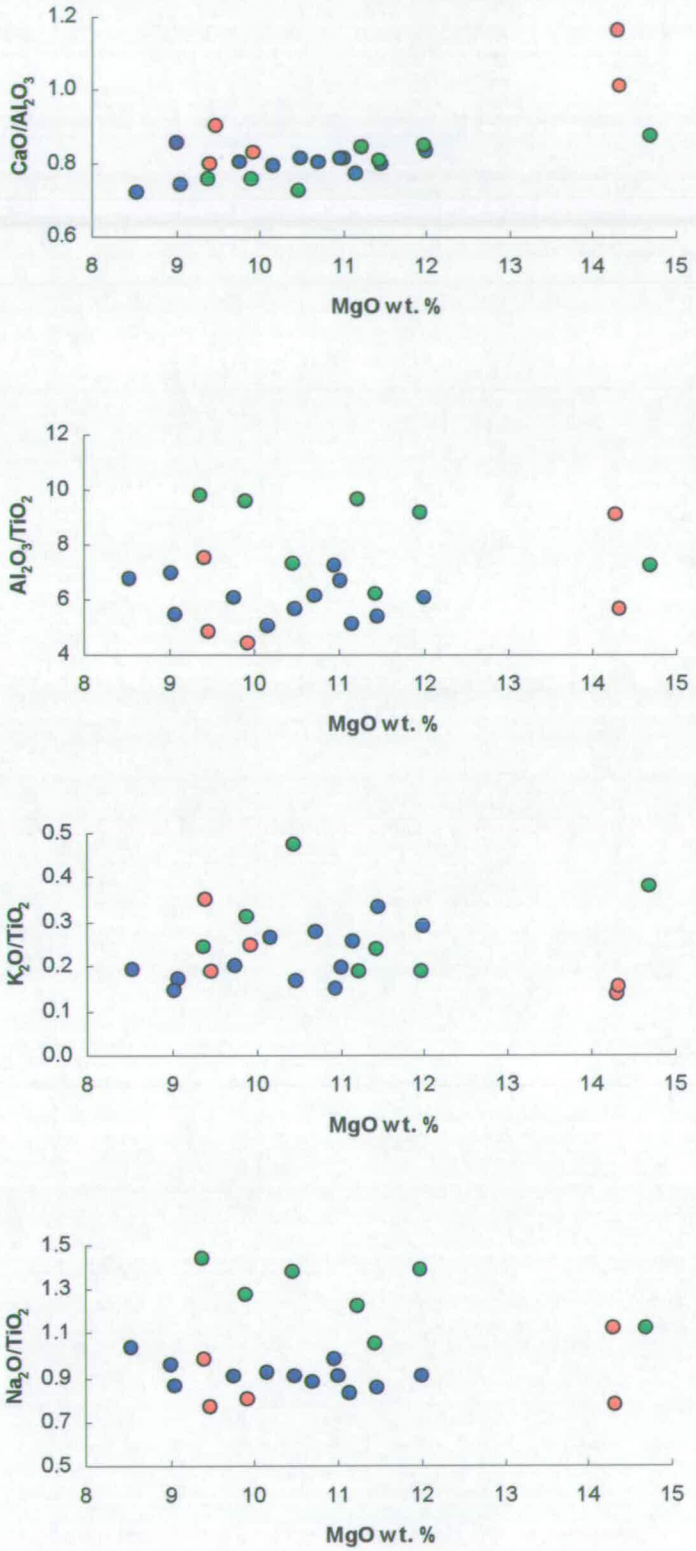

Figure 2.6 (a) Regional variation in major element oxide concentrations. Symbols as in Figure 2.3

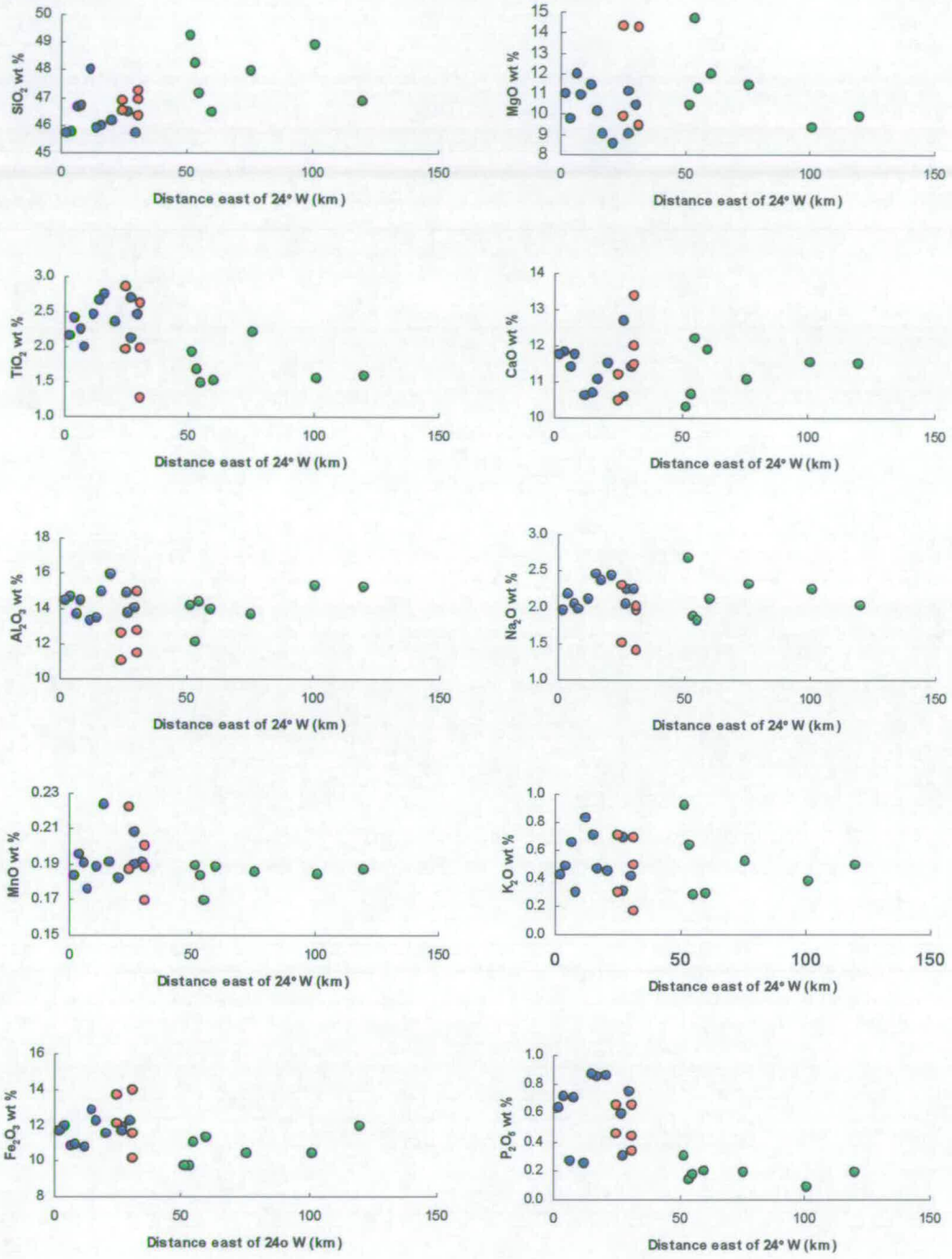

Figure 2.6 (b) Regional variation in major element oxide ratios. Symbols as in Figure 2.3

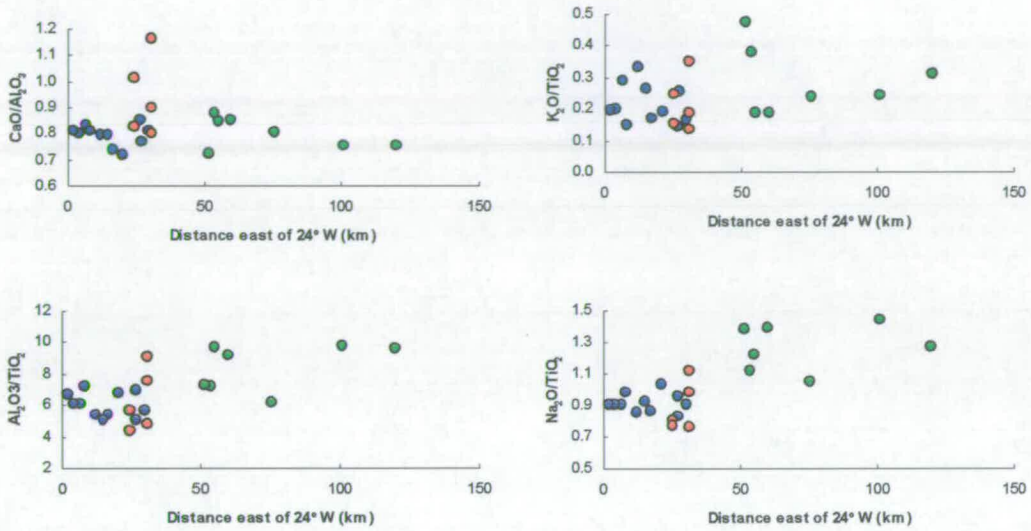

2.4.2 Trace elements

Trace element concentrations for each sample are presented in Table 2.3 and plotted against MgO in Figure 2.7. Correlations between MgO and the compatible trace elements (Ni, Sr, Cr and V) are observed, but correlations between MgO and the incompatible trace elements are not.

Basalts from Snæfellsjökull and Lýsuskarð are in general more enriched in the incompatible trace elements than basalts from Ljósufjöll. This is more clearly illustrated in Figure 2.8, in which primitive mantle (PM) normalized incompatible trace element abundances for all samples from Snæfellsnes are presented. All basalts exhibit enrichment in incompatible trace elements relative to PM. The Snæfellsjökull group are enriched relative to basalts from Lýsuskarð and Ljósufjöll. Moreover, basalts from the Snæfellsjökull and Lýsuskarð systems are, for the most part, more enriched in the very incompatible elements (VICE) and less enriched in the moderately incompatible elements (MICE) than basalts from Ljósufjöll. This is demonstrated by the steeper slope of the Snæfellsjökull group on the normalised incompatible element abundance diagrams. Y abundances are similar in

Snæfellsjökull and Ljósufjöll, but lower in Lýsuskarð. Likewise, Rb values are distinctly higher in Snæfellsjökull than Lýsuskarð, but Ljósufjöll values range from the highest Snæfellsjökull to the lowest Lýsuskarð values. These differences result in Ljósufjöll samples displaying flatter patterns in Figure 2.8. Finally, three Ljósufjöll basalts have distinctly low Ba abundances (SNS201, SNB130, H105) relative to the other Snæfellsnes samples.

Table 2.3: Trace element concentrations of Snaefellsnes basalts

Sample	Ba	Ce	Cr	La	Nb	Nd	Ni	Rb	Sr	V	Y	Zr
	ppm	ppm	ppm	ppm	ppm	ppm	ppm	ppm	ppm	ppm	ppm	ppm
Snæfellsjökull												
PSN1	302.0	56.5	444.5	24.5	43.7	30.2	159.8	20.7	578.6	350.4	23.7	160.7
PSN7	341.5	54.2	632.8	24.2	40.4	29.9	175.4	14.1	441.2	329.7	24.4	161.0
PSN8	233.0	42.3	398.4	19.5	32.0	23.7	127.3	11.5	409.4	344.8	21.0	122.0
PSN11	310.4	53.6	558.1	24.3	39.7	28.3	197.4	15.4	462.0	337.8	23.5	153.4
PSN13	374.0	68.7	505.0	30.8	49.9	37.3	179.3	20.5	492.6	282.9	28.5	164.1
PSN14	324.2	48.0	647.3	23.1	35.8	26.6	208.8	12.8	433.4	296.1	22.6	143.2
GSN9	272.0	46.8	856.0	23.1	36.3	25.8	294.6	13.9	475.2	327.2	19.1	126.7
GSN11	305.5	51.4	322.2	24.2	40.0	26.9	128.3	19.8	535.2	327.7	21.9	142.0
SNS214	324.7	55.2	719.0	26.2	46.0	28.3	218.3	20.7	496.0	321.2	22.7	168.3
SNS215	348.8	54.8	597.2	24.1	38.4	27.8	188.9	13.2	448.5	322.1	23.8	150.4
SNS219	348.1	57.6	576.5	24.3	41.3	29.0	175.3	13.5	455.3	324.8	24.5	159.6
SNS224	329.7	61.2	512.2	24.5	44.1	29.6	157.7	17.1	475.4	364.4	25.8	167.2
Lýsuskarð												
LB296	291.7	42.4	432.3	17.4	27.4	23.1	138.9	15.6	393.2	337.6	17.6	107.9
LB295	226.4	52.8	491.8	22.9	33.8	29.7	157.6	10.7	332.2	452.9	24.4	135.5
LB294	156.4	28.7	1154.0	12.9	18.1	17.6	316.8	8.4	259.1	279.4	12.4	77.4
LB232	213.3	56.2	538.8	23.5	34.0	30.9	166.8	8.3	427.3	330.7	22.4	119.7
LB229	154.0	37.6	1126.1	14.9	22.1	19.0	283.8	6.1	271.2	318.8	14.2	82.7
Ljósufjöll												
SNS201	105.3	26.1	298.8	10.5	15.1	14.9	140.1	8.0	255.4	270.8	23.2	93.4
SNS206	204.6	48.7	642.7	20.4	30.1	27.1	199.8	11.9	356.6	298.4	27.4	128.6
SNS209	231.7	45.9	1262.5	22.6	33.0	22.2	310.1	15.7	345.5	270.2	20.7	126.6
SNS211	293.2	58.1	731.1	26.0	43.2	28.9	194.9	20.7	428.9	252.8	25.6	168.6
IC7	146.0	32.5	299.0	12.2	20.2	18.1	146.0	10.6	280.9	326.0	22.7	102.3
SNB130	83.0	25.6	958.0	8.7	13.3	13.1	279.0	6.4	211.6	279.0	25.1	81.0
H105	103.0	n.d	751.0	14.0	15.0	n.d	197.0	9.0	206.0	276.0	26.0	81.0

Positive correlations are observed between different VICE/MICE (e.g., Ce/Y and Nb/Zr; Figure 2.9). The high VICE/MICE ends of the trends comprise basalts from Snæfellsjökull while the low VICE/MICE ends are defined by basalts from Ljósufjöll. Basalts from Lýsuskarð have similar Nb/Zr values to Snæfellsjökull, but are displaced to slightly higher Ce/Y.

Figure 2.7. Trace element concentrations (ppm) vs. MgO (wt. %)

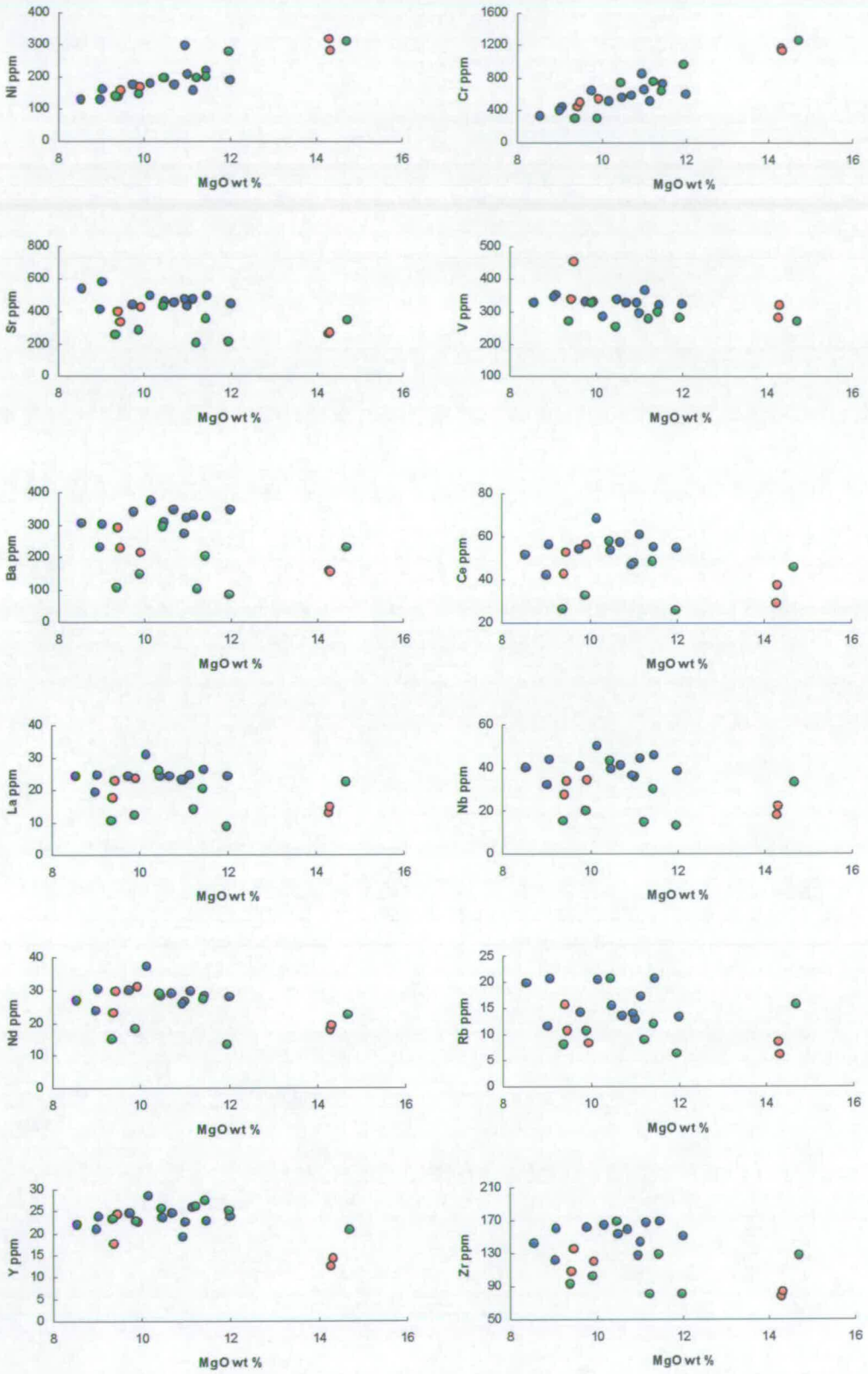

Figure 2.8: Incompatible trace element abundances of Snæfellsnes basalts normalized to primitive mantle values of Sun and McDonough (1989).

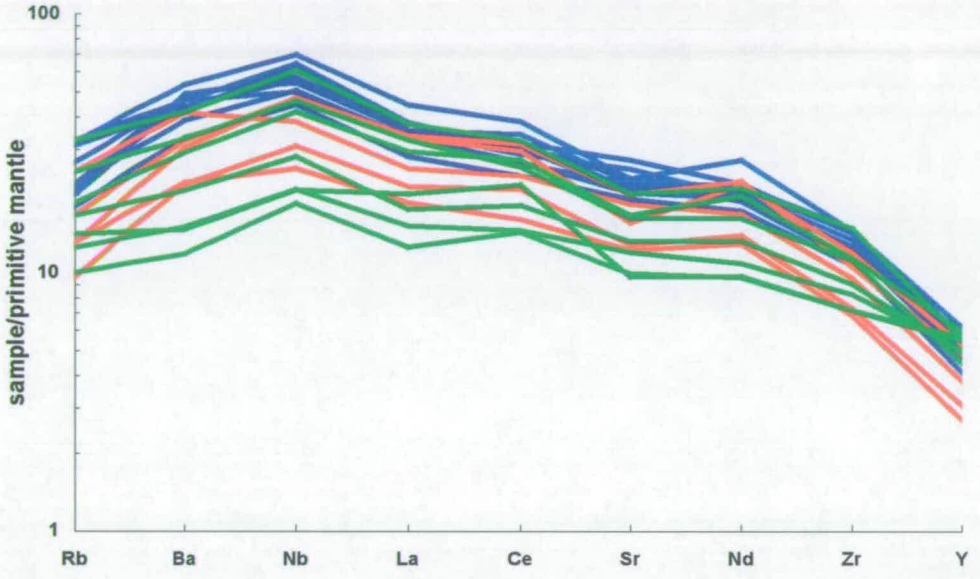

Figure 2.9: Ce/Y *vs.* Nb/Zr. Jan Mayen data from Stuart *et al.*, (*in prep.*). Average Icelandic basalt from Hardarson *et al.*, (1997).

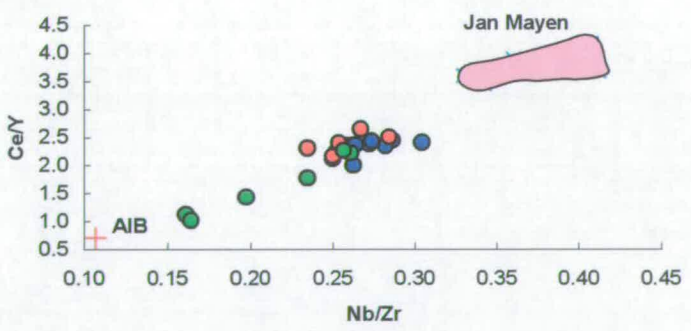

Regional variation in the degree of enrichment in incompatible trace elements is observed when VICE/MICE are plotted against sample location in km-east along the peninsula (Figure 2.10). Snæfellsjökull basalts are characterised by Nb/Zr > 0.25 and

Ce/Y > 2.0, which approach Jan Mayen compositions (Nb/Zr = 0.3 - 0.4; Ce/Y = 3.4 - 4.1; Stuart *et al.*, *in prep.*). Ljósufjöll compositions (Nb/Zr = 0.15 – 0.25; Ce/Y = 1.0 – 2.3) approach that of "average Icelandic basalt" (Nb/Zr = 0.1; Hardarson *et al.*, 1997).

Figure 2.10: Regional variation in VICE/MICE

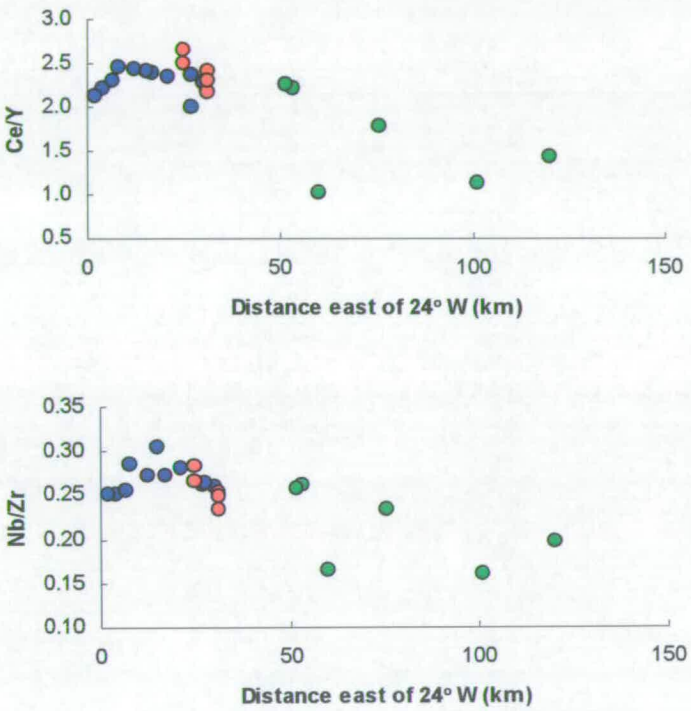

2.4.3 Helium isotopes

Helium isotope concentrations and ratios of olivine and pyroxene phenocrysts were determined following the procedures outlined in Appendix 2. Helium isotope data from crush analyses are presented in Table 2.4. Total He abundances released by *in vacuo* crushing range from 0.002×10^{-9} cc STP to 37.9×10^{-9} cc STP and $^3He/^4He$ range from 2.8 R_a to 11.6 R_a.

Table 2.4: Helium isotope data from crush extractions of He from olivine and pyroxene phenocrysts.

Volcanic system	Sample	Mineral	^4He 10^{-9} cc STP *	±	^4He blank %	^3He blank %	$^3He/^4He$ R_a §	±
Snæfellsjökull	**PSN1**	ol	9.32	0.03	2.31	0.70	**8.32**	**0.17**
		px	3.12	0.02	6.55	1.62	8.03	0.23
	PSN7	ol	9.14	0.01	2.34	0.55	**8.12**	**0.15**
		px	6.91	0.03	3.09	0.95	**8.55**	**0.18**
	PSN8	ol	16.4	0.02	1.32	0.31	**8.02**	**0.16**
		px	15.2	0.02	1.42	0.35	7.72	0.18
	PSN9	ol	0.79	0.004	21.84	7.74	*5.08*	*0.76*
		px	0.66	0.007	11.86	4.74	**6.47**	**0.37**
	PSN11	ol	6.48	0.03	3.28	1.05	**8.13**	**0.23**
		px	2.54	0.03	7.98	2.92	7.31	0.33
	PSN13	ol	4.49	0.02	4.67	1.56	**7.67**	**0.40**
		px	0.06	0.008	80.6	68.2	*5.09*	*8.71*
	PSN14	ol	5.40	0.009	5.01	1.20	**8.00**	**0.27**
		px	14.5	0.02	1.49	0.50	7.43	0.26
	GSN9	ol	8.31	0.02	2.58	0.86	**7.56**	**0.20**
		px	8.77	0.01	2.43	0.64	7.31	0.24
	GSN11	ol	5.89	0.02	3.58	0.91	**7.85**	**0.24**
		px	4.12	0.01	5.05	1.25	**8.13**	**0.17**
	SNB40	ol	2.09	0.01	12.0	3.75	6.48	0.53
		px	0.53	0.009	34.84	12.23	*9.81*	*1.67*
	SNS224	ol	8.55	0.007	0.13	0.30	**7.88**	**0.14**
		px	12.6	0.01	0.09	0.20	7.87	0.16
	SNS219	ol	6.36	0.008	0.27	0.36	**8.08**	**0.13**
	SNS215	ol	12.9	0.008	0.12	0.21	**8.29**	**0.09**
		px	12.3	0.01	0.09	0.21	7.79	0.08
	SNS214	ol	3.00	0.009	0.37	0.85	**7.88**	**0.24**

Volcanic system	Sample	Mineral	^{4}He 10^{-9} cc STP *	±	^{4}He blank %	^{3}He blank %	^{3}He/^{4}He R_a §	±
Lýsuskarð	**LB298**	ol	0.52	0.01	10.79	3.12	*6.96*	*1.04*
		ol	0.52	0.01	10.87	3.10	*7.08*	*0.77*
	LB296	ol	0.05	0.0001	0.31	0.17	**8.19**	**0.15**
	LB295	ol	4.71	0.009	5.71	1.27	**8.91**	**0.44**
		px	1.56	0.004	12.46	2.69	7.35	0.55
		px	0.82	0.01	7.19	2.13	*6.59*	*0.63*
		px	0.81	0.007	7.23	2.11	*6.71*	*0.33*
	LB294	ol	4.40	0.01	6.09	1.27	**9.30**	**0.27**
	LB232	ol	10.6	0.01	2.62	0.57	**8.60**	**0.33**
	LB231	ol	0.18	0.02	54.04	44.13	*2.81*	*1.59*
		px	1.17	0.02	29.06	11.66	*6.80*	*0.74*
	LB230	ol	0.002	0.0001	7.97	5.04	*8.73*	*1.63*
		px	0.31	0.02	41.96	19.66	*8.35*	*3.42*
	LB229	ol	5.52	0.02	3.84	1.24	**7.86**	**0.40**
		px	0.21	0.01	23.47	6.75	*7.86*	*1.47*
		px	0.20	0.008	24.22	6.75	*8.20*	*1.51*
Ljósufjöll	**IC7**	ol	37.9	0.03	0.05	0.04	**11.01**	**0.08**
	YS98-008	ol	17.8	0.009	0.21	0.13	**8.69**	**0.12**
		px	2.34	0.02	0.88	0.78	8.36	0.20
	H105	ol	11.3	0.03	0.18	0.16	**8.38**	**0.09**
		px	3.71	0.02	0.55	0.57	7.23	0.27
	SNS-211	ol	19.2	0.02	0.06	0.12	**8.51**	**0.07**
	SNS-209	ol	20.8	0.009	0.05	0.11	**8.53**	**0.08**
	SNS-206	ol	8.46	0.01	0.13	0.28	**8.49**	**0.12**
	SNS-201	ol	2.22	0.006	0.50	0.78	**11.61**	**0.30**

*Corrected for analytical blanks (Appendix 1) and atmospheric ^{4}He

§Bold type indicates values taken as representing the ^{3}He/^{4}He of the source. Italic type indicates ratios discarded on the basis of yielding [He] $< 1 \times 10^{-9}$ cc STP.

2.4.3.1 Effect of He abundance and blank corrections on ^{3}He/^{4}He

In Figure 2.11a, [He] extracted by crushing is plotted against ^{3}He/^{4}He. At [He] greater than 1×10^{-9} cc STP the range in ^{3}He/^{4}He is 6.9 – 11.6 R_a and the uncertainty in the measured ^{3}He/^{4}He is small (mean = 3.2 %, n = 38). In contrast, for [He] < 1 ×

10^{-9} cc STP, $^3He/^4He$ are more variable (2.88 – 10.70 R_a) and less reproducible and $^3He/^4He$ uncertainties are larger (mean = 22.6 %, n = 19) (Figure 2.11b).

The large uncertainty in $^3He/^4He$ of crush analyses yielding low [He] is due to larger blank corrections. $^3He/^4He$ values significantly decrease when blank corrections are greater than approximately 10% for ^3He and 20% for ^4He. The effect is larger for ^3He; a smaller % correction is required to reduce $^3He/^4He$ (Figure 2.12). Analyses that yielded less than 1×10^{-9} cc STP are considered to be imprecise and are excluded from the data-set examined below.

Figure 2.11 (a) Total He (cc STP) extracted by crushing olivine (squares) and pyroxene (circles) phenocrysts against $^3He/^4He$ (R/R_a). **(b)**: as (a) except Total He plotted on a log scale to emphasise variation in Total He < 1×10^{-9} cc STP.

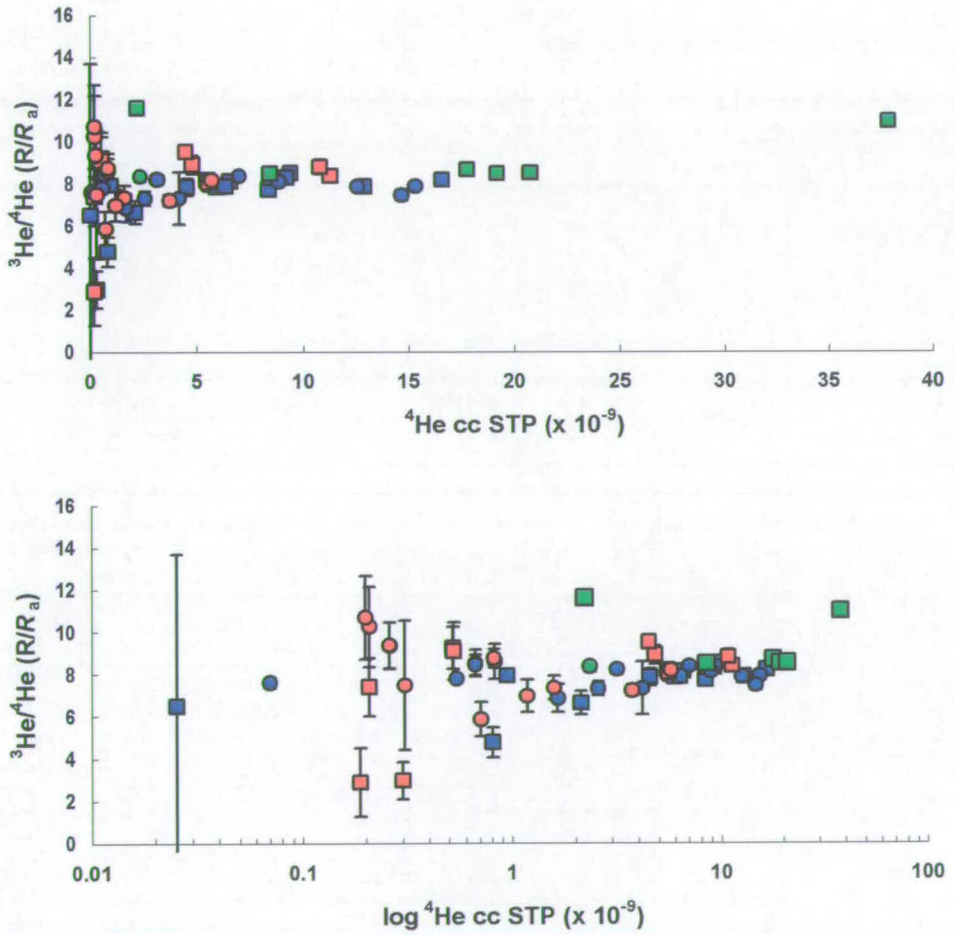

Figure 2.12: Plot of % blank correction against $^3He/^4He(R/R_a)$. Symbols as in Figure 2.13

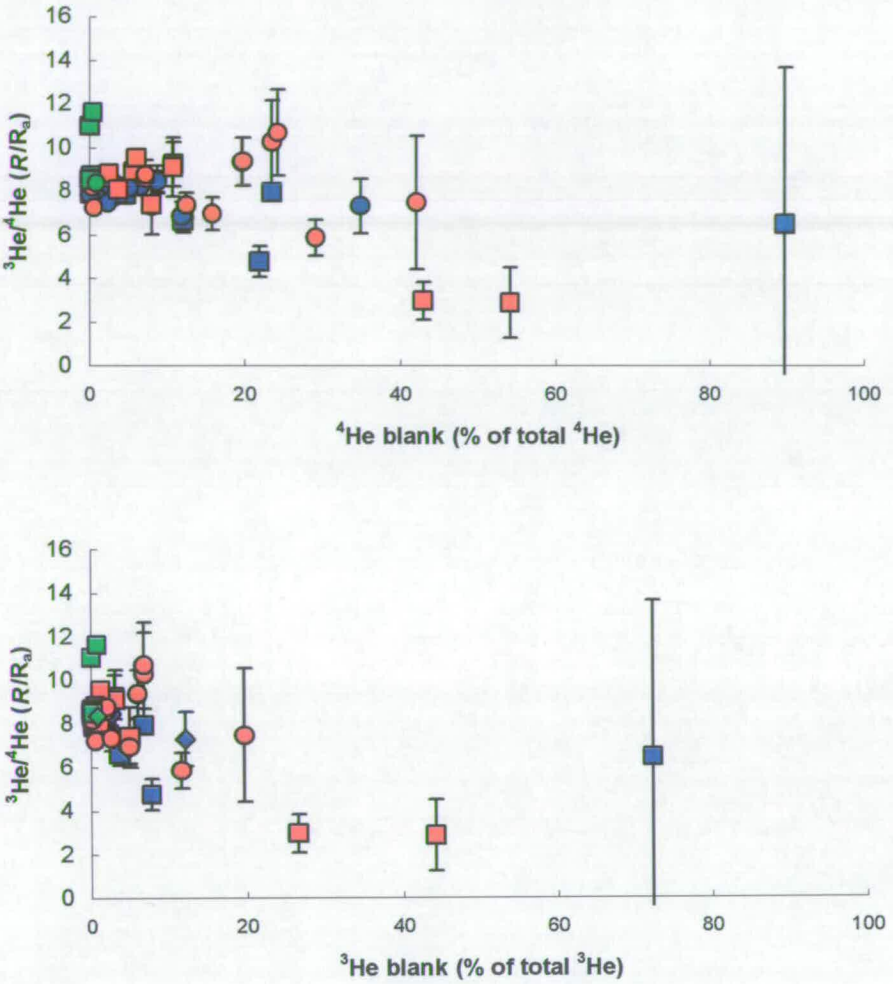

2.4.3.2 Variation in $^3He/^4He$ between olivine and pyroxene phenocrysts

The $^3He/^4He$ of olivines range from 7.7 to 11.6 R_a, and pyroxenes from 6.9 to 8.4 R_a. When cogenetic olivine and pyroxene (n=11) were analysed, the $^3He/^4He$ of olivines are equal to (within analytical uncertainty) the $^3He/^4He$ of co-existing pyroxenes in all except three samples (PSN11, LB295, H105) (Figure 2.13; Table 2.4). Lower $^3He/^4He$ of pyroxenes has been observed in previous studies of ocean island and island arc basalts (e.g., Marty *et al.*, 1994; Van Soest *et al.*, 2002; Martelli *et al.*, 2004) and can indicate post- or pre-eruptive addition of radiogenic ^4He to the pyroxene phenocrysts due to higher [U] and [Th] abundances and a higher diffusity of helium in pyroxenes (this is discussed in more detail in Section 2.5.2). In the

following discussions, the highest $^3He/^4He$ of any mineral pair (olivine in all except sample GSN11) is considered to best represent the $^3He/^4He$ of the mantle source.

Figure 2.13: Comparison of $^3He/^4He$ in co-existing olivines and pyroxenes. The diagonal line represents olivine-pyroxene equilibrium. Deviations of samples from the equiline show disequilibria.

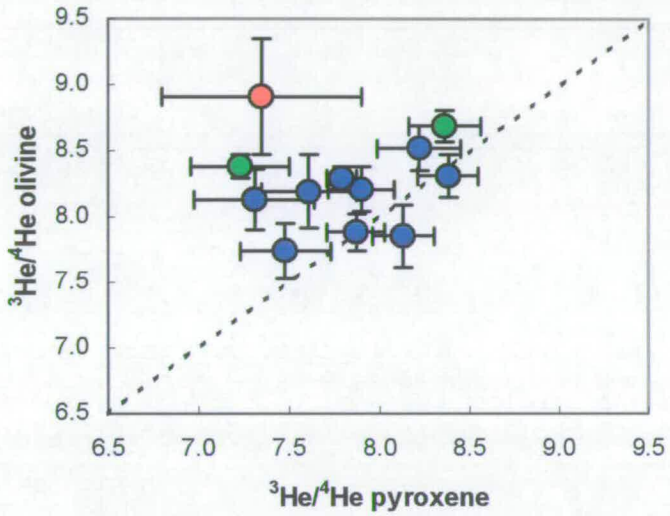

2.4.3.3 Regional variation in $^3He/^4He$

Samples from Snæfellsjökull have $^3He/^4He$ ranging from 6.9 - 8.5 R_a, which include the lowest $^3He/^4He$ on the Peninsula. Samples from Lýsuskarð range to higher $^3He/^4He$ (7.0 – 9.5 R_a). Samples from Ljósufjöll show the greatest range (7.2 – 11.6 R_a) and display the highest $^3He/^4He$ on the Peninsula (Table 2.4, Figure 2.11b). Previous $^3He/^4He$ measurements on phenocryst samples from Snæfellsjökull basalts have yielded 6.9 R_a (pyroxene) and 7.5 R_a (olivine) (Sigmarsson *et al.*, 1992).

In Figure 2.14(a) the olivine He-isotopic data for Snæfellsnes are plotted against distance east of 24° W. It is apparent that there is sharp increase in $^3He/^4He$ between 80 and 90 km-east. The samples from west of 100 km have He-isotope compositions within the range of MORB (8 ± 1 R_a) and higher than the He-isotope ratios of enriched basalts from Jan Mayen (5 - 6 R_a; Stuart *et al.*, *in prep.*). Samples east of 100 km have He-isotopic compositions at the lower end of the range recorded in olivines from the nearby Western Rift Zone (11-29 R_a: Skovgaard *et al*, 2001; Dixon

et al., 2000). In Figure 2.14(b) the samples from flows located west of 100-km-E are examined in more detail in order to identify smaller scale regional variation. Whilst basalts from Snæfellsjökull show a relatively restricted range of $^{3}He/^{4}He$, the Lýsuskarð basalts display local variation. Two trends appear to diverge from the low $^{3}He/^{4}He$ basalts of Snæfellsjökull. Whereas samples from western Ljósufjöll (~100 km E) have $^{3}He/^{4}He$ similar to Snæfellsjökull, the $^{3}He/^{4}He$ of samples from Lýsuskarð are distinctly higher.

Figure 2.14 (a) Variation in $^{3}He/^{4}He$ of olivines with distance east (0-150 km) along the Peninsula. **(b)** as (a) except enlarged to show variation between 0 and 80 km east.

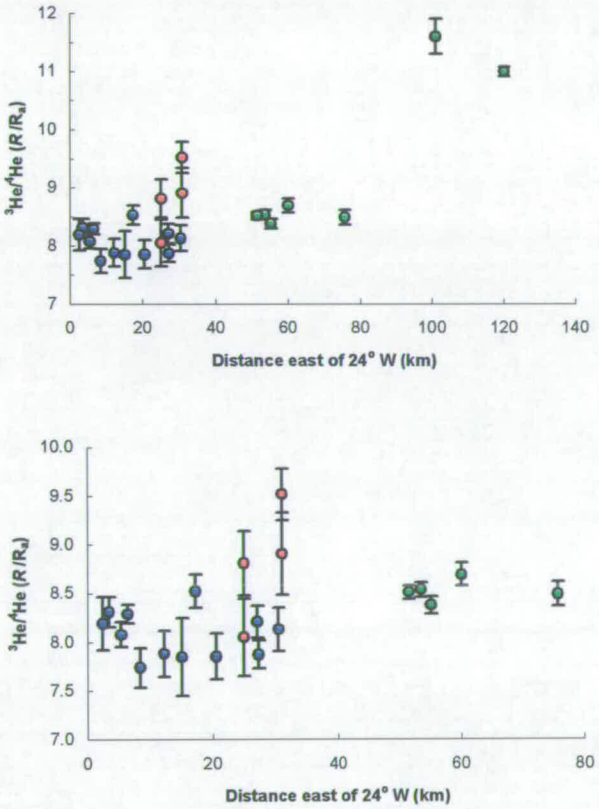

2.4.4 Sr-Nd-Pb isotopes

Strontium and neodymium isotope data for all samples for which $^{3}He/^{4}He$ were measured are presented in Table 2.5. $^{87}Sr/^{86}Sr$ ranges from 0.703230 (IC7) to 0.703537 (GSN9) and $^{143}Nd/^{144}Nd$ ranges from 0.51292 (LB229) to 0.51303 (GSN9). These are in agreement with measurements previously recorded for

Quaternary Snæfellsnes basalts (Sigmarsson *et al.*, 1992; Hardarson, 1993; Hémond *et al.*, 1993) but extend to more radiogenic $^{87}Sr/^{86}Sr$ and less radiogenic $^{143}Nd/^{144}Nd$.

Table 2.5: Sr, Nd and Pb isotope compositions of Snæfellsnes basalts

Sample	$^{87}Sr/^{86}Sr$	$^{143}Nd/^{144}Nd$	$^{206}Pb/^{204}Pb$	$^{207}Pb/^{204}Pb$	$^{208}Pb/^{204}Pb$	Δ7/4	Δ8/4
PSN1	0.703484	0.512972	18.85	15.54	38.56	0.4	13.5
PSN7	0.703403	0.513001	-	-	-	-	-
PSN8	0.703396	0.512954	-	-	-	-	-
PSN11	0.703381	0.512958	18.90	15.53	38.56	-1.2	8.5
PSN13	0.703403	0.512946		-	-	-	-
PSN14	0.703376	0.512987	18.84	15.52	38.48	-1.3	7.8
GSN9	0.703539	0.513025	18.92	15.51	38.54	-2.8	4.0
GSN11	0.703429	0.512971	-	-	-	-	-
SNS214	0.703457	0.512962	-	-	-	-	-
SNS215	0.703395	0.512956	-	-	-	-	-
SNS219	0.703387	0.512967	-	-	-	-	-
SNS224	0.703383	0.512974	18.84	15.51	38.48	-2.1	7.0
LB295	0.703411	0.512926	-	-	-	-	-
LB294	0.703420	0.512927	-	-	-	-	-
LB232	0.703381	0.512946	-	-	-	-	-
LB229	0.703442	0.512919	-	-	-	-	-
SNS201	0.703266	0.512973	-	-	-	-	-
SNS206	0.703361	0.512936	-	-	-	-	-
SNS209	0.703358	0.512963	-	-	-	-	-
SNS211	0.703384	0.512934	18.86	15.52	38.47	-1.5	3.9
IC7	0.703230	0.512960	18.80	15.49	38.34	-2.3	0.5
SNB130	0.703314	0.512944	18.82	15.51	38.39	-3.5	-1.3
H105	0.703391	0.512934	-	-	-	-	-

Mean % standard errors: $^{87}Sr/^{86}Sr = 0.0013$; $^{143}Nd/^{144}Nd = 0.0006$; $^{206}Pb/^{204}Pb = 0.0111$; $^{207}Pb/^{204}Pb = 0.0109$; $^{208}Pb/^{204}Pb = 0.0346$

In Sr-Nd isotope space, (Figure 2.15), the Snæfellsnes basalts form a cluster and there appears to be little correlation between the two isotope ratios (although, two extreme samples, IC7 and GSN9, may hint at a positive correlation). Comparing each of the three volcanic systems, samples from Ljósufjöll are characterised by the least-radiogenic $^{87}Sr/^{86}Sr$ and $^{143}Nd/^{144}Nd$ and samples from Snæfellsjökull the most-radiogenic ratios. Within the Lýsuskarð system a strong negative correlation is observed ($r^2 = 0.92$) and within Ljósufjöll there is a weaker negative correlation ($r^2 = 0.59$). No correlation is observed within the Snæfellsjökull system.

Regional variations in the Sr and Nd compositions of Snæfellsnes basalts are examined in Figure 2.16. $^{87}Sr/^{86}Sr$ decreases eastwards and towards the active rift

zones, from compositions comparable to those recorded in basalts from Jan Mayen (0.70338 – 0.70351; Stuart *et al.*, unpubl. data) to compositions within the upper-limit of the range of those recorded in lavas in the Western Rift Zone (0.70292 - 0.70343; Thirlwall *et al.*, 2004; Gee *et al.*, 1998). A regional trend for $^{143}Nd/^{144}Nd$ is less well-defined but appears to decrease eastwards through Snæfellsjökull and Lýsuskarð before increasing less steeply through the Ljósufjöll system. $^{143}Nd/^{144}Nd$ compositions approach Jan Mayen compositions (0.51284-0.51291) in eastern Snæfellsnes, and are comparable to WRZ compositions (0.51301-0.51316) in western Snæfellsnes (Figure 2.16). LB294 and LB229 from Lýsuskarð have anomalously low $^{143}Nd/^{144}Nd$, and SNS201 from Ljósufjöll has high $^{143}Nd/^{144}Nd$.

Pb isotope ratios of a subset of the Snæfellsnes samples are presented in Table 2.5 and Figure 2.17. $^{206}Pb/^{204}Pb$ range from 18.80 to 18.92, $^{207}Pb/^{204}Pb$ from 15.51 to 15.54 and $^{208}Pb/^{204}Pb$ from 38.34 to 38.56. Snæfellsnes basalts are all characterised by negative Δ7/4 (-3.5 to -0.4) and positive Δ8/4 (0.5 to 13.5). $^{206}Pb/^{204}Pb$, $^{207}Pb/^{204}Pb$ and $^{208}Pb/^{204}Pb$ all decrease with distance along the peninsula (Figure 2.18). Of note, GSN9, which has the most radiogenic Nd and Sr isotope ratios, is also characterised by the most radiogenic Pb isotope ratios. A positive correlation between $^{206}Pb/^{204}Pb$ and $^{87}Sr/^{86}Sr$ is observed but there is no correlation between $^{206}Pb/^{204}Pb$ and $^{143}Nd/^{144}Nd$ (Figure 2.19).

Figure 2.15 $^{87}Sr/^{86}Sr$ *vs.* $^{143}Nd/^{144}Nd$

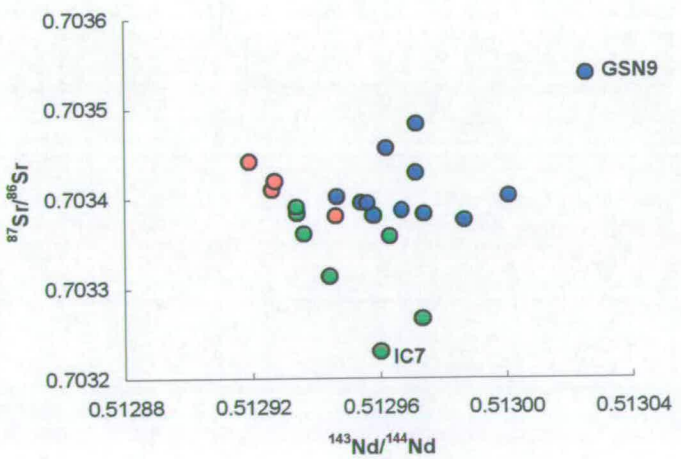

Figure 2.16: Regional variations in (a) $^{87}Sr/^{86}Sr$ and (b) $^{143}Nd/^{144}Nd$. Also marked are ranges for Jan Mayen (pink box; data from Stuart *et al.*, in prep.) and the WRZ (blue box; data from Thirlwall *et al.*, 2004 and Gee *et al.*, 1998)

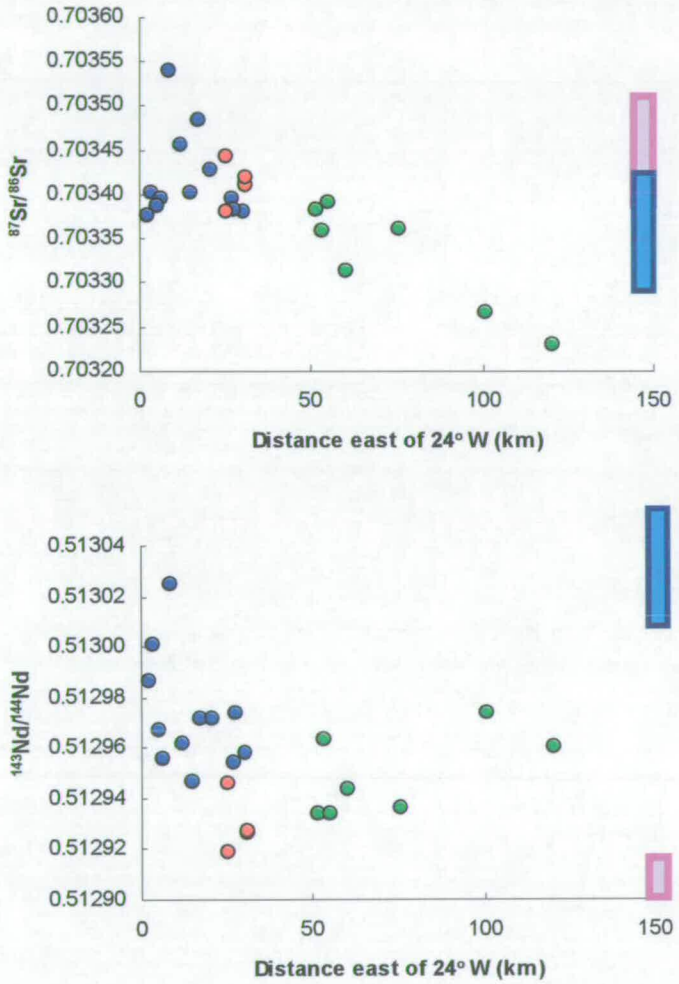

Figure 2.17 (a) $^{206}Pb/^{204}Pb$ *vs.* $^{207}Pb/^{204}Pb$ **(b)** $^{206}Pb/^{204}Pb$ *vs.* $^{208}Pb/^{204}Pb$. Solid line marks the NHRL of Hart (1984).

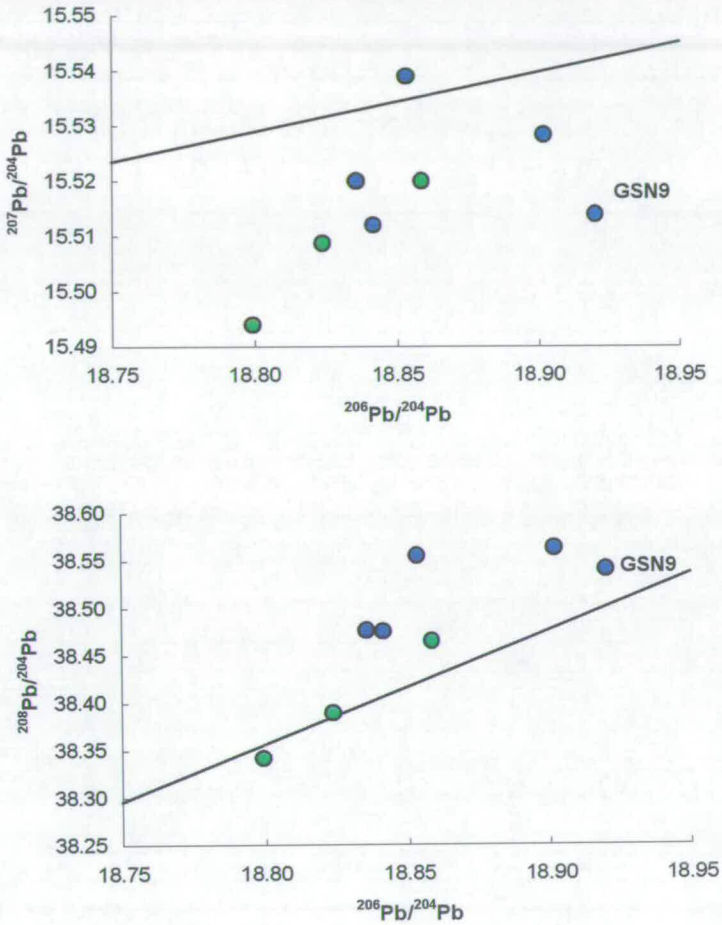

Figure 2.18: Regional variations in (a) $^{206}Pb/^{204}Pb$; (b) $^{207}Pb/^{204}Pb$ and (c) $^{208}Pb/^{204}Pb$

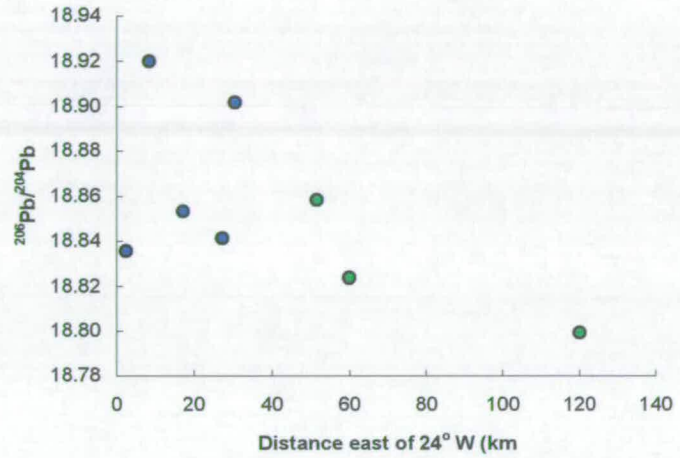

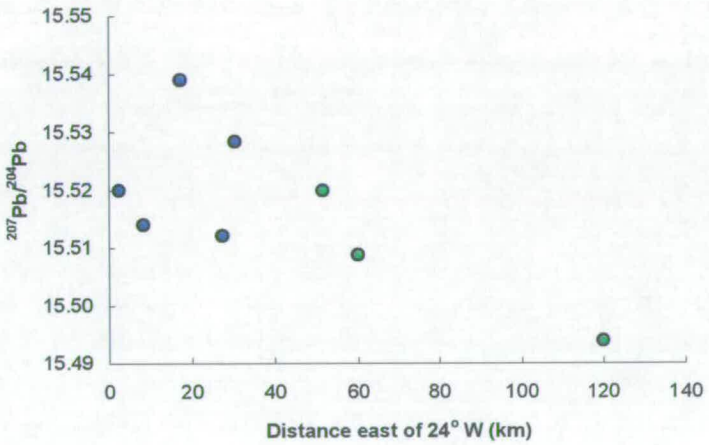

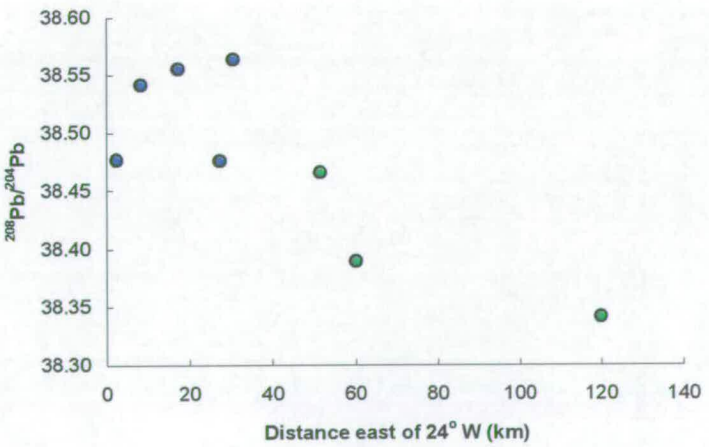

Figure 2.19 $^{206}Pb/^{204}Pb$ *vs.* (a) $^{87}Sr/^{86}Sr$ and (b) $^{143}Nd/^{144}Nd$

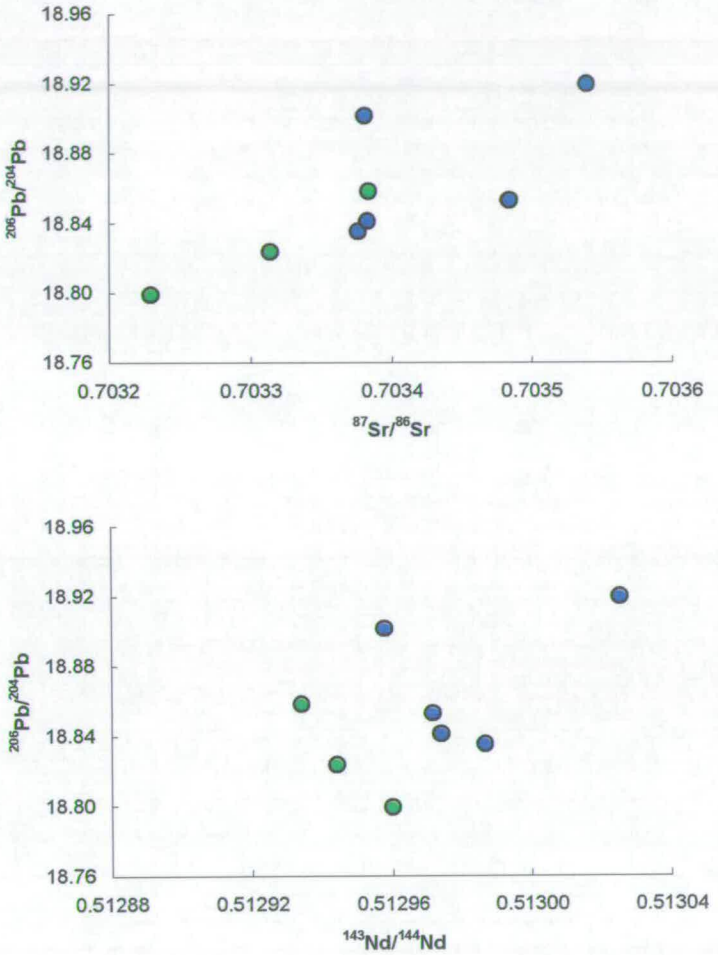

2.5 Discussion

2.5.1 Introduction

The results demonstrate regional variation in geochemistry along the Snæfellsnes Peninsula. Progressive east to west enrichment in incompatible elements may reflect variation in the extent and depth of partial melting; however, it could also reflect enrichment in the source. East-west source heterogeneity is inferred from $^{3}He/^{4}He$ and $^{87}Sr/^{86}Sr$, and to a lesser extent Nd and Pb isotope ratios. The simplest

interpretation is that the mantle beneath Snæfellsnes contains westward-increasing amounts of enriched material, which is also characterised by high $^{87}Sr/^{86}Sr$ and low $^{3}He/^{4}He$. However, if incompatible element enrichment is largely a consequence of partial melting, then this implies that melting conditions determine the proportion of enriched material that is sampled. Before examining the respective roles of melting processes and source heterogeneity in more detail, it is necessary to consider alternative explanations for the apparent geochemical variations.

2.5.2 Integrity of He isotope data

The crushing method employed at SUERC is capable of extracting magmatic He from olivines as old as 61 Ma, including the highest terrestrial $^{3}He/^{4}He$ measured to date (Stuart *et al.*, 2003). However, a number of pre-eruptive and post-eruptive processes may modify $^{3}He/^{4}He$ (e.g., Kurz, 1986a,b; Marty *et al.*, 1994; Hilton *et al.*, 1995; Van Soest *et al.*, 2002). The minor variation in the helium isotopic compositions of co-existing olivine and pyroxene phenocrysts, and variation between samples from the same volcanic systems, might be a result of such processes. Before discussing the helium isotope results in the context of mantle source characterisation it is necessary to examine these processes and to ensure that the phenocryst $^{3}He/^{4}He$ accurately reflect the time-integrated $^{3}He/(U + Th)$ history of the mantle source.

2.5.2.1 Ingrowth of radiogenic ^{4}He in phenocrysts

The $^{3}He/^{4}He$ of phenocrysts may be lowered by the ingrowth of ^{4}He from the decay of U and Th, either in the magma chamber or after eruption. The *in vacuo* crushing procedure adopted for this study is designed to release only magmatic He contained within fluid or melt inclusions without extracting lattice-hosted radiogenic ^{4}He (Kurz, 1986). Previous experiments using the crushing apparatus at SUERC have demonstrated that lattice-hosted radiogenic ^{4}He is not released by crushing phenocrysts from Tertiary basalts (Stuart *et al.*, 2000; 2003). Most of the samples analysed in this study have post-glacial eruption ages (though the five samples from Lýsuskarð are significantly older than 10,000 yrs) which should rule out significant modification of the $^{3}He/^{4}He$ by post-eruptive processes.

U and Th concentrations in phenocrysts can be estimated from whole-rock concentrations and mineral-melt distribution coefficients. Quaternary Snæfellsnes basalts, which include samples used in this study, have maximum whole-rock U and Th concentrations of 1.3 and 3.9 ppm respectively (analysed by ICP-MS, by T. Kokfelt and T.S. Johansen (Geomar, Kiel)). Assuming maximum eruption ages of 2 Ma for samples LB296, 295, 294, 232 and 229, and 20 ka for all other samples, radiogenic decay produces 1.9×10^{-13} to 1.9×10^{-11} cc ^{4}He STP/g in olivines, and 7.3×10^{-11} to 7.3×10^{-9} cc ^{4}He STP/g in clinopyroxenes (Table 2.6). Even if all the ingrown radiogenic ^{4}He in phenocrysts were released by crushing it would not significantly affect olivine or pyroxene ^{3}He/^{4}He.

Table 2.6 Production of radiogenic ^{4}He in olivines and pyroxenes.

Mineral	K_D U	K_D Th	[U] ppb	[Th] ppb	P^4He_{rad} cc STP/g/a^{-1}	^{4}He cc STP/g 20 kyrs	^{4}He cc STP/g 2 myrs
Olivine	0.00002	0.000052	0.03	0.2	9.3×10^{-18}	1.9×10^{-13}	1.9×10^{-11}
Pyroxene	0.013	0.014	17	55	3.6×10^{-15}	7.3×10^{-11}	7.3×10^{-9}

Mineral-melt distribution coefficients from Rollinson (1993). Radiogenic ^{4}He production rate (P^4He_{rad}) from Andrews (1989).

Prior to eruption, magmas may incorporate crustal He in the magma chamber (e.g., Hilton *et al.*, 1993, 1995). Such processes are often invoked to explain ^{3}He/^{4}He disequilibria between olivines and pyroxenes. The diffusity of He is around an order of magnitude greater in pyroxenes than in olivines at magmatic temperatures (Trull and Kurz, 1983), and consequently, pyroxenes are more likely to incorporate any crustal He from the magma (Hilton *et al.*, 1993; Marty *et al.*, 1994; Hilton *et al.*, 1995; Hilton *et al.*, 2000b). Additionally, pyroxene crystallises at lower temperatures than olivine and is therefore more likely to trap melt inclusions with modified ^{3}He/^{4}He. The near equilibrium (within analytical uncertainty) recorded in the Snæfellsnes olivine and pyroxene pairs suggests that pre-eruptive modification of ^{3}He/^{4}He has been negligible. Furthermore, the short magma-chamber residence times in Snæfellsnes (Sigmarsson *et al.*, 1992) make it unlikely that ingrowth of radiogenic

^{4}He in the magma chamber would be sufficient to have reduced phenocryst ^{3}He/^{4}He from Iceland-plume-like ^{3}He/^{4}He (50 R_a; Stuart *et al.*, 2003) to the measured values (8.0 – 11.6 R_a). If phenocrysts have in-grown ^{4}He during residence in a magma chamber there may be a relationship between ^{3}He/^{4}He and Mg#, the most primitive basalts having the highest ^{3}He/^{4}He (Gasparon *et al.*, 1994). However, there is no positive correlation between whole-rock Mg# and phenocryst ^{3}He/^{4}He, which suggests that radiogenic ^{4}He ingrowth is unrelated to fractional crystallisation in a magma chamber (Figure 2.20).

Figure 2.20: ^{3}He/^{4}He *vs.* Mg# of Snæfellsnes basalts. For samples where both olivine and pyroxene ^{3}He/^{4}He measurements are available, the highest value (usually olivine) is used.

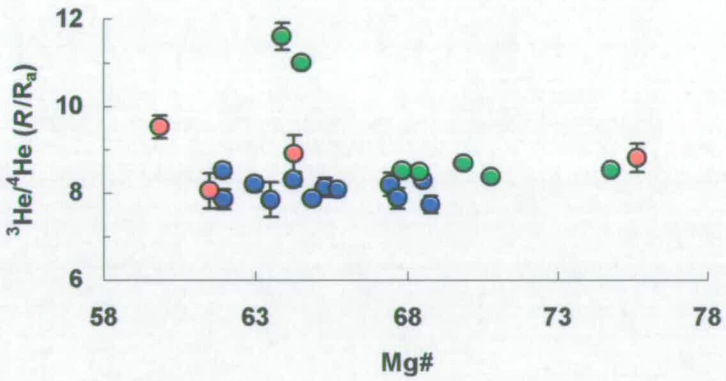

2.5.2.2 Post-eruptive production of cosmogenic ^{3}He

Cosmogenic ^{3}He is produced in the crystal lattice of ferromagnesian minerals from exposure to cosmic-rays and production is greatest at high-latitudes and altitudes (e.g., Kurz, 1986a, b; Craig and Poreda, 1986; Marti and Craig, 1987; Lal, 1988, 1991; Porcelli *et a.l*, 1986). While an effort was made to collect samples from outcrops shielded from cosmic-rays (see Appendix 1.1), it is possible that some samples have accumulated cosmogenic ^{3}He, and that as a result their ^{3}He/^{4}He are higher than that of the mantle source. Though cosmogenic ^{3}He is unlikely to have been released through crushing at SUERC (e.g., Williams *et al.*, 2005), modification of ^{3}He/^{4}He by cosmogenic ^{3}He accumulation could explain the higher helium isotopic compositions of samples LB294, and IC7 and SNS201, relative to other samples from the Lýsuskarð and Ljósufjöll systems respectively. Because the ^{3}He/^{4}He of cosmogenic He is so high, as it is dominated by ^{3}He, a negative

relationship between $^3He/^4He$ and ^4He concentration would be observed if a significant contribution of cosmogenic ^3He was released by crushing each sample. The absence of this correlation indicates that there has been no significant amount of cosmogenic ^3He released (Figure 2.21). In particular, the $^3He/^4He$ of $SNS201_{olivine}$ and $IC7_{olivine}$ are similar (11.01 ± 0.08 and 11.61 ± 0.30 R_a, respectively) despite the large difference in their ^4He concentrations.

To test for the effects of cosmogenic ^3He further the powders remaining from crushing sample $SNS201_{olivine}$ were melted in order to extract any lattice-hosted helium (Table 2.7).

Figure 2.21: $^3He/^4He$ against ^4He measured by crush extraction of He from olivines

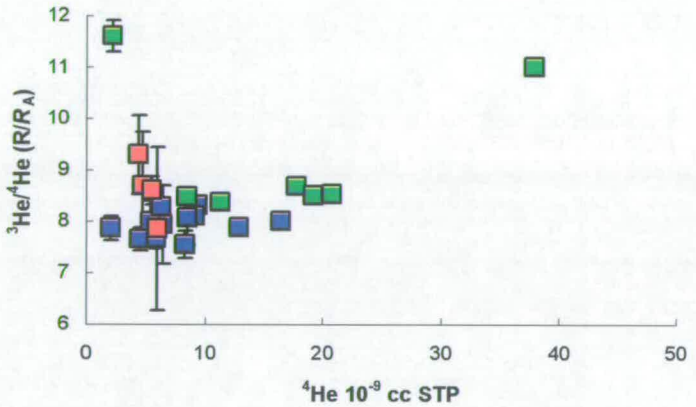

Table 2.7 Helium isotope data for furnace and crush extractions of helium from $SNS201_{olivine}$.

Sample	Extraction	^4He 10^{-10} cc STP g	^3He 10^{-15} cc STP g	$^3He/^4He$ R/R_a
SNS201	Melt - 900° C	1.32 ± 0.06	1.25 ± 0.23	7.37 ± 1.28
	Melt - 1600° C	0.69 ± 0.06	0.34 ± 0.09	3.54 ± 0.96
SNS201	Crush	22.17 ± 0.06	35.82 ± 0.93	11.61 ± 0.30

The low ^3He concentration and low $^3He/^4He$ released by melting powders of $SNS201_{olivine}$ ($^3He_{melt}$ and $^3He/^4He_{melt}$ respectively) confirms that cosmogenic ^3He production has been negligible in this sample. $^3He_{melt}$ is only ~ 5% of the ^3He extracted by crushing and most likely originates from magmatic He in inclusions that were not ruptured during the crushing procedure. In conclusion, the crushing

procedure is unlikely to have released any cosmogenic ^{3}He which could have modified the ^{3}He/^{4}He of olivines.

2.5.3 Crustal contamination

The assimilation of partial melts from the underlying young (<15 Myr) Icelandic oceanic crust would have a significant effect on both the isotopic and elemental compositions of the basalts (e.g., Condomines *et al.*, 1983; Meyer *et al.*, 1985; Oskarsson *et al.*, 1985; Steinþórsson *et al.*, 1985; Nicholson *et al.*, 1991). Contamination would result in enrichment in incompatible elements and radiogenic ^{3}He/^{4}He (through the addition of ^{4}He), both of which characterise the compositions of basalts from Snæfellsjökull.

Crustal contamination has been shown to play a significant role in the genesis of many evolved lavas in Iceland (e.g., O'Nions and Gronvold, 1973; Hemond *et al.*, 1988, Nicholson *et al.*, 1991). However, enrichment in incompatible elements in *primitive* lavas (Mg# >55) is not consistent with crustal contamination. Furthermore, correlations between fluid-mobile elements, such as K_2O or Rb, and immobile elements, such as Nb, suggest that contamination by crustal fluids is unimportant in the genesis of the basalts from Snæfellsnes (Figure 2.22) because any contaminant is likely to be relatively enriched in the more mobile elements.

Figure 2.22: Plots of mobile elements (K_2O, Rb) against the immobile element Nb demonstrating the minimal role of crustal assimilation.

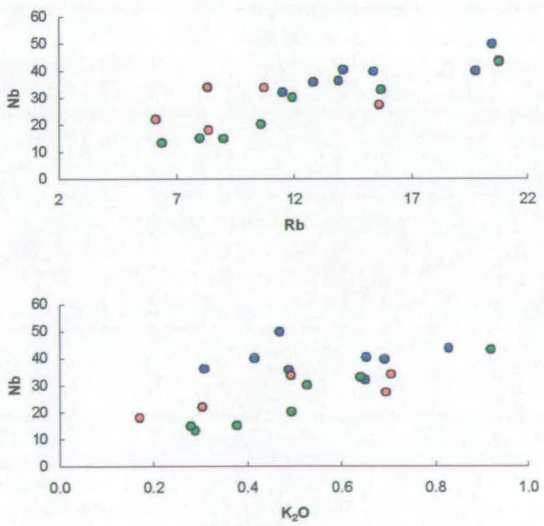

The lower $^{3}He/^{4}He$ of olivines from Snæfellsnes basalts compared to the rift zones could result from interaction of melts with altered Icelandic crust. Assuming U and Th concentrations in the old Icelandic crust of 0.1 and 0.3 ppm, respectively, 3×10^{-7} cc STP/g ^{4}He would be produced in the 15 Myr since formation. If the undegassed lower-mantle plume source has a [He] concentration of $1\text{-}3 \times 10^{-5}$ cc STP/g (e.g., Allègre *et al.*, 1986), then it would be necessary to incorporate over 90% crust in order to change $^{3}He/^{4}He$ from plume-like values (50 R_a; Stuart *et al.*, 2003) to Snæfellsjökull values of ~ 8 R_a.

Oxygen isotopes can provide further constraints on the extent of crustal contamination in volcanic rocks (e.g., James, 1981). Studies of whole-rock and olivine separates from Quaternary basalts from the Snæfellsnes Peninsula (Sigmarsson *et al.*, 1992; Hardarson, 1993; Kokfelt *et al.*, *in press*) demonstrate that the alkalic basalts are characterised by $\delta^{18}O$ = +4.6 - 5.9 ‰, a range that extends to values slightly higher than the range of Icelandic mantle values (+4.9 to + 5.5 ‰; Mattey *et al.*, 1994; Gautason and Muelenbachs, 1998; Thirlwall *et al.*, 1999; Gee *et al.*, 1998; Eiler *et al.*, 2000a; Kokfelt *et al.*, *in press*). Such compositions are contrary to what might be expected from the interaction of mantle-derived melts with the upper crust (e.g. Hattori and Muelenbachs, 1982; Gautason and Muelenbachs, 1998). Furthermore, the absence of a correlation between $\delta^{18}O$ and MgO concentration in Quaternary Snæfellsnes basalts also indicates that crustal assimilation has been negligible (Hardarson, 1993; Muelenbachs *et al.*, 1974). Measurements of high ^{230}Th excesses in the post-glacial basalts also indicate the minimal role of crustal assimilation in the genesis of the basalts (Kokfelt *et al*, 2003).

2.5.4 Fractional crystallisation

Fractional crystallisation can be identified in trends in MgO *vs.* major oxide concentration diagrams. For example, the slight increases in Al_2O_3, Na_2O and Fe_2O_3 with decreasing MgO are consistent with olivine fractionation and/or accumulation (Figure 2.4). Correlations between MgO and the abundances of the compatible elements can be explained by the fractionation of olivine (Ni), plagioclase (Sr) and clinopyroxene (Cr and V) (Figure 2.7).

Regional variation is observed in the concentrations of incompatible trace elements and TiO_2 and P_2O_5 (Figures 2.6, 2.10). Since the concentrations of these elements do not vary with MgO (Figure 2.4), the variations must reflect either enrichment in the source or variation in the degree of partial melting.

2.5.5 Partial melting

Relative enrichment or depletion in incompatible elements can also be explained by the degree of partial melting of a single source. Small-degree melts, from greater depths in the melting column, will be more enriched in incompatible elements and less enriched in compatible elements. Melting experiments (e.g., Langmuir *et al.*, 1992, Baker and Stolpher, 1994; Baker *et al.*, 1995) have shown that the following major oxide variations result from small-degree and/or high-pressure melting: high concentrations of incompatible major element oxides Na_2O, TiO_2, K_2O and P_2O_5 (ii) low CaO/TiO_2, Al_2O3/TiO_2 and $CaO/Al2O_3$ (as long as clinopyroxene remains in the residue).

Basalts from Ljósufjöll have lower Na_2O, K_2O, TiO_2, and P_2O_5 concentrations and higher Al_2O_3/TiO_2 than basalts from Snæfellsjökull (Figures 2.4-2.6; this study, see also Hardarson, 1993), suggesting that Ljósufjöll basalts have formed from greater degrees and/or shallower depths of partial melting. There is little difference between Snæfellsjökull and Ljósufjöll in CaO/Al_2O_3. Slight negative correlations with CaO/Al_2O_3 suggest that the degree of partial melting may account for at least some of the variations in Na_2O concentrations along the peninsula (Figure 2.23). Negative trends observed in the Lýsuskarð data-set in CaO/Al_2O_3 *vs.* TiO_2, K_2O or P_2O_5 are defined by the two most primitive basalts (LB232 and LB295). These have higher concentrations of Al_2O_3 than the less-primitive basalts (Figure 2.4) suggesting that Al_2O_3 concentration is affected by fractional crystallisation at high MgO concentrations. If these two samples are excluded, the absence of correlations between TiO_2, K_2O and P_2O_5 and CaO/Al_2O_3 and the displacement of Snæfellsjökull basalts to higher TiO_2, K_2O and P_2O_5 than Ljósufjöll basalts at comparable CaO/Al_2O_3, suggests that basalts from either end of the peninsula are derived from melting of sources with differing major element compositions.

Figure 2.23: Plots of incompatible major element concentrations against CaO/Al_2O_3, an index of melting degree.

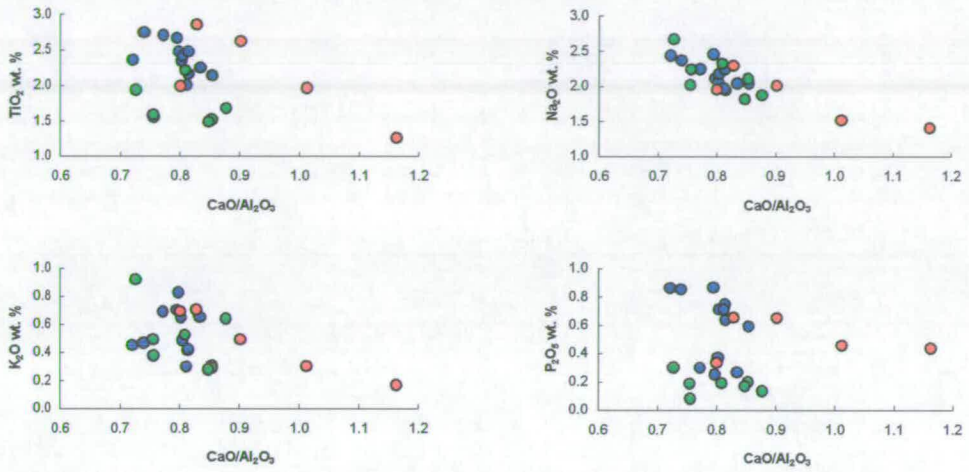

The ratios of very to moderately incompatible trace elements can be used to model the effects of partial melting of sources with different compositions. In Figure 2.24, a Ce/Y- Zr/Nb diagram, the Snæfellsnes basalts are plotted alongside modelled fractional melting curves for a spinel-lherzolite and a garnet-lherzolite mantle source. The basaltic compositions cannot be produced from fractional melting of either a spinel-lherzolite or garnet-lherzolite, but are derived from melting across the garnet-spinel transition. The displacement of two Lýsuskarð basalts (LB294 and LB229) to higher Ce/Y suggests a slightly greater proportion of garnet in their source. The two samples from the western end of Ljósufjöll appear to be derived from similar degrees of melting to the Snæfellsjökull and Lýsuskarð basalts, but the degree of melting appears to increase eastwards along the volcanic system, with the remaining samples from Ljósufjöll derived from the largest degrees of melting.

Trace-element ratios, however, may be less sensitive to variation in degrees of partial melting than major elements in basaltic rocks (e.g., Stracke *et al.*, 2003). If CaO/Al_2O_3 is used as a more robust indicator of the extent of partial-melting then negative trends should be observed when plotted against Nb/Zr or Ce/Y. Figure 2.25 clearly demonstrates that such correlations do not exist, which suggests that the

regional variation in incompatible-trace-element enrichment may be dominantly a reflection of source-variation.

Figure 2.24: Ce/Y *vs.* Zr/Nb. Non-modal fractional melting curves of primitive spinel-lherzolite (SL) and a garnet-lherzolite (GL) demonstrate that Snæfellsnes basalts formed from small-degree partial melting within a melting-column extending across the garnet-spinel transition. Source mineralogies from McKenzie and O'Nions, 1991. Partition co-efficients from Shaw, 1979.

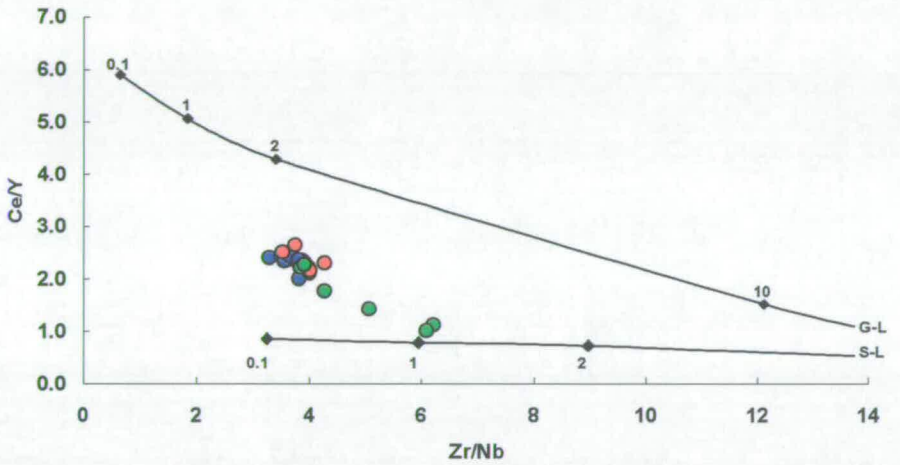

Figure 2.25: CaO/Al_2O_3 *vs.* Ce/Y and Nb/Zr

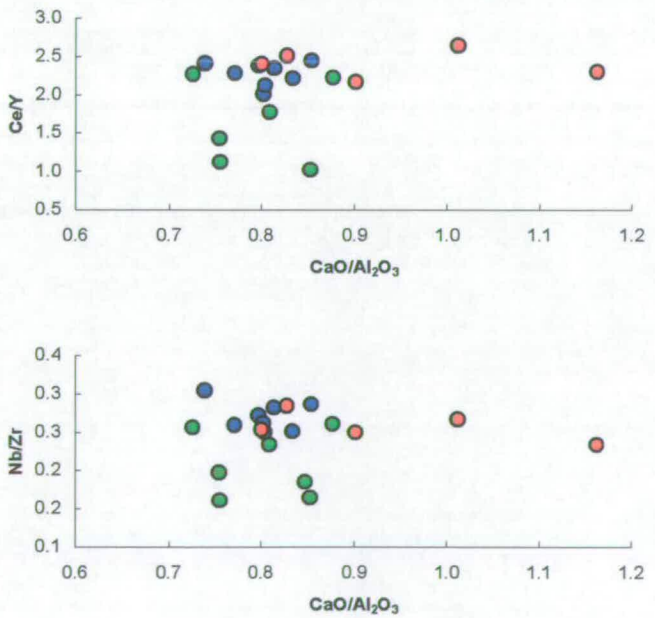

2.5.6 Source-characterisation: constraints from isotope ratios and major and trace element geochemistry

The strongest evidence for source heterogeneity along the Snæfellsnes Peninsula in this study is gained from He and Sr isotope ratios. Both show significant regional variation, with basalts from Ljósufjöll in the east characterised by the lowest $^{87}Sr/^{86}Sr$ and highest $^{3}He/^{4}He$ measured in this study. Less well-defined regional variation is seen in $^{143}Nd/^{144}Nd$ and Pb isotope ratios. Regional isotopic variation has previously been identified in Snæfellsnes using Sr and Nd isotopes (Hardarson, 1993), Re-Os isotopes (Smit *et al.*, 1999), and U-Th isotopes (Sigmarsson *et al.*, 1992; Kokfelt *et al.*, 2003). Source heterogeneity may also be reflected in the trace and major element composition of basalts. East-west variation in the degree of enrichment in incompatible elements is most apparent in Ce/Y and Nb/Zr and in the concentrations of TiO_2 and P_2O_5 (Figures 2.4 and 2.10) and it was suggested above that these variations result, at least to some degree, from differences in source composition. However, the extent of partial melting also appears to exert a control on the degree of enrichment in incompatible elements. Co-variations between the degree of incompatible element enrichment and isotope ratios should enable the respective roles of source composition and partial melting to be assessed.

When $^{3}He/^{4}He$ is plotted against VICE/MICE or concentrations of TiO_2 or P_2O_5, two divergent trends can be identified (Figure 2.26). Each trend radiates from an incompatible-element enriched end-member characterised by relatively low $^{3}He/^{4}He$ (~7.8 R_a). The two depleted end-members vary only in their $^{3}He/^{4}He$. The depleted end of the upper trend is defined by the two samples from easternmost Snæfellsnes, which have $^{3}He/^{4}He$ of >11.6 R_a. The depleted end of the lower trend is defined by the remaining Ljósufjöll basalts, which are characterised by $^{3}He/^{4}He$ of ~ 8.5 R_a. Snæfellsjökull basalts comprise the enriched end of the trends. The correlations between $^{3}He/^{4}He$ and the degree of enrichment (Nb/Zr, Ce/Y, TiO_2 and P_2O_5), defined by the upper trend in Figure 2.26, demonstrate that the regional differences in incompatible element enrichment between easternmost and westernmost Snæfellsnes are due to variation in source composition. Basalts from Lýsuskarð also plot along this upper trend, suggesting that source variation affects the incompatible

element compositions of basalts in this system. However, the weak relationship between $^{3}He/^{4}He$ and the degree of enrichment throughout Snæfellsjökull and in the western parts of the Ljósufjöll system, as defined by the lower trend in Figure 2.26, suggests that along most of the peninsula variations in incompatible element concentrations result from variation in the degree of partial melting rather than source heterogeneity.

If these interpretations are correct, similar trends should be identifiable in co-variation diagrams involving $^{87}Sr/^{86}Sr$, $^{143}Nd/^{144}Nd$ or Pb isotope ratios with trace and major elements. In fact, only single, negative trends are identified in the $^{87}Sr/^{86}Sr$ or $^{206}Pb/^{204}Pb$ against Nb/Zr or Ce/Y diagrams, and no relationships are observed between $^{87}Sr/^{86}Sr$ or $^{206}Pb/^{204}Pb$ and the major elements (Figures 2.27 and 2.29). No correlations between $^{143}Nd/^{144}Nd$ and trace or major elements are present (Figure 2.28). These observations imply that the $^{87}Sr/^{86}Sr$ and $^{206}Pb/^{204}Pb$ compositions of the two depleted end-members in Figure 2.26 are similar, and that the Nd isotopic compositions of all three end-members (enriched and depleted) in Figure 2.26 are similar. Furthermore, while Ce/Y and Nb/Zr trace source variations, TiO_2 and P_2O_5 do not. Along much of the peninsula, variation in the degree of incompatible element enrichment is associated with only small changes in the $^{87}Sr/^{86}Sr$ composition of the source – only in westernmost Snæfellsjökull and in easternmost Ljósufjöll do $^{87}Sr/^{86}Sr$ vary significantly. Based on Figures 2.27 - 2.29 then, the degree of enrichment appears to be a result of source composition only at either end of the peninsula.

In Figure 2.30, $^{3}He/^{4}He$ is plotted against $^{87}Sr/^{86}Sr$, $^{143}Nd/^{144}Nd$, and Pb isotope ratios. Two divergent trends are observed in He-Sr isotope space. Since, unlike trace element ratios, $^{87}Sr/^{86}Sr$ variation can only reflect source variation, this demonstrates that the two depleted end-members in Figure 2.27 do represent two distinct depleted source compositions, which are characterised by similar $^{87}Sr/^{86}Sr$ but different $^{3}He/^{4}He$. Thus, the lower trend in Figure 2.26 and the weak correlations in Figure 2.27 do indeed reflect variations in the degree of incompatible element enrichment in the source rather than degree of partial melting.

Figure 2.26 $^{3}He/^{4}He$ *vs.* (a) Ce/Y (b) Nb/Zr (c) TiO_2 and (d) P_2O_5

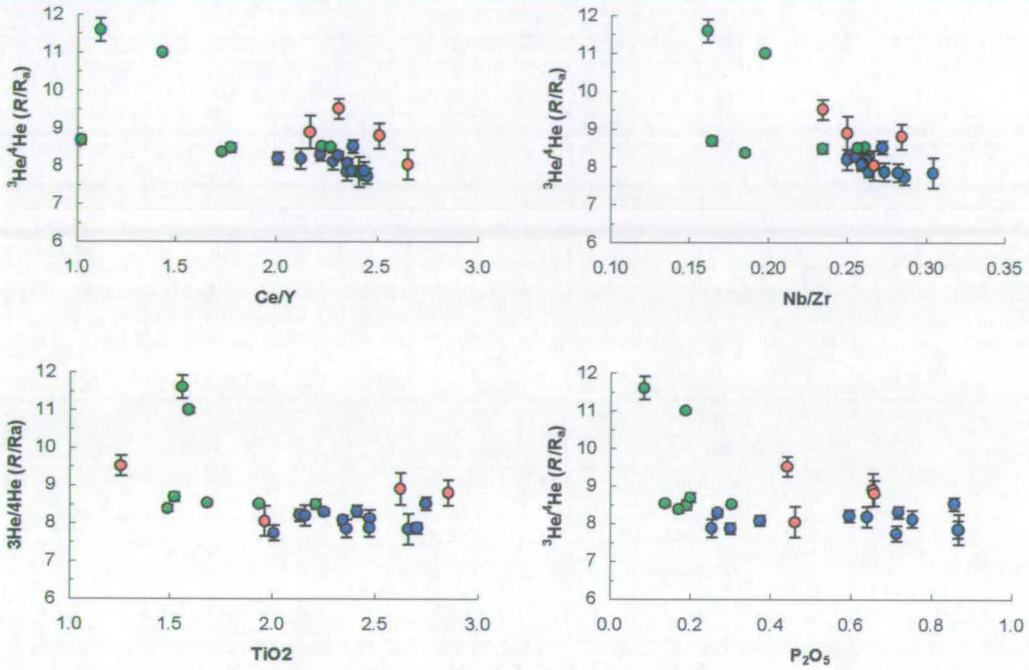

Figure 2.27 $^{87}Sr/^{86}Sr$ *vs.* (a) Nb/Zr (b) Ce/Y (c) TiO_2 and (d) P_2O_5

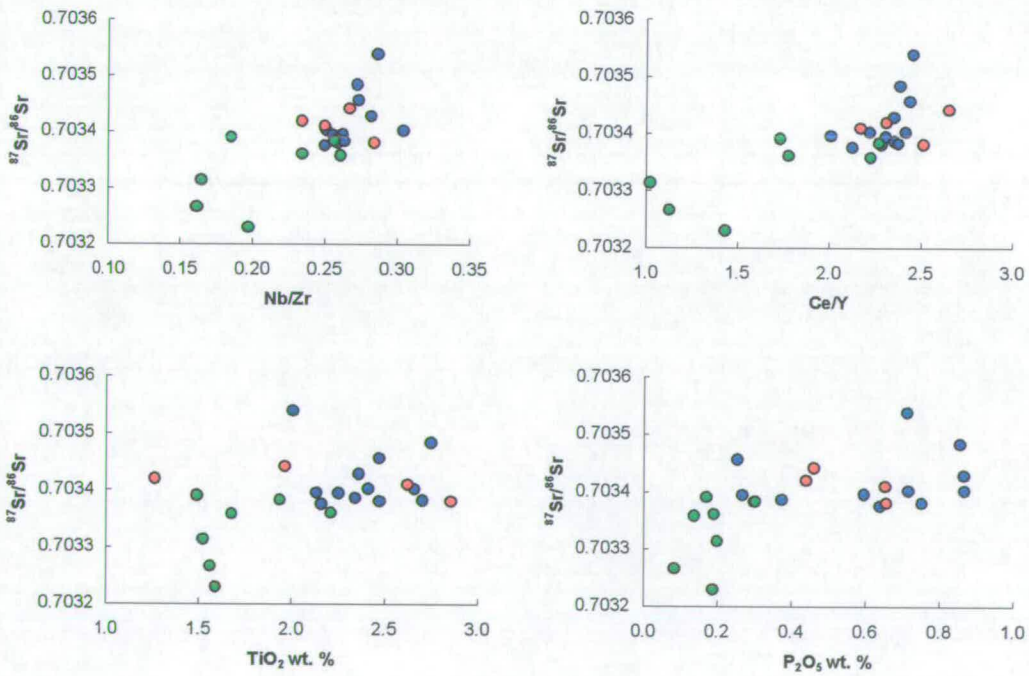

Figure 2.28 $^{143}Nd/^{144}Nd$ *vs.* (a) Nb/Zr (b) Ce/Y (c) TiO_2 and (d) P_2O_5

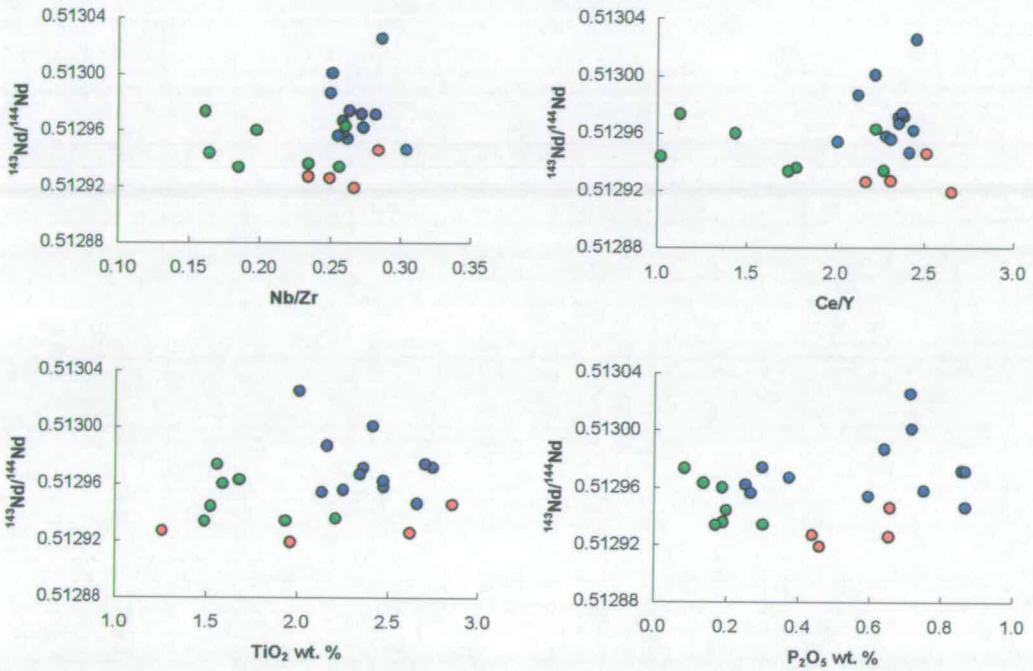

Figure 2.29 $^{206}Pb/^{204}Pb$ *vs.* (a) Nb/Zr (b) Ce/Y (c) TiO_2 and (d) P_2O_5

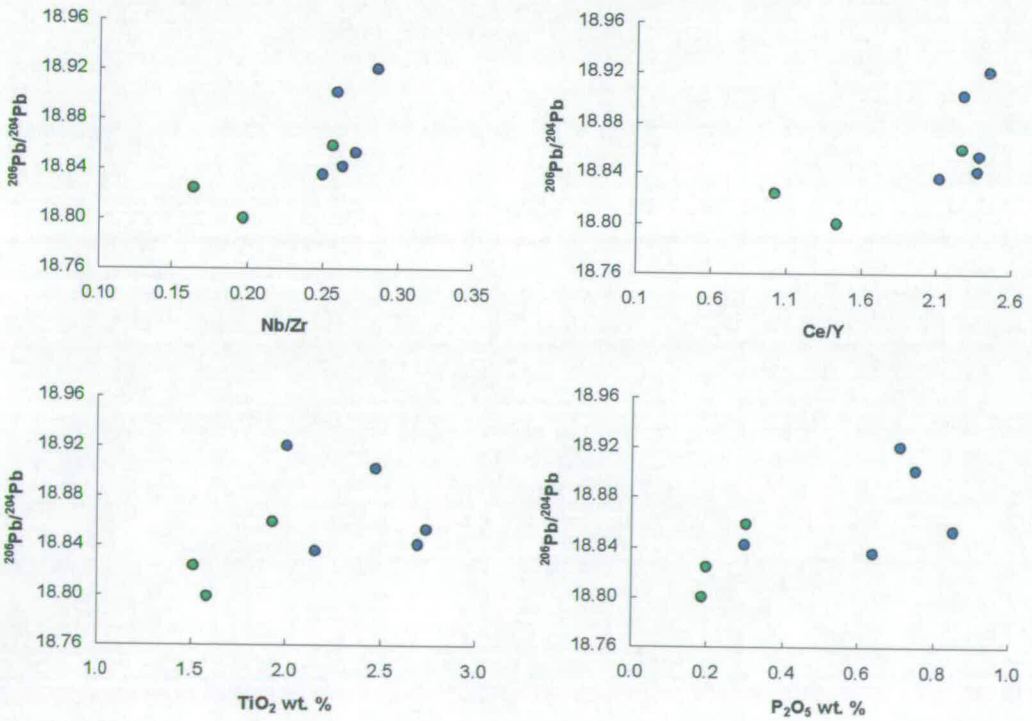

Figure 2.30 $^{3}He/^{4}He$ *vs.* (a) $^{87}Sr/^{86}Sr$; (b) $^{143}Nd/^{144}Nd$ and (c) $^{206}Pb/^{204}Pb$

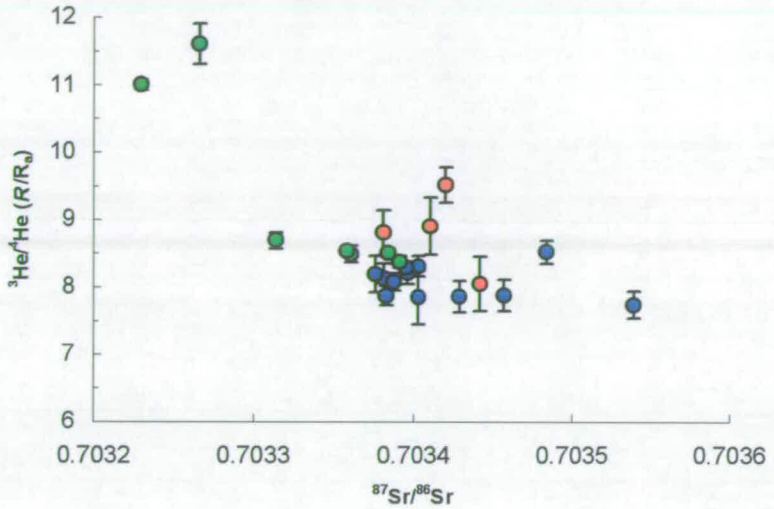

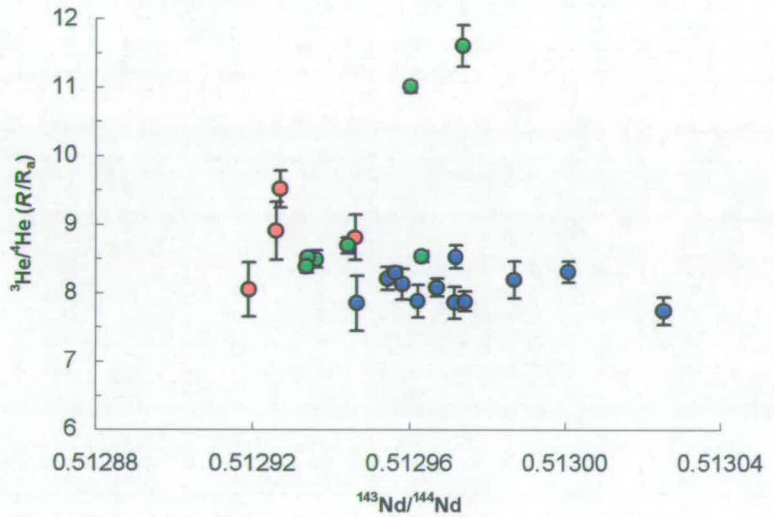

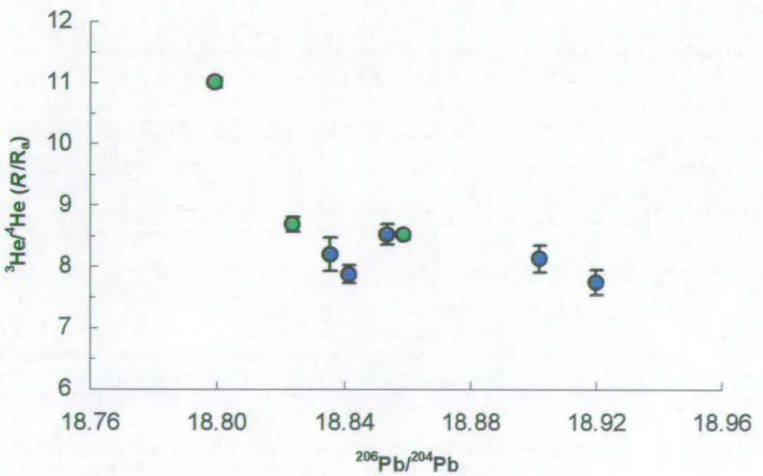

In summary, the trends in Figures 2.26, 2.27 and 2.30 are most easily explained by mixing between three local source compositions in the mantle beneath the Snæfellsnes Peninsula. These are characterised as:

- An enriched (high Nb/Zr and Ce/Y) source that is common throughout the region, but is most prevalent in Snæfellsjökull. It is characterised by radiogenic $^{87}Sr/^{86}Sr$ (~0.7035) and low $^{3}He/^{4}He$ (<7.8 R_a).
- One depleted (low Nb/Zr and Ce/Y) source that is sampled only beneath the farthest eastern parts of the peninsula and is characterised by less-radiogenic $^{87}Sr/^{86}Sr$ (<0.7032) and relatively high $^{3}He/^{4}He$ (>11.6 R_a).
- A second depleted source (also low Nb/Zr and Ce/Y) that is prevalent in western Ljósufjöll, and which also has less-radiogenic $^{87}Sr/^{86}Sr$, but is distinguished from the former depleted source by its lower $^{3}He/^{4}He$ (~9 R_a).

Snæfellsjökull basalts are derived from three-component mixtures involving either or both of the depleted sources, but are dominated by the enriched source. Lýsuskarð basalts originate from mixtures involving the high-$^{3}He/^{4}He$ depleted source and the enriched source. Ljósufjöll basalts are derived from mixtures of the enriched source and, in the west, the low-$^{3}He/^{4}He$ depleted source, and in the east, the high-$^{3}He/^{4}He$ depleted source. The simplest explanation for the regional variation in the type of depleted mantle sampled is that the high-$^{3}He/^{4}He$ depleted mantle in Snæfellsnes is most abundant close to the active rift zones, where it is preferentially sampled by the larger degrees of melting. The origins of the enriched and the high- and low-$^{3}He/^{4}He$ depleted mantle sources will be discussed in detail in Chapter 5.

2.5.7 Previous conclusions regarding melting *vs.* source

Previous interpretations of the relationships between melting processes and source-heterogeneity in Snæfellsnes have suggested a more significant role for melting, and the results of these studies should not be overlooked. Bunce (2002)

modelled the changes in source-composition from the Tertiary to the Quaternary in the Setberg region of Snæfellsnes and concluded that the change from depleted to enriched compositions in association with changes in the tectonic regime highlighted the role of dynamic melting. The more depleted and refractory source melted to greater degrees at shallower depths in the melt column beneath the active rift zones during the Tertiary. After rifting ceased, melts at the base of the melting column may have become trapped until the re-opening of the Snæfellsnes crust, in response to the initiation of rifting in the ERZ, allowed the melts to rise to the surface. These melts from greater depths would have been derived from the more enriched material. While this model explains the change in source-composition in relation to rejuvenated volcanism, it seems unlikely that the trapped melts could have been preserved during the 2.5 Myr period of inactivity. Sigmarsson *et al.*, (1992) and Kokfelt *et al.*, (2003) have used U-Th disequilibria determinations to show that increasing degrees of melting, possibly related to upwelling rates and/or lithospheric thickness, occur eastwards along the Snæfellsnes Peninsula, and that these correlate with $^{87}Sr/^{86}Sr$ and $^{143}Nd/^{144}Nd$ variations. Hardarson (1993) also argued that $^{87}Sr/^{86}Sr$ and $^{143}Nd/^{144}Nd$ co-variations with VICE/MICE require that the tapping of enriched and depleted mantle domains is controlled by the extent and depth of melting, possibly reflecting the thickness of the lithospheric lid.

In light of these interpretations a model for Snæfellsnes can be envisaged in which the depth and degree of melting determines whether a depleted or enriched mantle domain is sampled by a volcano. The depth and degree of melting may be controlled by the thermal regime (proximity to the inferred plume head and active rift-zones), rate of mantle upwelling or thickness of the overlying lithosphere. However, while this will result in more depleted material being sampled in the eastern parts of the peninsula, and more enriched material being sampled in the western parts, it will not necessarily exert a control over which type (high- or low-$^{3}He/^{4}He$) of depleted mantle is tapped. This appears to be controlled by the relative abundances of these in the source region of any particular volcanic system. A schematic representation of this model is presented in Figure 2.31.

Figure 2.31 Schematic cross-section illustrating the distribution of mantle sources and controls on melting processes and preferential source-tapping in Snæfellsnes.

The tapping of enriched or depleted sources in Snæfellsnes is controlled by the depth and degree of melting, which in turn is determined by the thickness of the lithosphere and hence the length of the melting column. Enriched mantle domains are preferentially tapped in western Snæfellsnes where the lithosphere is thickest and the melting column is shortest and therefore initial enriched melts are less diluted by depleted material. The depleted material present in the mantle beneath Snæfellsnes can be subdivided into two types; that characterised by $^{3}He/^{4}He > \sim 11.8\ R_a$, which is most abundant close to the active rift-zones to the east, and that characterised by $^{3}He/^{4}He = \sim 9\ R_a$ which dominates the depleted mantle in central and western Snæfellsnes.

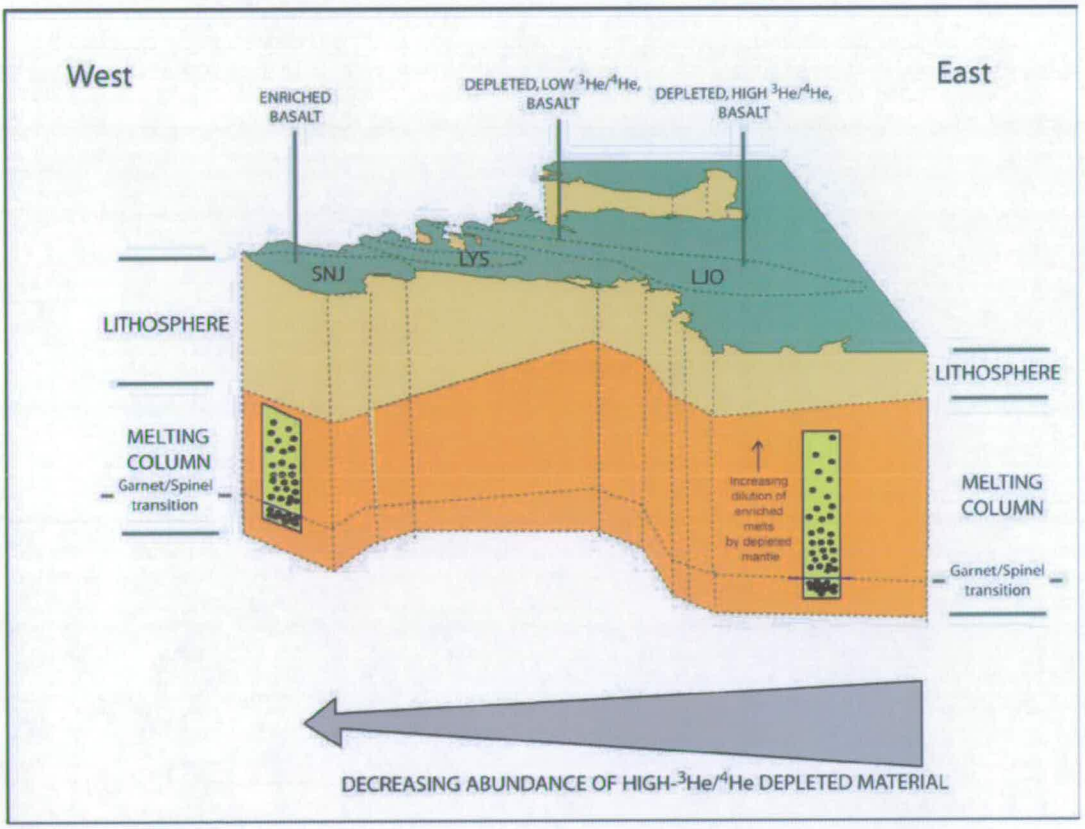

2.6 Summary and conclusions

Quaternary-age primitive basalts from the Snæfellsnes Peninsula in western Iceland are characterised by mildly alkaline compositions, typical of Recent flank zone basalts found in Iceland. The basaltic lavas were erupted within three en echelon volcanic systems trending east-west along the Peninsula. Geochemical variation between and within the systems is observed.

In major and trace element composition, basalts from the Snæfellsjökull system at the western tip of the peninsula are relatively enriched in incompatible trace elements and in P_2O_5 and TiO_2. Basalts from the centrally located Lýsuskarð system have compositions broadly similar to the Snæfellsjökull basalts, whereas basalts from the easternmost Ljósufjöll system are relatively depleted in incompatible elements. Fractional crystallisation and crustal contamination play negligible roles in the production of geochemical variation within the sample suite and therefore the general east-west variation in the degree of enrichment can be interpreted as reflecting either differences in mantle source-composition and/or the depth and degree of melting.

Isotopic ratios, such as $^{3}He/^{4}He$, $^{87}Sr/^{86}Sr$, $^{143}Nd/^{144}Nd$ and $^{206}Pb/^{204}Pb$, are robust indicators of source variation. $^{3}He/^{4}He$ were measured in olivine and pyroxene phenocrysts separated from a suite of 29 samples collected from along the length of the peninsula. $^{3}He/^{4}He$ of olivine and pyroxene phenocrysts are equal within analytical uncertainty and have not been modified by pre-eruptive or post-eruptive processes. The highest ratio recorded for a sample (usually olivine) is considered to reflect that of the source. Regional variation in $^{3}He/^{4}He$ indicates source heterogeneity beneath the peninsula, with lavas in westernmost Snæfellsnes being derived from a source characterised by $^{3}He/^{4}He \leq 7.8R_a$ and lavas from easternmost Snæfellsnes being derived from a source characterised by $^{3}He/^{4}He \geq 11.6\ R_a$. $^{87}Sr/^{86}Sr$ increases in the opposite direction, with the most radiogenic compositions present in basalts from Snæfellsjökull. Regional variation in $^{143}Nd/^{144}Nd$ and Pb isotope ratios are less well-defined.

Correlations between $^{3}He/^{4}He$ and $^{87}Sr/^{86}Sr$ or the degree of incompatible trace element enrichment suggest that three distinct sources are present in the mantle beneath Snæfellsnes, which are characterised as follows:

- Incompatible element enriched; $^{3}He/^{4}He \leq 7.8\ R_a$, $^{87}Sr/^{86}Sr \geq 0.7035$
- Incompatible element depleted; $^{3}He/^{4}He \geq 11.6\ R_a$, $^{87}Sr/^{86}Sr \leq 0.7032$
- Incompatible element depleted; $^{3}He/^{4}He \sim 9\ R_a$; $^{87}Sr/^{86}Sr < 0.7032$

Mixing between these end-members produces the range of compositions observed. The enriched end-member is dominant in the mantle beneath Snæfellsjökull in the west, the high-$^{3}He/^{4}He$ depleted end-member beneath eastern Ljósufjöll, and the low-$^{3}He/^{4}He$ depleted end-member beneath western Ljósufjöll. Relationships between incompatible element enrichment and isotopes indicate that the type of mantle domain sampled is to some degree controlled by the extent and depth of melting. Increasing degrees of partial melting, and a lengthening of the melt column towards the east of the peninsula and the active rift-zones, results in increasing dilution of enriched melt-fractions by depleted mantle melts. The depleted mantle sources are not distributed equally along the peninsula however: the high $^{3}He/^{4}He$ material is most abundant in the east, and the low $^{3}He/^{4}He$ depleted mantle dominates the depleted material in the west.

Chapter 3

CHARACTERISATION OF CHEMICALLY ENRICHED BASALTS FROM THE EASTERN FLANK-ZONE

3.1 Introduction

The second volcanic flank-zone examined in this study is located in eastern Iceland (Figure 3.1). Previous studies of the Eastern Flank-zone (EFZ) demonstrate that the Quaternary basalts are moderately enriched in incompatible trace elements and mildly alkaline, suggesting small-degrees of mantle melting at deeper levels than under the rift-zones (e.g. Hards *et al.*, 1995; 2000; Prestvik *et al.*, 2001;). Furthermore, Sr-Nd-Pb isotope data from these studies suggest that the EFZ mantle source is not homogeneous and that the source of lavas erupted at Öræfajökull volcano at the southern end of the flank-zone (Figure 3.1) may be derived from a discrete enriched component characterised by the most radiogenic $^{87}Sr/^{86}Sr$ (average of 15 samples = 0.70370) and highest Δ7/4Pb and Δ8/4Pb (average of 10 samples = + 2.9 and + 45.0, respectively) in the North Atlantic (Prestvik *et al.*, 2001). In contrast, basalts from the Snæfell volcanic centre, in the north of the flank-zone (Figure 3.1), appear to be characterised by Sr-Nd-Pb compositions that are slightly less radiogenic than Snæfellsnes basalts, suggesting dilution of the enriched component present in the Snæfellsnes mantle by more depleted material (Hards *et al.*, 1995; 2000). In this chapter enriched basalts from the EFZ are characterised further using He isotope data from olivine separates, in addition to major and trace element and Sr-Nd-Pb isotope data, in order to examine the nature of enriched mantle components present in the EFZ source. Comparisons of the EFZ data with data from the other flank-zones will be made in subsequent chapters.

3.2 Geology of the Eastern Flank-zone

The non-rifting Eastern Flank-zone was first identified by Walker (1975) and consists of three NNE-SSW-aligned volcanic centres: Öræfajökull, Esjufjöll, and Snæfell (Figure 3.1). It is located approximately 50 km east of the active Eastern and Northern Rift Zones (Bjornsson and Einarsson, 1990). Crustal thickness beneath the flank-zone is up to 35 km (e.g., Staples *et al.*, 1997). The basement rocks in the region are dominated by sub-horizontal tholeiitic basalt flows, typical of those produced in an axial rift-zone. Smaller volumes of basement rhyolites are associated with old volcanic centres such as Skafatafellsfjöll close to Öræfajökull (Prestvik *et al.*, 1993) (Figure 3.1). The basement rocks were formed at around 10 Ma, consistent

with eruption in the Reykjanes-Skagi rift zone, which is now located to the west of the active rift zones and became extinct at approximately 6.5 Ma (e.g. Sæmundsson , 1974, Sæmundsson, 1979).

Quaternary volcanic activity in the region has been confined to the three off-axis volcanic centres. The cause of the initiation of flank volcanism is uncertain. Hards *et al.*, (2000) interpreted the flank-zone as an incipient rift-zone, similar to the present-day tip of the Eastern Rift Zone, but, noting the southward-waning of volcanic activity, suggested it was abandoned as a result of a westward relocation of the NRZ at around 0.7 Ma (Helgason, 1985). It has been suggested that the eruption of dominantly mildly alkaline basaltic hyaloclastite in Snaefell in glacial periods suggests that depths of melting were greater during these times (e.g., Bourgeois *et al.*, 1998).

Öræfajökull is the most southerly of the three volcanoes (Figure 3.1). It is currently active and has erupted twice in historic times (1362 AD and 1727 AD). The northern parts of the edifice are submerged by the Vatnajökull ice-cap, and the Svinafellsjökull and Breiðamerkurjökull glaciers mark its western and eastern boundaries respectively (Figure 3.1). The Quaternary volcanic rocks of Öræfajökull are transitional to sodic alkaline (Na_2O - 2.0 $\geq$ K_2O) with compositions ranging from basalt through to rhyolite. The basic rocks are evolved (MgO = ~6 wt. %) relative to other basalts from the flank-zone (e.g. Hards *et al.*, 1995; Holm, 2004; Prestvik *et al.*, 2001) and comprise mainly lava flows and hyaloclastite formations of Upper Pleistocene (<0.8 Ma) age, but with a minor volume of post-glacial basalts in the Kvisker region (Prestvik *et al.*, 1980; Jóhannesson & Sæmundsson, 1998). Post-glacial volcanic activity has been dominated by explosive eruptions, the products of which include large volumes of tephra and pumice deposits, and silicic rocks, including rhyolitic lava flows and obsidian. The rhyolites are thought to have been derived largely from fractional crystallisation of basic melts (Holm *et al.*, 2004b; Prestvik *et al.*, 2001). Previous Sr-Nd-Pb isotope studies of Öræfajökull have noted its high $^{87}Sr/^{86}Sr$ (0.70366 – 0.70383) for its moderate $^{143}Nd/^{144}Nd$ (0.51285 – 0.51303), and its high $^{207}Pb/^{204}Pb$ (15.515 – 15.555) and $^{208}Pb/^{204}Pb$ (38.433 - 38.601) for its $^{206}Pb/^{204}Pb$ (18.475 – 18.663) compared to other Icelandic rocks. These isotopic characteristics have been related to a mantle component derived from

either recycled pelagic sediments (EM1-type) or recycled continental crust (EM2-type) (Sigmarsson *et al.*, 1992; Prestvik *et al.*, 2001).

The Esjufjöll stratovolcano (Figure 3.1), located approximately 30 km NW of Öræfajökull, is thought to be currently active; a minor eruption was recorded in 1927. Much of the volcano, including its large caldera (~ 40 km^2) is sub-glacial, so the compositions of the rocks are largely unknown. The exposed parts of the volcano consist of mainly evolved, aphyric, mildly alkaline basaltic rocks (MgO = 4 to 5 wt %) with minor volumes of rhyolite in the north-western margin (Holm *et al.*, 2004). The more evolved basalts appear to have been affected by anatectic contributions of hydrothermally-altered rift zone tholeiites, as indicated by $\delta^{18}O$ (+4 to +5) that are lower than observed elsewhere in the flank-zone (+5.0 to +5.7 ‰; Kokfelt *et al.*, *in press.*, Prestvik *et al.*, 2001, Sigmarsson *et al.*, 1992) (Holm *et al.*, 2004). The rhyolites have major and trace element compositions similar to rift-zone rhyolites, with lower Al_2O_3 and K_2O than rhyolites from Snæfell and Öræfajökull. This has been interpreted to suggest that AFC-processes may be more important at Esjufjöll than at the other EFZ volcanoes (Holm *et al.*, 2004).

The Snæfell volcano (Figure 3.1), in the northern part of the Eastern Flank-zone, is an elongate edifice overlying Pliocene basaltic flows. Steep sides rise to a 1500 m-high plateau formed of sub-horizontal lava flows, from which the slopes rise more gently to its summit at 1833 m. The youngest Snæfell lavas are approximately 10 ka. The volcanic rocks in the area are dominated (>70%) by mildly alkaline basaltic flows and subglacially erupted hyaloclastite, but a small volume (~10%) of highly evolved silicic rocks is associated with the central volcano. The basalts are fine-grained and generally phenocryst-poor (< 3%). They are enriched in incompatible trace elements relative to the rift-zone tholeiites, but less so than basalts from Snæfellsnes or Vestmannaeyjar. Rocks of intermediate compositions (benmoreites and trachytes) are scarce and appear to be the products of magma-mixing. The rhyolites are peralkaline (molecular $[Na_2O + K_2O]/Al_2O_3 > 1$) and have more enriched trace element compositions than rhyolites erupted in the rift-zones. The rhyolites have $^{87}Sr/^{86}Sr$ that are higher than the basaltic rocks (>0.7035 compared to ~0.7033), thought to be indicative of a crustal input in the genesis in the evolved rocks (Hards *et al.*, 2000).

Figure 3.1: Simplified map of the EFZ and showing locations of Öræfajökull, Esjufjöll and Snæfell volcanoes and sample localities.

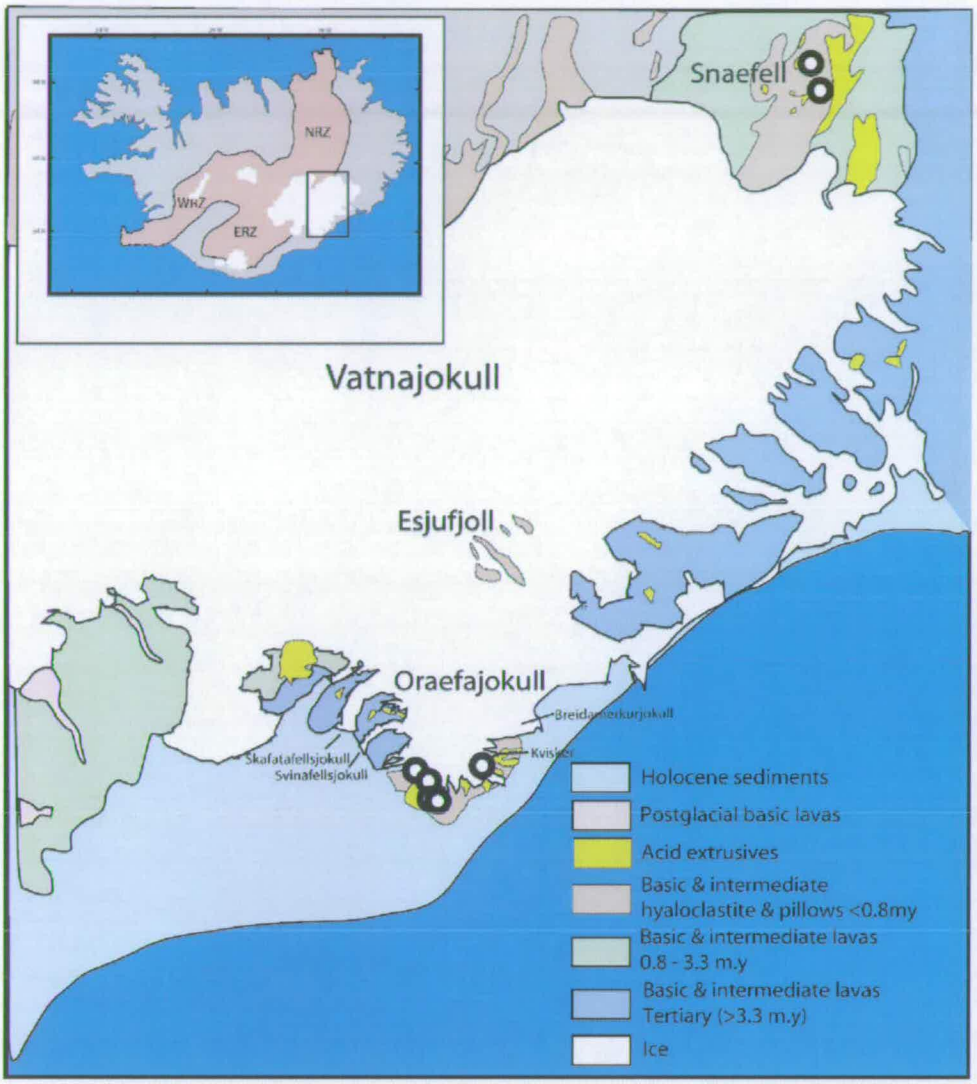

3.3 Sample descriptions

Access to sample locations in the EFZ is difficult due to a lack of roads and the glaciated terrain so only a small number of samples were collected from the region. As in Snæfellsnes, sampling was restricted to Quaternary, olivine- and pyroxene-phyric lava flows, from outcrops shielded from cosmic rays. In Öræfajökull the Quaternary geology is dominated by silicic rocks and hyaloclastite, and olivine-

phyric basalts are scarce. Three olivine- and pyroxene-rich samples were collected from basalt flows on the flanks of the Öræfajökull edifice, and additional samples from a stream-bed were donated by Kaj Hoernle (GEOMAR, Kiel). Esjufjöll volcano is largely submerged by the Vatnajökull ice-cap and access to basaltic rocks from this volcano was not possible. The alkali basalts erupted at Snæfell are typically phenocryst-poor (<3%) but two olivine-bearing samples were donated by Kaj Hoernle (GEOMAR, Kiel). Brief sample details are given in Table 3.1 and Appendix 1.2 and sample localities shown in Figure 3.1.

Table 3.1: Sample details

Volcanic centre	Sample Name	Location	Approximate Age
Öræfajökull	AW20	Small flow in shallow gorge north of Hnappavellir	<0.8 m.y
	AW24	Nr. radiomast, NE of Hnappavellir	<0.8 m.y
	AW27	Small gorge on western edge of jokull, ESE of Kvisker	<0.8 m.y
	H52	Öraefajökull, 2.5km NW Öräfi, river pebbles[1]	Unknown[2]
	H54	Öraefajökull, 2.5km NW Öräfi, river pebbles[1]	Unknown[2]
Snæfell	H136	Snæfell, east of the hut upslope[1]	Glacial
	H140	NNW of Snæfell, 1km W of Hafursfell[1]	Glacial

[1] Locality details from K. Hoernle, *pers. comm*

[2] Unknown age, but inferred to be younger than 0.8m.y based on location of river-source in NW Oraefi.

3.4 Results

Major and trace element concentrations, He isotope compositions and radiogenic lithophile isotope compositions were determined using the procedures outlined in Appendix 2. Major and trace element data for samples donated by Kaj Hoernle (H52, H54, H136 and H140) were determined by XRF at GEOMAR following the procedures outlined in Kokfelt *et al.*, (*in press*). Pb, Sr and Nd isotope data for H136 were also determined at GEOMAR following the procedures outlined in Kokfelt *et al.*, (*in press*). All results are presented in Tables 3.2 to 3.4.

3.4.1 Major elements

Major element oxide concentrations are presented in Table 3.2. On the TAS rock classification diagram, all samples from this study are transitional to sub-alkaline basalts, with the exception of two Öræfajökull samples (H52 and H54) which are andesites (Figure 3.2) (Le Maitre, 1979). Inclusion of data from Prestvik *et al.*, 2001 and Hards *et al.*, 1995, extends the compositional range in the EFZ to rhyolite. According to the IUGS classification, the Öræfajökull basalts are more sodic alkaline (Na_2O-2.0 ≥ K_2O) than the Snæfell basalts.

Figure 3.2: Total alkalis-silica (TAS) diagram of Snæfell and Öræfajökull basalts (after Le Maitre, 1979). Dark purple circles: Snæfell. Light purple circles: Öræfajökull. Previously published data shown for comparison (small circles) (Hards *et al.*, 1995, 2000; Prestvik *et al.*, 2001). Diagonal line marks the Hawaiian alkaline-subalkaline division of MacDonald and Katsura (1964).

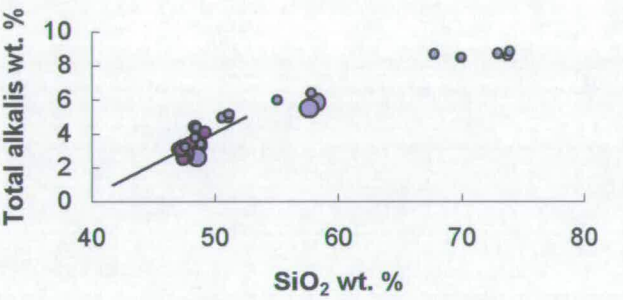

In Figure 3.3, major element oxides are plotted against MgO wt%. Data from previous studies of Snæfell (Hards *et al*, 1995; 2000) and Öræfajökull (Prestvik *et al.*, 2001) are shown for comparison. The Öræfajökull andesites are displaced to higher SiO_2, Al_2O_3 and K_2O, and lower CaO, TiO_2, P_2O_5 and MnO, than the intermediate rocks analysed by Prestvik *et al* (1993; 2001). The basalts, however, have similar compositions to the published data, with the exception of AW27 which has higher CaO and Al_2O_3, and lower TiO_2, Na_2O, K_2O, Fe_2O_3, P_2O_5 and MnO. The Snæfell basalts have major element compositions in agreement with the data of Hards *et al.* (2001), and have slightly higher P_2O_5 and lower CaO, Na_2O and Fe_2O_3 concentrations than basalts from Öræfajökull, consistent with their more primitive compositions (higher MgO concentrations).

Positive trends are observed between MgO and Al_2O_3/TiO_2 and CaO/Al_2O_3 at MgO > 5 wt. % (Figure 3.4). With the exception of AW27 from Öræfajökull, the major element oxide ratios of the basalts are consistent with the previous data from Öræfajökull and Snæfell.

Table 3.2: Major element oxide concentrations of EFZ samples

Sample	SiO_2	TiO_2	Al_2O_3	Fe_2O_3	MnO	MgO	CaO	Na_2O	K_2O	P_2O_5	Mg#
	wt. %	wt. %	wt. %	wt. %	wt. %	wt. %	wt. %	wt. %	wt. %	wt. %	
Öræfajökull											
AW20	48.59	2.21	15.12	13.14	0.20	6.28	10.85	2.75	0.62	0.25	51.25
AW24	47.47	2.12	15.80	12.92	0.19	6.37	11.82	2.65	0.45	0.21	52.02
AW27	48.53	1.50	17.61	10.22	0.15	6.67	12.58	2.27	0.34	0.15	58.95
H52	58.17	1.43	15.58	8.44	0.13	3.68	6.49	3.63	2.24	0.22	48.96
H54	57.62	1.37	16.03	8.09	0.13	4.15	6.89	3.41	2.10	0.21	53.06
Snæfell											
H136	47.72	1.79	15.03	11.40	0.17	10.13	10.90	1.94	0.66	0.25	66.16
H140	47.30	2.14	15.25	12.51	0.18	8.58	11.00	2.24	0.55	0.25	60.13

Note: All data corrected for loss on ignition. Range: 1.05 to 0.19%

Mg# = 100MgO/(MgO+FeO) (mol.); FeO = 0.9 $Fe_2O_3^t$

Figure 3.3: Major element oxide concentrations *vs.* MgO concentrations for samples from Öræfajökull and Snæfell. Published data from Prestvik *et al.*, (2001) and Hards *et al.*, (1995) are shown for comparison. Symbols as in Figure 3.2.

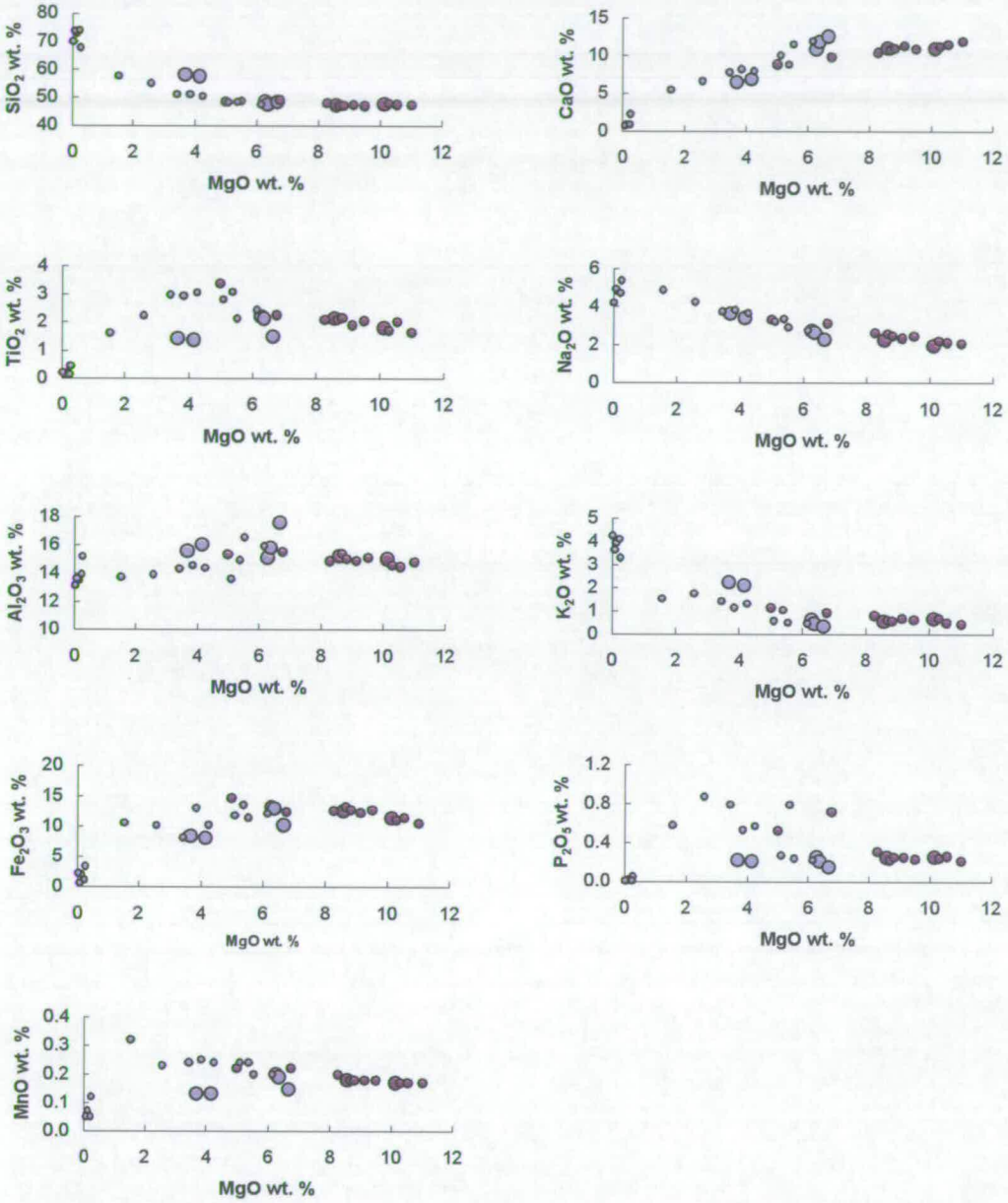

Figure 3.4: Major element oxide ratios *vs.* MgO concentrations (>5 wt. %). Symbols as in Figure 3.2.

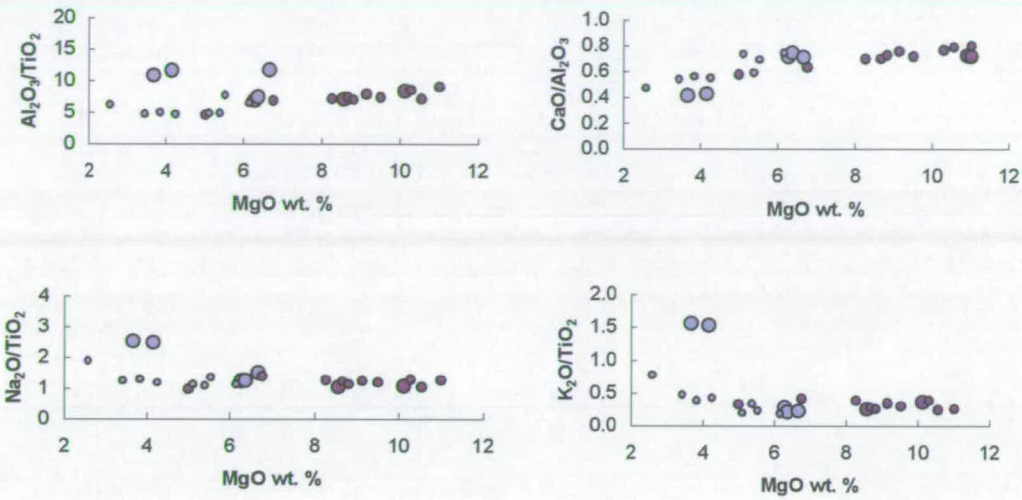

3.4.2 Trace elements

Trace element concentrations are presented in Table 3.3 and Figure 3.5, with published data from Öræfajökull and Snæfell shown for comparison (Prestvik *et al.*, 2001; Hards *et al.*, 1995). The trace element concentrations of the Snæfell and Öræfajökull basalts are similar, and in close agreement with the published data. The two evolved lavas from Öræfajökull (H52 and H54) are less enriched in compatible elements and more enriched in incompatible trace elements than the basalts, consistent with their lower MgO content. H52 and H54 are highly enriched in Rb. The relative enrichment in incompatible elements in the andesites is illustrated in primitive-mantle normalised trace element abundance diagrams (Figure 3.6). The basalts from Snæfell and Öræfajökull have smoother patterns than the andesites. The Snæfell basalts have negative Ce and positive Sr anomalies and the Öræfajökull basalts have negative Ba anomalies. The Snæfell and Öræfajökull basalts have comparable Ce/Y, but Snæfell basalts are characterised by slightly higher Nb/Zr (Figure 3.7). ΔNb (calculated using equation in Fitton *et al.*, 1997) of the EFZ basalts are positive and range from 0.19 to 0.25, and there is no difference between basalts from the two volcanoes.

Table 3.3: Trace element concentrations of EFZ samples

Sample	Ba	Ce	Cr	La	Nb	Nd	Ni	Rb	Sr	V	Y	Zn	Zr
	ppm	ppm	ppm	ppm	ppm	ppm	ppm	ppm	ppm	ppm	ppm	ppm	ppm
Öræfajökull													
AW20	155.26	39.01	109.48	23.47	21.40	24.70	59.65	11.76	341.28	324.30	31.74	100.70	164.08
AW24	122.63	29.74	124.32	13.47	16.80	17.74	62.50	12.32	342.97	357.40	26.94	104.38	130.84
AW27	86.19	22.52	111.49	9.78	11.35	14.26	59.32	11.69	343.40	240.40	19.99	73.59	95.68
H52	385.00	82.50	68.50	16.00	39.50	-	39.00	61.00	247.00	167.50	46.50	84.00	369.50
H54	364.00	71.00	83.00	17.00	35.00	-	36.00	57.00	253.00	163.00	43.00	79.00	342.00
Snæfell													
H136	183.00	27.00	835.00	16.61	21.00	-	198.00	17.00	357.00	269.00	21.00	75.00	126.00
H140	175.00	21.00	376.00	14.00	18.00	-	129.00	13.00	359.00	311.00	27.00	88.00	141.00

Figure 3.5: Trace element concentrations *vs.* MgO concentration of samples from Snæfell and Öræfajökull. Symbols as in Figure 3.3.

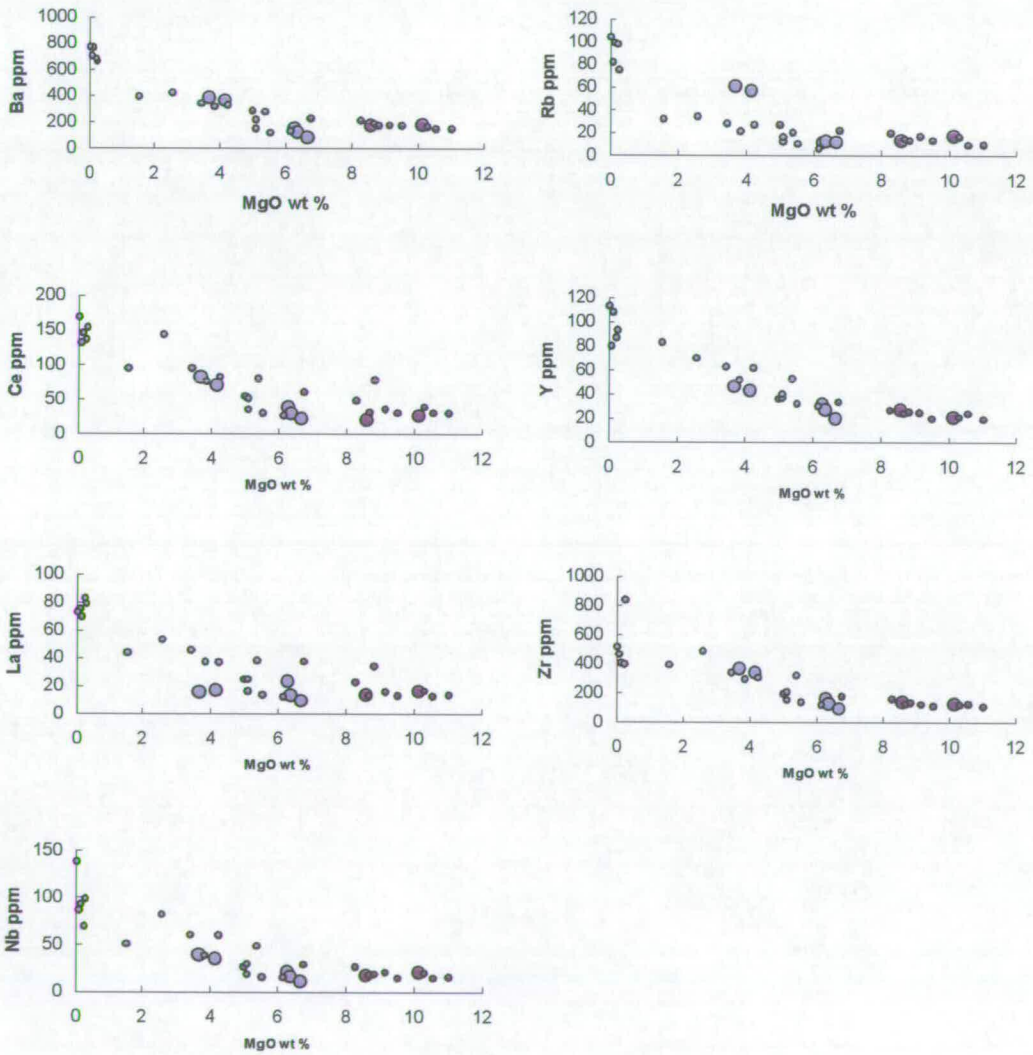

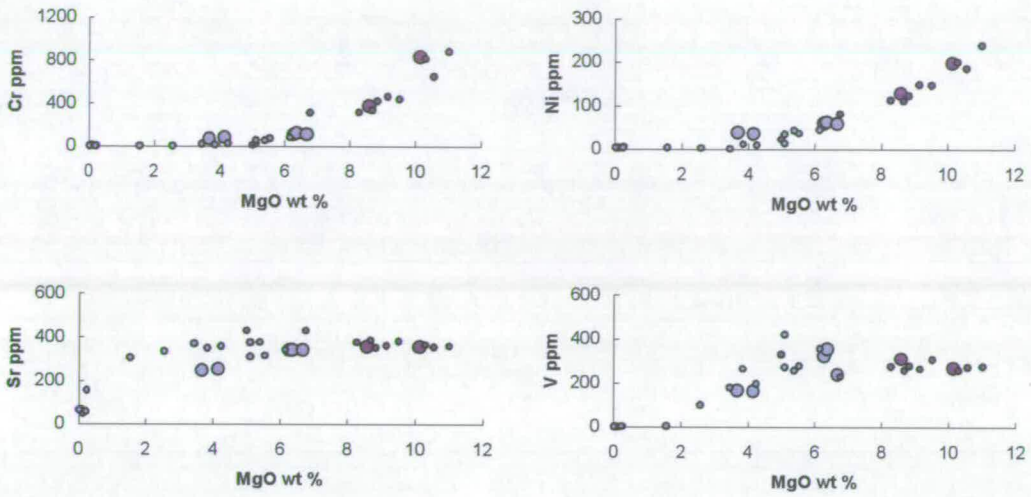

Figure 3.6: Primitive-mantle normalised diagrams of Öræfajökull and Snæfell trace element abundances.

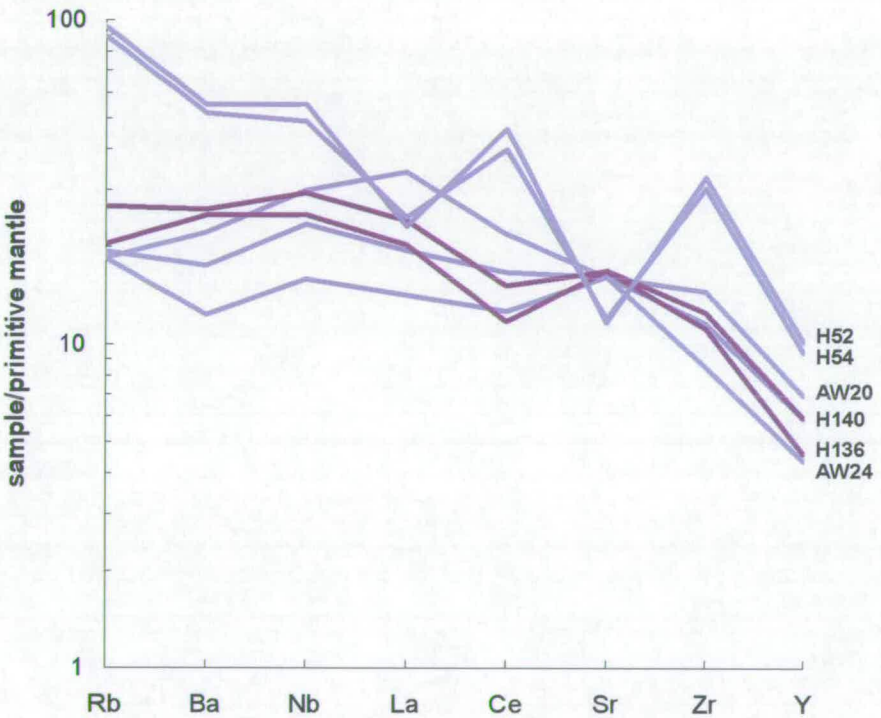

Figure 3.7 Ce/Y vs Nb/Zr of EFZ basalts (MgO > 5 wt. %) Symbols as in Figure 3.3.

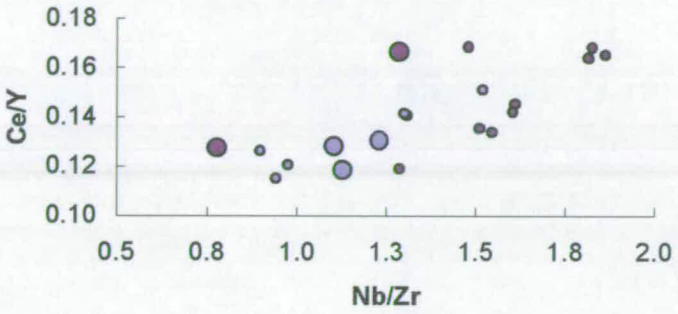

3.4.3 Helium isotopes

Helium concentrations and isotope ratios of olivine and pyroxene phenocrysts are presented in Table 3.4 and Figure 3.8. Helium extracted by *in vacuo* crushing ranged from 0.3 to 37.5 × 10^{-9} cc STP. $^{3}He/^{4}He$ range from 5.6 to 7.8 R_A in Öræfajökull and 6.4 to 7.0 R_A in Snæfell. The $^{3}He/^{4}He$ of co-genetic olivines and pyroxenes in AW20 are identical within analytical uncertainty. Olivines from AW24 yielded higher $^{3}He/^{4}He$ than the co-existing pyroxenes. Pyroxenes from AW27 yielded less than 1 × 10^{-9} cc STP He and consequently the $^{3}He/^{4}He$ has much greater uncertainty than the other samples from Öræfajökull. The anomalous major element chemistry (see Section 3.4.1 above) of AW27 is consistent with this basalt having undergone a degree of contamination resulting in modified $^{3}He/^{4}He$. Low He concentrations render a melt susceptible to contamination and pyroxenes are also more susceptible to this than olivines (see Section 2.5.2.1). In light of the possibility of contamination, this sample will be excluded in subsequent discussions of the data-set. The Öræfajökull samples are characterised by marginally higher $^{3}He/^{4}He$ than Snæfell samples. The highest Öræfajökull $^{3}He/^{4}He$ determinations are in agreement with a previous olivine measurement (8.0 ± 0.2 R_A; Sigmarsson *et al.*, 1992). No previous measurements of $^{3}He/^{4}He$ from Snæfell have been published.

Table 3.4: Helium isotope data from crush extractions of olivine and pyroxene phenocrysts.

Volcanic centre	Sample	Mineral	^{4}He 10^{-9} cc STP *	±	^{4}He blank %	^{3}He blank %	^{3}He/^{4}He R_A	±
Öræfajökull	AW20	Olivine	37.51	0.020	0.05	0.03	7.75	0.08
		Pyroxene	7.74	0.014	0.23	0.14	7.65	0.10
	AW24	Olivine	10.86	0.013	0.17	0.10	7.67	0.17
		Pyroxene	8.23	0.012	0.22	0.13	7.34	0.08
	AW27	Pyroxene	0.33	0.011	5.16	4.87	5.59	0.92
	H54	Olivine	2.60	0.007	0.39	0.42	7.81	0.13
	H52	Olivine	2.33	0.006	0.53	0.50	7.44	0.29
Snæfell	H136	Olivine	3.26	0.017	0.63	0.67	6.99	0.21
	H140	Olivine	1.36	0.021	1.50	1.74	6.35	0.22

Figure 3.8: ^{3}He/^{4}He and total He released by crushing of olivine (squares) and pyroxene (circles) phenocrysts.

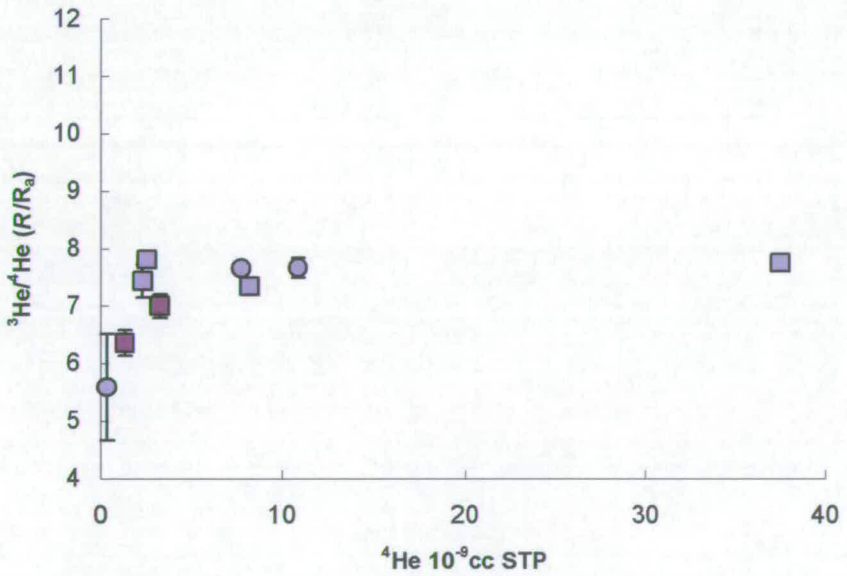

3.4.4 Sr, Nd and Pb isotopes

Sr, Nd and Pb isotope data are presented in Table 3.5 and in Figure 3.9. $^{87}Sr/^{86}Sr$ ranges from 0.70373 to 0.70375 in Öræfajökull and from 0.70318 to 0.70338 in Snæfell. $^{143}Nd/^{144}Nd$ ranges from 0.51294 to 0.51297 in Öræfajökull and from 0.51299 to 0.51301 in Snæfell. $^{87}Sr/^{86}Sr$ and $^{143}Nd/^{144}Nd$ for both volcanic centres are in agreement with previous measurements (Prestvik *et al.*, 2001; Sigmarsson *et al.*, 1992; Hards *et al.*, 1995; Figure 3.9a). Within Öræfajökull, there is no variation in $^{87}Sr/^{86}Sr$ or $^{143}Nd/^{144}Nd$ with rock type. Öræfajökull $^{87}Sr/^{86}Sr$ are the most radiogenic measured in Icelandic basalts, however, the high $^{87}Sr/^{86}Sr$ are not coupled with the most unradiogenic $^{143}Nd/^{144}Nd$. $^{143}Nd/^{144}Nd$ of Öræfajökull samples are comparable to eastern Snæfellsnes values (Ljósufjöll = 0.51293 – 0.51297; this study), and slightly higher than Jan Mayen values (0.51288 – 0.51291; Stuart *et al.*, *in prep.*). Snæfell basalts are characterised by $^{87}Sr/^{86}Sr$ and $^{143}Nd/^{144}Nd$ comparable to the most and least radiogenic compositions, respectively, of rift-zone basalts ($^{87}Sr/^{86}Sr < 0.7033$, $^{143}Nd/^{144}Nd > 0.51298$).

The samples analysed for Pb isotope ratios show $^{206}Pb/^{204}Pb = 18.56$, $^{207}Pb/^{204}Pb = 15.48$ and $^{208}Pb/^{204}Pb = 38.21$ in Snæfell (n=1), and $^{206}Pb/^{204}Pb = 18.33 - 18.55$, $^{207}Pb/^{204}Pb = 15.53 - 15.56$ and $^{208}Pb/^{204}Pb = 38.28 - 38.49$ in Öræfajökull (n=3). The Pb isotope ratios of AW20 and AW24 are less radiogenic than those in the andesite H54 and the samples from Prestvik *et al.* (2001) (Figure 3.9b,c). Snæfell Pb isotope ratios are in agreement with determinations by Hards *et al.* (1995) (Figure 3.9b,c). In diagrams of $^{206}Pb/^{204}Pb$ vs. $^{207}Pb/^{204}Pb$ or $^{208}Pb/^{204}Pb$, the data from each volcanic centre form trends parallel to the NHRL. Öræfajökull samples are displaced to higher $^{207}Pb/^{204}Pb$ and $^{208}Pb/^{204}Pb$ at similar $^{206}Pb/^{204}Pb$ to Snæfell basalts. The positive $\Delta 7/4$ and strongly positive $\Delta 8/4$ determined in previous studies of Öræfajökull are confirmed in this study. Snæfell basalts are characterised by negative $\Delta 7/4$ and slightly positive $\Delta 8/4$. There are no apparent relationships between $^{206}Pb/^{204}Pb$ and $^{87}Sr/^{86}Sr$ or $^{143}Nd/^{144}Nd$ in the EFZ (Figure 3.9d,e).

Table 3.5: Sr, Nd and Pb isotope compositions of EFZ samples

Sample	$^{87}Sr/^{86}Sr$	±	$^{143}Nd/^{144}Nd$	±	$^{206}Pb/^{204}Pb$	±	$^{207}Pb/^{204}Pb$	±	$^{208}Pb/^{204}Pb$	±	$\Delta^{207}Pb$	$\Delta^{208}Pb$
Öræfajökull												
H52	0.703737	0.0014	0.512937	0.0009	18.55	0.011	15.53	0.011	38.49	0.035	3.1	43.8
H54	0.703757	0.0012	0.512936	0.0006	-	-	-	-	-	-	-	-
AW20	0.703733	0.0013	0.512936	0.0007	18.38	0.011	15.56	0.011	38.38	0.035	7.9	53.2
AW24	0.703744	0.0011	0.512937	0.0005	18.33	0.011	15.53	0.011	38.28	0.034	5.3	49.3
AW27	0.703771	0.0014	0.512941	0.0007	-	-	-	-	-	-	-	-
Snæfell												
H136	0.703179	n.g	0.512994	n.g	18.56	n.g	15.48	n.g	38.21	n.g	-2.5	14.1
H140	0.703378	0.0014	0.513009	0.0007	-	-	-	-	-	-	-	-

Mean % standard errors: $^{87}Sr/^{86}Sr = 0.0013$; $^{143}Nd/^{144}Nd = 0.0006$; $^{206}Pb/^{204}Pb = 0.0111$; $^{207}Pb/^{204}Pb = 0.0109$; $^{208}Pb/^{204}Pb = 0.0346$

Figure 3.9: (a) $^{87}Sr/^{86}Sr$ *vs.* $^{143}Nd/^{144}Nd$, **(b)** $^{206}Pb/^{204}Pb$ *vs.* $^{207}Pb/^{204}P$, **(c)** $^{206}Pb/^{204}Pb$ *vs.* $^{208}Pb/^{204}Pb$, **(d)** $^{206}Pb/^{204}Pb$ *vs* $^{87}Sr/^{86}Sr$ and **(e)** $^{206}Pb/^{204}Pb$ *vs.* $^{143}Nd/^{144}Nd$, for samples from Snæfell and Öræfajökull. Additional data from Hards *et al.*, (1995; 2000) and Prestvik *et al.*, (2001) shown for comparison. Symbols as in Figure 3.2. Solid diagonal line represents the NHRL of Hart (1984).

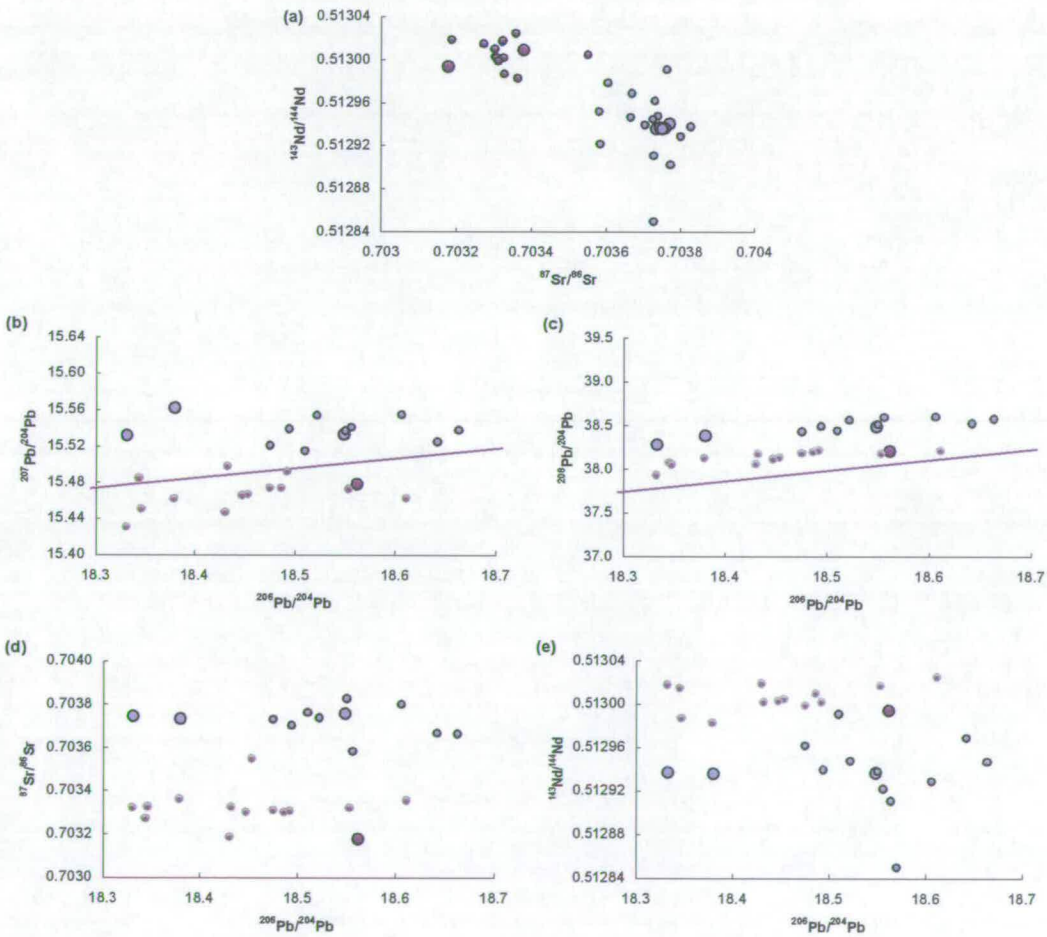

3.5 Discussion

The results demonstrate a clear isotopic distinction between the two volcanoes, with Öræfajökull displaying significantly higher $^{87}Sr/^{86}Sr$, $^{207}Pb/^{204}Pb$, $^{208}Pb/^{204}Pb$ and $^{3}He/^{4}He$ than Snæfell. The simplest interpretation of the trace element and isotope data is that the basalts are derived from isotopically distinct sources which have similar incompatible element ratios. However, it is possible that (i) the isotopic enrichment observed at Öræfajökull results from crustal contamination, or (ii) that the trace element ratios reflect crystallisation or melting processes rather than source composition. In order to examine the relationship between the two and to draw conclusions about the nature and number of enriched components in the EFZ it is necessary to evaluate the potential effects of crustal contamination, fractional crystallisation and melting on the trace element, major element and isotopic chemistry of the samples.

3.5.1.1 Assimilation of old Icelandic crust

The relatively high $^{87}Sr/^{86}Sr$ of the Öræfajökull basalts may be a result of assimilation of crustal rocks with radiogenic Sr. The basement rocks in Öræfajökull consist of tholeiites and minor silicic rocks produced in the extinct Reykjanes-Skagi rift around 10 Ma (Prestvik *et al.*, 1993). The basement tholeiites have $^{87}Sr/^{86}Sr$ compositions of 0.7031-0.7034, whereas the Quaternary basalts and andesites both have $^{87}Sr/^{86}Sr$ of ~0.7037 (this study; Prestvik *et al.*, 2001), so neither the andesites nor basalts can have been affected by assimilation of tholeiitic basement rock. Remelting and assimilation of silicic basement rocks with high Rb/Sr could increase $^{87}Sr/^{86}Sr$. In order to produce $^{87}Sr/^{86}Sr$ of 0.7037 from 13 Ma silicic rock with initial $^{87}Sr/^{86}Sr$ of 0.7032, the Rb/Sr of the silicic material would need to be >1.0 (Prestvik *et al.*, 2001). This is relatively high for Icelandic rhyolites (Oskarsson *et al.*, 1982), and the timescale involved is unrealistic. The re-melting and assimilation of silicic material would predict extremely low (radiogenic) $^{3}He/^{4}He$. $^{3}He/^{4}He$ as low as ~1 R_A have been observed elsewhere in Iceland and are generally associated with rhyolites or basaltic glasses that have been inferred to have undergone crustal contamination (e.g. Condomines *et al.*, 1983, Macpherson *et al.*, 2005).

The $^{3}He/^{4}He$ of the basalts may have been reduced from lower mantle plume-type ratios (~50 R_A) by assimilation of tholeiitic Icelandic crust. A reduction in olivine $^{3}He/^{4}He$ to EFZ values (6.5 – 8.0 R_A), requires more than 95 % crustal assimilation (see Section 2.5.3 for calculations). The absence of a relationship between $^{3}He/^{4}He$ and total He released by crushing provides strong evidence against contamination of high $^{3}He/^{4}He$ by crustal assimilation (Figure 3.8). Furthermore, such a contribution of crust would be evident in oxygen isotope data. Published olivine and whole-rock $\delta^{18}O$ data from the EFZ indicate that crustal contamination is negligible in both Snæfell and Öræfajökull (Hards *et al.*, 1995; Kokfelt *et al.*, *in press*; Sigmarsson *et al.*, 1992; Prestvik *et al.*, 2001). The $\delta^{18}O$ of EFZ basalts range from +4.9 to +5.7 ‰ and are comparable to the other flank-zones in Iceland (Condomines *et al.*, 1983; Kokfelt *et al.*, *in press*; Hardarson, 1993; Prestvik *et al.*, 2001; Sigmarsson *et al.*, 1992). They overlap and extend to values lower than minerals in equilibrium with N-MORB (+5.2 ± 0.3 ‰) but are within the range estimated for the Icelandic mantle (+4.9 to +5.5 ‰) (e.g., Mattey *et al.*, 1994; Gautason and Muelenbachs, 1998; Gee *et al.*, 1998; Thirlwall *et al.*, 1999; Eiler *et al.*, 2000a; 2000b; Kokfelt *et al.*, *in press*). Lower $\delta^{18}O$ (+2.0 to +4.8 ‰) measured in Iceland are generally associated with rift zone tholeiites and rhyolites and have been interpreted to indicate secondary hydrothermal alteration and interaction of primary magmas with hydrothermally altered crust (e.g., Condomines *et al.*, 1983; Hattori and Muelenbachs, 1982, Nicolson *et al.*, 1991). The higher $\delta^{18}O$ measured in the EFZ are therefore inconsistent with crustal contamination or secondary alteration.

3.5.1.2 Involvement of continental crust

Mesozoic and Palaeozoic age determinations of zircons collected from the Öræfajökull area suggest that a sliver of continental crust may be present beneath SE Iceland (Amundsen *et al.*, 2002) This might be related to the Jan Mayen microcontinent; a fragment of continental crust torn from the Greenland margin at 25 - 43 Ma (Foulger, 2004). The anomalously high $^{87}Sr/^{86}Sr$, $^{207}Pb/^{204}Pb$ and $^{208}Pb/^{204}Pb$ of the Öræfajökull rocks could result from involvement of underlying continental crust and associated sediments. Continental crustal contamination in Tertiary lavas from the North Atlantic Igneous Province is typically manifest in elevated Ce/Y and

Zr/Y at high SiO_2 (Fitton *et al.*, 1998; Dickin *et al.*, 1981). The two most evolved Öræfajökull samples analysed in this study (H52 & H54) have anomalously high Ce/Y and Zr/Y for their Nb/Zr but these samples do not have higher $^{87}Sr/^{86}Sr$ than the Öræfajökull basalts (Table 3.3, Figure 3.9).

As with contamination by oceanic crust, oxygen isotope data can be used to identify contamination by continental crust. Granitic rocks from the North Atlantic region, such as from southern Greenland, are characterised by elevated $\delta^{18}O$ (mean = +10.2 ; Brown *et al.*, 1999). If assimilation of continental material has occurred a positive correlation would exist between $\delta^{18}O$ and $^{87}Sr/^{86}Sr$ (James, 1981). Olivines from Öræfajökull sample H52, which is characterised by high SiO_2 and anomalous Ce/Y and Zr/Y, have been analysed for $\delta^{18}O$ by laser fluorination by J. Fiebig at Lausanne (see Kokfelt *et al.*, *in press*).The measured value of +4.91 ± 0.05 ‰ is at the lower end of the range previously reported for Öræfajökull (+5.0 to +5.7) (Sigmarsson *et al.*, 1992; Prestvik *et al.*, 2001) and is significantly lower than would be expected if continental crustal contamination had occurred.

3.5.1.3 Fractional crystallisation

In plots of MgO vs. major element or trace element concentrations, all basalt samples from the EFZ lie on crystallisation trends defined previously (Figures 3.3 and 3.5; Hards *et al.*, 1995; Prestvik *et al.*, 1982). The andesites H52 and H54 are displaced from the crystallisation trends despite having similar SiO_2 concentrations, possibly indicative of magma-mixing (as has previously been proposed for EFZ intermediate rocks; Hards *et al.*, 1995). Within the Öræfajökull suite however, the isotopic compositions of the basalts and andesites are identical within analytical uncertainty which suggests that the two suites are derived from the same source. Therefore, while the trace element and major element compositions of the andesites cannot be used to infer source compositions, the isotopic compositions of the andesites are unaffected by crystallisation or magma-mixing and can be used for source characterisation.

3.5.1.4 Melting processes

Major element oxide ratios such as CaO/Al_2O_3 were used in Chapter 2 to examine variations in the depth and extent of partial melting because, compared to trace element ratios, they are insensitive to source-variation (see Section 2.5.5). However, CaO/Al_2O_3 can not be used for the same purpose in this section as in the EFZ it varies with fractional crystallisation (Figure 3.4) Partial-melting modelling using Ce/Y and Nb/Zr suggests the Snæfell and Öræfajökull basalts contain similar proportions of garnet and have therefore been derived from similar depths in the melting column (Figure 3.10). In general, the Snæfell basalts plot at higher Ce/Y and lower Zr/Nb suggesting that they have formed from slightly smaller-degrees of melting of the same source. ΔNb values are the same for each volcano (ΔNb of Snæfell basalts = 0.15 – 0.29, n = 13; ΔNb of Öræfajökull basalts = 0.20 – 0.28, n = 8), also suggesting derivation from the same source.

Figure 3.10: Ce/Y- Zr/Nb diagram of EFZ basalts with modelled partial melting curves of garnet- and spinel-lherzolites (see Figure 2.24 for initial compositions and melting parameters). Symbols and data sources as in Figure 3.2.

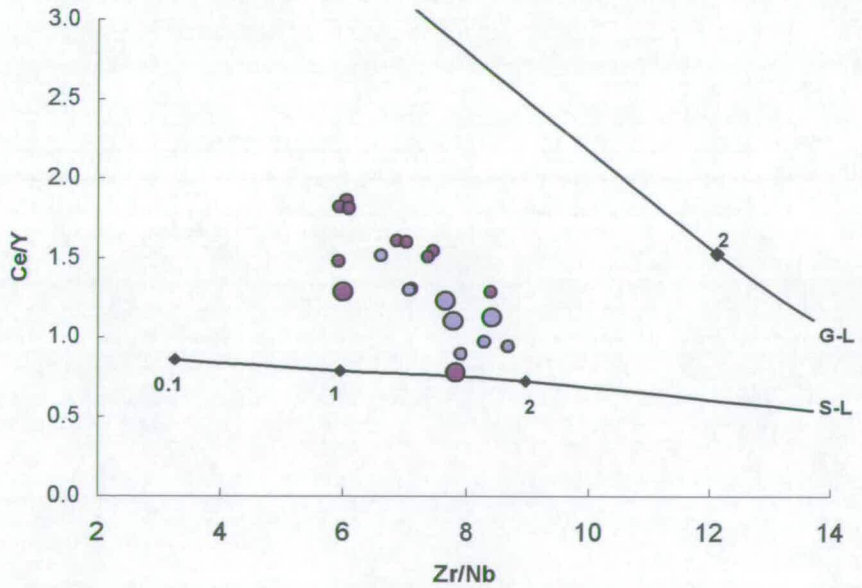

3.5.2 Source characterisation

Having ruled out contamination by Icelandic or continental crust and examined the effects of melting and fractional crystallisation on major and trace element compositions, the data can be used to constrain the number and nature of source components present in the EFZ mantle. The differences between Snæfell and Öræfajökull in $^{3}He/^{4}He$, $^{87}Sr/^{86}Sr$, $^{207}Pb/^{204}Pb$ and $^{208}Pb/^{204}Pb$ indicate the involvement of at least two components in the EFZ source. On the basis of the EFZ data alone however, it is difficult to determine whether or not the two volcanoes have source affiliation (i.e., if they are derived from mixtures involving common source components).

In Sr-Nd isotope space, the negative correlation in the EFZ as a whole suggests that the EFZ source compositions may be derived from mixing between two components (Figure 3.9a). The isotopically enriched component is characterised by extremely radiogenic $^{87}Sr/^{86}Sr$ (>0.70378) and low $^{143}Nd/^{144}Nd$. The more depleted component has lower $^{87}Sr/^{86}Sr$ and higher $^{143}Nd/^{144}Nd$ (and may be the component that is dominant in the rift-zone mantle source). In this mixing scenario, the Öræfajökull source contains a greater proportion of the enriched component than the Snæfell source.

In agreement with previous studies, the compositions of Öræfajökull and Snæfell basalts also differ significantly in Pb isotopes (Hards *et al.*, 2000; Prestvik *et al.*, 2001). On a plot of $^{206}Pb/^{204}Pb$ *vs.* $^{207}Pb/^{204}Pb$ the Öræfajökull samples are distinct from other Icelandic and North Atlantic basalts in that they plot above the NHRL of Hart (1984) (Figure 3.9b), suggesting the presence of a discrete enriched component in the Öræfajökull source. The Snæfell data appear to trend towards the Öræfajökull group. On a plot of $^{206}Pb/^{204}Pb$ *vs.* $^{208}Pb/^{204}Pb$, however, the data from the two volcanoes form distinct sub-parallel arrays, suggesting that the enriched Öræfajökull-type component is *not* involved in the generation of Snæfell isotopic compositions and that a second enriched component, characterised by lower $^{207}Pb/^{204}Pb$ and $^{208}Pb/^{204}Pb$ and higher $^{206}Pb/^{204}Pb$, must be invoked in Snæfell. Therefore, while Pb and Sr isotope ratios can be used to identify a distinct Öræfajökull enriched component, discerning relationships between the two volcanic centres on the basis of

these isotopes alone is problematic. Helium isotopes do not shed further light on mixing systematics with both volcanoes characterised by $^{3}He/^{4}He$ similar to or slightly lower than N-MORB (Figure 3.11).

Using Nd isotope ratios, which cannot be used to distinguish the Öræfajökull enriched component, the trend observed in Figure 3.9a suggests that a common depleted component with $^{143}Nd/^{144}Nd > 0.51302$ is tapped in the EFZ. This could be either the depleted component that is present in the rift-zone source, or it could also be the N-MORB component. The higher $^{143}Nd/^{144}Nd$ of Snæfell samples suggest its abundance is greatest in Snæfell. However, Snæfell samples are characterised by slightly lower $^{3}He/^{4}He$ than Öræfajökull, the opposite of the effect expected if the proportion of a depleted plume or MORB component is greatest in the Snæfell mantle.

In conclusion, the identification of mantle components and constraining the nature of source-mixing is difficult in the EFZ, in part due to a lack of significant chemical variation within the sample set. It is clear that the Öræfajökull volcano samples a extreme enriched mantle source, not seen elsewhere in Iceland, but it is difficult to determine the extent of its involvement in Snæfell. Pb isotope characteristics imply that it is not involved in the Snæfell source. The nature of depleted source in the EFZ is also difficult to constrain. It must have low Sr- and high Nd-isotope ratios, and $^{3}He/^{4}He$ greater than ~8 R_a, but it is not clear if it is a MORB-type or depleted plume component. Comparisons with data from the other flank-zones may aid the identification and characterisation of depleted mantle component(s) in the EFZ and this will be undertaken in Chapter 5.

Figure 3.11 $^{3}He/^{4}He$ *vs.* **(a)** $^{87}Sr/^{86}Sr$, **(b)** $^{143}Nd/^{144}Nd$ and **(c)** $^{206}Pb/^{204}Pb$ of samples from Snæfell and Öræfajökull. Symbols as in previous figures.

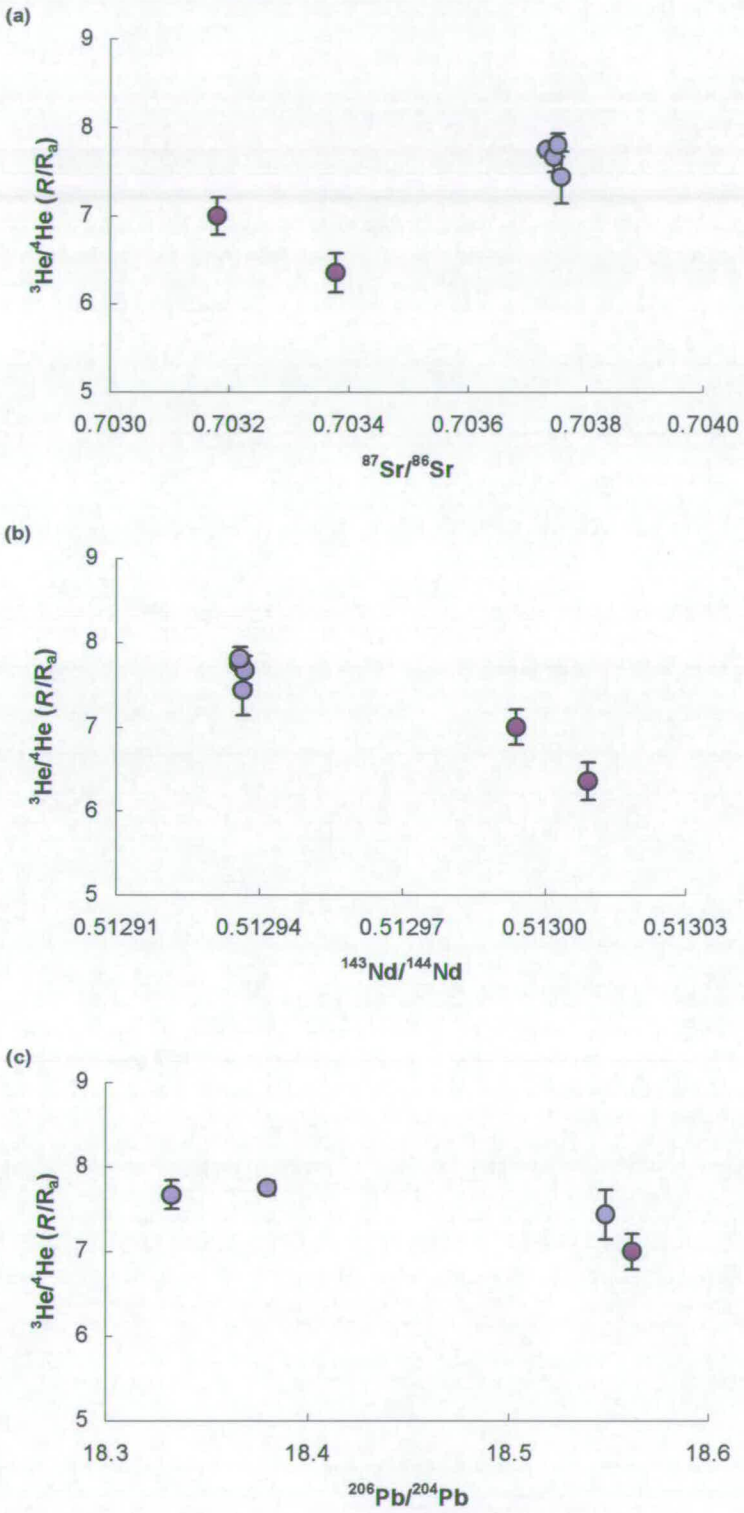

3.6 Summary

Isotopic data from Öræfajökull and Snæfell indicate the presence of at least two components in the EFZ source region; however, the compositions of the Öræfajökull rocks may have been affected by contamination. Contamination by old Icelandic crust can be excluded on the basis of trace element compositions, the low $^{87}Sr/^{86}Sr$ of basement rocks in the EFZ, the unradiogenic $^{3}He/^{4}He$ of Öræfajökull basalts and the relatively high $\delta^{18}O$ of the basalts. Oxygen isotope data also preclude significant assimilation of continental crust; a fragment of which has been postulated to underlie Öræfajökull. Consequently, the isotopic distinction between the two volcanoes is considered to be mainly the result of source-variation.

Fractional crystallisation can explain the more enriched nature of the Öræfajökull andesites, but does not explain the incompatible element enrichment of the EFZ basalts relative to rift zone tholeiites. Variation in the degree and depth of partial melting has been examined using incompatible trace element ratios of Öræfajökull and Snæfell basalts. Basalts from both volcanoes appear to be derived from small-degrees of partial melting of the same source.

Closer examination of the isotopic compositions of the Snæfell and Öræfajökull samples tentatively suggests the presence of two enriched components in the EFZ mantle. The Öræfajökull-type component is characterised by anomalously high $^{207}Pb/^{204}Pb$, $^{208}Pb/^{204}Pb$ for its $^{206}Pb/^{204}Pb$, and radiogenic $^{87}Sr/^{86}Sr$. The enriched component present in the Snæfell source is characterised by more radiogenic $^{206}Pb/^{204}Pb$. The differences in the $^{3}He/^{4}He$ of the Snæfell and Öræfajökull samples may simply reflect differing degrees of involvement of depleted MORB-type or plume-derived mantle in their sources. However, the presence of the Öræfajökull component as a discrete blob in the mantle cannot be ruled-out on the basis of the EFZ data alone.

Chapter 4

CHARACTERISATION OF CHEMICALLY ENRICHED BASALTS FROM THE SOUTHERN FLANK ZONE

4.1 Introduction

The Southern Flank Zone (SFZ) is the third flank zone considered in this study. It is located at the southern tip of the ERZ, and extends from Torfajökull in the north to Vestmannaeyjar in the south (Figure 4.1). Basalts from the SFZ are transitional to mildly alkaline and are enriched in incompatible elements compared to tholeiitic basalts from Veiðivötn and other fissure systems in the ERZ to the north (e.g., Jakobsson, 1979; Steinþórsson *et al.*, 1985; Furman *et al.*, 1991, 1995). SFZ basalts are characterised by more radiogenic $^{87}Sr/^{86}Sr$ and Pb-isotope compositions and less radiogenic $^{143}Nd/^{144}Nd$ than the depleted ERZ basalts (e.g., Meyer *et al.*, 1985; Furman *et al.*, 1991; 1995, Sigmarsson *et al.*, 1992; Stecher *et al.*, 1999). It has been proposed that the SFZ represents the propagating tip of the ERZ (Oskarsson *et al.*, 1982, 1985; Steinþórsson *et al.*, 1985; Meyer *et al.*, 1985) and that the observed gradation from tholeiitic through transitional (Fe-Ti-rich) to alkaline compositions results from interaction of primitive mantle-derived melts with altered basaltic crust (e.g., Oskarsson *et al.*, 1982, 1985). The absence of correlations between major elements and isotopes however, suggests that source heterogeneity plays an important role in the generation of the regional variation in the SFZ (e.g., Sigmarsson *et al.*, 1992; Hémond *et al.*, 1993; Furman *et al.*, 1995; Stecher *et al.*, 1999).

In this chapter, the He-Sr-Nd-Pb isotopic compositions of Quaternary SFZ volcanic rocks are determined and, in conjunction with trace and major element data, used to characterise the SFZ mantle sources. Regional geochemical variation is examined in order to assess the roles of partial melting and local tectonics on geochemical heterogeneity. In Chapter 5, the SFZ source compositions will be compared to those of the previous two flank zones studied in order to constrain the number, nature and origin of enriched mantle components in Iceland and the North Atlantic.

4.2 Geology of the Southern Flank Zone

The SFZ is located at the south-eastern end of the ERZ, which started propagating south from the NRZ at around 2-3 Ma ago (e.g., Sæmundsson, 1978; Johannesson, 1980) (Figure 4.1). The underlying basement rock is dominantly tholeiitic Icelandic oceanic crust produced in the WRZ at around 10 Ma (Jakobsson,

1979b). Crustal thickness along the SFZ decreases southerly from ~35km beneath the Vatnajökull ice-cap to around ~25 km beneath Vestmannaeyjar (Kaban *et al.*, 2002). The SFZ is bounded to the north by the Veiðivötn and Eldgjá fissure systems, the latter of which links the SFZ with the Grimsvötn system beneath the Vatnajökull ice-cap (Jakobsson, 1979b) (Figure 4.1). Basalts from Veiðivötn and Eldgjá are dominantly tholeiitic and relatively depleted in incompatible trace elements (e.g., Furman *et al.*, 1995). Recent volcanism in the SFZ is most likely a result of the southward propagation of the ERZ, however, it may also be in part related to incipient rifting in the EFZ (see Section 3.2).

The northernmost part of the SFZ is dominated by the Torfajökull volcanic complex (Figure 4.1). Torfajökull is the largest silicic eruptive site in Iceland and covers an area of around 400 km^2 up to elevations of ~1280m. The Torfajökull caldera was formed during the last glaciation and is approximately 12km in diameter. The volcanic system is considered to be a continuation of the Veiðivötn system to the north but can be distinguished petrologically by more alkaline compositions (e.g., Blake *et al.*, 1984). Rhyolitic lava flows and hyaloclastites comprise around 80% of the total volume of volcanic rocks in the region and only minor volumes of basaltic and intermediate lavas have erupted (McGarvie *et al.*, 1990).

The central part of the SFZ consists of the Katla, Tindfjöll, Eyjafjöll volcanic systems (Figure 4.1). The central volcanoes are partly submerged by the Mýdarsjökull, Tindfjallajökull and Eyjafjallajökull ice-caps, respectively. The Katla central volcano rises to ~1500m elevation. It has produced around 300 $km^3$of lava and hyaloclastite during the past 220 kyrs and the most recent eruption occurred in 1918. Historical activity is characterised by frequent eruptions, on average every 50 yrs. It has the largest caldera in Iceland with a volume of ~70 km^3 (Bjornsson, 1977; Sæmundsson, 1982; Bjornsson *et al.*, 1994). Its magma chamber has a volume of 10-12 km^3 and is situated at shallow depths of 1-1.5 km. The volcanic products are dominated (>90%) by aphyric Fe-Ti rich basalts, with minor volumes of rhyolites and tephra (e.g., Hildebrand, 1999; Jakobsson, 1979; Meyer *et al.*, 1985). The Eyjafjöll volcanic system is located to the west of the Katla system. It reaches elevations of 1668 m and has a 2.5 km wide caldera. The majority of volcanic activity at Eyjafjöll occurred during the last two glacial periods. Only one historical

eruption has occurred (1821-23). The volume of post-glacial lavas in the Eyjafjöll system is approximately 0.26 km^3 of which the majority are of intermediate compositions. Only ~0.006 km^3 of the lavas are basaltic (Jakobsson, 1979; Steinþórsson *et al.*, 1985). The Tindfjöll volcanic system is located to the north of the Eyjafjöll system and covers an area of ~360 km^2. The central volcano reaches a height of 1460m and has a 5 km-wide caldera. The volcano has been active since 0.8 Ma but only one eruption occurred during the Holocene, and none have been recorded in historic times. The volcanic products associated with the Tindfjöll system consist of rhyolitic lava flows and basaltic to intermediate hyaloclastite (Jóhannesson, 1998).

The Vestmannaeyjar archipelago forms a 40 km-long volcanic system in the southernmost part of the SFZ (Figure 4.1). It is comprised of around 18 islands, the largest two being Heimaey (13.5 km^2) and Surtsey (~1.8 km^2), and a number of small seamounts. Post-glacial volcanism has been of low intensity and four volcanic episodes are tentatively suggested to have occurred since late upper Pleistocene. Two historic eruptions have occurred; the 1973 eruption of Eldfell on Heimaey and the 1963-67 submarine eruption and formation of the island of Surtsey. Post-glacial volcanic rocks are dominated by mildly alkaline, olivine-phyric basalts. The total volume of the alkaline basalts of post-glacial age is greater than 3.2 km^3 whereas the volume of intermediate products is 0.25 km^3.

4.3 Sample descriptions

Sample collection in the SFZ was restricted by the glaciated terrain, lack of access roads and paucity of olivine-phyric basaltic flows. One post-glacial sample was collected from the Stórhöfði Peninsula, Heimaey (Vestmannaeyjar) and two additional samples, from Heimaey and Surtsey, were donated by Kaj Hoernle (GEOMAR, Kiel) and John Faithfull (University of Glasgow). In addition, two samples from the northern and southern flanks of Eyjafjöll were donated by Kaj Hoernle. Sample localities are presented in Figure 4.1 and detailed in Table 4.1. Sample descriptions are presented in Appendix 1.2.

Figure 4.1: Simplified map of the SFZ illustrating locations referred to in text and sample localities.

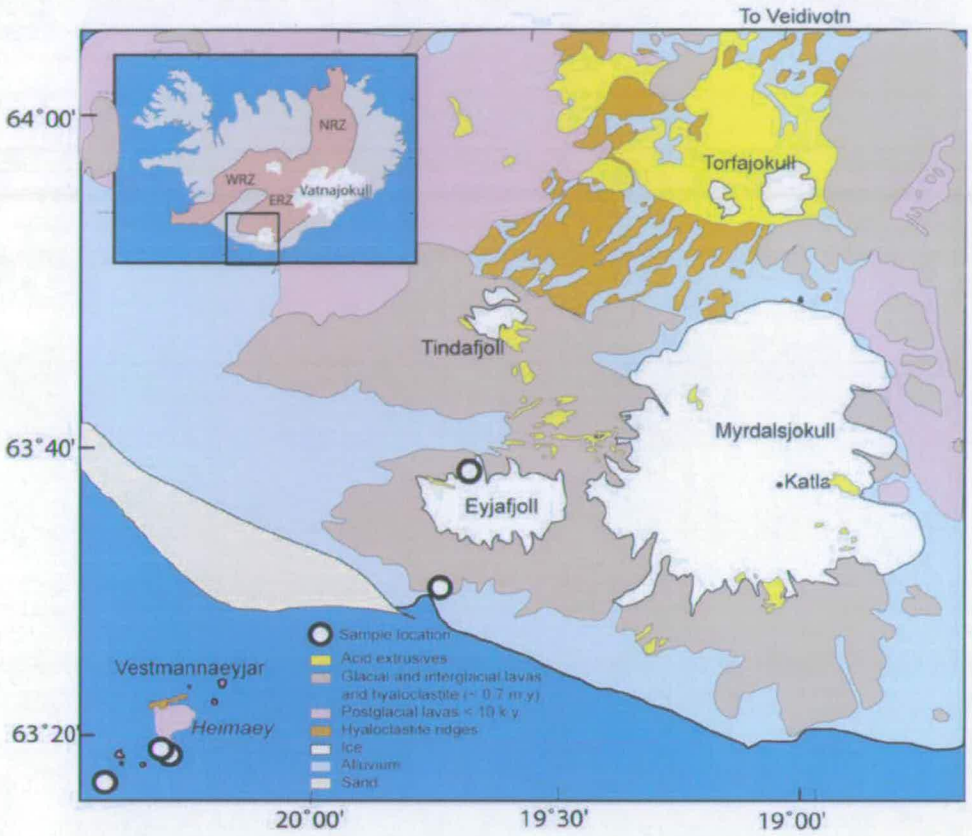

Table 4.1: Details of samples collected from the SFZ

Region	Sample Name	Location	Approximate Age
Vestmannaeyjar	AW31	Heimaey - Storhofdi,	6000 yrs
	H119	Heimaey - Storhofdi: lower section[1]	6000 yrs
	R23684	Surtsey - beach sand	Historic (1965-1967 eruptions)
Eyjafjöll	H76	Hvammsmuli	Glacial/interglacial
	H78	Seljalandfoss[1]	Post-glacial

[1] Locality details from K. Hoernle, *pers. comm*

4.4 Results

Major and trace element concentrations, helium isotope compositions and lithophile element isotope compositions were determined using the procedures outlined in Appendix 2. Major and trace element concentrations (H119, H76, H78) and Sr, Nd and Pb isotope ratios (H119, H76) for samples donated by Kaj Hoernle were determined by XRF and TIMS at GEOMAR following the procedures outlined in Kokfelt *et al.*, (*in press*). All results are presented in Tables 4.2 to 4.4.

4.4.1 Major elements

Major element oxide concentrations are presented in Table 4.2. On the TAS rock classification diagram, all samples from this study straddle the alkaline-subalkaline boundary and are basalts, with the exception of H78 from Eyjafjöll which is an andesite (according to the nomenclature of Le Maitre, 1979) (Figure 4.2). Data from previous studies of Vestmannaeyjar (Jakobsson, 1973, 1979; Steinþórsson *et al.*, 1985; Hemond *et al.*, 1993; Mattson *et al.*, 2003), Eyjafjöll (Jakobsson, 1979; Steinþórsson *et al.*, 1985) and Torfajökull and Katla (Jakobsson, 1979; Meyer *et al.*, 1985; McGarvie *et al.*, 1990; Macdonald *et al.*, 1990; Steinþórsson *et al.*, 1985) are shown for comparison. A south-north gradation from alkaline to transitional compositions is observed. Major element concentrations and ratios are plotted against MgO wt. % in Figures 4.3-4.4. The SFZ data from each region fall on trends defined by the published data. North-south regional variation in major element geochemistry is observed. The Eyjafjöll and Katla volcanic rocks have higher concentrations of P_2O_5, TiO_2 and Fe_2O_3 at any MgO concentration than Vestmannaeyjar and Torfajökull. Na_2O and Al_2O_3 concentrations are highest in Vestmannaeyjar, and SiO_2 and K_2O concentrations are highest in Torfajökull. Vestmannaeyjar lavas have lower CaO/Al_2O_3 than Eyjafjöll, Torfajökull and Katla, and Katla rocks have the lowest CaO/TiO_2 and Na_2O/TiO_2.

Table 4.2: Major element oxide concentrations of EFZ samples

Sample	SiO_2	TiO_2	Al_2O_3	Fe_2O_3	MnO	MgO	CaO	Na_2O	K_2O	P_2O_5	Mg#
	Wt. %	wt. %	wt. %	wt. %	wt. %	wt. %	wt. %	wt. %	wt. %	wt. %	
South - Vestmannaeyjar											
H119	46.29	1.63	14.51	12.23	0.18	11.15	11.60	1.95	0.29	0.17	67.99
AW31	45.82	1.63	15.04	12.4	0.19	11.16	10.88	2.33	0.35	0.16	66.38
R23684	45.91	1.96	14.27	13.5	0.20	11.22	9.50	2.783	0.44	0.23	64.67
North – Eyjafjöll											
H76	46.52	2.19	10.97	12.28	0.18	14.10	11.53	1.58	0.39	0.26	72.80
H78	54.50	2.12	15.13	11.87	0.22	2.93	6.92	4.13	1.49	0.68	36.52

Note: All data corrected for loss on ignition.

Mg# = 100MgO/(MgO+FeO) (mol.); FeO = 0.9 $Fe_2O_3^t$

Figure 4.2 Total alkalis *vs.* silica diagram of SFZ samples. Diagonal line represents the alkaline-subalkaline division of Hawaiian basalts from MacDonald and Katsura (1964).
Key (south to north) - Blue: Vestmannaeyjar. Yellow: Eyjafjöll & Tindafjöll. Purple: Katla. Orange: Torfajökull. Large circles: this study. Small circles: published data (see text for references).

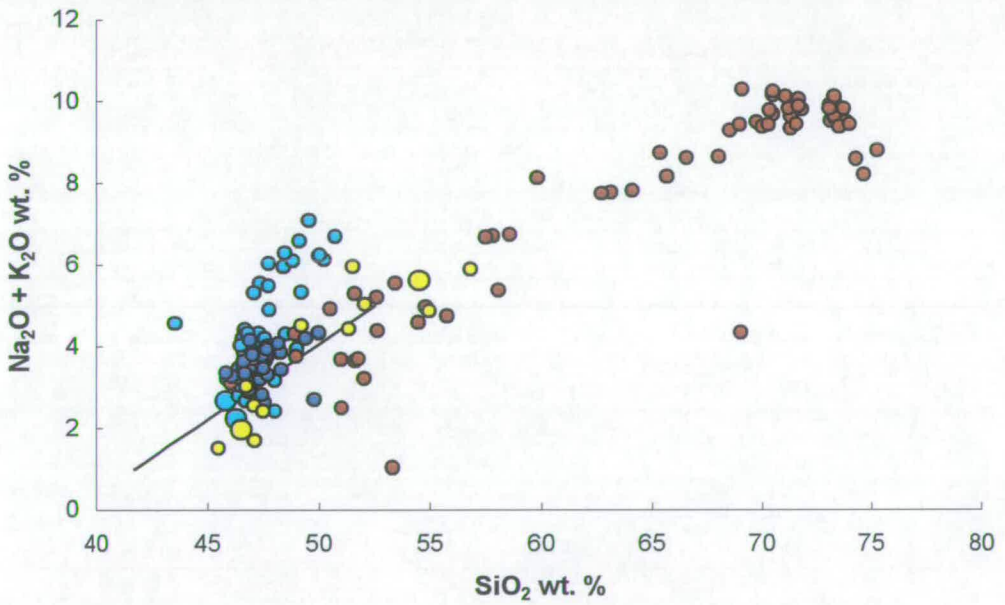

Figure 4.3 MgO (wt. %) vs. major element oxide concentrations (wt. %)

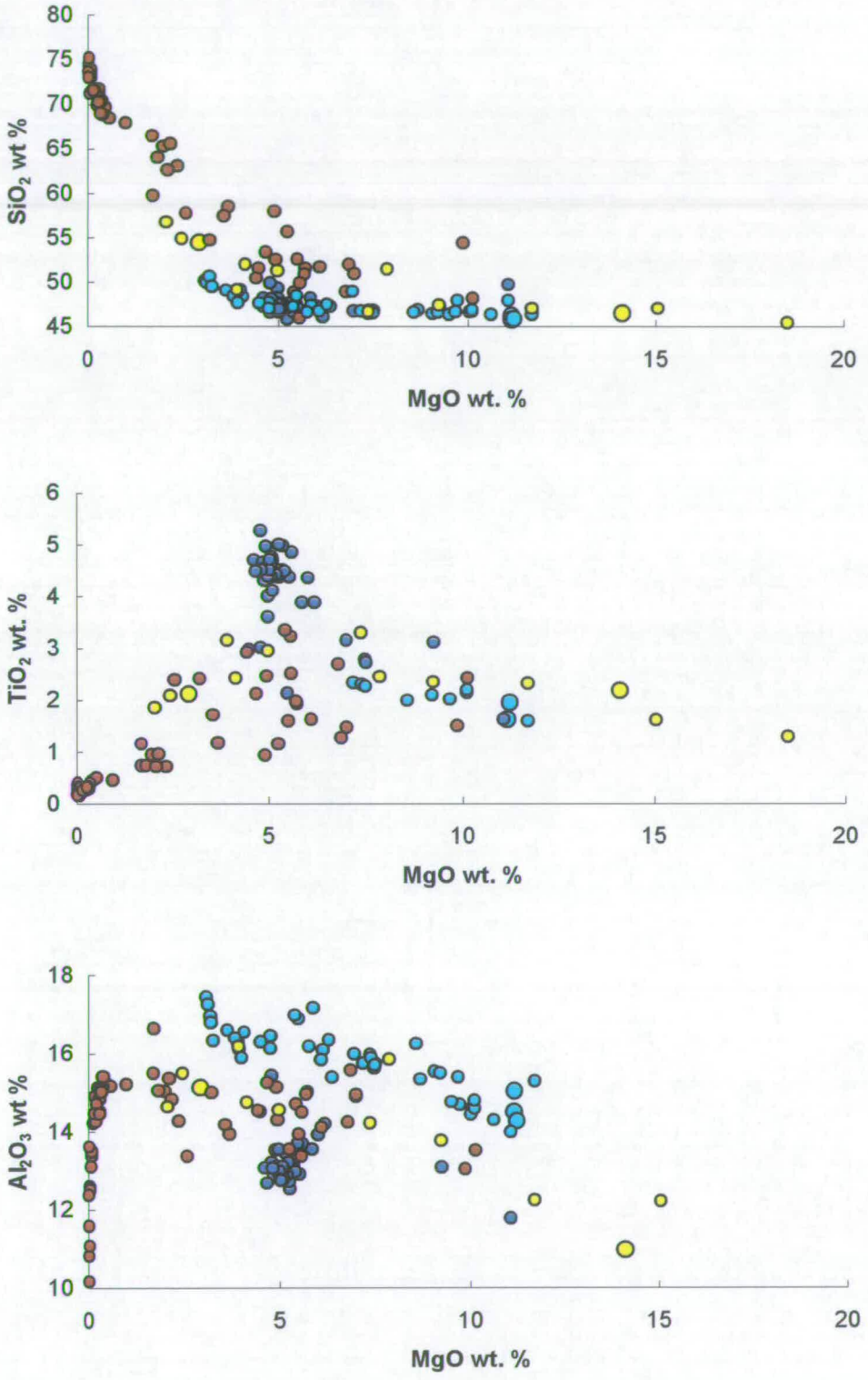

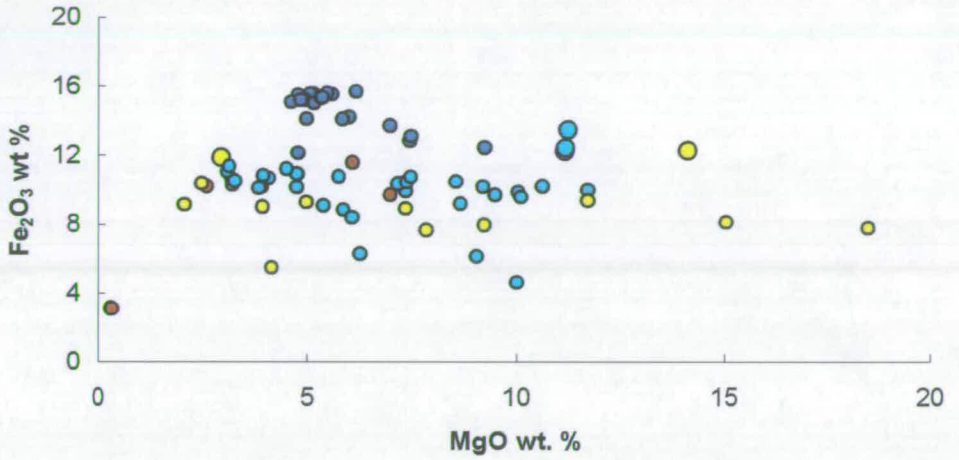
20
16
12
8
4
0
Fe_2O_3 wt %
0
5
10
15
20
MgO wt. %

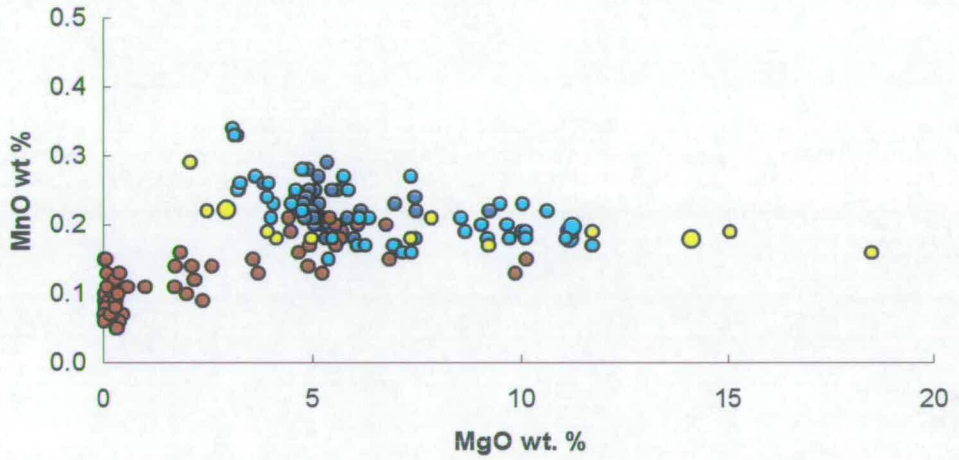
0.5
0.4
0.3
0.2
0.1
0.0
MnO wt %
0
5
10
15
20
MgO wt. %

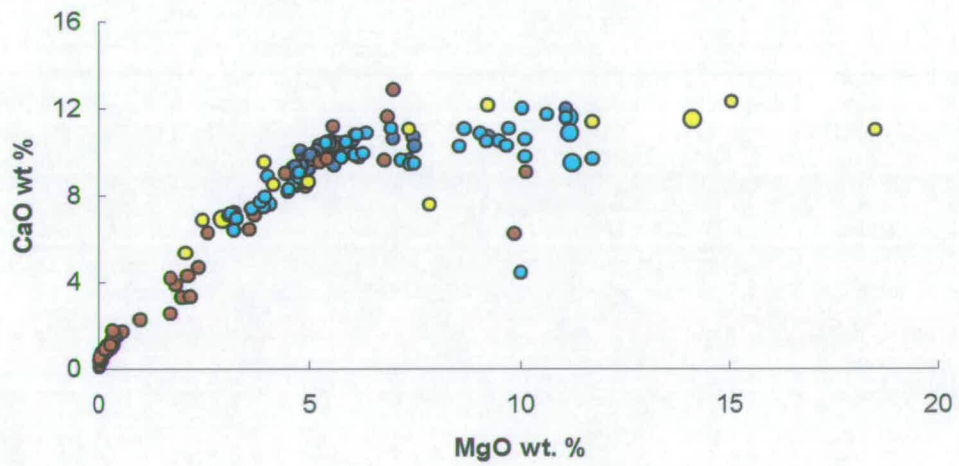
16
12
8
4
0
CaO wt %
0
5
10
15
20
MgO wt. %

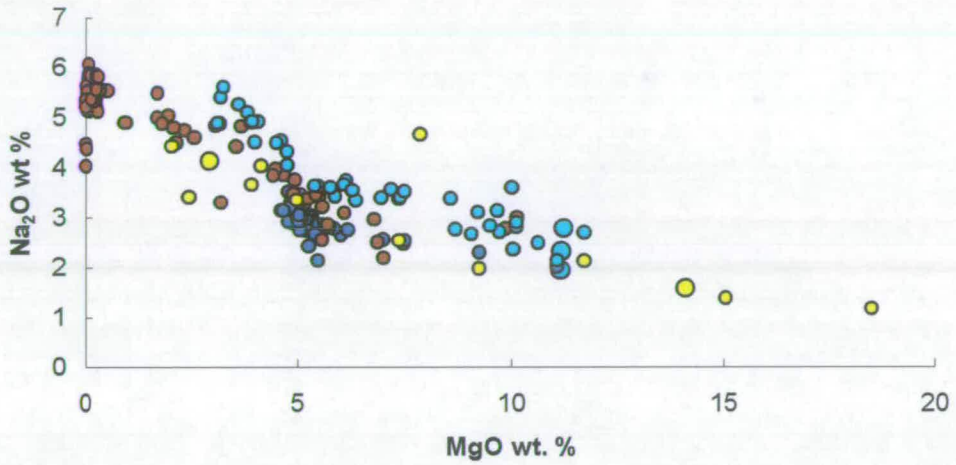
7
6
5
4
3
2
1
0
Na_2O wt %
0
5
10
15
20
MgO wt. %

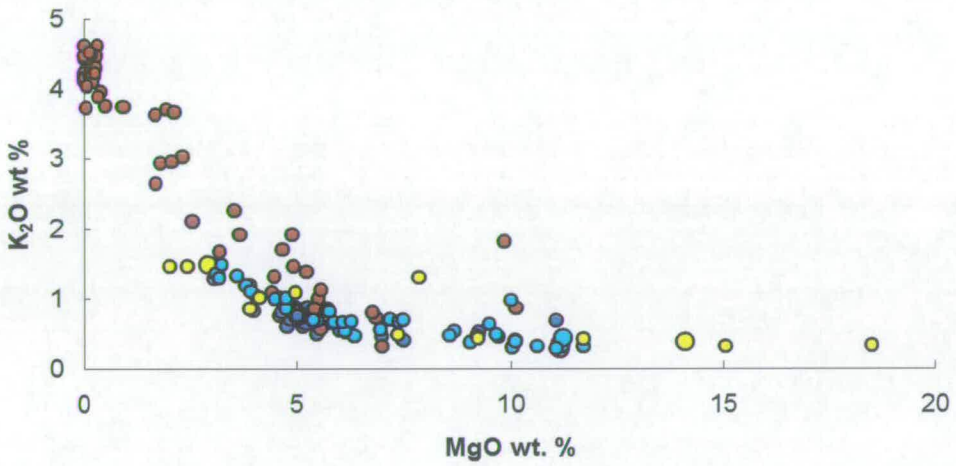
5
4
3
2
1
0
K_2O wt %
0
5
10
15
20
MgO wt. %

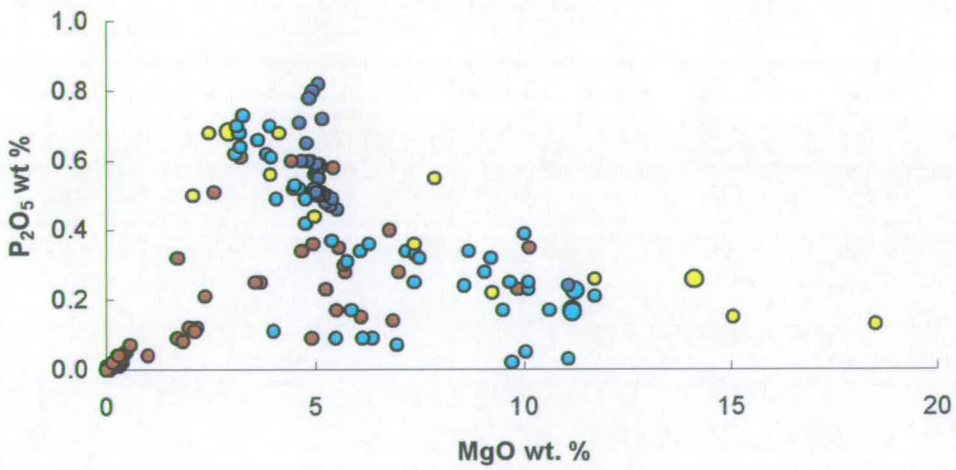
1.0
0.8
0.6
0.4
0.2
0.0
P_2O_5 wt %
0
5
10
15
20
MgO wt. %

Figure 4.4 MgO *vs.* major oxide ratios of SFZ basalts (MgO > 5 wt. %)

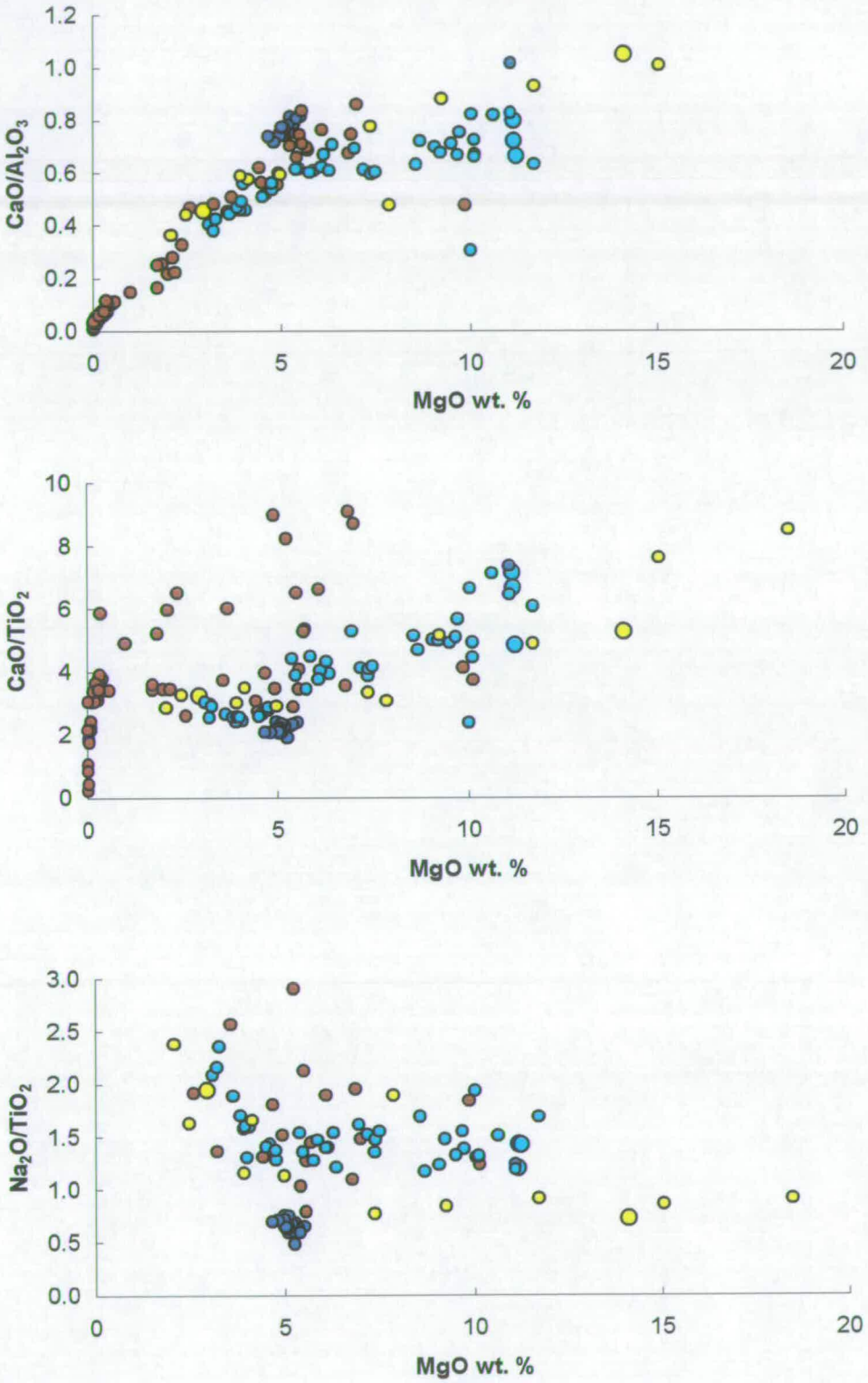

4.4.2 Trace elements

Trace element data are presented in Table 4.3 and Figures 4.5-4.6, with published data from the SFZ shown for comparison (Jakobsson, 1972; O'Nions *et al.*, 1973; Meyer *et al.*, 1985; McGarvie *et al.*, 1990; Macdonald *et al.*, 1990; Furman *et al.*, 1991; Hardarson, 1993; Gunnarsson *et al.*, 1998). The trace element concentrations and ratios of the SFZ samples are in close agreement with the previously published data for each region. Incompatible trace element concentrations increase with decreasing MgO and the Eyjafjöll andesite H78 has the highest concentrations of incompatible trace elements of the samples used in this study, consistent with its lower MgO content (Figure 4.5). The Eyjafjöll samples have similar trace element compositions to the Torfajökull data and basalts from both regions have higher incompatible trace element abundances than those from Vestmannaeyjar. Positive correlations are observed between different VICE/MICE (Figure 4.6). The Torfajökull data form the high VICE/MICE end of the Ce/Y-Nb/Zr array and Vestmannaeyjar basalts comprise the low end. The Eyjafjöll basalt of this study falls in the centre of the array.

Table 4.3: Trace element concentrations of EFZ samples

Sample	Ba	Ce	Cr	La	Nb	Nd	Ni	Rb	Sr	V	Y	Zn	Zr
	ppm	ppm	ppm	ppm	ppm	ppm	ppm	ppm	ppm	ppm	ppm	ppm	ppm
South - Vestmannaeyjar													
H119	89.00	20.00	611.00	8.78	11.00	nd	266.00	6.00	244.00	286.00	23.00	75.00	96.00
AW31	86.71	22.42	663.00	10.00	11.67	15.03	276.44	6.29	252.67	275.20	25.00	80.17	104.82
R23684													
North – Eyjafjöll													
H76	114.00	40.00	666.00	14.00	17.00	-	309.00	12.00	270.00	283.00	24.00	87.00	126.00
H78	337.00	146.00	49.00	55.00	53.00	-	15.00	36.00	427.00	139.00	62.00	158.00	469.00

Figure 4.5 Trace element concentrations (ppm) vs. MgO (wt. %)

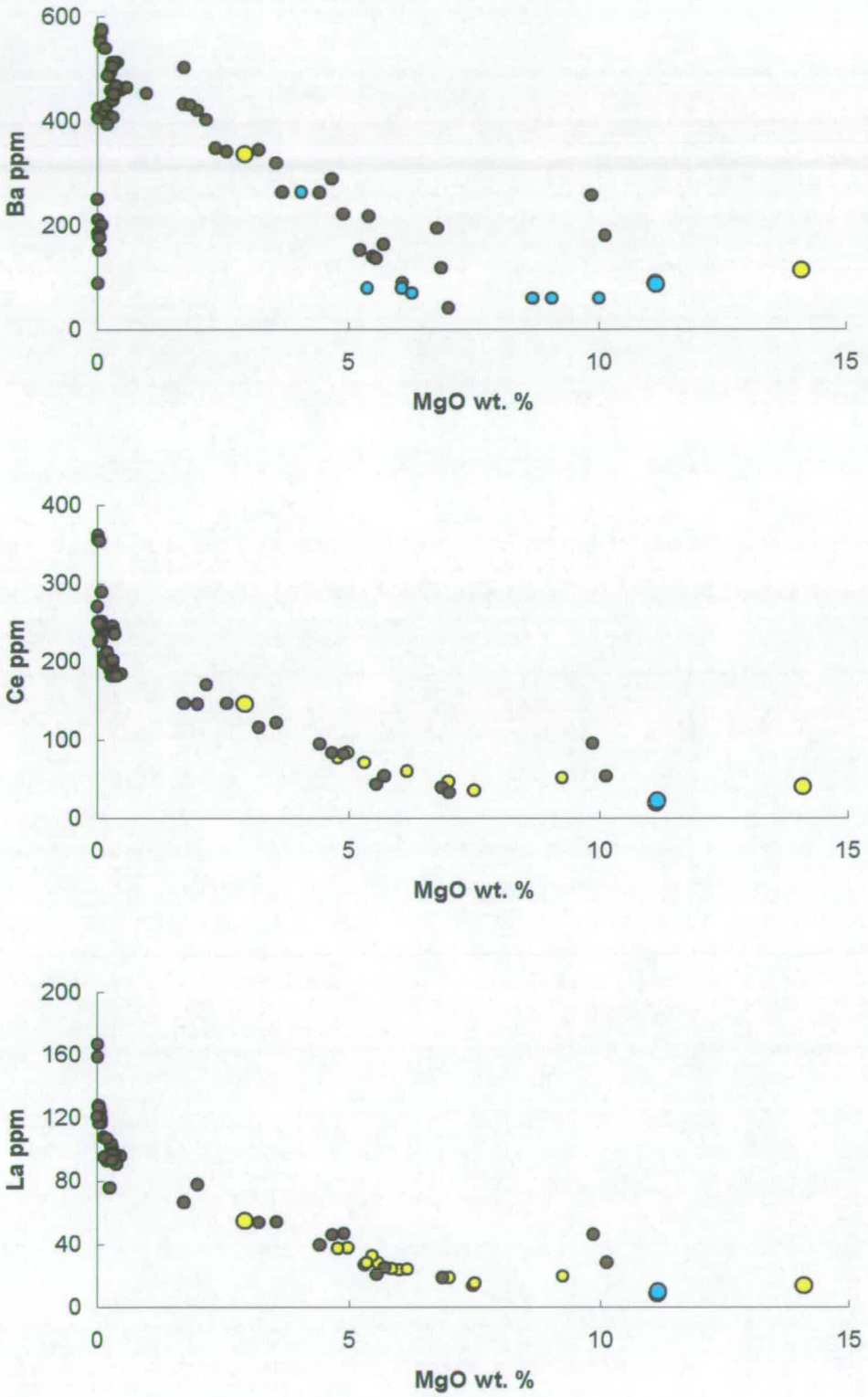

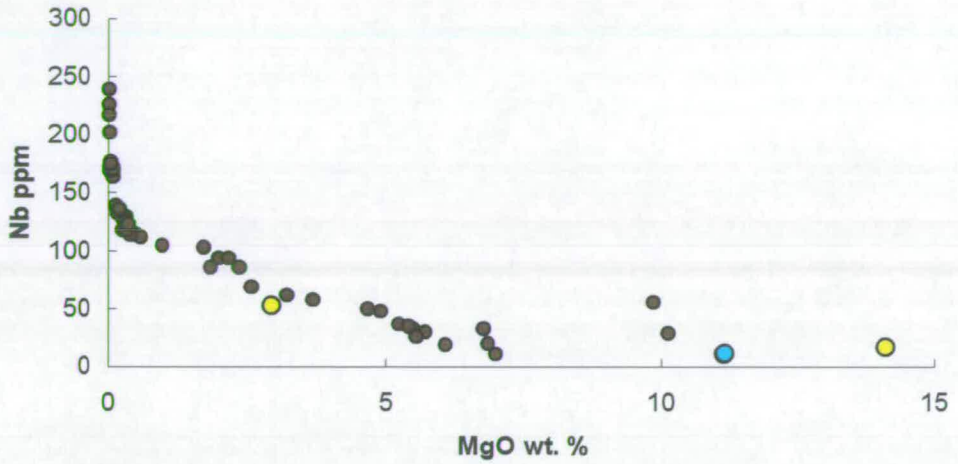
300
250
200
150
100
50
0
Nb ppm
0
5
10
15
MgO wt. %

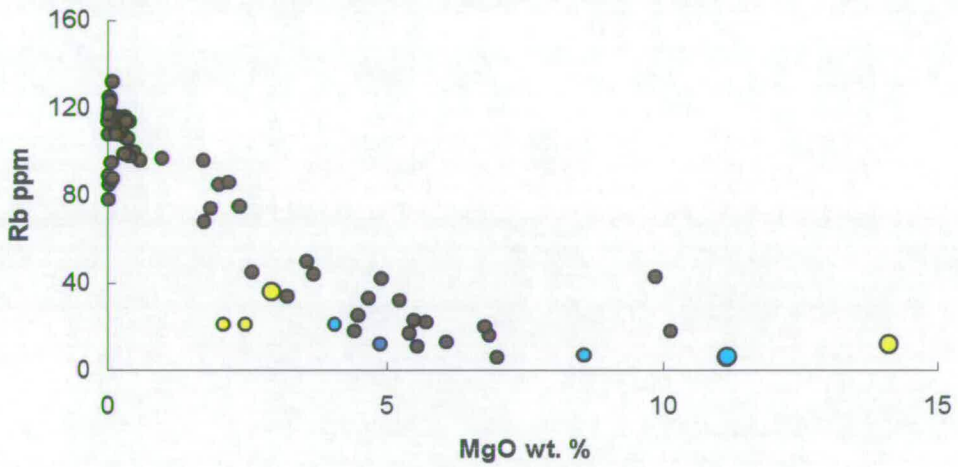
160
120
80
40
0
Rb ppm
0
5
10
15
MgO wt. %

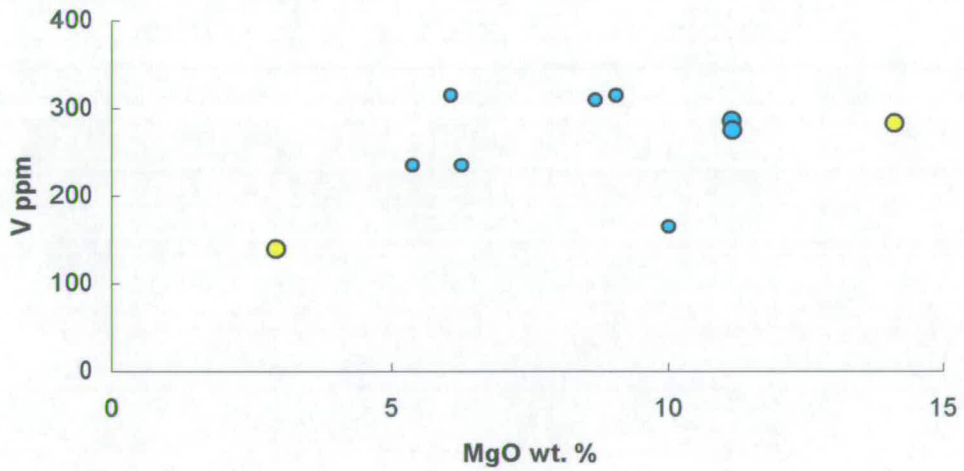
400
300
200
100
0
V ppm
0
5
10
15
MgO wt. %

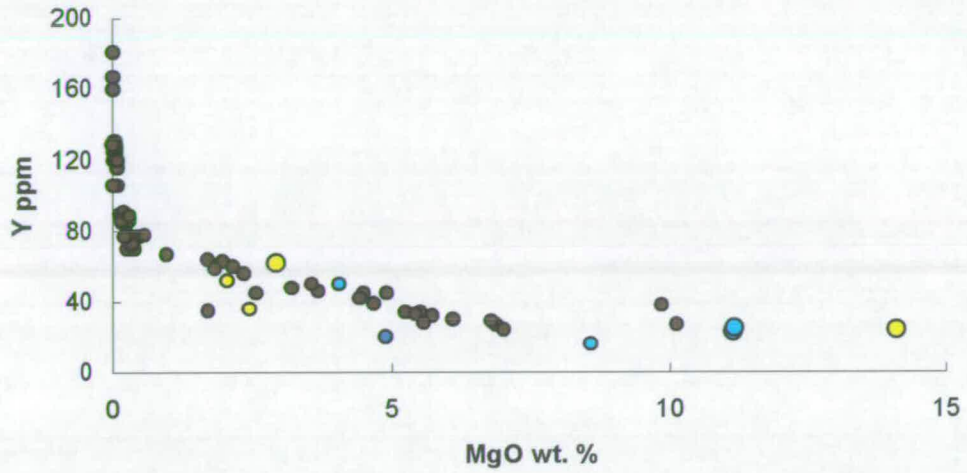
200
160
120
80
40
0
Y ppm
0
5
10
15
MgO wt. %

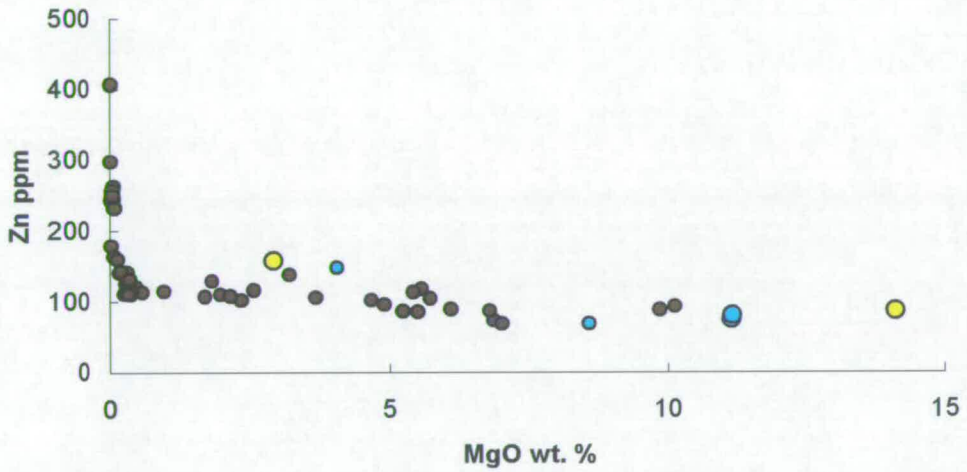
500
400
300
200
100
0
Zn ppm
0
5
10
15
MgO wt. %

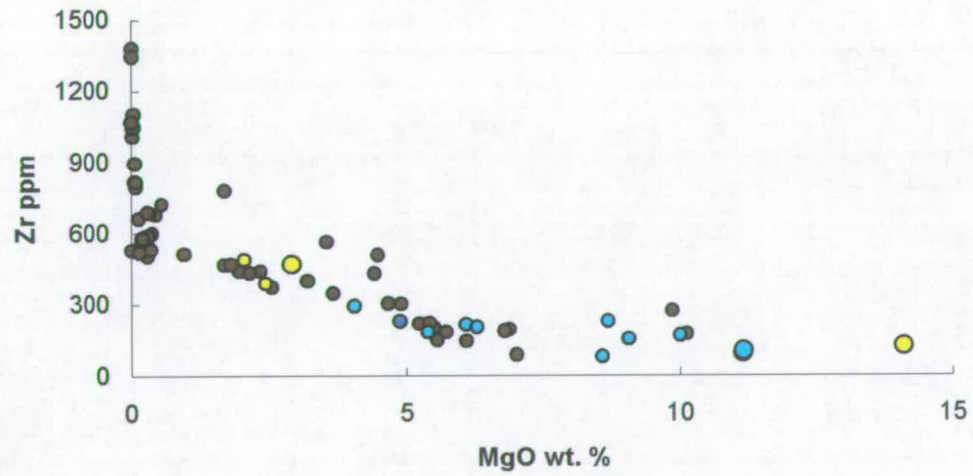
1500
1200
900
600
300
0
Zr ppm
0
5
10
15
MgO wt. %

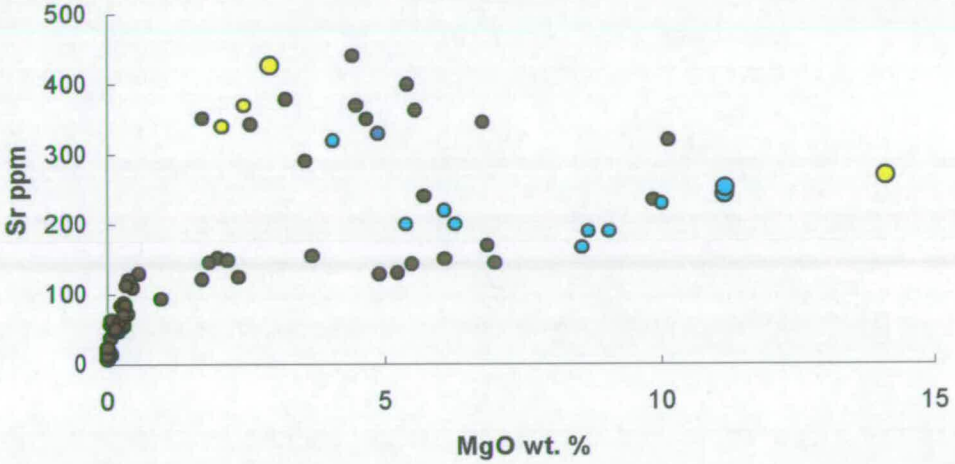
500
400
300
200
100
0
Sr ppm
0
5
10
15
MgO wt. %

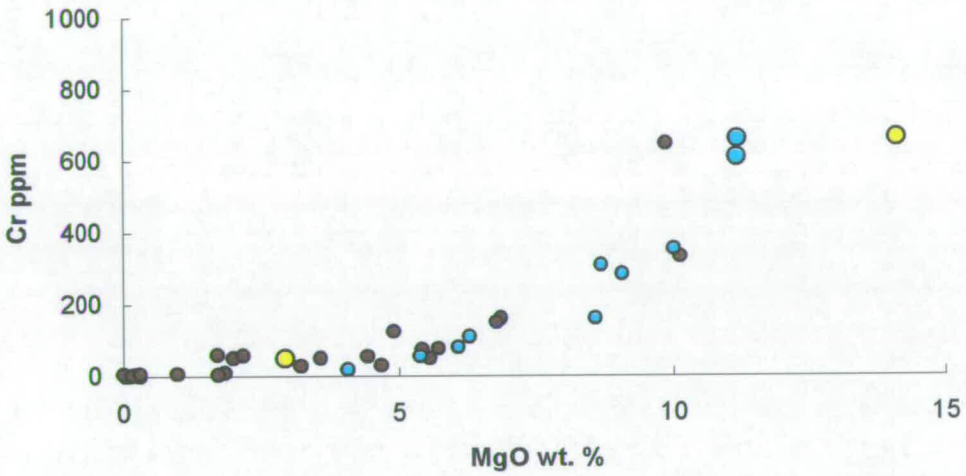
1000
800
600
400
200
0
Cr ppm
0
5
10
15
MgO wt. %

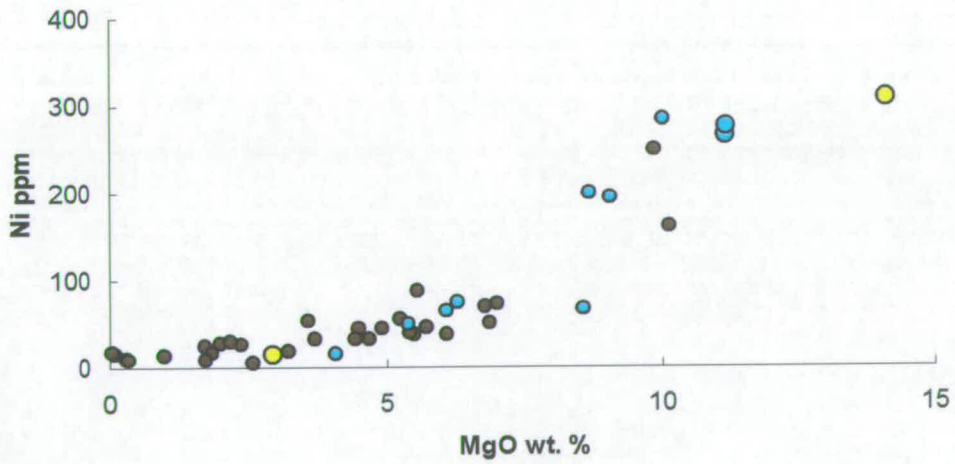
400
300
200
100
0
Ni ppm
0
5
10
15
MgO wt. %

Figure 4.6 Ce/Y *vs.* Nb/Zr for SFZ basalts (MgO > 5 wt. %)

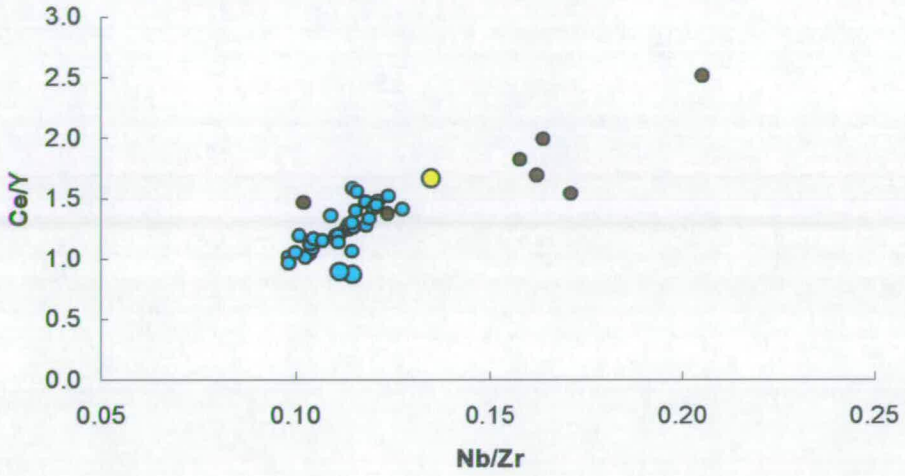

4.4.3 Helium isotopes

Helium concentrations and isotope ratios of olivine and pyroxene phenocrysts are presented in Table 4.4 and Figure 4.7. Helium extracted by *in vacuo* crushing ranged from 0.17 to 8.65 × 10^{-9} cc STP. $^{3}He/^{4}He$ range from 17.3 to 19.7 R_A in Eyjafjöll and 13.2 to 15.5 R_A in Vestmannaeyjar. In sample H76 the $^{3}He/^{4}He$ of pyroxenes (14.76 ± 1.74) are lower than co-genetic olivines (17.29 ± 0.42). H78 olivines have low He contents (<1 × 10^{-9} cc STP) but notably have the highest $^{3}He/^{4}He$ measured in this study (19.65 ± 2.30), which is also within error of H76 olivines. Eyjafjöll olivines have higher $^{3}He/^{4}He$ than Vestmannaeyjar olivines. The Vestmannaeyjar $^{3}He/^{4}He$ are slightly higher than a previous olivine measurement (~11.0 R_A; Kurz *et al.*, 1985). A single published olivine measurement from Pjorsadalur near Eyjafjöll yielded 18.3 R_a (Macpherson *et al.*, 2005), similar to the data from this study. $^{3}He/^{4}He$ of the olivines from Eyjafjöll are lower than subglacially erupted basaltic glasses from Hrauneyjarfoss (21.3 ± 0.2; Condomines *et al.*, 1983) and Sigalda (20.8; Breddam *et al.*, 2000) in the northern part of the flank-zone, and Thrihyrningur (26.2; Breddam *et al.*, 2000) farther south.

Table 4.4: Helium isotope data from crush extractions of olivine and pyroxene phenocrysts.

Volcanic centre	Sample	Mineral	^{4}He 10^{-9} cc STP *	±	^{4}He blank %	^{3}He blank %	^{3}He/^{4}He R_A	±
Vestmannaeyjar	H119	Olivine	8.65	0.064	0.14	0.07	14.07	0.23
	AW31	Olivine	2.10	0.073	0.53	0.73	13.20	0.33
	R23684	Olivine	4.85	0.066	0.26	0.11	15.52	0.28
Eyjafjöll	H76	Olivine	1.94	0.066	0.85	0.47	17.29	0.42
		Pyroxene	0.30	0.045	4.14	4.59	14.76	1.74
	H78	Olivine	0.17	0.064	5.66	2.78	19.65	2.30

* Corrected for atmospheric ^{4}He and analytical blanks (Appendix 2)

Figure 4.7 Total ^{4}He concentrations (released by crushing) *vs.* ^{3}He/^{4}He for SFZ olivines (squares) and pyroxenes (circles).

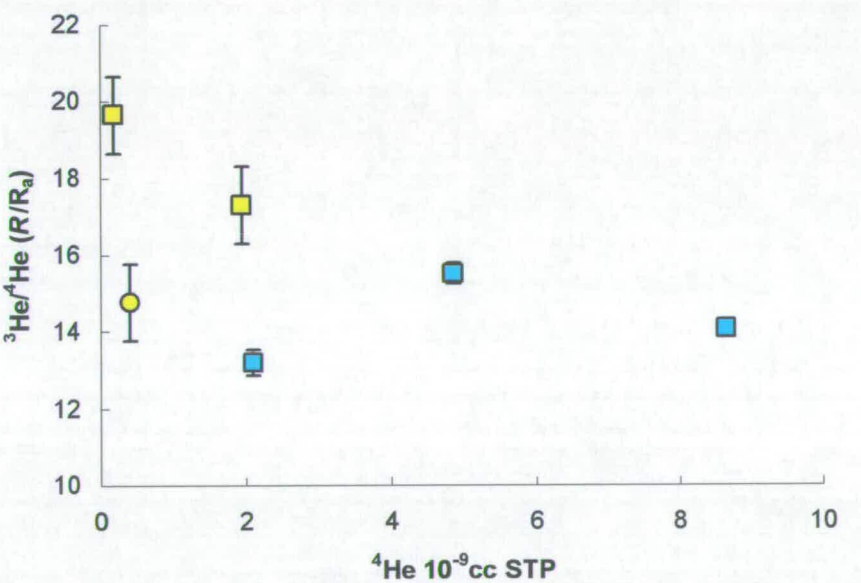

4.4.4 Sr, Nd and Pb isotopes

Sr, Nd and Pb isotope data are presented in Table 4.5 and in Figures 4.8-4.9. ^{87}Sr/^{86}Sr range from 0.703309 to 0.703312 in Eyjafjöll and from 0.70314 to 0.70317 in Vestmannaeyjar. ^{143}Nd/^{144}Nd range from 0.51298 to 0.51299 in Eyjafjöll and from 0.51301 to 0.51302 in Vestmannaeyjar. Of the samples analysed for Pb isotope ratios ^{206}Pb/^{204}Pb = 18.98, ^{207}Pb/^{204}Pb = 15.53 and ^{208}Pb/^{204}Pb = 38.57 in Vestmannaeyjar

(n=1) and $^{208}Pb/^{204}Pb$ = 19.18 - 19.19, $^{207}Pb/^{204}Pb$ = 15.54 - 15.55, $^{206}Pb/^{204}Pb$ = 38.80 - 38.81 in Eyjafjöll (n=2). $^{87}Sr/^{86}Sr$, $^{143}Nd/^{144}Nd$ and Pb isotope ratios for both volcanic systems are in agreement with previous measurements from the SFZ (Figure 4.9) (Gunnarsson *et al.*, 1998; Stecher *et al.*, 1999; Sigmarsson *et al.*, 1992; Furman *et al.*, 1995; Hémond *et al.*, 1993; Macdonald *et al.*, 1990). Eyjafjöll Sr-Nd-Pb isotope compositions are within the range of Torfajökull and are characterised by more radiogenic $^{87}Sr/^{86}Sr$, $^{206}Pb/^{204}Pb$, $^{207}Pb/^{204}Pb$ and $^{208}Pb/^{204}Pb$, and less radiogenic $^{143}Nd/^{144}Nd$ than Vestmannaeyjar. In Sr-Nd and Pb isotope space, the Vestmannaeyjar and Eyjafjöll/Torfajökull samples form separate clusters (Figure 4.9). Both Vestmannaeyjar and Eyjafjöll/Torfajökull are characterised by negative Δ7/4 and Δ8/4, however, the Eyjafjöll samples have slightly less-negative Δ7/4 and Δ8/4 than the Torfajökull samples of Stecher *et al.*, 1999 (Figure 4.9).

Table 4.5: Sr, Nd and Pb isotope compositions of EFZ samples

Sample	$^{87}Sr/^{86}Sr$	±	$^{143}Nd/^{144}Nd$	±	$^{206}Pb/^{204}Pb$	±	$^{207}Pb/^{204}Pb$	±	$^{208}Pb/^{204}Pb$	±	Δ7/4	Δ8/4
South - Vestmannaeyjar												
H119*	0.703171		0.513016		18.98		15.53		38.57		-1.93	-0.78
AW31	0.703143		0.513011		-	-	-	-	-	-	-	-
R23684	0.703171		0.513018		-	-	-	-	-	-	-	-
North – Eyjafjöll												
H76*	0.703312		0.512980		19.18		15.54		38.80		-3.14	-1.58
H78	0.703309		0.512989		19.19		15.55		38.81		-2.40	-2.02

* Sr, Nd and Pb isotope analyses by F. Hauff, GEOMAR

Mean % standard errors: $^{87}Sr/^{86}Sr$ = 0.0011; $^{143}Nd/^{144}Nd$ = 0.0006; $^{206}Pb/^{204}Pb$ = 0.0111; $^{207}Pb/^{204}Pb$ = 0.0109; $^{208}Pb/^{204}Pb$ = 0.0246

Figure 4.8 $^{87}Sr/^{86}Sr$ *vs.* $^{143}Nd/^{144}Nd$. Symbols as in Figure 4.2. See text for sources of published data.

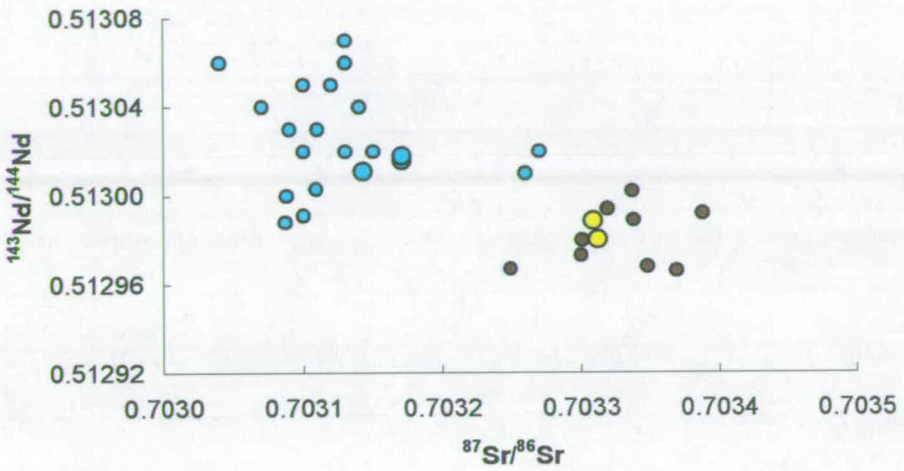

Figure 4.9 $^{206}Pb/^{204}Pb$ *vs.* (a) $^{207}Pb/^{204}Pb$ and (b) $^{208}Pb/^{204}Pb$. Diagonal line marks the NHRL of Hart (1984).

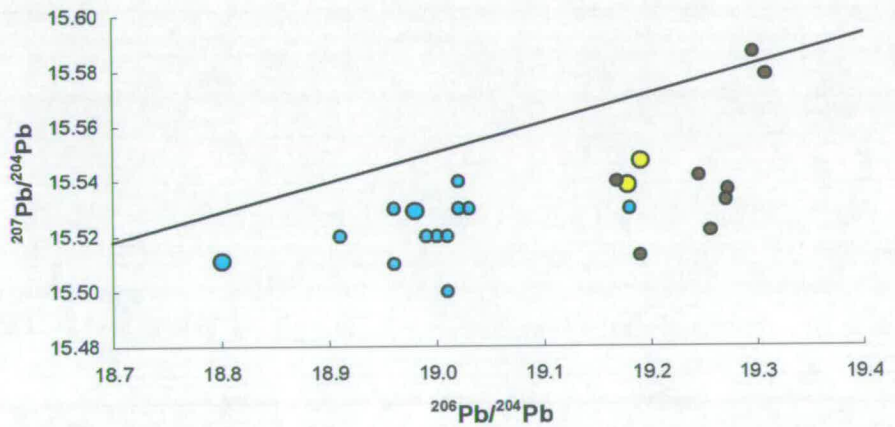

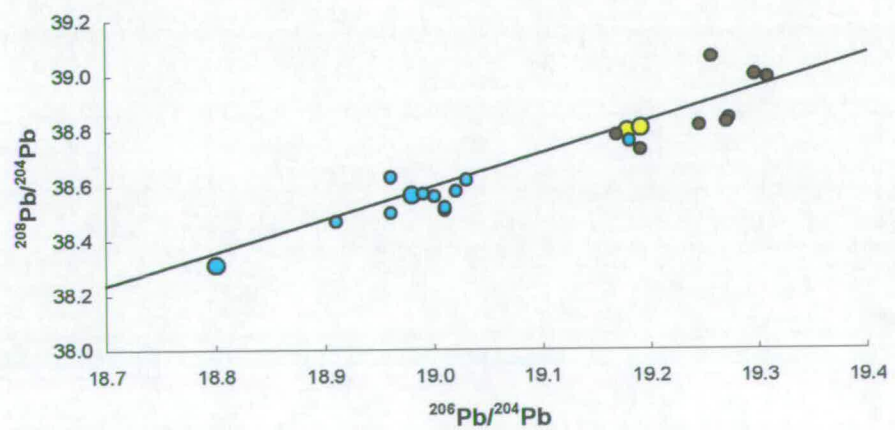

4.5 Discussion

Regional variations in Sr-Nd-Pb isotopic compositions are observed in the SFZ. These variations have previously been attributed to source heterogeneity on a scale of individual volcanoes (10-20 km) (e.g., Furman *et al.*, 1995) or to interaction with altered basaltic crust (e.g., Oskarsson *et al.*, 1982, 1985). The Sr-Nd-Pb data in this study are in agreement with those of previous studies, and demonstrate that northward increases in $^{87}Sr/^{86}Sr$ and Pb isotope ratios coincide with decreasing $^{143}Nd/^{144}Nd$. In addition, $^{3}He/^{4}He$ increase from Vestmannaeyjar to Eyjafjöll. Progressive enrichment in incompatible trace elements also occurs in a northerly direction and basalts grade from alkaline to transitional to tholeiitic northwards and towards the ERZ. At face value, the He-Sr-Nd-Pb isotope data indicate that the mantle source beneath the SFZ is increasingly dominated by an incompatible element enriched component, characterised by high $^{3}He/^{4}He$ and radiogenic Sr and Pb isotope ratios, towards the inferred centre of the Iceland plume. This is the opposite of the regional variation observed in Snæfellsnes, where increasing $^{3}He/^{4}He$ towards the active rift-zones coincided with decreasing Sr and Pb isotope ratios and incompatible element enrichment (see Section 2.5.6). Elevated $^{87}Sr/^{86}Sr$ and incompatible trace element enrichment may result from interaction with basaltic crust as a result of the propagation of the ERZ (e.g., Steinþórsson *et al.*, 1985; Oskarsson *et al.*, 1985). The change from alkaline to tholeiitic compositions along the ERZ is most likely a consequence of increasing depths of melting towards the active rift zones (e.g., Furman *et al.*, 1995; Thy, 1991; Kokfelt *et al.*, 2003; Kokfelt *et al.*, *in press*). Before examining the nature of the SFZ mantle sources it is necessary to evaluate the potential influences of crustal interaction, melting processes and fractional crystallisation on the compositions of SFZ basalts.

4.5.1.1 Assimilation of Icelandic crust

It is indisputable that crustal contamination is significant in the generation of many evolved volcanic rocks in the ERZ (e.g., Oskarsson *et al.*, 1982, 1985; Meyer *et al.*, 1985; Nicolson *et al.*, 1991; Hemond *et al.*, 1993; Gunnarsson *et al.*, 1999). Interaction of tholeiitic mantle-derived melts with altered Icelandic crust will not only affect major element compositions but could also modify isotopic compositions,

and this process has been invoked to explain elevated $^{87}Sr/^{86}Sr$ in the SFZ (e.g., Hemond *et al.*, 1993; Oskarsson *et al.*, 1982, 1985). The positive correlations between mobile and immobile elements (K_2O or Rb and Nb) in the SFZ (Figure 4.10) indicate that contamination by crustal fluids is negligible in the generation of SFZ magmas. Furthermore, the Vestmannaeyjar and Eyjafjöll samples fall on the same trends in Figure 4.10, despite the latter having higher $^{87}Sr/^{86}Sr$.

Olivine $^{3}He/^{4}He$ in the SFZ are higher than those determined in Snæfellsnes and the EFZ (see Sections 2.4.3 and 3.4.3) but are still lower than the highest ratios recorded in Quaternary Icelandic basalts (~34 R_A; Macpherson *et al.*, 2005). $^{3}He/^{4}He$ may have been reduced by assimilation of Icelandic crust. In order to change olivine $^{3}He/^{4}He$ from >35 R_A to 13 R_A, as recorded in Vestmannaeyjar olivines, requires over 90% assimilation (see Section 2.5.3 for calculations). Moreover, the southward decrease in $^{3}He/^{4}He$ would therefore suggest that crustal assimilation is greatest in Vestmannaeyjar. This is the opposite conclusion to that made if $^{87}Sr/^{86}Sr$ or incompatible trace element concentrations were used to examine crustal interaction, both of which are highest in Torfajökull: a positive correlation between $^{3}He/^{4}He$ and $^{87}Sr/^{86}Sr$ is not compatible with crustal contamination. Furthermore, such a contribution of crustal material would be evident in oxygen isotope data.

Published whole-rock $\delta^{18}O$ data from the SFZ strongly suggest that contamination of melts by Icelandic crust may be important in the genesis of silicic lavas (e.g., Gunnarsson *et al.*, 1998). In Torfajökull, rhyolites are characterised by $\delta^{18}O$ of +3.6 - 4.4 ‰ (Gunnarsson *et al.*, 1998), significantly lower than both N-MORB (+5.2 ± 0.3 ‰) and the Icelandic mantle (+4.9 ± 5.5 ‰) (e.g., Mattey *et al.*, 1994; Gautason and Muelenbachs, 1998; Thirlwall *et al.*, 1999; Gee *et al.*, 1998; Eiler *et al.*, 2000a; Kokfelt *et al.*, *in press*; Eiler *et al.*, 2000b). In contrast, basaltic rocks show limited interaction with Icelandic crust and are characterised by olivine and whole-rock $\delta^{18}O$ of +5.0 - 5.7 ‰ in Vestmannaeyjar, +4.3 - 4.8 ‰ in Katla and +4.8 - 4.9 ‰ in Torfajökull (Muelenbachs *et al.*, 1974; Sigmarsson *et al.*, 1992; Kokfelt *et al.*, *in press*; Gunnarsson *et al.*, 1998) These ranges are similar to other flank zones in Iceland (+4.9 - 5.7 ‰: Condomines *et al.*, 1983; Sigmarsson *et al.*, 1992; Hardarson, 1993; Prestvik *et al.*, 2001; Kokfelt *et al.*, *in press*), though the lowest $\delta^{18}O$ values in Katla may indicate some degree of crustal interaction.

Figure 4.10 Plots of mobile elements (K_2O, Rb) against the immobile element Nb demonstrating the minimal role of crustal assimilation.

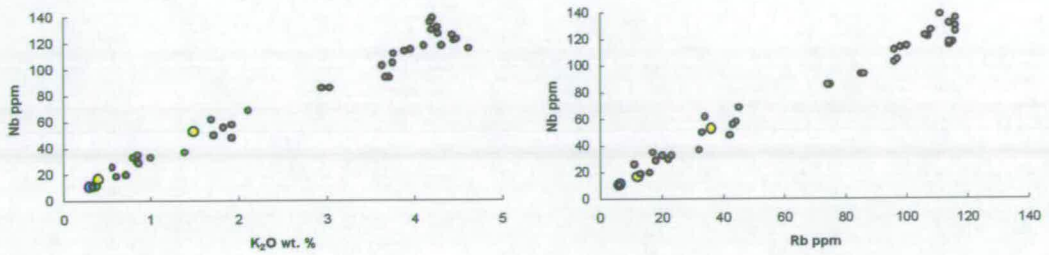

4.5.1.2 Fractional crystallisation

In plots of MgO *vs.* major element or trace element concentrations, all of the samples from the SFZ lie on previously defined crystallisation trends (Figures 4.3 and 4.4). The differences in major element and compatible trace element concentrations *within* each volcanic system can be explained by fractional crystallisation. Inflections in the major oxide-MgO correlations represent the onset of crystallisation of one or more new minerals. For example, the sharp decrease in CaO concentration below 6-8 wt. % MgO represents the onset of plagioclase and clinopyroxene crystallisation and the inflexion in the P_2O_5-MgO trend represents apatite crystallisation at low MgO. Increasing concentrations of compatible trace elements also reflect crystallisation. For example, the positive correlation between Ni and MgO is indicative of olivine fractionation.

Variation in major element concentrations between systems, however, indicates either differences in source composition or degree of melting. For example, the displacement of Katla samples to high TiO_2 at a given MgO concentration indicates that the parental magma in Katla was relatively enriched in this incompatible element. The higher FeO concentrations of Katla samples, could be a consequence of the suppression of plagioclase crystallisation as a result of a higher water (also an incompatible element) content in the source (Asimow and Langmuir, 2003). This is supported by the relatively high Sr concentration of the Katla basalt in Figure 4.5. The displacement of Vestmannaeyjar data to lower CaO/Al_2O_3 at high MgO, indicates that clinopyroxene is an important phase in the source mineralogy. The

main differences between magmas from each volcanic system are summarised below.

- Torfajökull magmas have the highest concentrations of SiO_2 and K_2O.
- Vestmannaeyjar volcanic rocks are characterised by enrichment in Al_2O_3 and Na_2O whereas Katla shows the most depletion in these elements.
- Katla magmas are anomalously rich in Fe_2O_3 and TiO_2 and also have the highest concentrations of P_2O_5 and MnO.

4.5.1.3 Melting processes

Regional variation in major oxide concentrations suggests that differences in the degree of partial melting may occur between each volcanic system. The well-documented regional gradation from alkaline to transitional compositions observed in the SFZ is indicative of increasing degrees of partial melting from Vestmannaeyjar to Torfajökull. However, a northward increase is observed in the degree of enrichment in incompatible trace elements. This suggests the opposite – that the degree of partial melting decreases northwards (Figures 4.5-4.6).

In the previous chapters, major element oxide concentrations and ratios were used to examine variations in the depth and extent of partial melting because, compared to trace element concentrations, they are insensitive to source variation. At MgO > 5 wt.%, concentrations of incompatible major oxides (Na_2O, TiO_2, K_2O and P_2O_5) and Al_2O_3 indicate that Vestmannaeyjar magmas are generated by the smallest degrees of melting and Torfajökull and Katla by similar and larger degrees of melting (Figure 4.4). Exceptions are TiO_2 and P_2O_5 which are more enriched in Katla. Negative correlations between TiO_2 or P_2O_5 and CaO/Al_2O_3 (in basalts with MgO > 5 wt. %) within individual systems suggest that, on a local scale, enrichment in these incompatible elements is controlled by the extent of melting (Figure 4.11). However, the absence of correlations within the SFZ as a whole suggests that TiO_2 and P_2O_5 enrichment in Katla is due to enrichment in the source material.

Incompatible trace element concentrations in basaltic rocks (MgO > 5 wt. %) increase northwards such that Torfajökull has the highest VICE/MICE (Figure 4.6). If interpreted in terms of melting this suggests that they are derived from the smallest-degrees or greatest depths of melting. This is the opposite of the

interpretation from major element compositions and, as concluded by Furman *et al.*, (1995), suggests that the processes governing enrichment in incompatible major elements and incompatible trace elements are decoupled in the SFZ. It is likely therefore, that variations in the degree of incompatible trace element enrichment results from source heterogeneity. In this case, the enriched material is a dominant component in the plume and is therefore preferentially sampled in the northern parts of the SFZ.

4.5.2 Source characterisation

Having examined the effects of crustal interaction, fractional crystallisation and melting processes on the compositions of SFZ volcanic rocks, the data presented in this chapter can now be used to characterise the SFZ mantle-source and assess regional source-heterogeneity.

The isotopic data provide the strongest evidence for regional variation in the composition of the SFZ mantle-source. Linear trends in Pb and Sr-Nd isotope space suggest that the mantle-source is progressively enriched in a component characterised by radiogenic $^{87}Sr/^{86}Sr$ (> 0.7034), radiogenic Pb isotopes ($^{206}Pb/^{204}Pb$ > 19.03, $^{207}Pb/^{204}Pb$ > 15.58, $^{208}Pb/^{204}Pb$ > 38.99) and unradiogenic $^{143}Nd/^{144}Nd$ (< 0.51297) in a northwards direction (Figures 4.8-4.9, 4.12). The isotopically enriched ends of the trends are comprised of Torfajökull samples (Stecher *et al.*, 1999). The Eyjafjöll samples of this study are characterised by only slightly less radiogenic Sr and Pb isotope ratios. Unlike the regional trends observed along the Snæfellsnes Peninsula, however, the most radiogenic Sr and Pb isotope ratios appear to coincide with the highest $^{3}He/^{4}He$ (19.7 R_a). The small number of olivine $^{3}He/^{4}He$ determinations means that trends in He-Sr, He-Nd, or He-Pb isotope space are not well-defined and interpretations of regional source variation using $^{3}He/^{4}He$ are therefore limited (Figure 4.13). However, two alternative hypotheses may account for the apparent regional variation in the composition of the SFZ mantle source, and these will be examined in more detail and in conjunction with data from the other flank zones in Iceland in the next chapter:

(i) Regional source variation represents different degrees of mixing between three components, as occurs in Snæfellsnes. The incompatible-trace-element enriched component is characterised by low $^{3}He/^{4}He$ and radiogenic Pb and Sr isotope ratios. In Eyjafjöll (and Torfajökull and Katla) this component is mixed with a depleted component characterised by $^{3}He/^{4}He > 19\ R_A$ whereas in Vestmannaeyjar it is mixed with a depleted component characterised by lower $^{3}He/^{4}He$. The high $^{3}He/^{4}He$ depleted component may therefore be plume derived.

(ii) Only two components are present in the SFZ mantle; one depleted component characterised by low $^{3}He/^{4}He$ ($< 11\ R_a$), and one enriched component characterised by high $^{3}He/^{4}He$ ($>19\ R_a$). The enriched component is contained within the plume, and therefore dominates the mantle source in the northern parts of the flank zone. The depleted component infiltrates the mantle in the south.

Figure 4.11 Incompatible major oxide concentrations *vs.* CaO/Al_2O_3

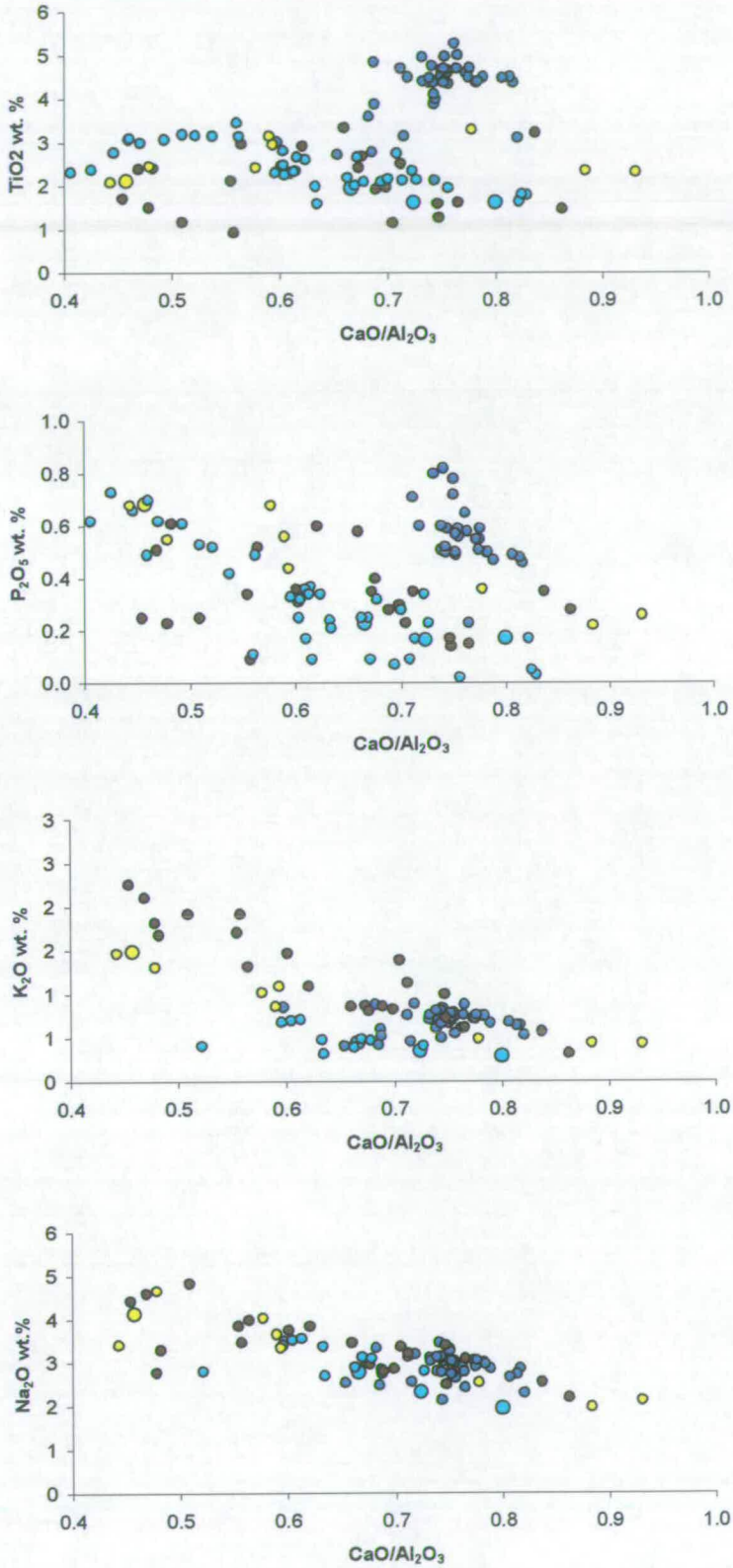

Figure 4.12 $^{206}Pb/^{204}Pb$ *vs.* $^{87}Sr/^{86}Sr$ and $^{143}Nd/^{144}Nd$

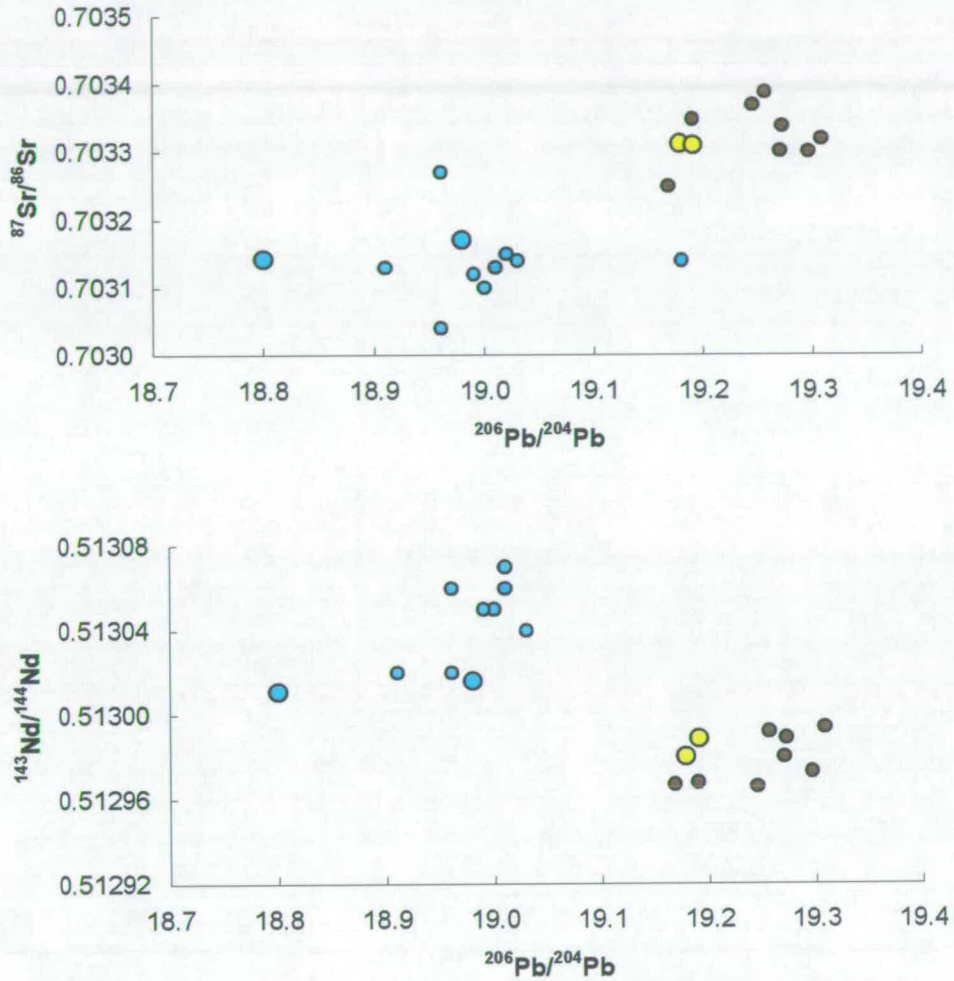

Figure 4.13 $^{3}He/^{4}He$ *vs.* $^{87}Sr/^{86}Sr$, $^{143}Nd/^{144}Nd$ and $^{206}Pb/^{204}Pb$

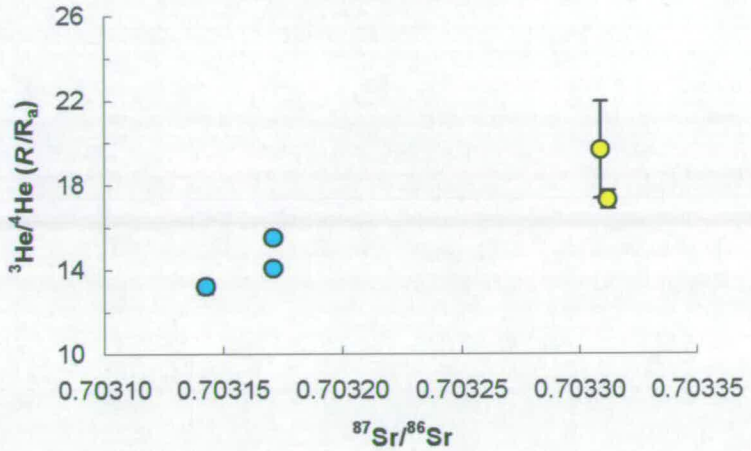

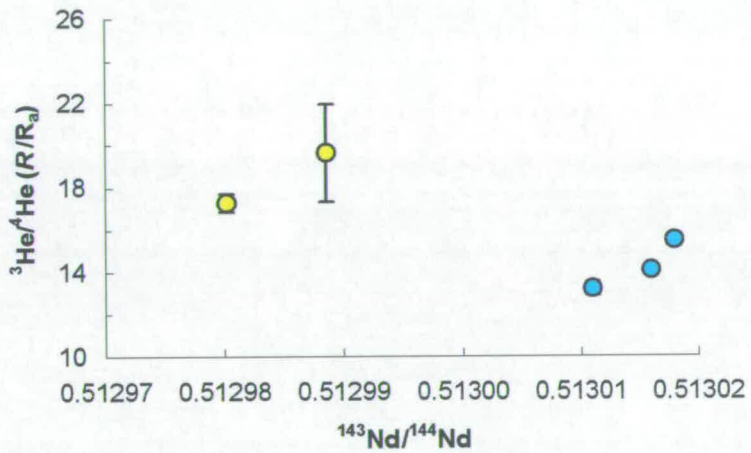

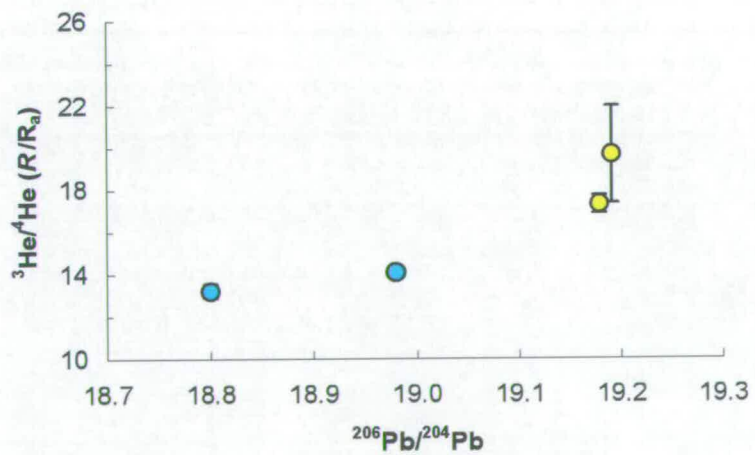

4.6 Summary

Basalts from the SFZ, located at the tip of the propagating ERZ, range in composition from highly incompatible-element-enriched, transitional basalt at Torfajökull and Eyjafjöll in the north of flank-zone, to more depleted and mildly-alkaline basalt at Vestmannaeyjar at the southern end of the flank-zone. Some of the variation in major element composition can be explained by fractional crystallisation at individual volcanic centres, but source heterogeneity is required to explain differences between volcanoes. Regional variation is also observed in the isotope data, such that the most incompatible-element-enriched basalts are also the most isotopically-enriched, and this does not appear to be a consequence of interaction with oceanic crust during rift-propagation as has been proposed by Oskarsson *et al.*, (1982, 1985). $^{206}Pb/^{204}Pb$ ranges from ~18.8 (Vestmannaeyjar) to ~19.4 (Torfajökull), and correlates positively with $^{87}Sr/^{86}Sr$ (~0.7031-0.7034) and negatively with $^{143}Nd/^{144}Nd$ (~0.51296 - 0.51301). While $^{3}He/^{4}He$ increases northwards with proximity to the inferred centre of the plume (~13-19 R_a), unlike at the Snæfellsnes Peninsula $^{3}He/^{4}He$ is highest in the more enriched basalts. The regional co-variations in He, Sr, Nd and Pb isotopes might be explained either by (i) two-component mixing between enriched mantle characterised by high $^{3}He/^{4}He$ (>~19 R_a) and depleted mantle characterised by lower $^{3}He/^{4}He$ (< 11 R_a); or (ii) by mixing between enriched mantle characterised by low $^{3}He/^{4}He$ with local depleted mantle domains characterised by variable $^{3}He/^{4}He$ (as appears to occur in Snæfellsnes).

Chapter 5

THE NATURE, ORIGINS, DISTRIBUTION OF AND INTER-RELATIONSHIPS BETWEEN ENRICHED COMPONENTS IN THE SUB-ICELANDIC MANTLE

5.1 Introduction

The principal objectives of this research, as detailed in section 1.3, were to: (i) use He, Sr, Nd and Pb isotopes and trace and major element data to characterise the mantle sources of geochemically enriched basalts from Iceland's three flank-zones; (ii) identify the number and composition of enriched components in the local mantle; (iii) examine the inter-relationships between these enriched components; and (iv) constrain the main factors controlling the geographic distribution of mantle enrichments.

In the preceding three chapters the results of the chemical analyses of basalts from each of the flank-zones were presented and interpretations of the data in the context of mantle sources were made. Trace element data confirmed previous observations that basalts from each flank-zone are characterised by enrichment in incompatible trace elements relative to basalts from the Icelandic rift-zones (Furman *et al.*, 1991; Hardarson, 1993; Hards *et al.*, 1995; Stecher *et al.*, 1999; Prestvik *et al.*, 2001; Bunce, 2002). On the basis of the trace element data alone it is difficult to assess the relative roles of source enrichment and melting processes on the compositions of basalts, and the two factors are undoubtedly coupled.

This study shows that the enriched basalts are derived from a mantle source or sources that are isotopically distinct from the source of rift-zone basalts, consistent with the interpretations of previous studies (Sigmarsson *et al.*, 1992; Furman *et al.*, 1995; Hards *et al.*, 1995; Stecher *et al.*, 1999; Prestvik *et al.*, 2001). The radiogenic $^{87}Sr/^{86}Sr$ and unradiogenic $^{143}Nd/^{144}Nd$ that characterise flank-zone basalts demonstrate that they originate in mantle that has had a higher time-integrated Rb/Sr and Nd/Sm than the source of rift-zone basalts. Pb isotope data of flank-zone basalts show that the "enriched" mantle is also characterised by more radiogenic Pb isotope ratios than the "depleted" mantle source of active rift-zones. He, Sr, Nd and Pb isotope characteristics of the flank-zone basalts require explanations in terms of mixing between depleted and enriched mantle in order to produce local flank-zone source-compositions. In this chapter, the results from the previous chapters are brought together in order to assess the nature and number of enriched components in the Icelandic mantle. Mixing relationships between these components are examined in order to explain the extent of source heterogeneity within and between the flank-

zones. The mixing-model is then applied to rift-zone and adjacent Mid-Atlantic Ridge (MAR) basalts in order to provide constraints on the distribution of enriched domains in the North Atlantic mantle.

5.2 Characterisation of enriched mantle components

5.2.1 Defining "enriched" mantle: evidence from trace elements

Enriched basalts in Iceland and the North Atlantic are defined as having VICE/MICE that are greater than those of "average Icelandic basalt" (e.g., Nb/Zr > 0.1; Hardarson *et al.*, 1997; Fitton *et al.*, 2003; Thirlwall *et al.*, 2004). Outwith Iceland, Quaternary enriched basalts are also found at Jan Mayen (Trønnes *et al.*, 1999; Stuart *et al.*, (*in prep.*), along the Jan Mayen Platform (JMP) (Schilling *et al.*, 1989) and at Vesteris Seamount (Haase and Devey, 1994).

Use of a logarithmic Nb/Y – Zr/Y diagram enables incompatible element enrichment in the mantle source to be distinguished from enrichment from relatively small degrees of partial-melting (Fitton *et al.*, 1997). Within each of the three flank-zones, variation in Nb/Y and Zr/Y mainly results from partial-melting rather than source composition. In Figure 5.1 the Nb-Y-Zr compositions of flank-zone basalts are compared to basalts from Iceland rift-zones and elsewhere in the North Atlantic. At the enriched end of the Iceland array, the flank-zone basalts form two separate parallel arrays, indicative of derivation from small-degree melting of two compositionally distinct sources. The upper array comprises Jan Mayen and Snæfellsnes basalts and the lower array comprises the remaining flank-zone basalts. The function ΔNb (ΔNb = 1.74 + log(Nb/Y) - 1.92 log(Zr/Y)), is used by Fitton *et al.*, (1997) to define source variation between N-MORB (negative ΔNb) and the Iceland Plume (IP) (positive ΔNb). The ΔNb of basalts from Snæfellsnes range from 0.38-0.52 and are comparable to Jan Mayen (0.42 - 0.55; Trønnes *et al.*, 1999; Stuart *et al.*, *in prep.*) demonstrating a common source. The ΔNb of the EFZ and the SFZ basalts are similar (0.21-0.23; 0.19-0.25, respectively) and distinctly lower than the Jan Mayen and Snæfellsnes basalts, testifying to derivation from a mantle source which is less enriched in Nb.

Figure 5.1: Log(Nb/Y)-log(Zr/Y) diagram showing all Icelandic data. Parallel lines represent the Icelandic array of Fitton *et al.*, 1997.

Key: Small circles – published data. Large circles - this study.

Data sources: Jan Mayen basalts: Stuart *et al.*, *in prep*. Rift-zone basalts: see Figure. 1.3. Flank-zone basalts: this study; Furman et al., 1995; Hards et al., 1995; Prestvik et al., 2001

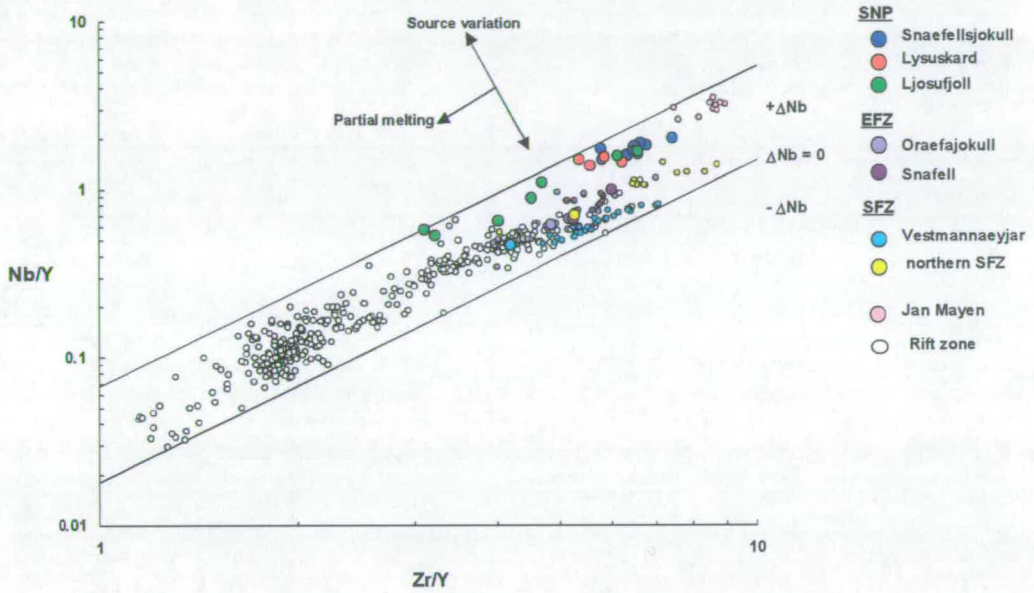

5.2.2. Isotopes as source discriminants

Strong constraints on mantle heterogeneity are also provided by isotopic data (Chapters 2-4). In Snæfellsnes, regional variation in He, Sr and Pb isotope ratios demonstrated that basalts from either end of the peninsula were derived from isotopically distinct sources. In the EFZ, Sr and Pb isotopes provide strong evidence for a unique mantle component supplying Öræfajökull. The Snæfell mantle source appears to be characterised by less extreme Sr and Pb isotopic compositions, but the extent of involvement of the Öræfajökull component in the Snæfell source cannot be assessed. In the SFZ, regional variation was observed in He, Sr, Nd and Pb isotopes, with the highest He, Sr and Pb isotope ratios, and the lowest Nd isotope ratios, characterising basalts from the northern parts of the flank-zone, closest to the inferred axis of the Iceland plume. In order to determine the extent of mantle heterogeneity within the flank zones and Iceland as a whole, the compositions of the

heterogeneity within the flank zones and Iceland as a whole, the compositions of the flank-zone basalts (as determined in this study) are now compared with each other and with basalts from elsewhere in the North Atlantic region.

Published Sr and Nd isotope data for the North Atlantic region show a negative correlation between $^{87}Sr/^{86}Sr$ and $^{143}Nd/^{144}Nd$ that is interpreted as a binary mix between an enriched (high-$^{87}Sr/^{86}Sr$ – low-$^{143}Nd/^{144}Nd$) and a depleted (low-$^{87}Sr/^{86}Sr$ – high-$^{143}Nd/^{144}Nd$) mantle source (O'Nions and Pankhurst, 1973; Sun and Jahn, 1975; Zindler *et al.*, 1979; Sigmarsson *et al.*, 1992; Furman *et al.*, 1991, 1995; Hémond *et al.*, 1993; Taylor *et al.*, 1997; Gee *et al.*, 1998; Trønnes *et al.*, 1999; Kempton *et al.*, 2000). The enriched flank-zone basalts comprise the high $^{87}Sr/^{86}Sr$ – low $^{143}Nd/^{144}Nd$ end of the North Atlantic array (Figure 5.2). The triangular distribution of basalts in Figure 5.2 indicates the presence of at least three mantle components: a depleted (low $^{87}Sr/^{86}Sr$ – high $^{143}Nd/^{144}Nd$) component and two enriched (high $^{87}Sr/^{86}Sr$ – low $^{143}Nd/^{144}Nd$) components. The depleted component may be the shallow upper-mantle source of N-MORB (e.g., Mertz and Haase, 1997; Hanan *et al.*, 2000; Stracke *et al.*, 2003) or an intrinsic component of the Iceland Plume (e.g., Hémond *et al.*, 1993; Thirlwall, 1995; Hards *et al.*, 1995; Fitton *et al.*, 1997, 2003; Kempton *et al.*, 2000; Chauvel and Hémond, 2000; Breddam, 2002). The two enriched components, best represented by Jan Mayen and Öræfajökull basalts, are distinguished by different $^{87}Sr/^{86}Sr$ at low $^{143}Nd/^{144}Nd$. The negative trends between Sr and Nd isotopes in Iceland are not generally observed within individual flank-zones and imply that source heterogeneity is more complex than simple binary mixing. The SFZ enriched component defined in Figure 5.1 cannot be distinguished from Sr-Nd isotopes.

Pb isotope ratios reveal more complex source heterogeneity in Iceland and the North Atlantic than can be distinguished using Sr and Nd isotopes, and up to five components have been proposed (e.g., Thirlwall, 1995, 2004; Mertz and Haase, 1997; Hanan and Schilling, 1997; Taylor *et al*, 1997; Hanan *et al.*, 2000; Chauvel and Hémond, 2000; Kempton *et al.*, 2000; Murton *et al.*, 2002). In this study, Pb isotope data reveal at least three end-member compositions in Iceland's flank-zones. The Öræfajökull end-member is characterised by strongly-positive $\Delta 7/4$ and $\Delta 8/4$. Within both the Snæfellsnes and Southern flank zones, two different end-members

are required, one (enriched) characterised by negative Δ7/4, slightly positive Δ8/4 and radiogenic Pb isotope ratios, and the other (depleted) by slightly negative Δ7/4 and relatively unradiogenic Pb isotope ratios. In $^{206}Pb/^{204}Pb$ - $^{207}Pb/^{204}Pb$ and $^{206}Pb/^{204}Pb$ - $^{208}Pb/^{204}Pb$ plots (Figure 5.3) the enriched end-member is represented by basalts from the SFZ and the depleted end-member by rift-zone basalts. The Öræfajökull end-member is characterised by high $^{207}Pb/^{204}Pb$ and $^{208}Pb/^{204}Pb$ at moderately radiogenic $^{206}Pb/^{204}Pb$ values. Simple binary mixing between the SFZ and rift-zone end-members could account for the positive linear arrays of rift-zone and flank-zone basalts in Pb isotope plots. Notably, the Jan Mayen basalts, which represent an end-member in Sr-Nd isotopes and ΔNb, do not appear to define an extreme Pb isotope composition.

Figure 5.2: $^{87}Sr/^{86}Sr$ *vs.* $^{143}Nd/^{144}Nd$. Icelandic basalts form a triangular array suggestive of the presence of three mantle components: a depleted component and two enriched components. Flank-zone basalts are derived from sources dominated by enriched mantle. Jan Mayen and Öræfajökull basalts represent the two enriched source end-members.
Symbols as in Figure 5.1. Data sources: Flank-zones: this study; Furman *et al.*, 1991; Hards *et al.*, 1995; Srecher *et al.*, 1999; Prestivk *et al.*, 2001: Jan Mayen: Tronnes *et al.*, 1999; Stuart *et al.*, in prep. Rift zones: Thirlwall *et al.*, 1995; 2004; Hanan and Schilling, 1997; Chauvel and Hemond, 2000; Breddam *et al.*, 2000, 2002; Stracke *et al.*, 2003; Kempton *et al.*, 2000,

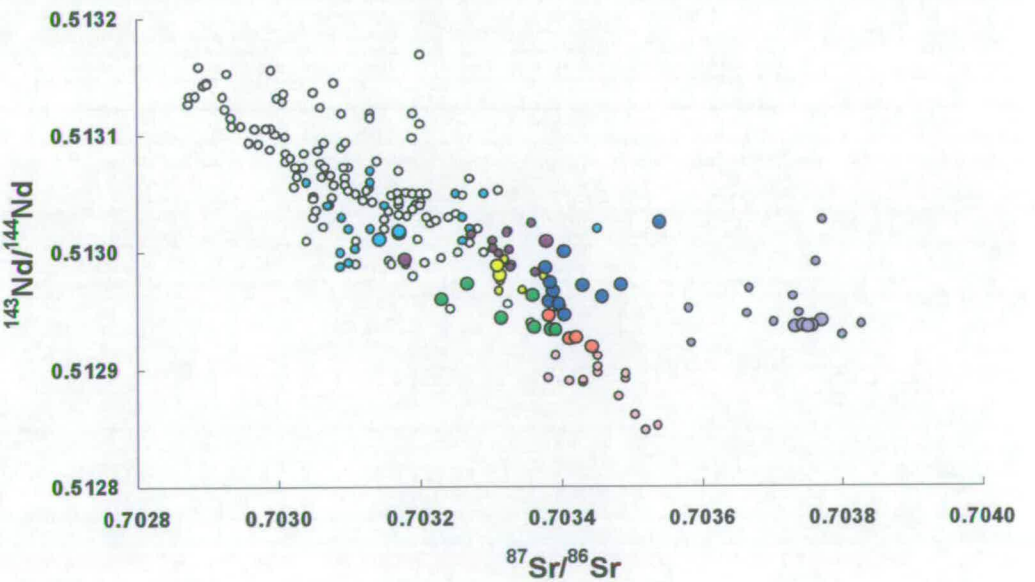

Figure 5.3 $^{206}Pb/^{204}Pb$ against (a) $^{207}Pb/^{204}Pb$ and (b) $^{208}Pb/^{204}Pb$.
Key as in Figure 5.1. Diagonal line marks the NHRL of Hart (1984). Data sources: as in Figure 5.2.

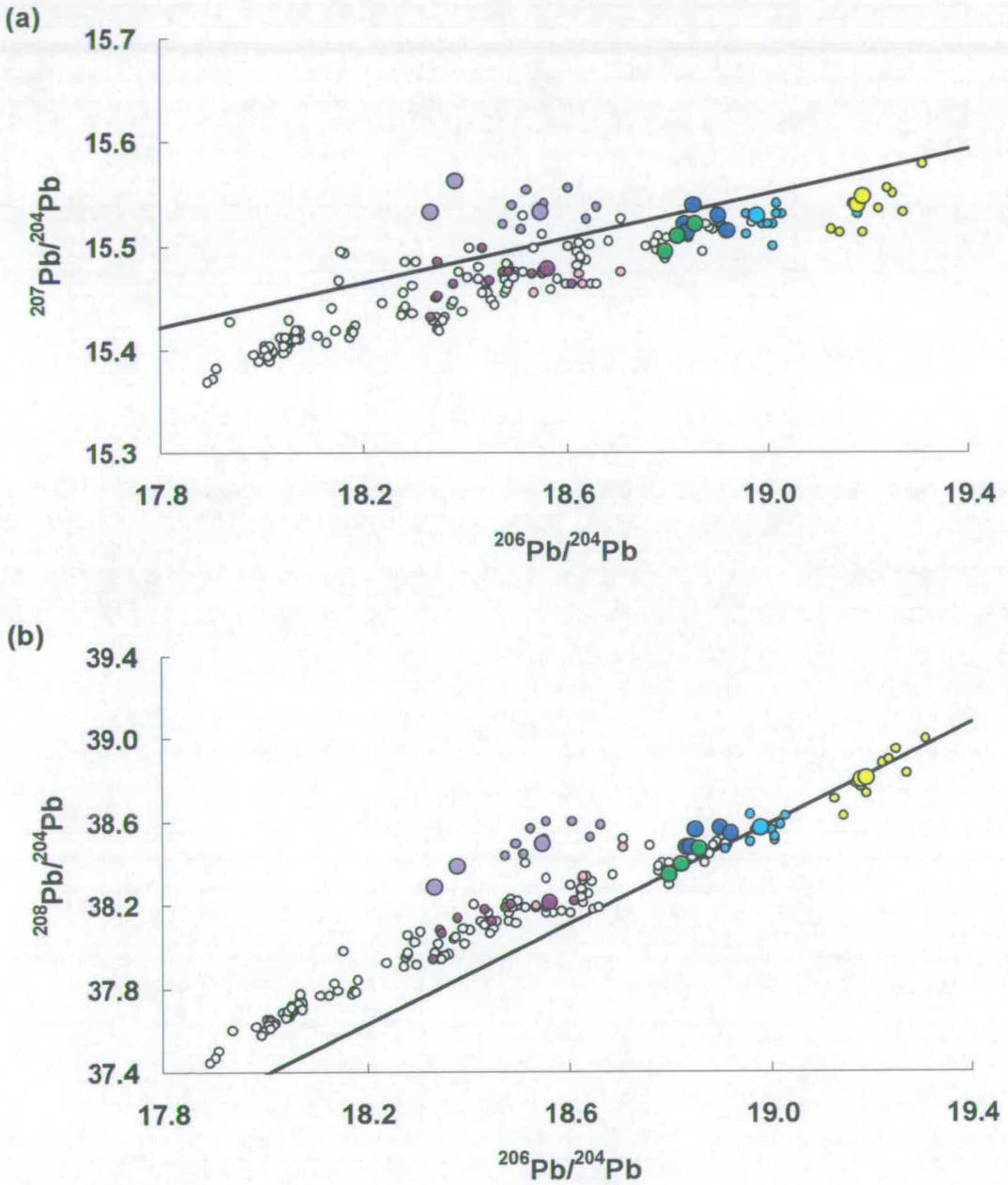

Helium isotope ratios provide further evidence for mantle heterogeneity in Iceland (Condomines *et al.*, 1983; Kurz *et al.*, 1985; Breddam *et al.*, 2000, 2002; Dixon *et al.*, 2000; Macpherson *et al.*, 2005). Basaltic lavas erupted along the rift-zones are generally characterised by high olivine phenocryst $^{3}He/^{4}He$ (up to 34.3 R_a; Macpherson *et al.*, 2005). High $^{3}He/^{4}He$ measured in basalts from ocean islands relative to N-MORB (8 R_a) are attributed to derivation from a deep undegassed mantle reservoir inferred to be sampled by mantle plumes (e.g., Kurz *et al.*, 1982; 1983). $^{3}He/^{4}He$ lower than 8 R_a can be explained by derivation from a radiogenic-He-rich, degassed and recycled source. A limited number of published $^{3}He/^{4}He$ from off-axis and flank-zone basalts and glasses from central Iceland indicate that the enriched mantle source in the North Atlantic is characterised by $^{3}He/^{4}He$ lower than or equal to N-MORB (Kurz *et al.*, 1985; Poreda *et al.*, 1986; Sigmarsson *et al.*, 1992; Macpherson *et al.*, 2005; Stuart *et al.*, *in prep.*).

In this study, geographical source variation in the Snæfellsnes and Southern flank-zones was identified using $^{3}He/^{4}He$. In these flank zones, $^{3}He/^{4}He$ increases towards the active rift zones and the centre of Iceland. In Snæfellsnes however the variation was from 7.7 – 11.6 R_a, and in the SFZ from 13 – 19 R_a. In the EFZ little $^{3}He/^{4}He$ variation is seen in the Snæfell (~6.5 R_a) and Öræfajökull (~7.7 R_a) basalts, although the number of samples are smaller. In Figure 5.4, the He isotope data from this study are compared to published rift-zone data and to the Jan Mayen data of Stuart *et al.* (*in prep.*). Restricting comparisons to olivine phenocryst crush analyses avoids using ratios that may have been corrupted by radiogenic in-growth or crustal assimilation, as is common in subglacial basaltic glasses or in pyroxene phenocrysts (see Sections 1.3 and 2.5.2). $^{3}He/^{4}He$ are lowest in Jan Mayen and highest in the ERZ and southern NRZ. N-MORB-like $^{3}He/^{4}He$ are observed in western Snæfellsnes, the EFZ and in the northern NRZ. The overall variation in $^{3}He/^{4}He$ in Iceland and Jan Mayen may represent simple two-component mixing between a low-$^{3}He/^{4}He$ Jan Mayen-type end-member and a high-$^{3}He/^{4}He$ rift-zone end-member. However, the involvement of a N-MORB-like component in the Icelandic mantle is apparent from neon isotopes (e.g., Dixon *et al.*, 2000; Dixon, 2003). Furthermore, high $^{3}He/^{4}He$ are apparent in both depleted (rift-zone) and enriched (northern SFZ) basalts.

Figure 5.4: $^{3}He/^{4}He$ released by *in vacuo* crushing of olivines from rift-zone and flank-zone basalts. Key as in Figure 5.1. Horizontal dashed line represents $^{3}He/^{4}He$ of N-MORB. Additional data from: Kurz *et al.*, (1985); Sigmarsson *et al.*, (1992); Dixon *et al.*, (2000); Breddam *et al.*, (2000), (2002); Macpherson *et al.*, (2005); Stuart *et al.*, (*in prep.*).

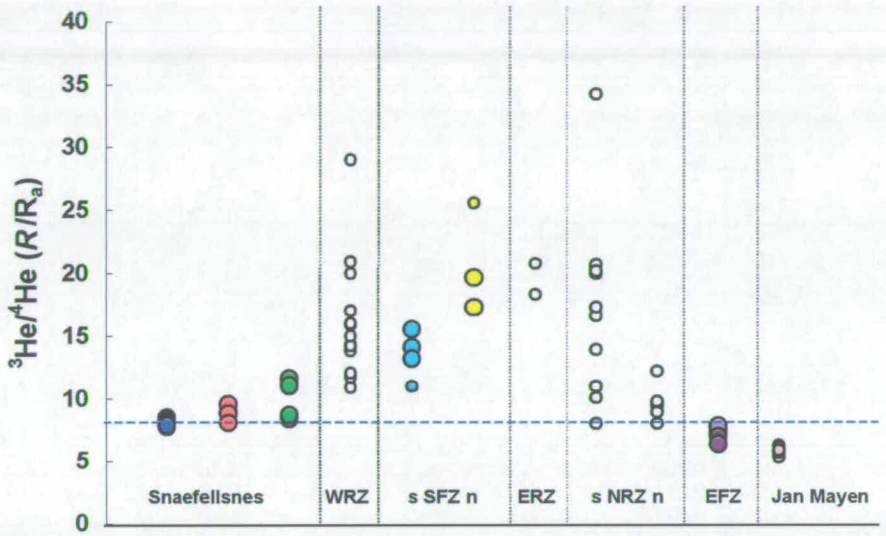

Note: The $^{3}He/^{4}He$ of pyroxenes and basaltic glasses may be modified by pre-eruptive processes such that they do not represent the time-integrated $^{3}He/(U+Th)$ of the mantle source and these data are not included for comparison.

5.2.3 Number and compositions of enriched mantle end-members: isotopic co-variations

Distinguishing between the different enriched end-members requires several source discriminants. For example, Jan Mayen basalts have extreme ΔNb and Sr, Nd and He isotopic compositions, but not Pb isotope ratios. The Öræfajökull source is characterised by extreme Sr and Pb isotope compositions, while basalt from the northern SFZ is distinguished from Jan Mayen basalt using ΔNb and Pb or He isotope ratios, but its He isotopic composition is similar to those of the depleted rift-zone basalts. Examination of isotopic co-variations is required to resolve the complexity and clarify the number and composition of enriched components present in the mantle beneath the flank-zones.

In Snæfellsnes, constraints on the number of end-members involved in mixing can be made in co-variation diagrams using He isotopes (Section 2.5.6). Assuming near-linear mixing trends, three end-members are required; an enriched, low-$^{3}He/^{4}He$ end-member (with radiogenic Sr and Pb isotope ratios) and two depleted end-members with moderate (~ 9.5 R_a) and high (>11.6 R_a) $^{3}He/^{4}He$, respectively. The Sr and Pb isotope compositions of the depleted end-members are similar to each other, and are less radiogenic than the enriched end-member. If the local trends in Snaefellsnes reflect regional mixing trends, the Jan Mayen, Öræfajökull and northern SFZ end-members should also be identifiable in He-Sr, He-Nd and He-Pb isotope co-variation diagrams. In Figure 5.5 the flank-zone basalts form linear trends radiating from a single enriched composition. Jan Mayen and Snæfell basalts form a lower trend and Snæfellsnes and Vestmannaeyjar basalts define the middle trends. Northern SFZ basalts fall on an extrapolated upper trend. Although Öræfajökull basalts are a discrete group in the He-Sr isotope plot, they plot along the Jan Mayen-Snæfell trend in He-Pb and He-Nd isotope diagrams. The approximate composition of a single enriched Icelandic end-member (EI_1) can therefore be constrained in these diagrams ($^{3}He/^{4}He \leq 5\ R_a$, $^{87}Sr/^{86}Sr \geq 0.7036$, $^{143}Nd/^{144}Nd \leq 0.5129$ and $^{206}Pb/^{204}Pb \geq 19.4$). The Öræfajökull basalts define a second enriched end-member (EI_2), characterised by extreme $^{87}Sr/^{86}Sr$ (~0.70375).

The He isotope co-variations (Figure 5.5) allow identification of only two enriched end-members and do not discriminate between the Jan Mayen and northern SFZ end-members proposed in Sections 5.2.1 and 5.2.2. The difference in the $^{3}He/^{4}He$ of basalts from Jan Mayen and the northern SFZ appears to be a consequence of mixing with depleted mantle characterised by variable $^{3}He/^{4}He$ (Figure 5.5). The higher $^{87}Sr/^{86}Sr$ and lower $^{143}Nd/^{144}Nd$ of Jan Mayen basalts compared to the SFZ basalts could be explained by a greater proportion of the EI_1 end-member in the Jan Mayen source; however, in this scenario the Pb isotope ratios of the Jan Mayen basalts should be more radiogenic than those in the northern SFZ basalts. Alternatively, the enriched Jan Mayen source could be derived from mixing

Figure 5.5: $^{3}He/^{4}He$ *vs.* (a) Nb/Zr, (b) $^{87}Sr/^{86}Sr$, (c) $^{143}Nd/^{144}Nd$ and (d) $^{206}Pb/^{204}Pb$. Inset sketch diagrams illustrate potential local enriched (E) and depleted (D) end-members and mixing trends. Key as in Figure 5.1. Data sources: this study; Stuart *et al.*, (*in prep.*).

Note: Data filtered to include only $^{3}He/^{4}He$ measured in olivines, and whole-rock Sr-Nd-Pb isotope measurements on the same samples.

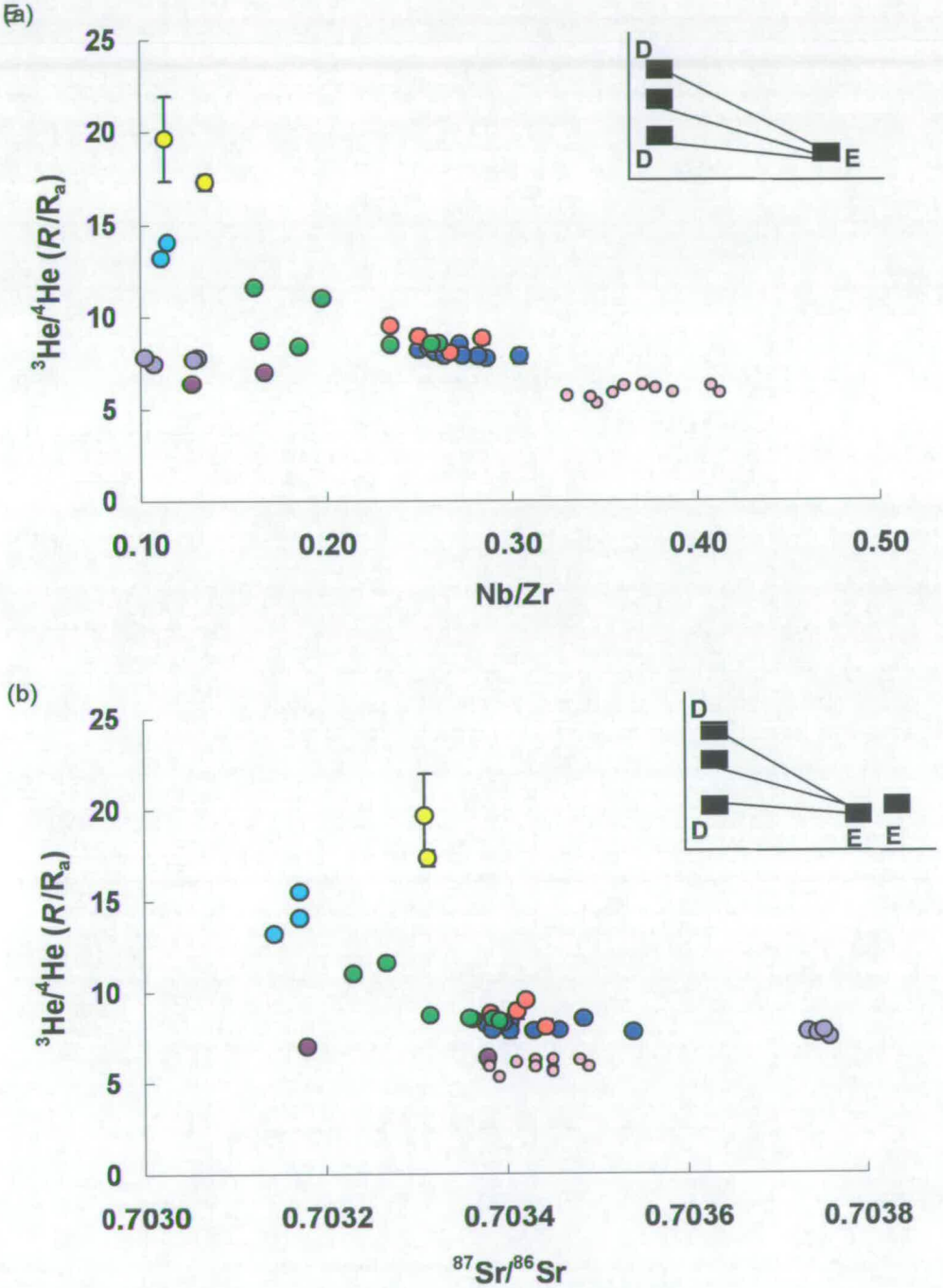

(c)

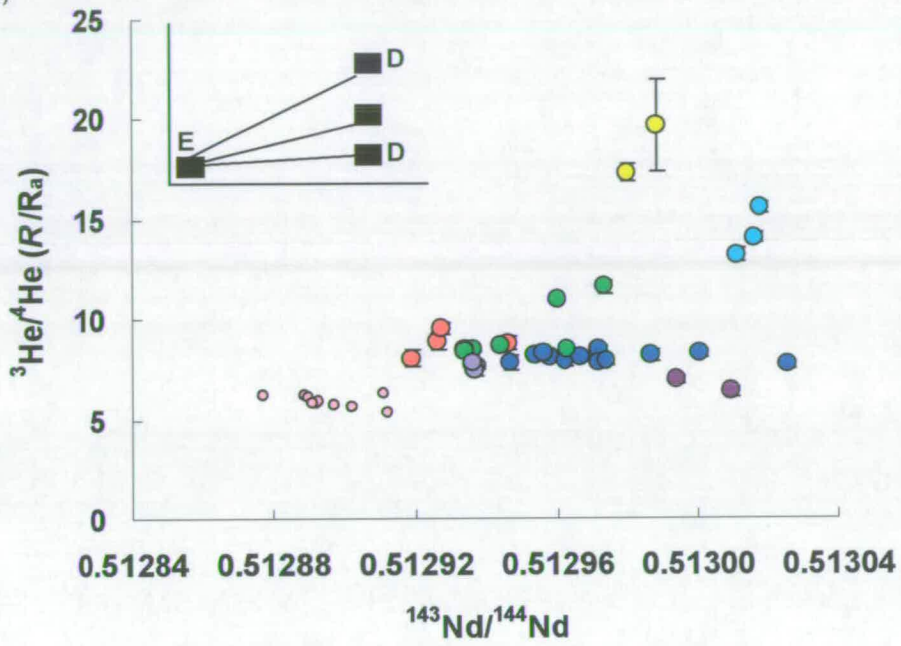
25
20
15
10
5
0
E
D
D
$^3He/^4He\ (R/R_a)$
0.51284
0.51288
0.51292
0.51296
0.51300
0.51304
$^{143}Nd/^{144}Nd$

(d)

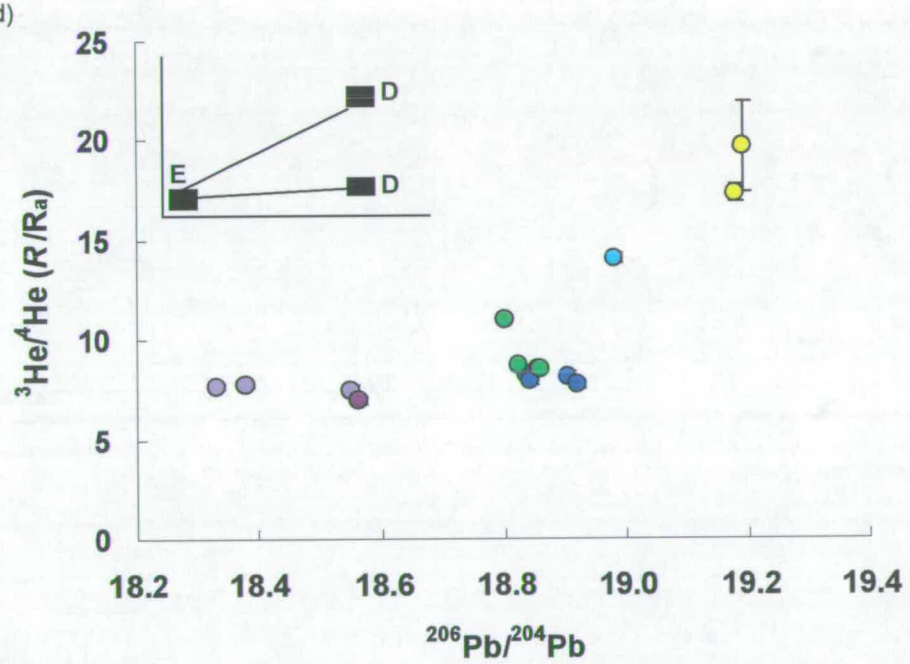
25
20
15
10
5
0
E
D
D
$^3He/^4He\ (R/R_a)$
18.2
18.4
18.6
18.8
19.0
19.2
19.4
$^{206}Pb/^{204}Pb$

Figure 5.6: $^{206}Pb/^{204}Pb$ *vs.* (a) $^{87}Sr/^{86}Sr$ and (b) $^{143}Nd/^{144}Nd$. Approximate compositions of three enriched end-members labelled. Key as in Figure 5.1. Data sources: As in Figure 5.2

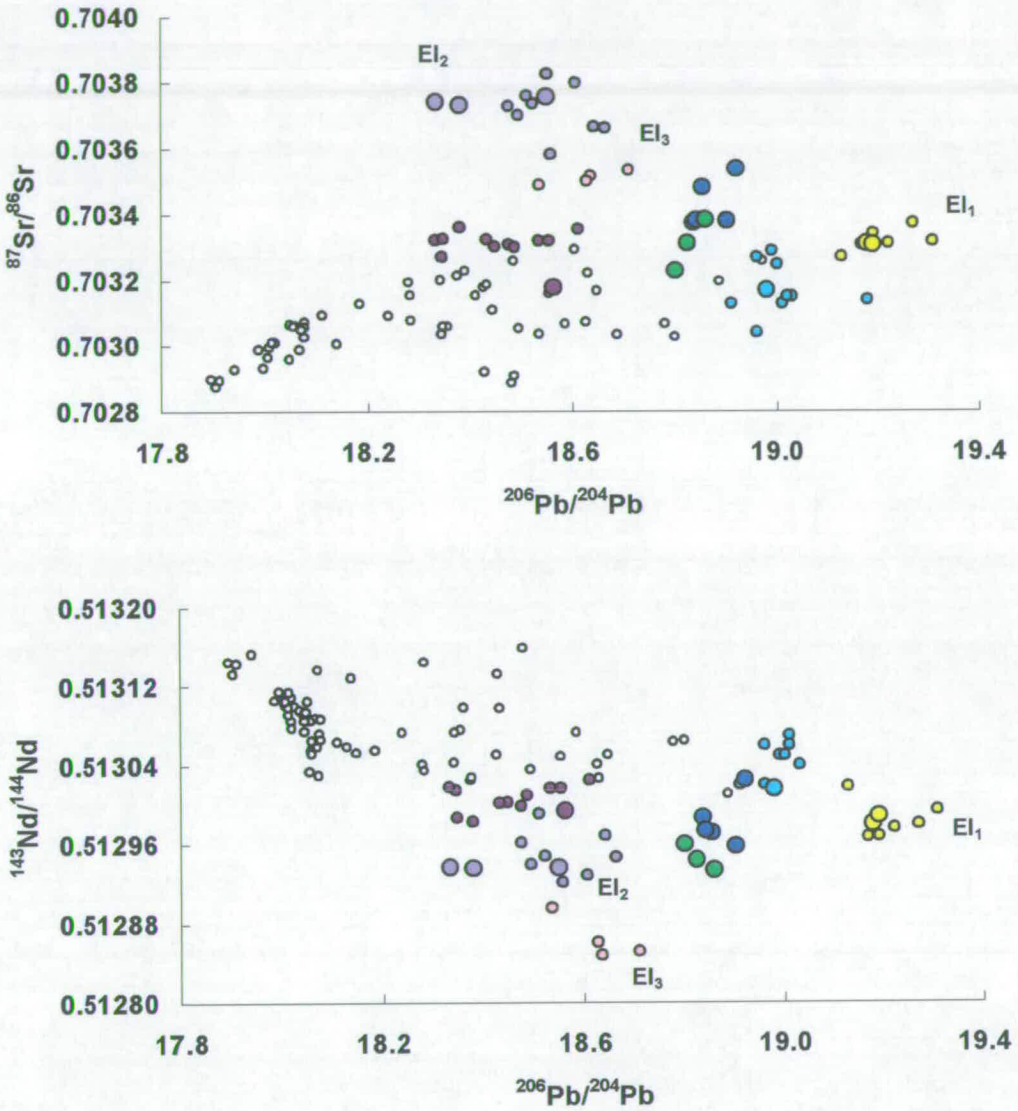

between EI_1 and EI_2, but the lower $^{143}Nd/^{144}Nd$ compared to Öræfajökull basalts (Figure 5.5c) and negative Δ7/4 (Figure 5.3a) of Jan Mayen basalts exclude this origin. The low Pb isotope ratios, high $^{87}Sr/^{86}Sr$, low $^{143}Nd/^{144}Nd$ and low $^{3}He/^{4}He$ could result from continental crustal contamination at Jan Mayen. However, Trønnes *et al.*, (1999) and Stuart *et al.*, (*in prep.*) argue that the isotopic and trace element compositions of Jan Mayen basalts are not consistent with contamination by the fragment of continental crust located south of the island. Homogeneity in isotope ratios and the similarity of the compositions of Jan Mayen basalts to those of basalts erupted along the Mohns Ridge to the north support this. If the compositions of Jan Mayen basalts represent that of their source it is necessary to invoke a third enriched end-member (EI_3) with less radiogenic Pb isotopic compositions than EI_1. EI_3 can be clearly identified in Pb-Sr and Pb-Nd isotope co-variation diagrams (Figure 5.6) and ΔNb also distinguishes EI_3 from EI_1 (Figure 5.1). By invoking EI_3, it is no longer necessary for the $^{3}He/^{4}He$ of EI_1 to be low. It could be greater than 19 R_a, as suggested in the first interpretation in Chapter 4 (Section 4.5.2). In the SFZ, therefore, depleted compositions are sampled in the south (Vestmannaeyjar) and enriched compositions are sampled in the north. The depleted component required is characterised by low $^{3}He/^{4}He$ and the enriched by high-$^{3}He/^{4}He$.

The compositions of the enriched end-members that have been identified are summarised in Table 5.1.

Table 5.1 Compositions of enriched end-members identified in the Icelandic flank-zones and Jan Mayen.

Component	$^{3}He/^{4}He$	$^{87}Sr/^{86}Sr$	$^{143}Nd/^{144}Nd$	$^{206}Pb/^{204}Pb$	ΔNb
EI_1	>19 R_a	0.7034	0.51299	19.35	0.2
EI_2	~8 R_a	0.7037	0.51294	18.7	0.2
EI_3	<5.5 R_a	0.70305	0.51305	18.0	0.6

5.2.4 Origins of mantle enrichment

5.2.4.1 EI_1

The EI_1 component dominates the SFZ mantle source, but is also present in the Snaefellsnes source. It is characterised by $^{87}Sr/^{86}Sr$ >0.7034, $^{143}Nd/^{144}Nd$ <0.51299, radiogenic Pb isotope ratios ($^{206}Pb/^{204}Pb$ >19.3), $^{3}He/^{4}He$ > ~19 R_a and ΔNb >0.2 (Table 5.1). This is similar to the chemically and isotopically enriched Icelandic component identified in numerous studies (e.g. Hanan and Schilling, 1997; Mertz and Haase, 1997; Fitton *et al.*, 1997, 2003; Stecher *et al.*, 1999; Chauvel and Hémond, 2000; Kempton *et al.*, 2000; Thirlwall *et al.*, 2004). The enriched (and depleted) Icelandic mantle components are argued to be derived from a mantle source in which μ has been enhanced (increased $^{238}U/Pb$ relative to the N-MORB-source) (e.g., Thirlwall, 1995, 2004; Chauvel and Hémond, 2000; Skovgaard *et al.*, 2001). Derivation of the EI_1 component from a HIMU-like mantle reservoir (originating from recycled oceanic crust) explains the radiogenic $^{206}Pb/^{204}Pb$ of Snæfellsnes and SFZ basalts. The $^{206}Pb/^{204}Pb$ of HIMU-derived OIB are typically > 22 (e.g., Zindler and Hart, 1986), which corresponds to isolation of subducted oceanic crust in the mantle for 2-3 Gyr (Woodhead *et al.*, 1996). The lower $^{206}Pb/^{204}Pb$ of EI_1 could result from a younger isolation age of the recycled oceanic crust, as has been proposed by Thirlwall *et al.* (2004), or from lower (U,Th)/Pb in the recycled material (Chauvel and Hémond, 2000). The negative Δ7/4 values that characterise most Icelandic basalts (except those from Öræfajökull) imply derivation from a young (<1.8 Ga) HIMU component (Thirlwall, 1997, 2004). Young-HIMU sources are also characterised by distinctive trace element ratios (e.g.,Thirlwall, 1997). The higher Nd/Pb (19.2-23.8; Kokfelt *et al*, unpubl. data) in SFZ basalts compared to old HIMU (15.8-17.5; Thirlwall, 1997), are compatible with derivation of EI_1 from a young-HIMU component. The age of this recycled component has been estimated as 400-500 Myr (Thirlwall, 1995).

$^{3}He/^{4}He$ of HIMU-dominated OIB sources are typically lower than MORB (e.g., St Helena: 4.3-5.9 R_a (Graham *et al.*, 1992); Guadalupe: 4.9-5.1 R_a (Eiler *et al.*, 1997); the Cameroon line: 5.0-6.7 R_a (Barfod *et al.*, 1999); the Cook-Austral Islands:

5.4-7.6 R_a (Hanyu and Kaneoka, 1998)). These values are higher than those predicted from pre-subduction He-degassing of oceanic crust and/or from post- or pre-subduction radiogenic ^{4}He ingrowth (e.g., Hanyu and Kaneoka, 1998; Moreira and Kurz, 2001). Subduction- and recycling-related processes should combine to produce extremely radiogenic ^{3}He/^{4}He signatures (~0.05 R_a) in a HIMU-mantle reservoir that has been isolated for 0.5 – 2 Gyr. The high ^{3}He/^{4}He of the EI_1 end-member therefore most likely originates from incorporation of mantle characterised by high ^{3}He/^{4}He.

5.2.4.2 EI_2

EI_2 is prevalent in only the Öræfajökull mantle source and is distinguished by its anomalously high ^{87}Sr/^{86}Sr (~0.7037) for ^{143}Nd/^{144}Nd (~0.51294), and high, positive Δ7/4 and Δ8/4. It has been recognised as a discrete Icelandic mantle component in previous studies (Sigmarsson *et al.*, 1992; Prestvik *et al.*, 2001). Thirlwall *et al.*, (2004) note similarities between Öræfajökull and their depleted component ID2. The distinct Pb isotopic composition of ID2 is also characteristic of the 'e' component of Hanan and Schilling (1997). These studies have related the isotopic characteristics to an origin in one of the EM-type mantle reservoirs of Zindler and Hart (1986). According to Hart (1988), EM1 mantle is characterised by extremely radiogenic ^{87}Sr/^{86}Sr (~0.705), high ^{207}Pb/^{204}Pb (~15.5) and ^{208}Pb/^{204}Pb (~37.3) and low ^{206}Pb/^{204}Pb (~17.6), and may be derived from recycled pelagic sediments (Hofmann, 1997) or from modified bulk-earth (Hart, 1984). EM2 is characterised by higher ^{206}Pb/^{204}Pb (~19.0), ^{207}Pb/^{204}Pb (~15.7) and ^{208}Pb/^{204}Pb (~38.75), and significantly more radiogenic ^{87}Sr/^{86}Sr (>0.722). This is likely derived from recycled continental crustal material (Hart, 1988; Weaver, 1991). Both Thirlwall *et al.*, (2004) and Hanan and Schilling (1997) relate their EI_2-like components to an EM1 source, in agreement with the interpretation of Öræfajökull Sr isotope-ratios by Sigmarsson *et al.*, (1992). In contrast, Prestvik *et al.*, (2001) suggest more significant involvement of an EM2-like component, based on Pb-Sr and Pb-Nd trends, and a slight but recognisable positive Pb anomaly in primitive mantle normalized trace element plots. Regardless of which EM-type component best represents the EI_2 end-member, it is clearly distinct from anything else erupted in Iceland, and most likely has a recycled origin.

OIB with EMI or EM2 characteristics have variable $^{3}He/^{4}He$, generally similar to or slightly higher than N-MORB (e.g., Hanyu and Kanaeoka, 1997; Farley and Neroda, 1998; Hanyu *et al.*, 1999), and this is also the case with the EI_2 end-member identified here. The $^{3}He/^{4}He$ signature of EM-characterised OIB may be the result of involvement of a relatively undegassed (lower-mantle) component (Hanyu *et al.*, 1999), since the recycled origin of EM-type mantle reservoirs implies that these basalts should develop extremely radiogenic He isotope compositions, even over relatively short timescales.

5.2.4.3 EI_3

The EI_3 component is similar to the high-Sr/low-Pb enriched component in the North Atlantic proposed by Mertz and Haase (1997). Most other isotopic studies have not identified this component in Iceland (although Kempton *et al.*, [2003] consider that there may be more than one enriched type of mantle domain present in the Iceland plume). Thirlwall *et al.*, (2004) require the presence of two enriched components in order to explain isotopic variations along the Reykjanes Peninsula, but while their IE1 is clearly similar to EI_1, their second enriched component (IE2) is characterised by significantly less-radiogenic isotopic compositions than EI_3. EI_3 differs significantly from EI_1 in its Pb and He isotope compositions and in ΔNb. Sr isotopic compositions approach those of EI_2, but EI_3 has more radiogenic $^{143}Nd/^{144}Nd$ than Oraefajokull basalts (Figure 5.6) and is characterised by more negative Δ7/4 than SFZ basalts (based on Jan Mayen compositions; Figure 5.3). This eliminates an origin in mixing of EI_1 and EI_2. The negative Δ7/4 (-1.2 to -4.8), positive Δ8/4 (15 - 35), low $^{3}He/^{4}He$ (5.6 - 6.7 R_a) and high (with respect to old HIMU) Nd/Pb (16.8 - 28.6) of Jan Mayen basalts (Trønnes *et al.*, 1999; Stuart *et al.*, *in prep.*) are consistent with the involvement of young (< 500 Myr-old) recycled oceanic crust. The less-radiogenic $^{206}Pb/^{204}Pb$ of EI_3 compared to EI_1 (EI_3 = ~18.7) could result from a shorter isolation time of recycled crust in the asthenospheric mantle, or from a lower (U, Th)/Pb. (It is unlikely to be a result of mixing with depleted mantle since Jan Mayen basalts are in every other way more enriched than the EI_1-characterised basalts.) A younger recycling age could produce the lower $^{206}Pb/^{204}Pb$ of EI_3, but would not result in Δ7/4 values that are more negative than EI_1

(Thirlwall., 1997). A lower μ-value in the young recycled material in the EI_3-source is therefore preferred for the origin of EI_3 Pb isotope characteristics.

5.3 Origins of source heterogeneity in flank-zones and off-axis regions: mixing between mantle components.

5.3.1 Mixing models

If representative of mixing trajectories, the near-linear trends between $^3He/^4He$ and the other isotope ratios in Figure 5.5 would, in the simplest mixing scenarios, imply that the He/Sr, He/Pb or He/Nd of the enriched components and the local depleted end-members are equal (e.g., $(He/Sr)_{enriched}/(He/Sr)_{depleted} = 1$ (*viz.* the κ-value = 1)). As inferred in Section 5.2.4 above, it is therefore unlikely that the end-members represent pure mantle components (i.e., N-MORB, HIMU or plume) but rather are derived from mixtures.

Two models can account for the observed trends (Figure 5.7). In the first, the local depleted end-member compositions are produced from near-linear mixing of two depleted mantle components which have significantly different $^3He/^4He$ (Figure 5.7a). One depleted Icelandic component (DI_1) must be characterised by $^3He/^4He$ ratios that are higher than measured in Recent Icelandic basalts (> 34.3 R_a; Figure 5.5). The composition of DI_1 is clearly similar to the depleted Icelandic component identified in numerous studies and commonly ascribed to the mantle plume (e.g., Hards *et al.*, 1995; Thirlwall *et al.*, 1995, 2004; Fitton *et al.*, 1997, 2003; Taylor *et al.*, 1997; Chauvel and Hémond, 2000; Kempton *et al*, 2000; Breddam, 2002; Murton *et al.*, 2002). The isotopic composition of this component is not well-defined except that it must be characterised by lower Sr and Pb isotope ratios and higher $^{143}Nd/^{144}Nd$ than the least enriched of the enriched basalts. If attributed to a mantle plume, the $^3He/^4He$ of the depleted Iceland component DI_1 can be assumed to be equivalent to the highest $^3He/^4He$ measured in any terrestrial basalts: 60-Ma old Baffin Island picrites have $^3He/^4He$ = ~49.5 R_a (Stuart *et al.*, 2003). The mantle source (termed HRDM: He-recharged depleted mantle, Stuart *et al.*, (2003)) is characterised by $^{87}Sr/^{86}Sr \approx 0.70305$, $^{143}Nd/^{144}Nd \approx 0.51305$. These values are similar to estimates of

the Sr-Nd isotopic composition of the depleted Iceland plume component by Taylor *et al.*, (1997) or Thirlwall *et al.*, (2004). The Pb isotope composition of HRDM cannot be constrained from Baffin Island picrites due the effects of crustal contamination. However, depleted Iceland plume mantle is assumed to have $^{206}Pb/^{204}Pb$ of 17.87-18.15 by Thirlwall *et al.*, (2004) and ~ 18.0 by Chauvel and Hémond (2000).

The second depleted component required in the mixing-model (DI_2) has $^{3}He/^{4}He$ of ~7-9 R_a (Figures 5.5, 5.7a). A potential candidate for DI_2, based on He isotopes, is therefore the shallow asthenospheric source of N-MORB. The Sr-Nd-Pb-isotopic composition of 'plume-free' North Atlantic MORB mantle has been estimated by Taylor *et al.*, (1997) and Chauvel and Hémond, (2000) to be $^{87}Sr/^{86}Sr \approx 0.70231$, $^{143}Nd/^{144}Nd \approx 0.51328$ and $^{206}Pb/^{204}Pb \approx 17.75$. These Sr and Nd isotope ratios are at the lower and upper ends respectively of the ranges given for the depleted Atlantic N-MORB source (compilation in Saunders *et al.*, 1988).

Many studies, however, dispute the involvement of North Atlantic N-MORB mantle in the Iceland plume (e.g., Hards *et al.*, 1995, Thirlwall, 1995; Fitton *et al.*, 1997, 2003; Breddam, 2002; Thirlwall *et al.*, 2004). The positive Δ7/4 and negative ΔNb that characterise N-MORB are not compatible with the compositional requirements of the low-$^{3}He/^{4}He$ depleted component DI_2. By invoking mixing of an enriched component with a N-MORB-dominated depleted component in Snæfellsnes, for example, would result in a trend towards negative ΔNb between Jan Mayen and Snæfellsnes in Figure 5.1. Such a trend is not apparent. Similarly, a trend towards positive Δ7/4 is not observed in Figure 5.3. However, N-MORB might be invoked for the depleted component present in the Snæfell mantle. Fields containing Jan Mayen and Snæfell in Figures 5.1 and 5.3 do trend towards a possible N-MORB-type end-member.

An alternative to North Atlantic MORB for the low $^{3}He/^{4}He$ depleted end-member could be the RRD1 component of Thirlwall *et al.*, (2004), which is isotopically similar to the 'plume-sheath' component of Kempton *et al.*, (2000). RRD1 may have its origins in contamination of the "plume-free" N-MORB source by an enriched mantle component (responsible for the negative Δ7/4 of RRD1-derived basalts).

Figure 5.7: Sketch diagrams demonstrating possible mixing systematics in Iceland. In (a), mixing between two depleted components (DI_1 and DI_2) produces the local depleted end-member compositions. In (b), the mixing-trends represent sections of hyperbolic mixing curves between a single depleted component (DI_1) and an enriched component (e.g. EI_3). Blue dashed arrow represents increasing κ-value.

(a)

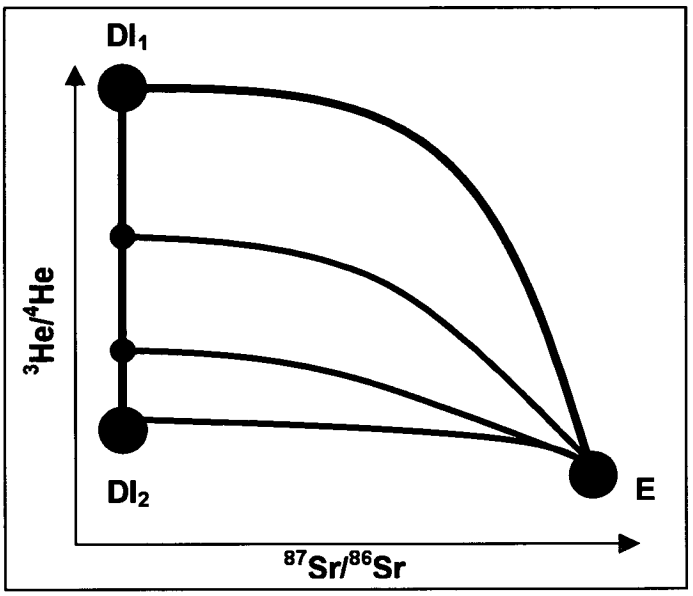

(b)

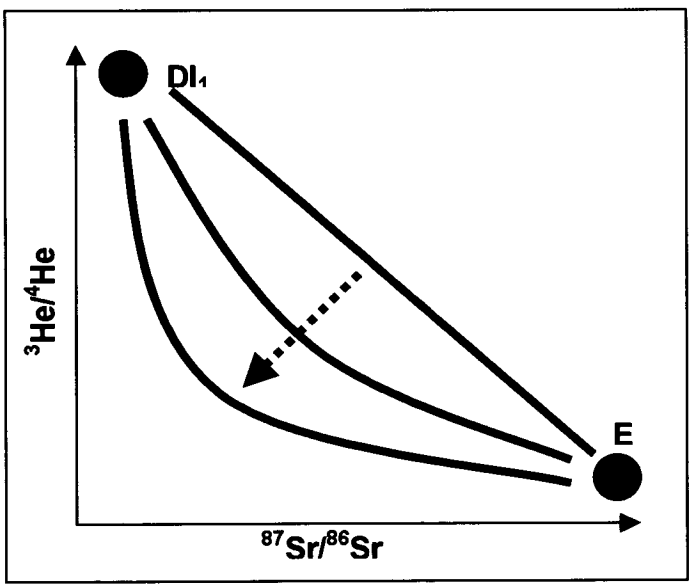

Involvement of a RRD1-type component could also explain the similarity between DI_1 and DI_2 in Pb-Sr-Nd isotope space. However, RRD1 should be characterised by high $^3He/^4He$ (equivalent to the $^3He/^4He$ of Reykjanes Ridge basalts (12.7 – 17.5 R_a; Hilton *et al.*, 2000) at latitudes of 58.3°N to 61.3°N (Thirlwall *et al.*, 2004)). The composition of RRD1 is therefore itself likely to have been affected by high-$^3He/^4He$ derived (plume-derived) mantle. Therefore, while a second depleted component, derived from N-MORB might be invoked for the depleted Snæfell-Jan Mayen end-member, this model does not appear to fully satisfy mixing requirements in the other flank zones.

In the second model, the trends identified in Figure 5.5 represent near-linear sections of hyperbolic mixing curves between a single depleted component with high $^3He/^4He$ (DI_1) and an enriched component of young-HIMU origin (Figure 5.7b). This model removes the need for an N-MORB-type component in the generation of Icelandic basalts. The degree of curvature of the mixing lines is then in each case dependent on the relative He/Sr, He/Pb or He/Nd of each component. To produce the strongly concave-upward curves ($\kappa > 1$) requires low (He/[Sr, Nd, Pb]) of DI_1 relative to the enriched component. Decreasing the (He/[Sr, Nd, Pb]) of DI_1, the inferred Iceland plume component, could be achieved by degassing prior to mixing with enriched mantle. This could be achieved if the depleted Iceland plume component contains a high water content, as has been suggested by Nichols *et al.*,(2002). Dehydration associated with small-volume melt loss (<<1%) at the wet solidus would also result the loss of up to 75% of the helium budget from the plume component prior to melting at the dry solidus (e.g., Ito *et al.*, 1999). Consequently, the depleted end-member required to explain trends in Figure 5.5 could have variable $^3He/^4He$ as a consequence of varying extents of volatile-loss.

In the following section, the two models are evaluated by examining mixing between a young-HIMU component (from which EI_1 and EI_3 are derived), a depleted plume component (DI_1 or HRDM), a depleted upper mantle component (DI_2 or NA-MORB) and a depleted component with variable $^3He/^4He$ (as a result of variable degassing of the plume).

5.3.2 Mixing parameters

The mixing parameters (isotope ratios and elemental concentrations of each component) are detailed in Table 5.2. In the model, the isotope ratios of each component are based on those expected for young-HIMU, MORB and HRDM, as determined in sections 5.2.4 and 5.3.1.1, above. For simplicity in the model degassing of the plume component is represented by variable $^{3}He/^{4}He$.

For the HIMU-like enriched components He concentrations can be estimated assuming complete degassing of oceanic crust during subduction, followed by radiogenic ^{4}He ingrowth during asthenospheric storage. Over time-scales of c. 500 Myr, appropriate for relatively young-HIMU in the Iceland plume (Thirlwall, 1995, 2004), the amount of ^{4}He produced in the recycled crust (assuming U and Th concentrations of ~0.066 and ~0.22 ppm, respectively) will be 7×10^{-6} cc STP/g (using calculations of Morrison and Pine, 1955). The concentrations of Pb, Sr and Nd in HIMU-like mantle are taken as approximately 0.2 ppm, 120 ppm and 7 ppm, respectively (Eiler *et al.*, 1997).

For the depleted mantle components, He, Pb, Sr and Nd concentrations are assumed to be broadly similar to depleted N-MORB-source mantle (Stuart *et al.*, 2003). The He concentration of NA-MORB is estimated as 1.5×10^{-5} cc STP/g from concentrations in gas-rich 'popping-rock' erupted along the Mid-Atlantic Ridge (Sarda *et al.*, 1988). A similar, but slightly higher He concentration is assumed for the depleted plume component (double the concentration of NA-MORB: 3×10^{-5} cc STP/g) based on the He concentration of HRDM (Stuart *et al.*, 2003). Pb, Sr and Nd and concentrations in the plume component and NA-MORB (based on depleted MORB mantle: DMM) are taken as 0.05 ppm, 15 ppm and 0.8 ppm, respectively (Eiler *et al.*, 1997 and references therein), with slight enrichment assumed in the plume component.

Table 5.2: Isotope ratios and element concentrations of mantle components used in mixing calculations.

Component	He (ccSTP/g)	Sr (ppm)	Nd (ppm)	Pb (ppm)	$^{3}He/^{4}He$	$^{87}Sr/^{86}Sr$	$^{143}Nd/^{144}Nd$	$^{206}Pb/^{204}Pb$
Y-HIMU	7×10^{-6}	120	7	0.23	0.05	0.7036 to 0.7038	0.5129 to 0.51283	18.7 to 19.4
PLUME	3×10^{-5}	16	3	0.05	49.5	0.70305	0.51305	18.0
N-MORB	1.5×10^{-5}	14.5	3	0.045	8	0.70231	0.51328	17.75

Note: $^{3}He/^{4}He$, $^{87}Sr/^{86}Sr$, $^{143}Nd/^{144}Nd$ and $^{206}Pb/^{204}Pb$ determined as detailed in sections 5.2.4 and 5.3.1.

Elemental concentrations in young HIMU (EI_1, EI_3), Plume (DI_1) and N-MORB mantle (DI_2) are as detailed in text.

5.3.3 Results of mixing model

How the He-Sr-Nd-Pb isotopic compositions of source end-members and flank-zone and off-axis basalts can be produced by mixing between the mantle components is shown in Figure 5.8. Local trends are well-defined in He-Sr, He-Nd and He-Pb diagrams. $^{3}He/^{4}He$ greater than 8 R_a can only be generated by involvement of the depleted plume component. The model also demonstrates the importance of a contribution of the variable-$^{3}He/^{4}He$ depleted component to the compositions of flank-zone mantle sources and this clearly has implications for the dynamics and structure of the Iceland plume. The relative proportions of enriched components involved in the flank-zone sources are best distinguished in the Pb-Sr and Pb-Nd co-variation diagrams.

In the following sections, the origins of enriched end-members and mantle source compositions in each flank-zone and in the other enriched regions (Jan Mayen and Vesteris Seamount) are considered in the context of the mixing model, and observations regarding the nature of mixing and distribution of components in the Icelandic mantle are noted.

5.3.3.1 Snæfellsnes Peninsula

According to the model, the compositions of Snæfellsnes basalts can be produced by mixing of the HIMU-type enriched component (with intermediate $^{206}Pb/^{204}Pb$ values) with depleted mantle, either dominated by MORB (DI_2) or characterised by variable $^{3}He/^{4}He$ (DI_1). The incorporation of MORB can be ruled-out based on Nb as discussed in Section 5.2.1 above. Therefore basalts from eastern Ljósufjöll are derived from mixing with a depleted mantle source derived from plume material with higher $^{3}He/^{4}He$ than basalts from western Ljósufjöll, Lysuskard or Snaefellsjokull. In the Pb-Sr and Pb-Nd diagrams, the Snæfellsnes basalts do not appear to lie on a mixing trajectory with the depleted plume component, but rather with a depleted component derived from MORB-plume mixing, or one characterised by higher $^{206}Pb/^{204}Pb$ and $^{143}Nd/^{144}Nd$ and lower $^{87}Sr/^{86}Sr$ than the plume component . Having ruled out involvement of N-MORB, this suggests that the isotopic composition of DI_1 is not the same as the HRDM composition inferred for the plume component The Sr-Nd-Pb isotopic composition of the HRDM component can be variable, as proposed by Ellam and Stuart (2004), and therefore the DI_1 component of this study might be a local variant of the global HRDM component (Figure 5.8(d-e)).

The apparent easterly increase in the proportion of depleted mantle in the Snæfellsnes source may be an artefact of melting conditions (with more-depleted mantle preferentially tapped by larger degree melts; see Section 3.5.5 and Section 5.5.2, below). However, the westerly decrease in the $^{3}He/^{4}He$ of DI_1 cannot be explained in this way and suggests that the process responsible for reducing $^{3}He/^{4}He$ is less prevalent closest to the active rift zones.

Figures 5.5(a-c) demonstrate that the enriched end-member that is present in Snæfellsnes is most similar to EI_3, as is also implied from trace element characteristics of Snæfellsnes basalts (Figure 5.1). However, involvement of EI_1 (or young-HIMU characterised by higher $^{206}Pb/^{204}Pb$) is also implied in the Pb-Sr and Pb-Nd mixing diagrams (Figure 5.5(d) and (e)). Only a minor contribution of EI_1 is required to modify the Pb isotope characteristics of Snæfellsnes basalts without significantly affecting the other isotope ratios.

5.3.3.2 Eastern Flank Zone

According to the model, the mantle beneath Snæfell is derived from a mixture of low-$^{3}He/^{4}He$ depleted material (N-MORB or highly degassed plume) and a HIMU-component with relatively unradiogenic $^{206}Pb/^{204}Pb$ (EI_3). The source composition has clear similarities to the Jan Mayen mantle source. None of the mixing diagrams exclude the potential incorporation of EI_2. Significant scatter in the data of Hards *et al.*, (1995) on the Pb-Sr plot suggests involvement of the depleted plume component rather than N-MORB in the Snæfell source, but as discussed above, the Pb-Sr-Nd composition of the depleted plume component DI_1 may be different to that inferred by Stuart *et al.*, (2003) for HRDM.

In Öræfajökull, the mantle source is dominated by EI_2, which, with the possible exception of Snæfell, has little influence outside of this volcanic centre. The uniqueness of Öræfajökull is best demonstrated in the Pb-Sr isotope plot where Öræfajökull compositions cannot be produced by mixing between any combination of the young-HIMU or depleted components.

5.3.3.3 Southern Flank Zone

The proportion of depleted mantle involved in the SFZ source is greatest beneath Vestmannaeyjar. This depleted mantle could be moderately-degassed plume or a mixture of N-MORB and high-$^{3}He/^{4}He$ plume, however trace element characteristics in the SFZ rule-out incorporation of N-MORB (Chapter 4; Figure 5.1). Mixing trends are observed in Figures 5.5(a-c) from the low $^{3}He/^{4}He$ depleted component, through Vestmannaeyjar basalts and n-SFZ basalts to EI_1. EI_1 appears itself to be derived from mixing between young-HIMU and relatively undegassed-$^{3}He/^{4}He$ plume. This suggests that the EI_1 component is intrinsic to the Iceland plume, which has important implications for the dynamics of melting and plume-degassing in Iceland. This will be examined further in the subsequent discussion sections.

5.3.3.4 Jan Mayen and Vesteris seamount

Like Snæfell basalts, Jan Mayen compositions can be explained by two-component mixing between young-HIMU (EI_3) and either high-$^{3}He/^{4}He$ plume or

N-MORB. Stuart *et al.*, (*in prep.*) conclude that a depleted plume-component is not required to explain the composition of the Jan Mayen source, and that this supports geophysical observations of the absence of a plume in the Jan Mayen region. The dominance of EI_3 in the Jan Mayen source makes it difficult to prove the absence of plume-derived depleted mantle, but the relationships between Snæfell and Jan Mayen compositions referred to above suggest that N-MORB may be the depleted component.

Helium isotope data are not available for Vesteris Seamount, but general mixing systematics can be inferred using the Pb, Sr and Nd isotope data of Mertz and Haase (1997). The model suggests that like Jan Mayen basalts, Vesteris Seamount basalts are derived from mixtures of EI_3 and minor N-MORB, implying the absence of plume-derived components. The involvement of an EI_2-like component can be excluded using Sr-Nd-Pb isotopic co-variation (Figure 5.10d-e). Vesteris seamount basalts have lower $^{143}Nd/^{144}Nd$ and lower $^{87}Sr/^{86}Sr$ than Öræfajökull basalts at similar $^{206}Pb/^{204}Pb$.

The presence of EI_3-dominated mantle at localities both far from and close to Iceland (at Snæfell and Snæfellsnes) also has important implications for the dynamics and structure of the Iceland plume, suggesting that EI_3 is not a plume-derived component but is present as an upper-mantle heterogeneity.

Figure 5.8: Results of mixing model calculations (based on Young-HIMU, NA-MORB and Plume components) for **(a)** He-Sr, **(b)** He-Nd **(c)** He-Pb, (d) Pb-Sr and (e) Pb-Nd. Mixing trajectories between components are marked as solid black lines with tick-marks representing 20% increments. The Snaefellsnes mixing trajectory is marked as a dashed line. The effect of a variably degassed plume source is indicated by the vertical line.

(a)

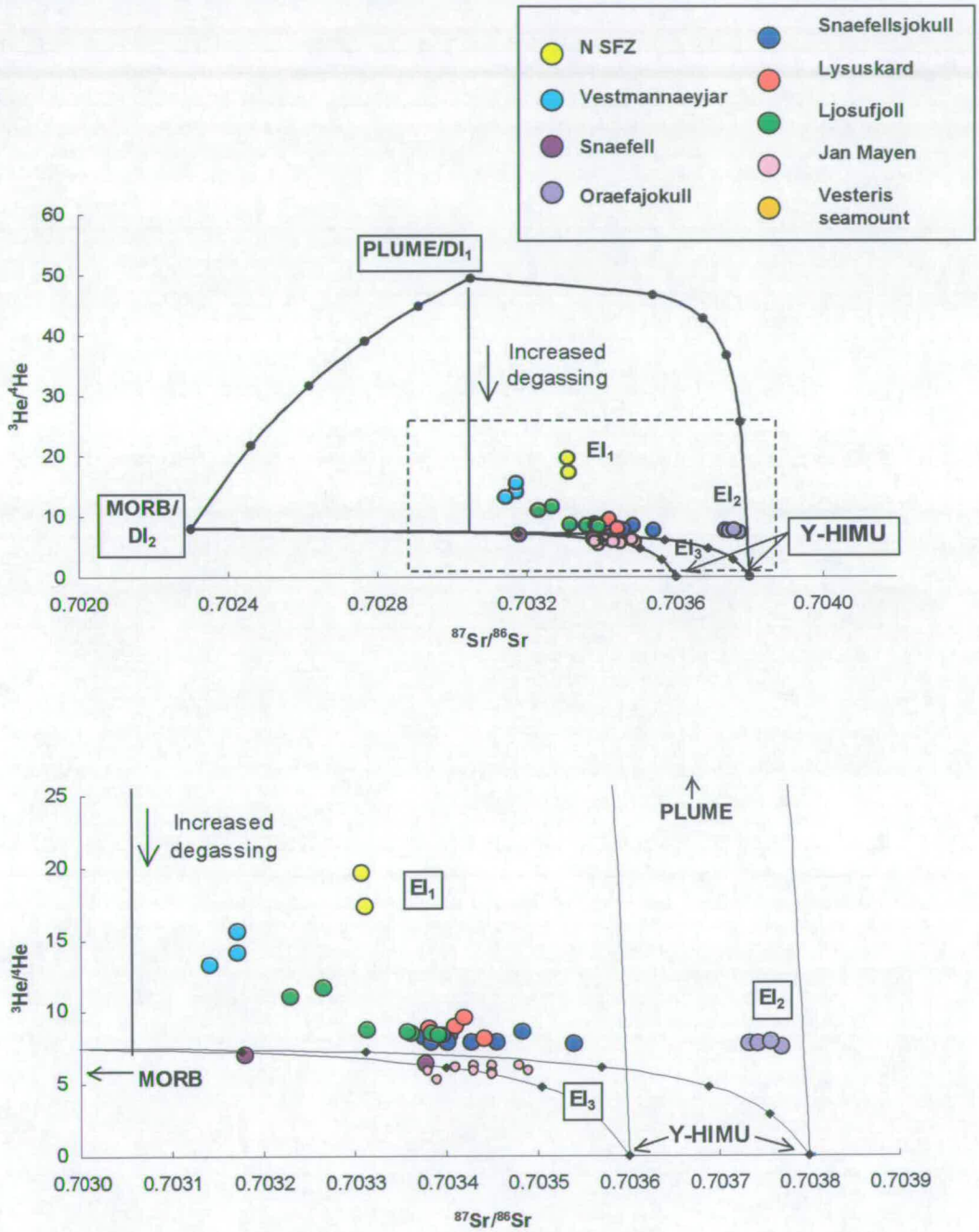

(b)

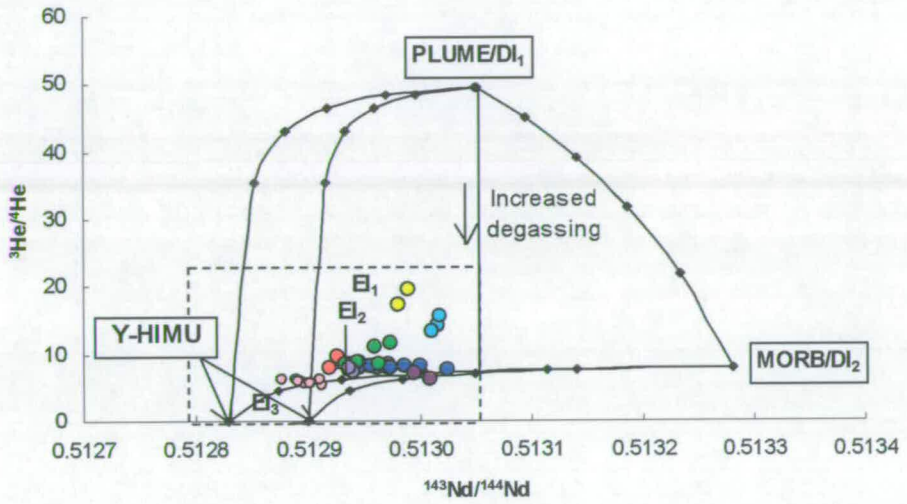
PLUME/DI1
Increased degassing
EI1
EI2
EI3
Y-HIMU
MORB/DI2
3He/4He
143Nd/144Nd
0
10
20
30
40
50
60
0.5127
0.5128
0.5129
0.5130
0.5131
0.5132
0.5133
0.5134

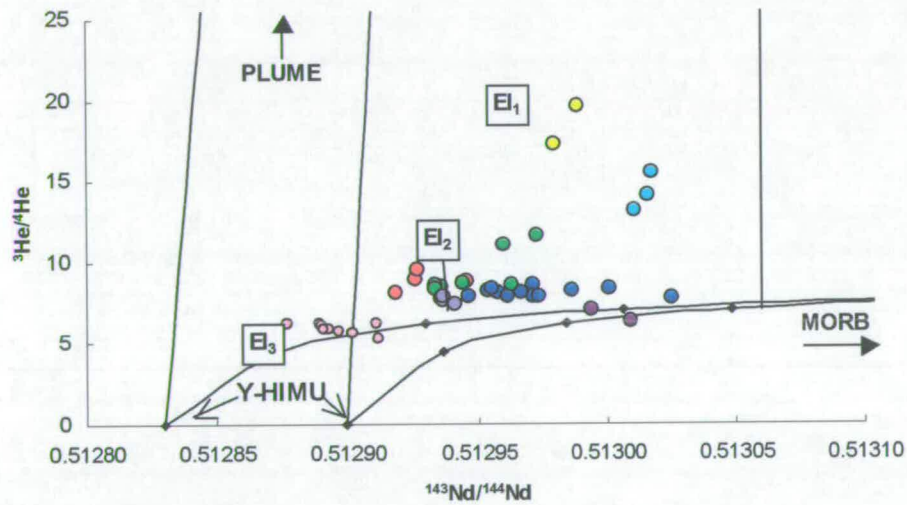
PLUME
EI1
EI2
EI3
MORB
Y-HIMU
3He/4He
143Nd/144Nd
0
5
10
15
20
25
0.51280
0.51285
0.51290
0.51295
0.51300
0.51305
0.51310

(c)

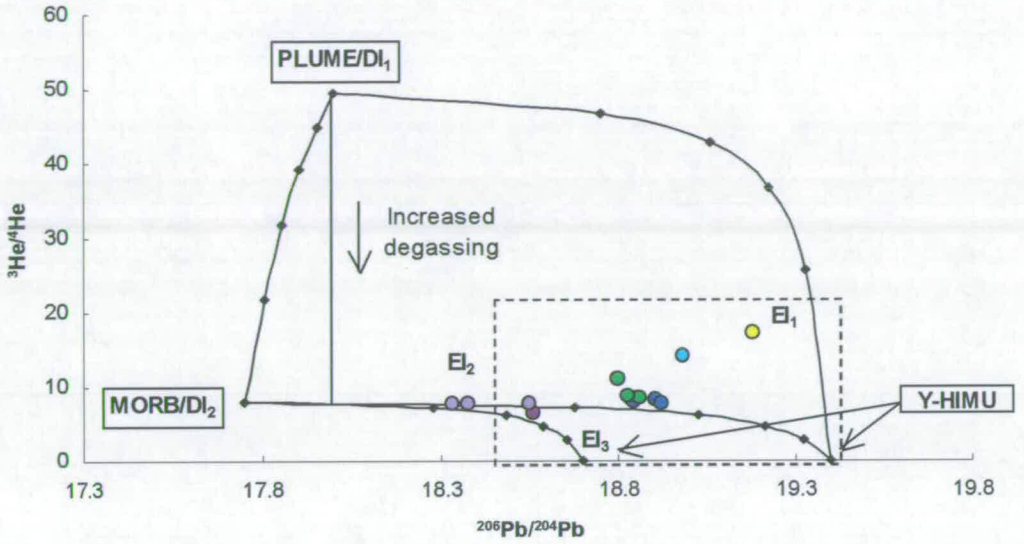
PLUME/DI1
Increased degassing
EI1
EI2
MORB/DI2
Y-HIMU
EI3
3He/4He
206Pb/204Pb

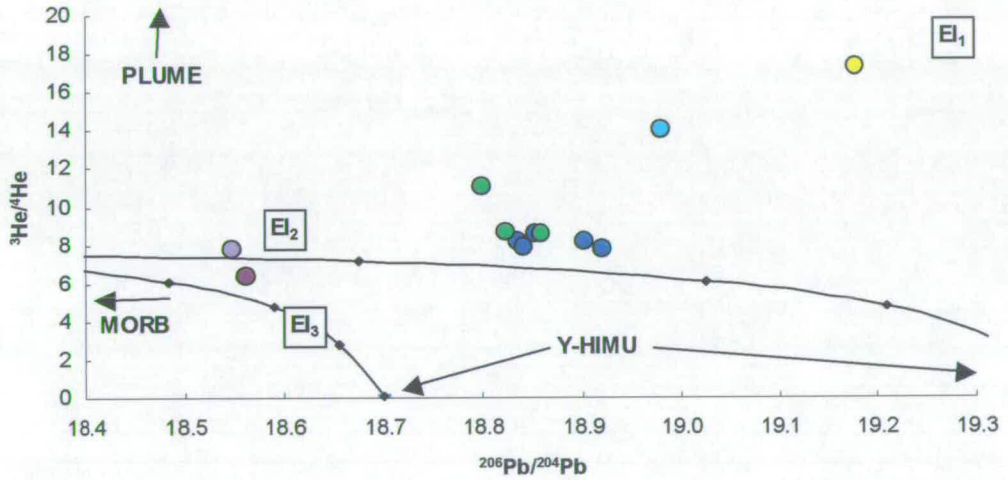
PLUME
EI1
EI2
MORB
EI3
Y-HIMU
3He/4He
206Pb/204Pb

(d)

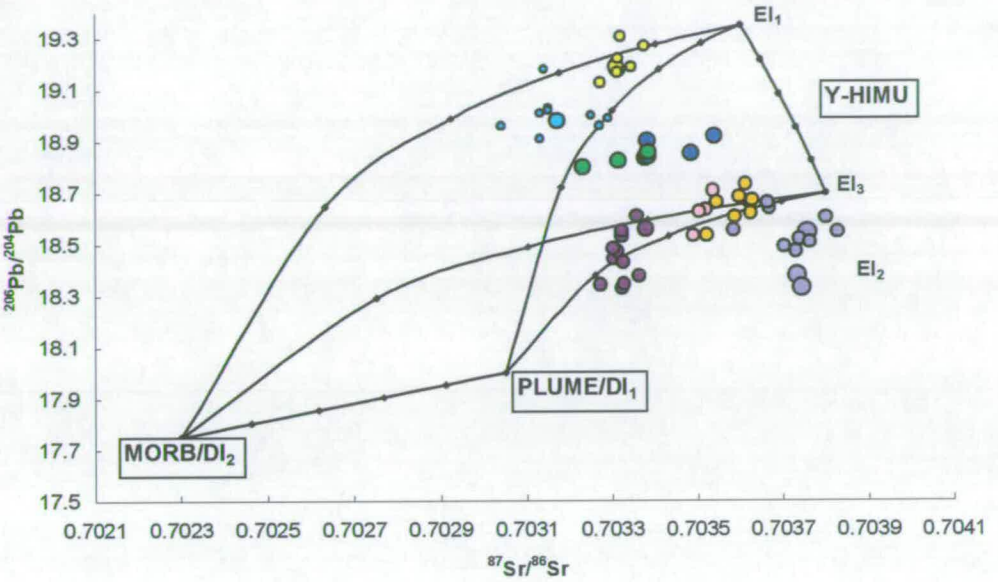
EI1
Y-HIMU
EI3
EI2
PLUME/DI1
MORB/DI2
19.3
19.1
18.9
18.7
18.5
18.3
18.1
17.9
17.7
17.5
206Pb/204Pb
0.7021
0.7023
0.7025
0.7027
0.7029
0.7031
0.7033
0.7035
0.7037
0.7039
0.7041
87Sr/86Sr

(e)

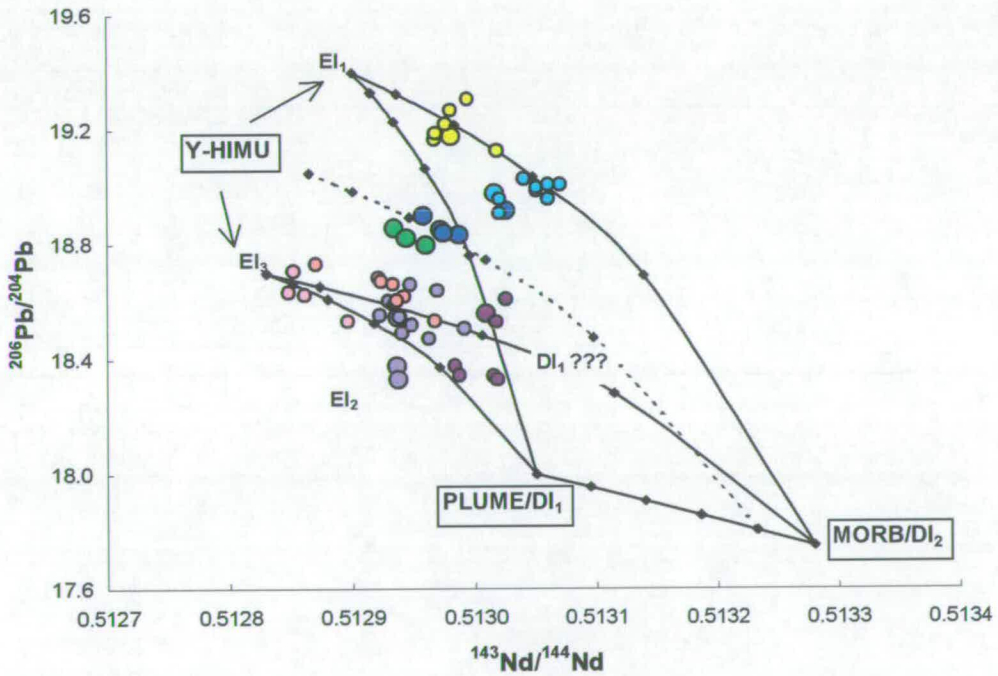
19.6
19.2
18.8
18.4
18.0
17.6
206Pb/204Pb
EI1
Y-HIMU
EI3
DI1 ???
EI2
PLUME/DI1
MORB/DI2
0.5127
0.5128
0.5129
0.5130
0.5131
0.5132
0.5133
0.5134
143Nd/144Nd

5.4 The influence of enriched components in the North Atlantic region

While enriched basaltic lavas in Iceland are erupted mainly in flank-zone regions, minor volumes of moderately enriched basalts are also found in the rift-zones. The involvement of enriched components in the generation of rift-zone source compositions should be detectable in He-Pb-Sr-Nd co-variation diagrams through displacement of data to more radiogenic He, Sr and Pb isotope ratios, and less radiogenic $^{143}Nd/^{144}Nd$, than the plume or N-MORB components. The proposed origins of EI_1 and EI_3 within the Iceland plume and the upper mantle, respectively, can also be confirmed by examining mixing trends defined by rift-zone and Mid-Atlantic Ridge data.

Tholeiitic basalts from Iceland's rift-zones and from the adjacent portions of the Mid-Atlantic Ridge (MAR) comprise the depleted ends of trends in Sr, Nd and Pb co-variation diagrams (Figure 5.6). Olivine phenocryst $^{3}He/^{4}He$ range to 34.3 R_a in lavas erupted in the rift-zones, testifying to the dominance of the high (relatively undegassed?) $^{3}He/^{4}He$ depleted component at the centre of the plume (Figure 5.4).

Basalt from the Reykjanes and Kolbeinsey Ridges (south and north of Iceland, respectively) has been shown to be contaminated by plume-derived mantle, possibly due to shallow deflection of the Iceland plume (e.g., Taylor *et al.*, 1997; Hilton *et al.*, 1999). Regional isotopic variations within the MAR mantle provide convincing evidence for plume-ridge interaction (Figure 5.9). The presence of EI_3 both within and away from the Iceland plume (e.g., at Snæfell and Jan Mayen), suggests it is a feature of a heterogeneous upper mantle source. If so, some of the variations in Sr, Nd and Pb compositions along the MAR might be explained by upper mantle heterogeneity rather than plume-contamination, in agreement with the interpretations of Mertz and Haase (1997), Hanan and Schilling (1997) and Hanan *et al.*, (2000). However, elevated $^{3}He/^{4}He$ between 53° N and 71° N cannot be explained by simple mixing of enriched and depleted N-MORB mantle, which would produce $^{3}He/^{4}He < 8\ R_a$. $^{3}He/^{4}He > 8\ R_a$ must therefore result from involvement of DI_1 in the MAR sources close to Iceland. Although the Sr, Nd and Pb isotope compositions of MAR basalts suggest plume contamination only as far south as 61° N along the Reykjanes

Ridge, basalts as far south as the Charlie Gibbs Fracture Zone at 53° N have elevated $^{3}He/^{4}He$. (Figure 5.9).

Selected data from the rift zones and from the MAR are examined in the context of the mixing model in Figure 5.10. For simplification, mixing is only examined in He-Sr and Pb-Sr co-variation diagrams since these best identify involvement of the different components. For reasons outlined earlier (Section 5.2.2), data plotted on the He-Sr diagram are restricted to olivine phenocryst $^{3}He/^{4}He$, and whole-rock $^{87}Sr/^{86}Sr$ from the same samples. This limits the available rift-zone data-set to only a few samples. However, it is still clear that elevated $^{3}He/^{4}He$ (>8 R_a) can only be explained by involvement of a plume component in source-mixing.

5.4.1 The Northern Rift-Zone and the adjacent Kolbeinsey Ridge

The NRZ comprises, from central Iceland northwards, the Kistufell, Askja, Krafla and Theistareykir volcanoes. Combined olivine-$^{3}He/^{4}He$ and Sr-Nd-Pb data are not available for the NRZ. Interpretations are therefore based solely on the Pb-Sr isotope plot. In the southern part of the NRZ, closest to the proposed centre of the Iceland plume, the mantle source appears to be derived from near-pure mixing between EI_1 and the depleted plume component. Olivine $^{3}He/^{4}He$ from volcanoes in the south of the rift-zone range from 16.6 to 34.3 R_a (Macpherson *et al.*, 2005) and thus appear to support this interpretation. In addition, the highest $^{3}He/^{4}He$ lava of Macpherson *et al.* (2005) (NAL-625) is classified as enriched (and is characterised by radiogenic Sr) and samples from the same study that are characterised by lower $^{3}He/^{4}He$ are more depleted. The source of enriched lavas examined by Macpherson *et al.*(2005) may therefore be related to the SFZ source.

In the north of the rift-zone, the Theistareykir source (N-NRZ field in Figure 5.10) appears to be derived from mixing between plume-mantle and minor EI_3. Olivine $^{3}He/^{4}He$ data from Theistareykir indicate that the source here is characterised by $^{3}He/^{4}He$ between 8 and 12 R_a (Skovgaard *et al.*, 2001; Macpherson *et al.*, 2005), which suggests that the depleted component involved has low $^{3}He/^{4}He$. Based on the Theistareykir field in the Pb-Sr diagram, a mixing trajectory could also be constructed between a depleted component and an enriched component characterised

Figure 5.9: Isotopic variation along the MAR in the North Atlantic. Shaded boxes mark locations of Iceland and Jan Mayen. Dotted lines mark the approximate compositions of 'plume-free' North Atlantic MORB. Data sources: Poreda *et al.*, (1986); Waggoner, (1989); Mertz *et al.*, (1991); Mertz and Haase, (1997); Schilling *et al.*, (1999); Hilton et al., (2000); Taylor *et al.*, (1997); Murton *et al.*, (2002).

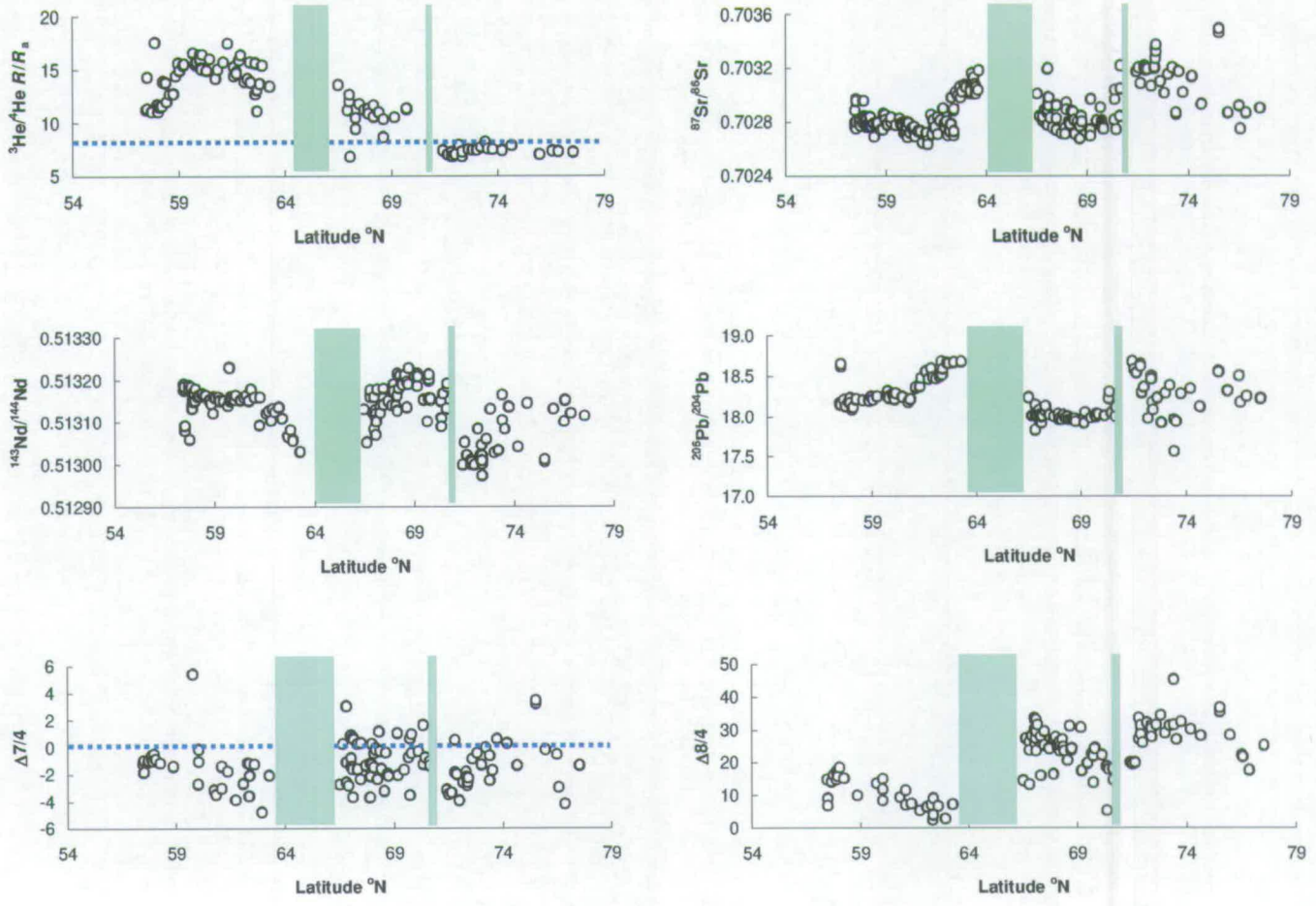

Figure 5.10: Results of mixing-model calculations based on two enriched – two depleted components, for **(a)** He-Sr and **(b)** Pb-Sr. Mixing trajectories are marked as solid black lines with tick-marks representing 20% increments. Data sources: MAR - as in Figure 5.9, rift-zones – as in Figure 5.6.

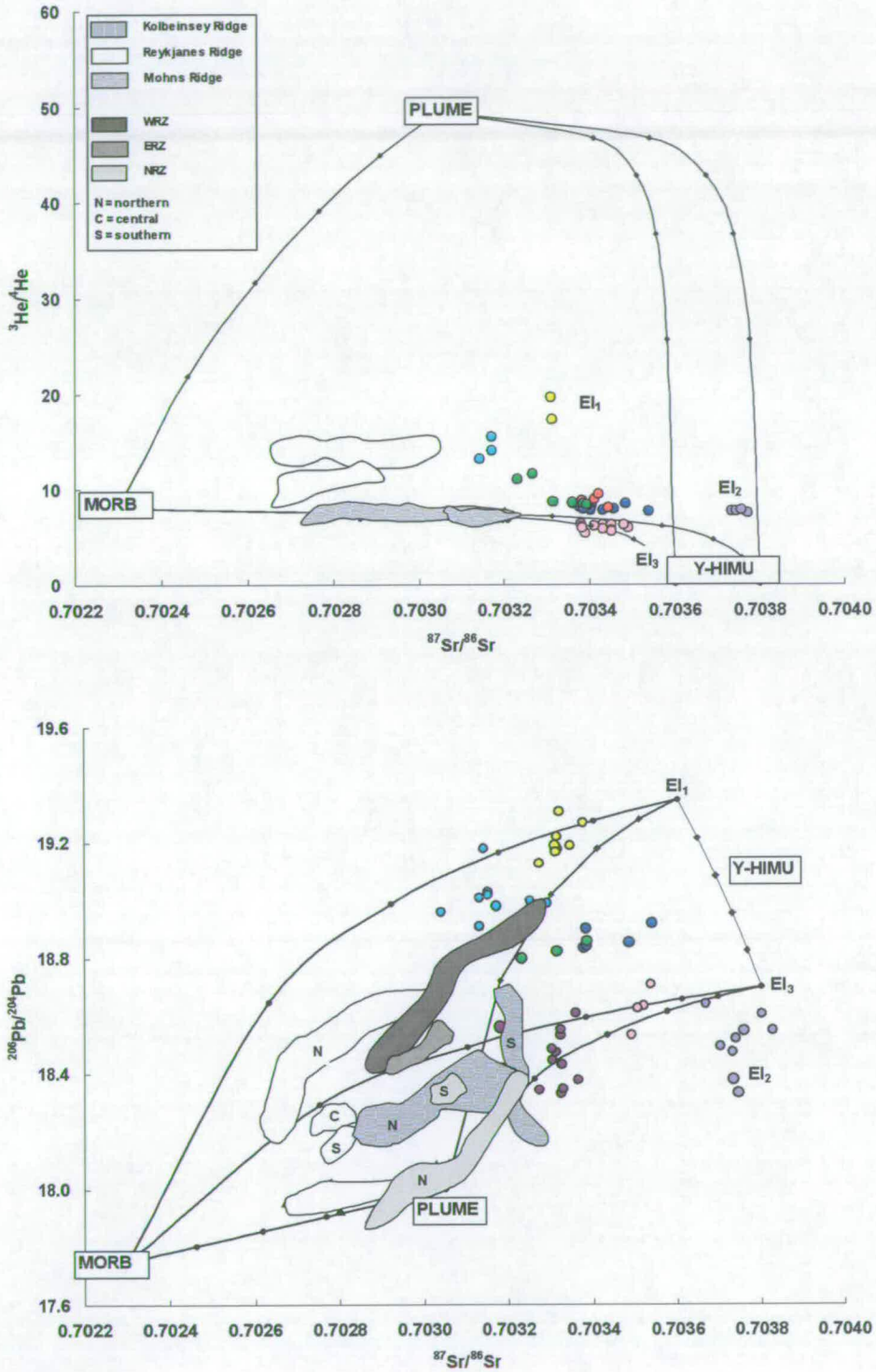

by more radiogenic $^{87}Sr/^{86}Sr$ and less radiogenic $^{206}Pb/^{204}Pb$ than EI_3. This could be EI_2 or an EI_2-like component.

The Kolbeinsey Ridge (KR) is the northern extension of the MAR adjacent to Iceland, and terminates at Jan Mayen. In the He-Sr plot the KR source appears to be derived from mixing between EI_1 and a depleted component that is either N-MORB or low-$^3He/^4He$ plume (Figure 5.10a). In this case it has similarities with the SFZ basalts, plotting at the depleted end of this trend. Alternatively, the KR source could be derived from mixing of EI_3 and low-$^3He/^4He$ plume. The Pb-Sr plot resolves this (Figure 5.10b). The compositions of KR basalts appear to be derived from a source containing a significant proportion of depleted material and neglible EI_1. EI_3, or even EI_2, appears to be responsible for any enrichment. The depleted material is in this diagram demonstrated to be derived from a N-MORB-plume mixture. The positive $\Delta 7/4$ of some Kolbeinsey Ridge basalts supports the involvement of N-MORB and/or EI_2 (Figure 5.9).

5.4.2 The Eastern Rift-Zone

Limited isotopic data are available from the ERZ. The rift-zone's proximity to the proposed centre of the Iceland plume implies that high proportions of plume-derived EI_1 and DI_1 should be present in the ERZ mantle, with the more DI_1-rich sources producing basalts characterised by the highest $^3He/^4He$. In the Pb-Sr isotope plot, ERZ basalts are derived from a mantle-source similar to that of Kistufell basalts (southern NRZ). Only one sample from the ERZ is available that has combined olivine $^3He/^4He$ and Pb isotope data (sk82-27; Kurz *et al.*, (1985)). Although a trend in the He-Pb isotope plot cannot be defined on the basis of this single sample, its high $^3He/^4He$ (20.8 R_a) and unradiogenic $^{206}Pb/^{204}Pb$ (18.45) supports derivation from the plume-derived mantle components.

5.4.3 The Western Rift-Zone and the Reykjanes Ridge

On the Pb-Sr co-variation diagram basalts from the WRZ define a mixing-trajectory between depleted (DI_1) and enriched (EI_1) plume mantle Combined olivine $^3He/^4He$ and Sr-Nd-Pb data are not available for WRZ basalts, however, olivine

$^3He/^4He$, ranging from 11 - 29 R_a (Kurz, 1985; Breddam *et al.*, 2000; Dixon, *et al.*, 2000), support this interpretation.

Variations in the isotopic compositions of Reykjanes Ridge (RR) basalts with proximity to Iceland are well-documented (e.g., Sun and Jahn 1975; Mertz *et al.*, 1991; Mertz and Haase, 1997; Taylor *et al.*, 1997; Murton *et al.*, 2002; Thirlwall *et al.*, 2004). Regional co-variation between Sr-Nd isotope ratios and $^3He/^4He$ led Taylor *et al.*, (1997) to suggest that the Reykjanes Ridge source composition is derived from mixing between N-MORB-type mantle and the Iceland plume. A similar conclusion based on He isotopes is reached by Poreda *et al.*, (1986) and Hilton *et al.*, (2000). These interpretations are supported in the mixing model presented here. The He-Sr compositions of Reykjanes Ridge basalts can be produced by mixing a minor amount of young-HIMU (EI_3-type) with depleted mantle derived from mixing of the MORB component with the high-$^3He/^4He$ plume component. The involvement of the depleted plume component increases with proximity to Iceland. This is supported by the Pb-Sr model (Figure 5.10b) which additionally demonstrates that the proportion of EI_1-type HIMU component in the enriched source mixture increases northwards towards Iceland.

5.4.4 The Mohns Ridge

The Mohns Ridge (MR) is the section of the MAR north of Jan Mayen (north of 71° N). Along the Mohns Ridge it is expected that the mantle source will be derived from mixing between the two upper-mantle components (N-MORB and EI_3). An increase in the proportion of EI_3 might be predicted at locations close to Jan Mayen. The plume-derived components should be absent. The He-Sr isotope compositions of MR basalts lie on the EI_3-MORB mixing trajectory (Figure 5.10a). Enriched mantle is apparently more abundant in the southern MR, near to Jan Mayen.

In the Pb-Sr co-variation diagram northern MR basalts form a broad field below the EI_3-N-MORB mixing trajectory. This may indicate additional involvement of an EI_2-like component. In contrast southern MR basalts form a near vertical array which cannot be explained by the mixing model. However, the array intersects the N-MORB-EI_3 mixing trajectory at a more enriched (EI_3) composition than characterises the northern MR basalts.

5.4.5 Summary

The roles of the different mantle components and Icelandic end-members in the generation of source compositions in the North Atlantic region, as determined from the model, are summarised in Figure 5.11, below.

Figure 5.11: Map of Iceland and the North Atlantic illustrating the different contributions of Icelandic end-members and mantle components to local source compositions

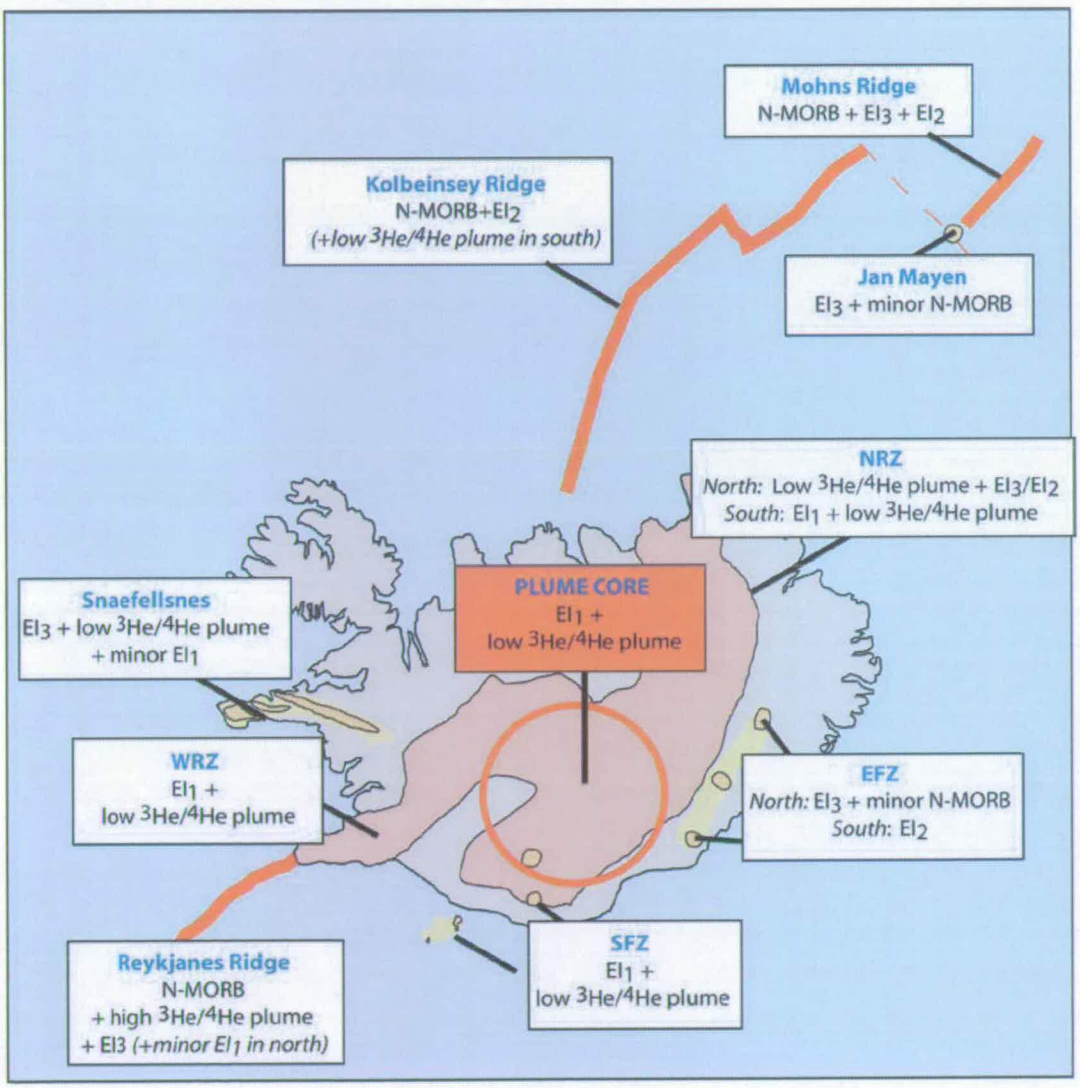

5.4.6 Comparison with previous models

The research presented in this thesis has provided new constraints on the number and nature of enriched mantle components in Iceland. As indicated in Chapter 1, previous investigations of mantle components in Iceland and the North Atlantic have tended to overlook the diversity of enriched basalts, often using data from only one flank-zone to constrain the composition of the "enriched" end-member. The interpretations of the present model are now compared to those of previous models in order to evaluate the extent to which the recognition of different enriched components weakens or strengthens these models.

The first of these studies, that of Murton *et al.*, (2002), examined geochemical variation along the Reykjanes Ridge, using Sr- and Nd-isotopes in conjunction with major and trace element data, to constrain the degree of interaction between plume- and ridge-derived mantle. Six components were proposed. Two enriched components were identified (defined as enriched on the basis of their isotopic compositions): a component intrinsic to the Iceland plume and equivalent to EI_1 of this study, and a trace-element poor version of the same component, that has been affected by melting processes. By not utilizing He and Pb data, and by disregarding data from flank-zones other than the SFZ, an EI_3-like component, demonstrated in this study to be an important constituent of Reykjanes Ridge mantle source, was not identified.

The four depleted components proposed by Murton *et al.*, (2002) can be divided into two intrinsic to the plume and two contained within a plume-sheath. The two depleted plume components were distinguished on the basis of ΔNb (the traditional 'depleted plume' with positive ΔNb and a isotopically similar component with negative ΔNb), and the two in the sheath using $^3He/^4He$ (a low $^3He/^4He$ component that is possibly a local variant of MORB and a version of this with high-$^3He/^4He$). Such a diversity of depleted components is not required in the model of this study, as a minor contribution from the either of the three enriched components can be used to explain small variations in the depleted MAR basalt compositions.

Thirlwall *et al.*, (2004) conducted a study of Icelandic mantle components using new high-precision Sr-, Nd- and Pb-isotope data, in conjunction with trace element data. Data was compiled from the Reykjanes and Kolbeinsey Ridges, the WRZ and NRZ, and the SFZ. For comparative purposes they also included the published data

of Prestvik *et al.*, (2001) for samples from Öræfajökull. Using trace element data to define "enriched" and "depleted", they identified four mantle end-members in Iceland and invoked another two to explain additional variation along the MAR segments.

The two enriched end-members identified include one, IE1, which is equivalent to the EI_1 end-member of this study. As in this study they recognize that an additional enriched end-member is required however, to explain variation in $^{206}Pb/^{204}Pb$ along the WRZ and in central Iceland, and they invoke a second enriched end-member, IE2. This end-member is not equivalent to either EI_2 or EI_3 of this study, which I use here to explain variation along the NRZ and WRZ, respectively, but has much lower Pb isotope ratios ($^{206}Pb/^{204}Pb$ =18.2) and moderate Sr and Nd isotope ratios. In this study, this end-member would in fact be classified as depleted, and therefore it may be a variant of the Icelandic depleted plume component (DI_1) that has been modified by incorporation of EI_3. Of the two depleted Icelandic components, their first is also associated with the dominant component in Iceland and the North Atlantic and is similar to the depleted component used for the models of this study. The second depleted component is invoked to explain the anomalous positive Δ7/4 of some highly depleted lavas from the Reykjanes Peninsula. However, it is isotopically similar to the EI_2 component of this study which is used to explain minor variation in the compositions of depleted Kolbeinsey Ridge and Theistareykir basalts. If EI_2 is an upper-mantle heterogeneity that is also present at the margins of Iceland, it is feasible to assume that it may be involved in local mantle sources along the Reykjanes Peninsula, even though it appears to be more prevalent to the north and east of Iceland.

5.5 Possible implications for the structure and dynamics of the Iceland mantle plume

The eruption of enriched lava flows in Iceland is largely confined to the three flank-zones. However, interpretations of the isotopic data presented in this study indicate that enriched components also form an important part of the mantle source beneath the rift zones. If, as the data suggest, one enriched component (EI_3) is

confined to the ambient upper-mantle, and another (EI_1) to the Iceland plume then the nature of mixing between plume-derived and upper-mantle-derived components that occurs in different regions could provide insights into the structure of the Iceland mantle plume.

While the spatial distribution of mantle components and the structure of the plume can explain the distribution of EI_1 or EI_3, they do not explain the concentration of enriched lavas (be they plume- or upper-mantle-derived) in the flank-zones and their relative scarcity in the rift-zones. The ultimate composition of basalts in terms of enrichment or depletion is strongly dependent on melting environment and it is generally accepted that small melt fractions preferentially sample more enriched domains in a heterogeneous mantle source (e.g., Fitton *et al.*, 2003). The restriction of the more-enriched basalts to the flank-zones must therefore tell us something about the melting conditions in the flank-zones. Various hypotheses are discussed in the final part of this section.

5.5.1 Interpretations of the spatial distribution of components in the North Atlantic mantle

The observations summarised in Section 5.4.5 (Figure 5.11) are consistent with a radial, but asymmetric, distribution of plume-derived components in the North Atlantic region. The abundance of high-$^3He/^4He$ plume-derived mantle (EI_1 and DI_1) appears to be greatest at the plume-core in the centre of Iceland where the three rift-zones converge, and deflected towards the south and south-east. At the western and northern margins of Iceland, and along sections of the MAR immediately adjacent to Iceland, only minor contributions of this plume-derived material are required to explain local source-heterogeneity. Perhaps surprisingly, given its proximity to the head of the mantle plume, there appears to be no flow of plume-derived material towards the EFZ.

Melt production in Iceland is often regarded as reflecting inter-play between active plume-driven upwelling and passive plate-driven upwelling (e.g., Maclennan *et al.*, 2001; Kokfelt *et al.*, 2003), but melting at Iceland might also be driven by dehydration (e.g., Ito *et al.*, 1999, Nichols *et al.*, 2003). This process has been invoked in the present study as a means to degas the depleted DI_1 component in the

plume. The association of EI_1 and EI_3 with the undegassed plume and upper-mantle, respectively, means that the degassing process requires further investigation here. While degassing the plume component DI_1 without degassing EI_3 can be explained if EI_3 is contained within the upper-mantle rather than the plume, it is not clear why, if present in the plume, the EI_1 component would not be affected by degassing at the same time as the depleted component DI_1.

The core of the Iceland plume is shown in this model to contain both enriched and depleted material characterised by high $^3He/^4He$. Ito *et al.*, (1999) demonstrate that when plume-mantle reaches the wet-solidus, hydrous, volatile-rich small-volume melts are formed as He is partitioned into the first-formed melts. We can assume that these are also preferentially derived from the most-enriched material. These melts rise vertically until they start to mix with the depleted, and partially degassed material in the melting zone above the dry solidus. The viscosity increase resulting from dehydration causes shallow lateral deflection of the plume and supplies high-$^3He/^4He$ depleted melts to the rift-zones. This model has been applied previously (e.g., Breddam *et al.*, 2000) and adequately explains the dominance of high $^3He/^4He$ material in centre of Iceland and along the rift-zones, but not why its distribution is asymmetrical.

Asymmetry in the distribution of mantle components has been recognised in Iceland (e.g., Thirlwall *et al.*, 2004), though an adequate explanation for it has not yet been provided by geodynamic models. Shen *et al.*, (2002) used geophysical modelling to suggest that the plume-stem beneath Iceland dips towards the south. The lateral deflection of shallow-level material, driven by plate-driven upwelling, might therefore be asymmetrical; concentrating the supply of high-$^3He/^4He$ melts along the ERZ and WRZ rather than the NRZ.

Asymmetry in the distribution of mantle components is also observed in the vicinity of Jan Mayen. EI_3 is largely absent along the Kolbeinsey Ridge south of Jan Mayen, but affects the isotopic compositions of basalts erupted along the southern Mohns Ridge to the north. This presents the possibility that EI_3 is not simply an upper-mantle heterogeneity but could represent a distinct Jan Mayen plume-component. This would also explain why EI_3-type upper-mantle mantle domains are not sampled along the Kolbeinsey Ridge in preference to EI_2-type mantle. However,

there is no geophysical evidence for a mantle plume in the vicinity of Jan Mayen (e.g., Haase *et al.*, 1996). Alternatively, EI_3 may have been an enriched component intrinsic to the ancestral Iceland Plume in which it was perhaps more abundant than it is in the present-day mantle plume. The presence of EI_3 in the vicinity of Jan Mayen could then be explained by lateral dispersion of the plume in the North Atlantic region (e.g., Trønnes *et al.*, 1999). However, if EI_3 is an ancestral plume component it is difficult to explain the absence of a degassed DI_1-type component (recognisable by positive ΔNb) beneath the Mohns Ridge. It seems more likely then that the EI_3-signature of basalts erupted in the vicinity of Jan Mayen is a result of the melting processes that determine the sampling of enriched or depleted mantle domains (see Section 5.5.2, below).

The higher proportion of low-$^3He/^4He$ mantle at the margins of Iceland (Snæfellsnes and adjacent ridge segments) suggests that the mantle plume is zoned. The mantle surrounding the core of the plume in central Iceland forms a sheath in which mixing of enriched and depleted upper-mantle and plume-derived components has occurred. If present, the extent of the sheath is also asymmetric, extending farther along the Reykjanes Ridge in the south, than along the Kolbeinsey Ridge in the north. The same processes responsible for southward deflection of the main plume would probably also cause asymmetry in the lateral extent of the plume sheath.

The concept of a concentrically zoned mantle plume has previously been proposed (e.g., Fitton *et al.*, 1997; Kempton *et al.*, 2000). In the model of Kempton *et al.*, (2000) the plume sheath is thought to be derived from mantle forming the thermal boundary layer at the base of the upper mantle and carried vertically by plume ascent. The authors infer an origin of the sheath at depth in the mantle in order to explain the trace element and isotopic distinction between the plume-sheath and N-MORB mantle source. If the plume sheath in the present model is also assumed to be derived from entrained upper-mantle at depth, then the chemical signature of the depleted upper-mantle (N-MORB) has been subsumed by that of the deep-mantle plume.

The core-sheath concept for the Iceland plume also explains the distribution of the enriched components. EI_1 is derived from mixing between a young-HIMU component and undegassed plume, and as a result is dominant in the core of the

plume in central Iceland and flows southwards along the ERZ and SFZ, and to a lesser extent the WRZ. In contrast, EI_3 appears to represent heterogeneity in the upper-mantle, since, with the exception of Snæfellsnes, involvement of EI_3 is always associated with N-MORB. The presence of EI_3 in the mantle at localities such as Snæfellsnes and along the Reykjanes Ridge can be explained if volcanism in these regions samples material derived from the plume sheath, which must have also preserved enrichments in the entrained upper-mantle even though the isotopic signatures of the depleted upper-mantle had been destroyed by the plume.

The above interpretations of the distribution of mantle components in Iceland and the North Atlantic are summarised in Figure 5.12, a schematic representation of the structure of the Iceland plume and dynamics of source generation.

Figure 5.12: Schematic diagram of the Iceland mantle plume

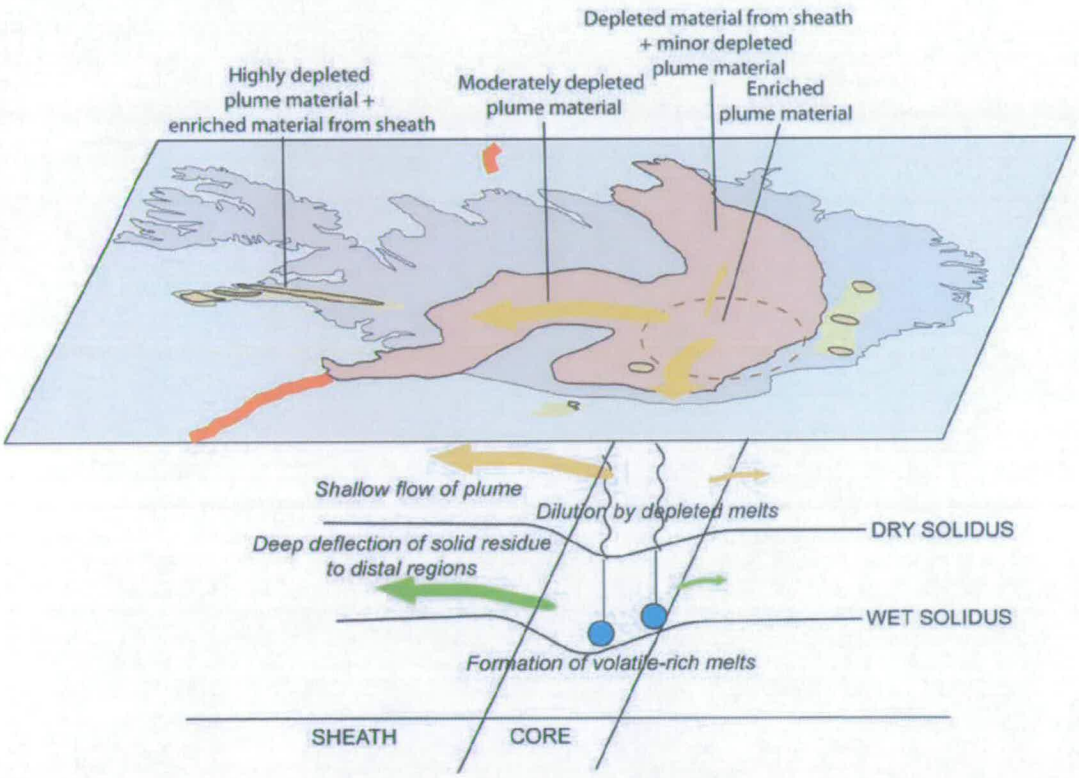

The dehydration of the core of the plume at the wet-solidus results in the formation of hydrous, volatile-rich small-volume melts. These segment and rise rapidly and vertically until they mix with depleted melts formed in the main melting zone. The extent of shallow-level mixing, controlled by the length of the melting column, determines the degree of depletion and $^3He/^4He$ of the resulting melt. Shallow-level melts are channeled into the rift-zones by deflection resulting from the associated viscosity increase. Model based in part on Shen *et al.*, 2002.

5.5.2 The role of melting processes in sampling source-heterogeneity

Inherent to any discussions of plume structure are variations in melting conditions imposed by the thermal influence of the plume and length of the melting column as determined by thickness of the mantle lithosphere and/or depth to the solidus. During dynamic melting in an upwelling mantle column, small-degree melt fractions of the enriched mantle form first within the garnet-stability field. As these melts rise in the column they are progressively diluted by larger-degree melts of the more depleted material (in the spinel-stability field) until further melting is prevented by the mantle lithosphere (e.g., Elliot *et al.*, 1991). Thus, the eruption of enriched or depleted lava flows, regardless of their plume or upper mantle derivation, must be determined by the local melting conditions.

The restriction of the most enriched flows to the flank-zones and the most depleted flows to the rift-zones indicates a radial pattern in the nature of melting environments (Figures 5.11, 5.12). The depth in the melting column at which the mantle melts influences the proportion of garnet in the enriched material. The apparently higher proportion of garnet in the Jan Mayen and SFZ sources (demonstrated by displacement to higher Ce/Y at any given Zr/Nb; Figure 5.13) therefore implies that the top of the melting zone is truncated at greater depths at these localities than beneath the other Icelandic flank-zones.

Lithospheric thickness will be greatest farthest from the centre of the Iceland plume along the Snæfellsnes Peninsula, so the length of the melting column in Iceland should be shortest beneath Snæfellsjökull. Thinner lithosphere and increasing mantle temperature and upwelling rates, towards Ljósufjöll in the east, result in a longer melting column and thus a decrease in the degree of enrichment of basalts along the peninsula. Consequently, the most-enriched basalts in Snæfellsnes are erupted in Snæfellsjökull and the most-depleted in Ljósufjöll (see Chapter 2, Figure 2.31).

Similar melting environments are observed in the EFZ. Although melting starts at a similar depth in the EFZ, mantle temperatures are likely to be higher, and therefore lithospheric thickness thinner, due to the proximity of the EFZ to the plume-head.

Figure 5.13: Ce/Y *vs.* Zr/Nb. Model non-modal fractional melting curves for spinel- and garnet-lherzolite (S-L and G-L) calculated as in Figure 2.24. Differences in the depths and degrees of melting are inferred in the flank-zones and in Jan Mayen. The proportion of garnet in the source is greatest in Jan Mayen and the SFZ and least in Ljósufjöll. The degree of melting is largest in Vestmannaeyjar and Öræfajökull.
Symbols and data-sources as in Figure 5.1.

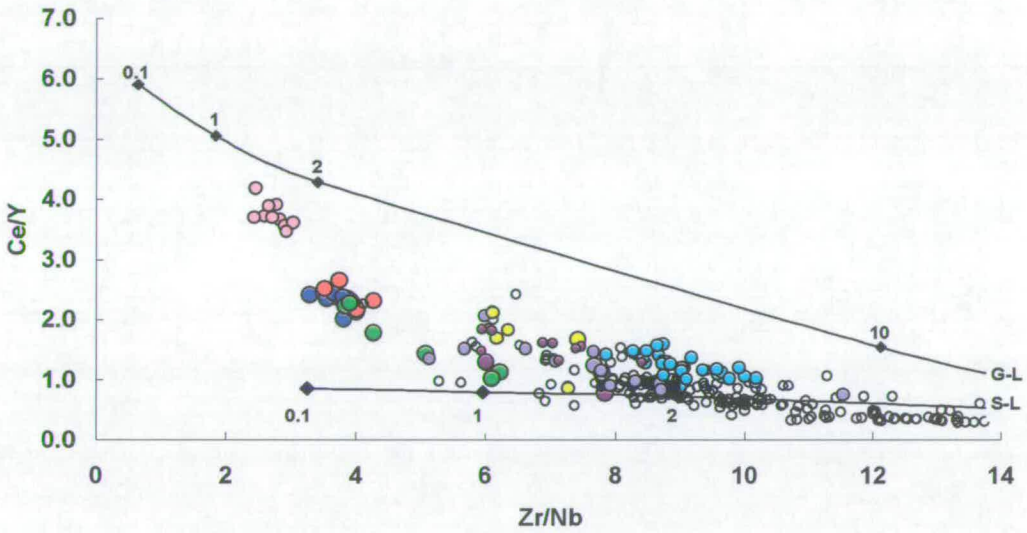

Melting in the column will progress to shallower levels, resulting in increased dilution of enriched melts by depleted melts.

In the SFZ, the degree of melting appears to increase away from the centre of the plume-head and towards Vestmannaeyjar. This is not consistent with the thinner lithospheric lid or higher mantle temperatures in the northern parts of the flank-zone. If the model of plume-dehydration is returned to here, an adequate explanation might be sought (Figure 5.12). If the northern SFZ basalts are derived from incipient melts formed where the depth to the wet solidus is greatest, and if the plume-stem is tilted, then at the point where these enriched melts cross the dry solidus, the melting column will be at its shortest and the melting rate rapid enough to prevent significant dilution by depleted, degassed mantle. In contrast, the Vestmannaeyar basalts will be derived from shallow-level plume outflow, during which time the material will be progressively diluted by depleted, large-degree melts.

5.5.3 Is there an alternative to the Iceland plume model?

The model presented here for explaining the origins and distributions of enriched and depleted mantle components in Iceland is based on the assumption that volcanism at Iceland is due to the presence of a mantle plume. Given the recent controversy regarding the existence of thermal mantle plumes (see Section 1.2.3), it is pertinent to conclude this discussion with a brief interpretation of the data in the context of alternatives.

In the interpretations above, the Iceland plume is assumed to consist of a dominant component: depleted mantle with high $^{3}He/^{4}He$ derived from depth. The deep origin is usually invoked to explain its high $^{3}He/^{4}He$. Ellam and Stuart (2004) propose that the high-$^{3}He/^{4}He$ plume component present in the North Atlantic in the Tertiary is in fact derived from helium-recharged depleted mantle, and they label their component HRDM. There is no prerequisite in their model that the helium reservoir, and therefore the ancestral Iceland plume, is derived from depth (however the prevalence of HRDM at islands normally associated with a deep plume on the basis of geophysical evidence implies that it is). Alternatives for the origins of high $^{3}He/^{4}He$ include storage of ancient helium in olivine cumulates (Natland, 2003) and preservation of helium in old (U+Th)-poor mantle (Anderson, 1998), both of which could be stored in reservoirs in the upper-mantle. In present-day Iceland, the highest $^{3}He/^{4}He$ recorded to date are in enriched basalts from the centre of Iceland (~34 R_a; Macpherson *et al.*, 2005). The high-$^{3}He/^{4}He$ ratios measured in Tertiary basalts from NW Iceland were also associated with enriched isotopic signatures (Hilton *et al.*, 1999) and likewise, in this study the highest $^{3}He/^{4}He$ are associated with the enriched end-member EI_1. The HIMU-derived EI_1 end-member is assumed to acquire its high-$^{3}He/^{4}He$ through mixing with the depleted high-$^{3}He/^{4}He$ component. Since it is perfectly feasible to have a heterogeneous upper-mantle containing enriched heterogeneities, such as EI_3 of this study, then there is no reason not to suppose that EI_1 might be an upper-mantle heterogeneity that has been 'recharged' with primordial helium at the same time as HRDM. Therefore only the location of the primordial helium reservoir needs to be constrained in order to distinguish between a shallow or deep mantle origin for the Iceland mantle source.

The second assumption associated with the plume is that it is hot and therefore that melting is induced by the increased temperatures. However, Nichols *et al.*, (2003) and Asimow and Langmuir (2003) have both demonstrated how the degree and rate of melting can instead be increased by raising the water content of the source. An increased H_2O content in the 'plume' components (EI_1 and HRDM) has already been invoked to explain the eventual variability in the $^3He/^4He$ value of the depleted component by dehydration and degassing. However, in the dehydration model of Ito *et al.*, (1999) an excess temperature of ~180°C in the source (the plume conduit) is still required in order to increase crustal thickness at Iceland without inducing the extreme along-axis melt flow predicted by previous models (see references in Ito *et al.*, 1999).

If an alternative mechanism to thermal-induced melting can be found that is capable of producing the large volumes of melt at Iceland, and reproducing the other geophysical characteristics, then the data presented in this study will not be inconsistent with a 'plume-free' model. Instead of a hot, deep-rooted plume, a hydrous heterogeneity ('blob') that has been recharged with primordial helium could be present in the shallow sub-Icelandic mantle. This may mix in with the surrounding mantle (which may contain other heterogeneities such as EI_3) at its edges in order to produce the 'sheath'. Dehydration of the 'blob' would enhance melting rates and lower the $^3He/^4He$ of the depleted, degassed material. The subsequent eruption of depleted or enriched lava flows would ultimately be determined by melting processes.

Chapter 6

Summary and conclusions

6.1 Introduction

Postglacial basalts erupted in the three Icelandic flank-zones (the Snæfellsnes Peninsula, the Southern Flank Zone, and the Eastern Flank Zone) are mildly alkaline and are highly enriched in incompatible elements compared to both tholeiitic basalt erupted in the Icelandic rift-zones and to normal mid-ocean ridge basalt (N-MORB) from the Mid-Atlantic Ridge to the north and south of Iceland. While a common theme in Icelandic geochemical research has been the nature and origins of the depleted component present in the sub-Icelandic mantle (and whether it is intrinsic to the Iceland mantle plume or the same as that present in the N-MORB source), less attention has been paid to the nature of the enriched components in the Iceland plume. A relatively limited number of isotopic studies of individual flank-zones and volcanic centres indicate that there may be more than one enriched component present in the plume; however their origins and relationships are uncertain. Similarities between the enriched mantle supplying volcanism the Snæfellsnes Peninsula and that present beneath volcanic centres elsewhere in the North Atlantic region (for example at Jan Mayen and Vesteris Seamount) might suggest that enriched mantle domains sampled in the flank-zones are not necessarily intrinsic to the plume, but exist as heterogeneities in the shallow asthenospheric mantle.

High helium isotopes (greater than the range for N-MORB: 8 ± 1 R_a) are regarded as unambiguous tracers of mantle plumes and enable the degassed and recycled mantle to be distinguished from plume-derived mantle. In conjunction with Sr, Nd and Pb data, and major and trace element data, He isotopes allow the numbers, nature, distribution of and relationships between enriched components in the sub-Icelandic mantle to be constrained.

6.2 The Snæfellsnes Peninsula

Quaternary-age primitive basalts from the Snæfellsnes Peninsula in western Iceland are characterised by mildly alkaline compositions, typical of Recent flank zone basalts found in Iceland. The basaltic lavas were erupted within three en echelon volcanic systems trending east-west along the Peninsula, and geochemical variation between and within the systems is observed.

In major and trace element composition, basalts from the Snæfellsjökull system at the western tip of the peninsula are relatively enriched in incompatible trace elements and in P_2O_5 and TiO_2. Basalts from the centrally located Lýsuskarð system have compositions broadly similar to the Snæfellsjökull basalts, whereas basalts from the easternmost Ljósufjöll system are relatively depleted in incompatible elements. Fractional crystallisation and crustal contamination play negligible roles in the production of geochemical variation within the sample suite and therefore the general east-west variation in the degree of enrichment can be interpreted as reflecting either differences in mantle source-composition and/or the depth and degree of melting.

Isotopic ratios, such as $^{3}He/^{4}He$, $^{87}Sr/^{86}Sr$, $^{143}Nd/^{144}Nd$ and $^{206}Pb/^{204}Pb$, are robust indicators of source variation. $^{3}He/^{4}He$ of olivine and pyroxene phenocrysts are identical within analytical uncertainty and have not been modified by pre-eruptive or post-eruptive processes. The highest ratio recorded for a sample (usually olivine) is considered to reflect that of the source. Regional variation in $^{3}He/^{4}He$ reflects source heterogeneity beneath the peninsula, with lavas in westernmost Snæfellsnes being derived from a source characterised by $^{3}He/^{4}He \leq 7.8R_a$ and lavas from easternmost Snæfellsnes being derived from a source characterised by $^{3}He/^{4}He > 11.6\ R_a$. $^{87}Sr/^{86}Sr$ increases in the opposite direction, with the most radiogenic compositions present in basalts from Snæfellsjökull. Regional variation in $^{143}Nd/^{144}Nd$ and Pb isotope ratios are less well-defined.

Correlations between $^{3}He/^{4}He$ and $^{87}Sr/^{86}Sr$ or the degree of incompatible trace element enrichment suggest that three distinct sources are present in the mantle beneath Snæfellsnes, which are characterised as follows:

- Incompatible element enriched; $^{3}He/^{4}He \leq 7.8\ R_a$, $^{87}Sr/^{86}Sr \geq 0.7035$
- Incompatible element depleted; $^{3}He/^{4}He \geq 11.6\ R_a$, $^{87}Sr/^{86}Sr \leq 0.7032$
- Incompatible element depleted; $^{3}He/^{4}He \sim 9\ R_a$; $^{87}Sr/^{86}Sr < 0.7032$

Mixing between these end-members produces the range of compositions observed. The enriched end-member is dominant in the mantle beneath Snæfellsjökull in the west, the high-$^{3}He/^{4}He$ depleted end-member beneath eastern Ljósufjöll, and the low-$^{3}He/^{4}He$ depleted end-member beneath western Ljósufjöll. The relationships between incompatible element enrichment and isotopes indicate that the type of mantle domain sampled is to some degree controlled by the extent and depth of

melting. Correlations between source-discriminants (e.g., $^{3}He/^{4}He$ and $^{87}Sr/^{86}Sr$) imply that the incompatible element depleted basalts are also isotopically distinct. Increasing degrees of partial melting, and a lengthening of the melt column towards the east of the peninsula and the active-rift zones, results in increasing dilution of enriched melt-fractions by depleted mantle melts.

6.3 The Eastern Flank Zone

Isotopic data from Öræfajökull and Snæfell indicate the presence of at least two components in the EFZ source region; however, the compositions of the Öræfajökull rocks may have been affected by contamination. Contamination by old Icelandic crust can be excluded on the basis of trace element compositions, the low $^{87}Sr/^{86}Sr$ of basement rocks in the EFZ, the unradiogenic $^{3}He/^{4}He$ of Öræfajökull basalts and the relatively high $\delta^{18}O$ of the basalts. Oxygen isotope data also preclude significant assimilation of continental crust; a fragment of which has been postulated to underlie Öræfajökull. Consequently, the isotopic distinction between the two volcanoes is considered to be mainly the result of source-variation.

Fractional crystallisation can explain the more enriched nature of the Öræfajökull andesites, but does not explain the incompatible element enrichment of the EFZ basalts relative to rift zone tholeiites. Variation in the degree and depth of partial melting has been examined using incompatible trace element ratios of Öræfajökull and Snæfell basalts. Basalts from both volcanoes appear to be derived from small-degrees of partial melting of the same source.

Closer examination of the isotopic compositions of the Snæfell and Öræfajökull samples tentatively suggests the presence of two enriched components in the EFZ mantle. The Öræfajökull-type component is characterised by anomalously high $^{207}Pb/^{204}Pb$, $^{208}Pb/^{204}Pb$ for its $^{206}Pb/^{204}Pb$, and radiogenic $^{87}Sr/^{86}Sr$. The enriched component present in the Snæfell source is characterised by more radiogenic $^{206}Pb/^{204}Pb$. The differences in the $^{3}He/^{4}He$ of the Snæfell and Öræfajökull samples may simply reflect differing degrees of involvement of depleted MORB-type mantle in their sources. However, the presence of the Öræfajökull component as a discrete blob in the mantle cannot be ruled-out on the basis of the EFZ data alone.

6.4 The Southern Flank Zone

Basalts from the SFZ, located at the tip of the propagating ERZ, range in composition from highly incompatible-element-enriched, transitional basalt at Torfajökull and Eyjafjöll in the north of flank-zone, to more depleted and mildly-alkaline basalt at Vestmannaeyjar at the southern end of the flank-zone. Some of the variation in major element composition can be explained by fractional crystallisation at individual volcanic centres, but source heterogeneity is required to explain differences between volcanoes. Regional variation is also observed in the isotope data, such that the most incompatible-element-enriched basalts are also the most isotopically-enriched, and this does not appear to be a consequence of interaction with oceanic crust during rift-propagation as has been proposed by Oskarsson *et al.*, (1982, 1985). $^{206}Pb/^{204}Pb$ ranges from ~18.8 (Vestmannaeyjar) to ~19.4 (Torfajökull), and correlates positively with $^{87}Sr/^{86}Sr$ (~0.7031-0.7034) and negatively with $^{143}Nd/^{144}Nd$ (~0.51296 - 0.51301). While $^{3}He/^{4}He$ increases northwards with proximity to the inferred centre of the plume (~13-19 R_a), unlike at the Snæfellsnes Peninsula, $^{3}He/^{4}He$ is highest in the more enriched basalts. The regional co-variations in He, Sr, Nd and Pb isotopes might be explained either by (i) two-component mixing between enriched mantle characterised by high $^{3}He/^{4}He$ (>~19 R_a) and depleted mantle characterised by lower $^{3}He/^{4}He$ (< 11 R_a); or (ii) by mixing between enriched mantle characterised by low $^{3}He/^{4}He$ with local depleted mantle domains characterised by variable $^{3}He/^{4}He$ (as appears to occur in Snæfellsnes).

6.5 The nature, number and origins of enriched components

Examination of flank-zone basalt isotopic compositions reveals coherent trends in He-Sr-Nd-Pb isotope co-variation diagrams which allow the identification of three subtly distinct enriched components in the North Atlantic mantle. Each enriched end-member is characterised by lower $^{143}Nd/^{144}Nd$ and more radiogenic Pb and Sr isotope ratios than the depleted mantle components sampled in the rift-zones and along the MAR. One enriched end-member, EI_1, is most prevalent in the mantle beneath the SFZ. It is distinguished from the other enriched end-members by its extreme Pb isotope composition ($^{206}Pb/^{204}Pb$ > 19.4) and higher $^{3}He/^{4}He$ (>19 R_a). It is probably

derived from recycled oceanic crust (a young-HIMU-like component). The second enriched end-member, EI_2, is only sampled at Öræfajökull (EFZ), and is distinguished by its extreme $^{87}Sr/^{86}Sr$ (> 0.7037) and positive $\Delta 7/4$. Its isotopic composition most likely has its origins in recycled pelagic or terrigenous sediments. The third enriched end-member, EI_3, dominates the Jan Mayen (North Atlantic) and Snæfell (EFZ) mantle sources. It has similar Sr and Nd isotopic compositions to EI_1, but is characterised by less-radiogenic Pb isotope ratios ($^{206}Pb/^{204}Pb$ ~18.6), lower $^3He/^4He$ (< 5 R_a) and higher ΔNb (~0.6). It is also most likely derived from young recycled oceanic crust. Enriched mantle beneath Snæfellsnes appears to be derived from mixing of EI_1 and EI_3.

Trends in isotope co-variation diagrams can be explained by mixing of enriched end-members and depleted mantle end-members that have variable $^3He/^4He$ as a consequence of degassing the depleted Iceland plume component. Degassing is initiated by dehydration and small-volume melt loss from the plume. A depleted N-MORB like component may also be involved in source generation in Jan Mayen, Snæfell, and along the MAR segments adjacent to Iceland.

The mixing model presented enables plume-derived enriched components to be distinguished from those present in the shallow asthenospheric mantle. Only EI_1 appears to be intrinsic to the plume, whereas EI_2 and EI_3 are upper-mantle heterogeneities. EI_2, or an EI_2-like component derived from continental material, while dominant in Öræfajökull, appears to be involved in the mantle sources of MORB in the North Atlantic, particularly along the northernmost parts of the MAR

The distribution of enriched and depleted components and mixing relationships between them, indicate that the Iceland mantle plume may be zoned, with pure plume-derived mantle (derived from mixing of high-$^3He/^4He$ EI_1 and depleted, degassed plume) only present at the very core of the plume in south-eastern Iceland. If so, both the shallow-level outflow of plume-derived material and the lateral extent of the sheath surrounding the plume appears to be asymmetric, extending farther to the south of Iceland than to the north (Figure 6.1a). Aswell as the strong source and provenance controls on the compositions of Icelandic basalts, the restriction of the most enriched basalts to the flank-zones is in part a result of melting processes.

Enriched sources will be preferentially sampled by small-degrees of partial melting of a heterogeneous source (Figure 6.1b).

Figure 6.1: (a) Dynamics and structure of the Iceland plume as interpreted from the results of this study. See Chapter 5 for details; **(b)** the role of melting in sampling enriched and depleted mantle in Snaefellsnes. See Chapter 2 for details.

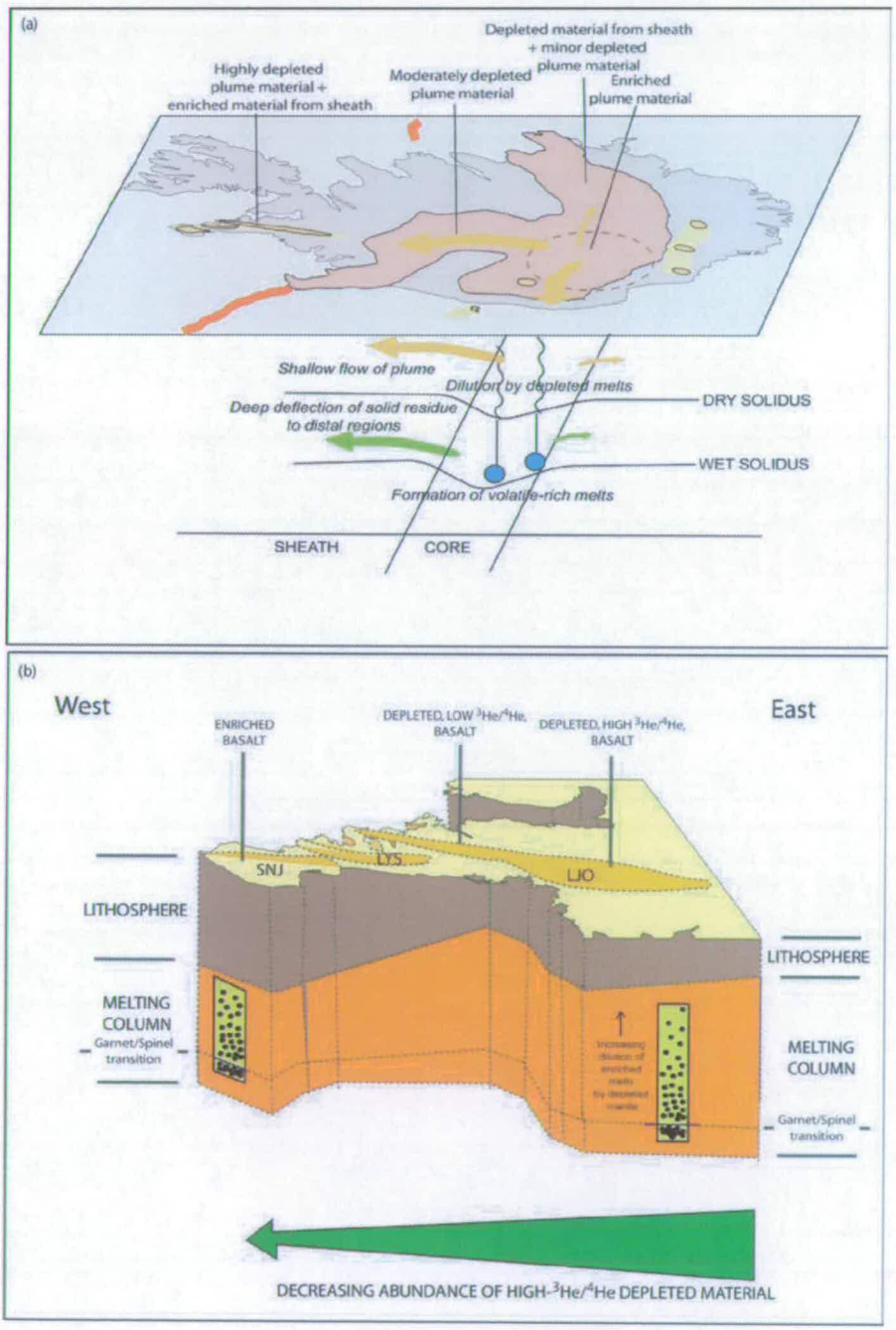

REFERENCES

Allègre, C.J., Staudacher, T., Sarda, P., 1986. Rare gas systematics: formation of the atmosphere, evolution and structure of the Earth's mantle. *Earth Planet. Sci. Lett.* **81,** 127-150.

Allègre, C.J., Moreira, M., Staudacher, T., 1995. $^{3}He/^{4}He$ dispersion and mantle convection. *Geophys. Res. Lett.* **22,** 2325-2328.

Amundsen, H.E.F., Schaltegger, U., Jamtveit, B., Griffin, W.L., Podladchikov, Y.Y., Torsvik, T., Gronvold, K., 2002. Reading the LIPs of Iceland and Mauritius, in: *15th Kongsberg Seminar,* B. Jamtveit, and H.E.F. Amundsen eds., Kongsberg, Norway.

Anderson, D.L., 1998. A model to explain the various paradoxes associated with mantle noble gas geochemistry. *Proc. Natl. Acad. Sci.* **95**, 9087-9092.

Anderson, D.L., 2000. The thermal state of the upper mantle: No role for mantle plumes. *Geophys. Res. Lett.* **27**, 3623-3626.

Anderson, D.L., 2001. Top-down tectonics? *Science* **293**, 2016-2018.

Anderson, D.L., 2003. Look again. *Astro. Geophys.* **44**, 1.10-1.11.

Anderson, D.L., Zhang, Y.-S., Tanimoto, T., 1992. Plume heads, continental lithosphere, flood basalts and tomography. *In*: Storey, B.C., Alabaster, T.U. & Pankhurst, R.J. (eds). Magmatism and the causes of continental break-up. *Geological Society Special Publication* **68**, 99-124.

Andrews, J.N., 1989. The isotopic composition of radiogenic helium and its use to study groundwater movements in confined aquifers. *Chem. Geol.* **49**, 339-351.

Asimow, P.D., Langmuir, C.H., 2003. The importance of water to oceanic mantle melting regimes. *Nature* **42**, 815-820.

Baker, M.B., Stolper, E.M., 1994. Determining the composition of high-pressure mantle melts using diamond aggregates. *Geochim. Cosmochim. Acta* **58**, 2811-2827.

Baker, M.B., Hirschmann, M.M., Ghiorso, M.S., Stolper, E.M., 1995. Compositions of near-solidus peridotite melts from experiments and thermodynamic calculations. *Nature* **375**, 308-311.

Barfod, D., Ballentine, C.J., Halliday, A.N., Fitton, J.G., 1999. Noble gases in the Cameroon line and the He Ne and Ar isotopic compositions of high μ (HIMU) mantle, *J. Geophys. Res.* **104,** 29509-29527.

Bijwaard, H., Spakman, W., 1998. Tomographic evidence for a narrow whole mantle plume below Iceland. *Earth Planet. Sci. Lett.* **166**, 121-126.

Bjarnason, I., Menke, W., Flovenze, O., Caress, D., 1993. Tomographic image of the spreading centre in southern Iceland. *J. Geophys. Res.* **98**, 6607-6622.

Bjornsson, A., Sæmundsson, K., Einarsson, P., Tryggvason, E., Gronvold, K., 1977. Current rifting episode in north Iceland. *Nature* **266**, 318-323.

Bjornsson, H., Einarsson, P., 1990. Volcanoes beneath Vatnajökull, Iceland: evidence from radio echo-sounding, earthquakes and jokulhlaups. *Jokull* **40** 147-168.

Bjornsson, H., Kristmannsdottir, H., 1984. The Grimsvötn geothermal area, Vatnajokull, Iceland. *Jokull* **34**, 25-50.

Blake S., 1984. Magma mixing and hybridization processes at the alkalic, silicic Torfajökull central volcano triggered by tholeiitic Veiðivötn fissuring, south Iceland. *J. Volcanol. Geotherm. Res.* **22,** 1-31.

Bonatti, E., 1990. Not so hot 'hot spots' in the oceanic mantle, *Science* **250**, 107-111.

Bourgeois, O., Dauteuil, O., Van Vliet-Lanoe, B., 1998. Pleistocene subglacial volcanism in Iceland: tectonic implications. *Earth Planet. Sci. Lett.* **164**, 165-178.

Bunce, L., 2002. Off-axis volcanism and the length-scale of mantle heterogeneity beneath the Snaefellsnes peninsula, western Iceland. Ph.D Thesis. University of Edinburgh.

Breddam, K., Kurz, M.D., Storey, M., 2000. Mapping out the conduit of the Iceland mantle plume with helium isotopes. *Earth Planet. Sci. Lett.* **176**, 45-55.

Breddam, K., 2002. Kistufell: Primitive melt from the Iceland mantle plume. *J. Petrol.* **43**, 345-373.

Brown, P.E., Fallick, A.E., Becker, S.M., Dempster, T.J., Hutton, D.H.W., 1999. The Rapakivi granites of south Greenland - stable isotope characteristics of their black and white facies and the nature of their protolith. *Lithos* **46**, 485-504.

Campbell, I.H, Griffiths, R.W., 1990. Implications of mantle plume structure for the evolution of flood basalts. *Earth Planet. Sci. Lett.* **99**, 79-93.

Chauvel, C., Hoffman, A.W., Vidal, P., 1992. HIMU-EM: The French Polynesian connection. *Earth Planet. Sci. Lett.* **110**, 99-119.

Chauvel, C., Hémond, C., 2000. Melting of a complete section of recycled oceanic crust: trace element and Pb isotopic evidence from Iceland. *Geochem. Geophys. Geosyst.* **1**, 1999GC000002.

Condomines, M., Grönvold, K., Hooker, P.J., Muehlenbachs, K., O'Nions, R.K., Óskarsson, N., Oxburgh, E.R., 1983. Helium, oxygen, strontium and neodymium isotopic relationships in Icelandic volcanics. *Earth Planet. Sci. Lett.* **66**, 125-136.

Courtillot, V., Davaille, A., Besse J., Stock, J., 2003. Three distinct types of hotspot in the Earth's mantle. *Earth Planet. Sci. Lett.* **205**, 295-308.

Craig, H., Poreda, R.J., 1986. Cosmogenic ^{3}He in terrestrial rocks: the summit lavas of Maui. *Proc. Nat. Acad. Sci. USA* **83**, 1970.

Darbyshire, F.A., White, R.S., Priestly, K.F., 2000. Structure of the crust and uppermost mantle of Iceland from combined seismic and gravity study. *Earth Planet. Sci. Lett.* **181**, 409-428.

Dickin, A.P., 1981. Isotope geochemistry of Tertiary Igneous rocks from the Isle of Skye, N.W. Scotland. *J. Petrol.* **22**, 155-189.

Dixon, E.T., 2003. Interpretation of Helium and Neon isotopic heterogeneity in Icelandic basalts. *Earth. Planet. Sci. Lett.* **206**, 83-99.

Dixon, E., Honda, M., McDougall, I., Campbell, I., Sigurdsson, I., 2000. Preservation of near-solar isotopic ratios in Icelandic basalts. *Earth Planet. Sci. Lett.* **180**, 309-324.

Eiler, J.M., Farley, K.A., Valley, J.W., Hauri, E., Craig, H., Hart, S.R., Stolper, E.M., 1997. Oxygen isotope variations in ocean island basalt phenocrysts. *Geochim. Cosmochim. Acta* **61**, 2281-2293.

Eiler, J.M., Grönvold, K., Kitchen, N., 2000. Oxygen isotope evidence for the origin of chemical variations in lavas from Theistareykir volcano in Iceland's northern volcanic zone. *Earth Planet. Sci. Lett.* **184,** 269-286.

Eiler, J.M., Crawford, A., Elliott, T., Farley, K.A., Valley, J.W., Stolpher, E.M., 2000. Oxygen isotope chemistry of oceanic arc lavas. *J. Petrol.* **41**, 229-256.

Ellam, R.M., Stuart, F.M., 2000. The sub-lithospheric source of North Atlantic Basalts: evidence for, and significance of, a common end-member. *J. Petrol.* **41**, 919-932.

Ellam, R.M., Stuart, F.M., 2004. Coherent He-Nd-Sr isotope trends in high 3He/4He basalts: implications for a common reservoir, mantle heterogeneity and convection, *Earth Planet. Sci. Lett.* **228**, 511-523.

Elliot, T.R., Hawkesworth, C.J., Grönvold, K., 1991. Dynamic melting of the Iceland Plume. *Nature* **351**, 201-206.

Farley K.A., Neroda, E., 1998. Noble gases in the Earth's mantle. *Ann. Rev. Earth Planet. Sci.* **26**, 189-218.

Fitton, J.G., Saunders, A.D., Norry, M.J., Hardarson, B.S. and Taylor, R.N., 1997. Thermal and chemical structure of the Iceland plume. *Earth Planet. Sci. Lett.* **153**, 197-208.

Fitton, J.G., Hardarson, B.S., Ellam, R.M., Rogers, G., 1998. Sr-, Nd-, and Pb-isotope composition of volcanic rocks from the southeast Greenland margin at 63°N: temporal variation in crustal contamination during continental breakup. *Proceedings of the Ocean Drilling Program, Scientific results* **152**, 351-357.

Fitton, J.G., Saunders, A.D., Kempton, P.D., Hardarson, B.S., 2003. Does depleted mantle form an intrinsic part of the Iceland plume? *Geochem. Geophys. Geosyst.* **4**, 2002GC000424.

Foulger, G.R., Pritchard, M.J., Julian, B.R., Evans, J.R., Allen, R.M., Nolet, G., Morgan, W.J., Bergsson, B.H., Erlendsson, P., Jakobsdóttir, S., Ragnarsson, S., Stefansson, R., Vogtfjörd, K., 2000. The seismic anomaly beneath Iceland extends down to the mantle transition zone and no deeper. *Geophys. J. Int.* **142**, F1-F5.

Foulger, G.R., 2004. On the apparent eastward migration of the spreading ridge in Iceland. *Penrose conference abstract vol.*

Foulger, G.R., Pearson, D.G., 2001. Is Iceland underlain by a plume in the lower mantle? Seismology and helium isotopes. *Geophys. J. Int.* **145**, F1-F5.

Foulger, G.R., Natland, J.H., Anderson, D.L., 2005. A source for Icelandic magmas in remelted Iapetus crust. *J. Volcanol. Geotherm. Res.* **141**, 23-44.

Furman, T., Frey, F.A., Park, K.-H., 1991. Chemical constraints on the petrogenesis of mildly alkaline lavas from Vestmannaeyjar, Iceland: the Eldfell (1973) and Surtsey (1963-1967) eruptions. *Contrib. Mineral. Petrol.* **109**, 19-37.

Furman, T., Frey, F., Park, K.-H., 1995. The scale of source heterogeneity beneath the Eastern neovolcanic zone, Iceland. *J. Geol. Soc. London* **152**, 997-1000.

Gasparon, M., Hilton, D.R., Varne, R., 1994. Crustal contamination processes traced by helium isotopes: examples from the Sunda Arc, Indonesia. *Earth Planet Sci. Lett.* **126**, 15-22.

Gautason, B., Muelenbachs, K., 1998. Oxygen isotopic fluxes associated with high temperature processes in the rift zones of Iceland. *Chem. Geol.* **145**, 275-286.

Gee, M.A.M., Taylor, R.N., Thirlwall, M.F., Murton, B.J., 1998. Glacioisostacy controls chemical and isotopic characteristics of tholeiites from the Reykjanes Peninsula, SW Iceland. *Earth Planet Sci. Lett.* **164**, 1-5.

Gee, M.A.M., Thirlwall, M.F., Taylor, R.N., Lowry, D., Murton, B. J., 1998. Crustal processes: major controls on Reykjanes peninsula lava chemistry, SW Iceland. *J. Petrol.* **39**, 819-839.

Graham, D.W., Humphries, S.E., Jenkins, W.J., Kurz, M.D., 1992. Helium isotope geochemistry of some rocks from St. Helena. *Earth Planet. Sci. Lett.* **110**, 121-132.

Graham D.W., 2002. Noble Gas Isotope Geochemistry of Mid-Ocean Ridge and Ocean Island Basalts: Characterization of Mantle Source Reservoirs, *in Eds*: Porcelli, D., Ballentine, C.J., Wieler, R. Noble gases in geochemistry and cosmochemistry. *Reviews in Mineralogy and Geochemistry* **47**

Graham, D.W., Kurz, M.D., Jenkins, W.J., Batiza, R., 1987. Helium isotope disequilibrum and geochronology of glassy submarine basalts; *Nature* **326**, 384-386.

Graham, D.W., Larsen, L.M., Hanan, B.B., Pedersen, A.K., Lupton, J.E., 1998. Helium isotope composition of the early Iceland mantle plume inferred from the Tertiary picrites of West Greenland. *Earth Planet. Sci. Lett.* **160**, 241-255.

Gunnarsson, B., Marsh, B.D.Jr., Taylor, H.P., 1998. Generation of Icelandic rhyolites: silicic lavas from the Torfajökull central volcano. *J. Volcanol. Geotherm. Res.* **83,** 1-45.

Haase, K.M., Devey, C.W., 1994. The petrology and geochemistry of Vesteris Seamount, Greenland Basin- an intraplate alkaline volcano of non-plume origin. *J. Petrol.* **35**, 295-328.

Hanan, B.B., Schilling, J.-G., 1997. The dynamic evolution of the Iceland mantle plume: the lead isotope perspective. *Earth Planet. Sci. Lett.* **151**, 43-60.

Hanan, B.B., Blichert-Toft, J., Kingsley, R., Schilling, J.-G., 2000. Depleted Iceland mantle plume geochemical signature: Artifact of multicomponent mixing? *Geochem. Geophys. Geosyst.* **1**, 1999GC000009.

Hanyu, T., Kaneoka I., 1997. The uniform and low $^{3}He/^{4}He$ ratios of HIMU basalts as evidence for their origin as recycled materials. *Nature* **390**, 273-276.

Hanyu, T., Kaneoka, I., 1998. Open system behaviour of helium in case of the HIMU source area. *Geophys. Res. Lett.* **25**, 687-690.

Hanyu, T., Kaneoka, I., Nagao, K., 1999. Noble gas study of HIMU and EM ocean island basalts in the Polynesian region. *Geochim. Cosmochim. Acta*, **63,** 1181-1201.

Hardarson, B.S., 1993. Alkalic rocks in Iceland with special reference to the Snaefelsjokull volcanic system. Ph.D. Thesis, Univ. Edinburgh.

Hardarson, B.S., Fitton, J.G., 1991. Increased mantle melting beneath Snæfellsjokull volcano during late Pleistocene glaciation. *Nature*, **353**, 62-64.

Hardarson, B.S., Fitton, J.G., Ellam, R.M., Pringle, M.S., 1997. Rift relocation- a geochemical and geochronical investigation of a palaeo-rift in northwest Iceland. *Earth Planet. Sci. Lett.* **153**, 181-198.

Hards, V.L., Kempton, P.D., Thompson, R.N., 1995. The heterogeneous Iceland plume: new insights from the alkaline basalts of the Snaelfell volcanic centre. *J. Geol. Soc. London* **152**, 1003-1009.

Hards, V.L., Kempton, P.D., Thompson, R.N., Greenwood, P.B., 2000. The magmatic evolution of the Snæfell volcanic centre; an example of volcanism during incipient rifting in Iceland, *J. Volc. Geotherm. Res.* **99**, 97-121.

Hart S.R., 1984. A large-scale isotopic anomaly in the southern Hemisphere mantle. *Nature* **309**, 753-757.

Hart, S.R., 1988. Heterogeneous mantle domains: signatures, genesis and mixing chronologies. *Earth Planet. Sci. Lett.* **90,** 273-296.

Hart, S.R., Schilling, J.-G., Powell, J.L. 1973. Basalts from Iceland and along the Reykjanes Ridge: Sr isotope geochemistry. *Nature Phys. Sci.* **246**(155), 104-107.

Hattori, K., Muehlenbachs, K., 1982. Oxygen isotope ratios of the Icelandic crust. *J. Geophys. Res.* **87**, 6559-6565.

Helgason, J., 1985. Shifts of the Plate Boundary in Iceland - Some Aspects of Tertiary Volcanism. *J. Geophys. Res.* **90**, 84-92.

Helmberger, D.V., Wen, L., Ding, X., 1998. Seismic evidence that the source of the Iceland hotspot lies at the core-mantle boundary. *Nature* **396**, 251-255.

Hémond, C., Condomines, M., Fourcade, S., Allègre, C.-J., Oskarsson, N., Javoy, M., 1988. Thorium, strontium and oxygen isotopic geochemistry in recent tholeiites from Iceland: crustal influence on mantle-derived magmas. *Earth Planet. Sci. Lett.* **87**, 273-285.

Hémond, C., Arndt, N.T., Lichtenstein, U., Hofmann, A.W., 1993. The heterogeneous Iceland plume: Nd-Sr-O isotopes and trace element constraints. *J. Geophys. Res.* **98**, (B), 15,833-15,850.

Hildebrand, L., Grönvold, K., Oskarsson, N., 1998. Geochemistry and evolution of the Katla Volcanic Centre, South Iceland. www.norvol.hi.is.

Hildebrand, L., Thorssander, P., 1999. Sulphur isotopes in rocks from the Karla volcanic centre, south Iceland. *Geosciences Society of Iceland, 1999 Spring Meeting, Abstract Volume*, **45**.

Hilton, D.R., Hammerschmidt, K., Teufel, S., Friedrichsen, H., 1993. Helium isotope characteristics of Andean geothermal fluids and lavas. *Earth Planet. Sci. Lett.* **120**, 265-282.

Hilton, D.R., Barling, J., Wheller, G.E., 1995. Effect of shallow-level contamination on the helium isotope systematics of ocean island lavas. *Nature* **373**, 330-333.

Hilton, D.R., Grönvold, K., Macpherson, C.G., Castillo, P.R., 1999. Extreme $^{3}He/^{4}He$ ratios in northwest Iceland: constraining the common component in mantle plumes. *Earth Planet. Sci. Lett.* **173**, 53-60.

Hilton, D.R., Thirlwall, M.F., Taylor, R.N., Murton, B.J., Nichols, A., 2000. Controls on magmatic degassing along the Reykjanes Ridge with implications for the helium paradox. *Earth Planet. Sci. Lett.* **183**, 43-50.

Hilton, D.R., Macpherson, C.G., Elliot, T.R., 2000. Helium isotope ratios in mafic phenocryst and geothermal fluids from La Palma, the Canary Islands (Spain): Implications for HIMU mantle source. *Geochim. Cosmochim. Acta* **64**, 2119-2132.

Hofmann, A.W., 1988. Chemical differentiation of the Earth: the relationship between mantle, continental crust, and oceanic crust. *Earth Planet. Sci. Lett.* **90**, 297-314.

Hofmann, A.W., 1997. Mantle Geochemistry: the message from oceanic volcanism. *Nature* **385**, 219-229.

Holm, P.M., Gill, R.C.O., Pedersen, A.K., Larsen, J.G., Hald, N., Nielsen, T.F.D., Thirlwall, M.F., 1993. The Tertiary picrites of West Greenland: contributions from 'Icelandic' and other sources. *Earth Planet. Sci. Lett* **115**, 227-244.

Holm, F., Trønnes, R.G., Grönvold, K., Karlsson, H., Torfason, H., 2004. Petrology and geochemistry of the Esjufjöll central volcano, south-east Iceland. *Geosciences Society of Iceland 2004 Spring Meeting Abstract Volume*, 30-31.

Ito, G., Shen, Y., Hirth, G., Wolfe, C.J., 1999. Mantle flow, melting and dehydration of the Iceland mantle plume. *Earth Planet. Sci. Lett.* **165**, 81-96.

Ivarsson G., 1992. Geology and Petrochemistry of the Torfajökull Central Volcano in Central South Iceland, in Association with the Icelandic Hot Spot and Rift Zones. Ph.D. dissertation. *Univ. Hawaii.*

Jakobsson, S.P., 1972. Chemistry and distribution of recent basaltic rocks in Iceland, *Lithos* **5**, 365-386.

Jakobsson, S.P., 1979a. Outline of the petrology of Iceland. *Jökull* **29**, 57-73.

Jakobsson, S.P., 1979b. Petrology of recent basalts of the Eastern Volcanic Zone, Iceland. *Acta Nat. Island.* **26**, 1-103.

Jakobsson, S.P., Pedersen, A.K., Ronsbo, J.G., Melchior Larsen, L., 1973. Petrology of mugearite-hawaiite: early extrusives in the 1973 Heimaey eruption, Iceland. *Lithos* **6**, 203-214.

James, D.E., 1981. The combined use of oxygen and radiogenic isotopes as indicators of crustal contamination. *Ann. Rev. Earth Planet. Sci.* **9**, 311-344.

Jancin, M., Young, K.D., Voight, B., Aronson, J.L., Sæmundsson, K., 1985. Stratigraphy and K/Ar ages across the west flank of the northeast Iceland axial rift zone, in relation to the 7 Ma volcano-tectonic reorganization of Iceland. *J. Geophys. Res.* **90**, 287-310.

Johannesson, H., 1980. Jardlagaskipan og throun rekbelta a Vesturlandi. *Natturufraedingurinn* **50**, 13-31.

Johannesson, H., 1982. *Summary of the geology of Snæfellsnes.* Arbok Ferdafelags Islands, 151-172.

Jóhannesson, H., Jakobsson, S.P., Sæmundsson, K., 1982. Geological map of Iceland, sheet 6, Icelandic Museum of Natural History and Iceland Geodectic Survey, Reykjavik.

Johannesson, H., 1994. Geological map of West Iceland, 2nd edition, Icelandic Museum of Natural History and Iceland Geodectic Survey, Reykjavik.

Jóhannesson, H., Sæmundsson, K., 1989. Bedrock Geology, Icelandic Museum of Natural History and Iceland Geodectic Survey, Reykjavik.

Jóhannesson, H., Sæmundsson, K., 1998. Bedrock Geology, Icelandic Museum of Natural History and Iceland Geodectic Survey, Reykjavik.

Jull, M., McKenzie, D., 1996. The effects of deglaciation on mantle melting beneath Iceland. *J. Geophys Res.* **101** (B10), 21815-21828.

Kaban, M.K., Flovenz, Ó.G., Palmason, G., 2002. Nature of the crust-mantle transition zone and the thermal state of the upper mantle beneath Iceland from gravity modelling. *Geophys. J. Int.* **149**, 281-299.

Kellog, L.H., Wasserburg, G.J., 1990. The role of plumes in mantle helium fluxes. *Earth Planet. Sci. Lett.* **99**, 276 89.

Kempton, P.D., Fitton, J.G., Saunders, A.D., Nowell, G.M., Taylor, R.N., Hardarson, B.S., Pearson, G., 2000. The Iceland plume in space and time: a Sr-Nd-Pb-Hf study of the North Atlantic rifted margin. *Earth. Planet. Sci. Lett.* **177**, 255-271.

Kerr, A.C., Saunders, A.D., Tarney, J., Berry, N.H., Hards, V.L., 1995. Depleted mantle-plume geochemical signatures: No paradox for plume theories. Geology **23**, 843-846.

Kirstein, L.A., Timmerman, M.G., 2000. Evidence of the proto-Iceland plume in north-western Ireland at 42 Ma from helium isotopes. *J. Geol. Soc. London* **157**, 923-927.

Kokfelt, T. F., Hoernle, K.A., Hauff, F., 2003. Upwelling and melting of the Iceland plume from radial variation of 238U-230Th disequilibria in postglacial volcanic rocks. *Earth Planet. Sci. Lett.* **214**, 167-186.

Kokfelt, T.F., Hoernle, K., Hauff, F., Fiebeg, J., Werner, R., Garbe-Schonberg, D., Combined trace element and Pb-Nd-Sr-O isotope evidence for recycled oceanic crust (upper and lower) in the Iceland mantle plume. *J.Petrol.* in press.

Kristjansson, L., Jóhannesson, H., 1999 Secular variation and reversals in a composite 2.5 km thick lava section in central Western Iceland. Earth Planets and Space **51**, 261-276.

Kurz, M.D., 1986a. Cosmogenic helium in a terrestrial igneous rock. *Nature* **320**, 435-439.

Kurz, M.D., 1986b. In situ production of terrestrial cosmogenic helium and some applications to geochronology. *Geochim. et Cosmochim. Acta* **50**, 2855-2862.

Kurz, M.D., Jenkins, W.J., Hart, S.R., 1982a. Helium isotope systematics of ocean islands and mantle heterogeneity. *Nature* **297**, 43-46.

Kurz, M.D., Jenkins, W.J., Schilling, J.-G., Hart, S.R., 1982b. Helium isotopic variation in the mantle beneath the central North Atlantic Ocean. *Earth Plant. Sci. Lett.* **58**, 1-14.

Kurz, M.D., Meyer, P.S., Sigurdsson, H., 1985. Helium isotope systematics within the neovolcanic zones of Iceland. *Earth Planet. Sci. Lett.* **74** , 291-305.

Lal, D., 1991. Cosmic ray labelling of erosion surfaces: In situ production rates and erosion models *Earth and Planet. Sci. Lett.* **104**, 424-439.

Langmuir, C.H., Klein, E.M., Plank, T., 1992. Petrological systematics of mid-ocean ridge basalts: constraints on melt generation beneath ocean ridges. In *Mantle Flow and Melt Generration at Mid-Ocean Ridges*, eds. J. Phipps Morgan, D.K. Blackman and J.M. Sinton, pp. 183-280, Geophys. Mon. 71, Am. Geophys. Union.

Lawver, L.A., Müller, R.D., 1994. Iceland hotspot track. *Geology* **22**, 311-314.

Le Maitre, R.W., Bateman, P., Dudek, A., Keller, J., Lameyre, J., Le Bas, M.J., Sabine, P.A., Schmid, R., Sorensen, H., Streckeisen, A., Woolley, A,R., Zanettin, B., 1989. A classification of igneous rocks and glossary of terms: recommendations of the International Union of Geological Sciences Subcommision on the Systematics of Igneous Rocks. *Blackwell Scientific Publications*, Oxford.

Lupton, J.E., Craig, H., 1975. A major helium-3 source at 15° S on the East Pacific Rise. *Science* **214**, 1981 13-18.

MacDonald, G.A., Katsura, T., 1964. Chemical composition of Hawaiian lavas. *J. Petrol.* **5**, 83-133.

Macdonald, R., McGarvie, D.W., Pinkerton, H., Smith, R.L., Palacz, Z.A., 1990. Petrogenetic evolution of the Torfajökull volcanic complex, Iceland: I. Relationship between the magma types. *J. Petrol.* **31**, 429-459.

Maclennan, J., McKenzie, D., Gronvöld, K., 2001. Plume-driven upwelling under central Iceland. *Earth. Planet. Sci. Lett.* **194**, 67-82.

Maclennan, J., Jull, M., McKenzie, D., Slater, L., Gronvold, K., 2002. The link between volcanism and deglaciation on Iceland, *Geochem. Geophys. Geosyst.* **3**, 2001GC000282.

Macpherson, C.G., Hilton, D.R., Sinton, J.M., Poreda, R.J., Craig, H., 1998. High $^{3}He/^{4}He$ ratios in the Manus back-arc basin: implications for mantle mixing and the origin of plumes in the western Pacific Ocean. *Geology* **26**, 1007-1010.

Macpherson, C.G., Hilton, D.R., Day, J.M.D., Lowry, D., Gronvold, K., 2005. High $^{3}He/^{4}He$, depleted mantle and low $\delta^{18}O$, recycled oceanic lithosphere in the source of central Iceland lavas. *Earth Planet Sci. Lett.* **233**, 411-427.

Martelli, M., Nuccio, P.M., Stuart, F.M., Burgess, R., Ellam, R.M., Italiano, F.M., 2004. Helium-strontium isotope constraints on mantle evolution beneath the Roman Comagmatic Province, Italy. *Earth Planet Sci. Lett.* **224**, 295-308.

Marti, K. and Craig, H. 1987. Cosmic-ray-produced neon and helium in the summit lavas of Maui. *Nature* **325**, 335.

Marty B., Trull T., Luzziez P., Basilei, I., Tanguy, J.C., 1994. He, Ar, O, Sr and Nd isotope constraints on the origin and evolution of Mount Etna magmatism. *Earth Planet. Sci. Lett.* **126**, 23-39.

Marty, B., Upton, B.G.J., Ellam, R.M., 1998. Helium isotopes in early Tertiary basalts, northeast Greenland: Evidence for 58 Ma plume activity in the North Atlantic-Iceland volcanic province. *Geology* **26**, 407-410.

Mattey, D.P., Lowry, D., Macpherson, C.G., 1994. Oxygen isotope composition of mantle peridotite. *Earth Planet. Sci. Lett.* **128**, 231-241.

Mattson, S.R., Höskuldsson, A., 2003. Geology Of The Heimaey volcanic centre, south Iceland: early evolution of a central volcano in a propagating rift? *J. Volcanol. Geotherm. Res.* **127**, 55-71.

McDonough, W.F., Chauvel, C., 1991. Sample contamination explains the Pb isotopic composition of some Rurutu island and Sasha seamount basalts. *Earth Planet. Sci. Lett.* **105**, 397-404.

McDonough, W.F., Sun, S.S., 1995. The composition of the Earth. *Chem. Geol.* **120**, 223-253.

McGarvie, D.W., Macdonald, R., Pinkerton, H., Smith, R.L., 1990. Petrogenetic evolution of the Torfajökull volcanic complex, Iceland II. The role of magma mixing. *J. Petrol.* **31**, 461-481.

McKenzie, D., Bickle, M.J,. 1988. The volume and composition of melt generated by extension of the lithosphere. *J. Petrol.* **29**, 625-679.

McKenzie, D., O'Nions, R.K., 1995. The source regions of ocean island basalts. *J. Petrol.* **36**, 133-159.

Mertz, D.F., Haase, K.M., 1997. The radiogenic isotope composition of the high-latitude North Atlantic mantle. *Geology* **25**, 411-414.

Mertz, D.F., Devey, C.W., Todt, W., Stoffers, P., Hofmann, A.W., 1991. Sr-Nd-Pb isotope evidence against plume-asthenosphere mixing north of Iceland. *Earth Planet. Sci. Lett.* **107**, 243-255.

Meyer P.S., Sigurdsson,H., Schilling, J.-G., 1985. Petrological and geochemical variations along Iceland's neovolcanic zones. *J. Geophys. Res.* **B90**, 10043-10072.

Moreira, M., Allègre, C.J., 1998. Helium-neon systematics and the structure of the mantle. *Chem. Geol.* **147**, 53-59.

Moreira, M., Doucelance, R., Dupré, B., Kurz, M., Allègre, C.J., 1999. Helium and lead isotope geochemistry in the Azores archipelago. *Earth Planet. Sci. Lett.* **169**, 189-205.

Moreira, M., Kurz, M., 2001. Subducted oceanic lithosphere and the origin of the 'high μ' basalt helium isotopic signature. *Earth Planet. Sci. Lett.* **189**, 49-57.

Morgan, W.J., 1971. Convection plumes in the lower mantle. *Nature* **230**, 42-43.

Morgan, W.J., 1972. Plate motions and deep mantle convection. *Mem. Geol. Soc. Am.* **132**, 7-22.

Morrison, P., Pine, J, 1955. Radiogenic origin of the helium isotopes in rocks. *Annu. NY Acad. Sci.* **62**, 189-205.

Muehlenbachs, K., Anderson, A.T., Sigvaldsson, G.E., 1974. Low-δ18O basalts from Iceland. *Geochimica et Cosmochimica Acta* **38**, 577 588.

Murton, B.J., Taylor, R.N., Thirlwall, M.F., 2002. Plume-ridge interaction: a geochemical perspective from the Reykjanes ridge. *J. Petrol.* **43**, 1987-2012.

Nichols, A.R.L., Carroll, M.R., Hoskuldsson, A., 2002. Is the Iceland hot spot also wet? Evidence from the water contents of undegassed submarine and subglacial pillow basalts. *Earth Planet. Sci. Lett.* **202**, 77-87.

Nicholson, H., Condomines, M., Fitton, J.G., Fallick, A.E., Grönvold, K., Rogers, G., 1991. Geochemical and isotopic evidence for crustal assimilation beneath Krafla, Iceland. *J. Petrol.* **32**, 1005-1020.

O'Nions, R.K., Grönvold, K., 1973. Petrogenetic relationships of acid and basic rocks in Iceland: Sr isotopes and rare-earth elements in Late and post-glacial volcanics. *Earth Planet. Sci. Lett.* **19**, 397-409.

O'Nions, R.K., Pankhurst, R.J., 1973. Secular variation in the Sr-isotope composition of Icelandic volcanic rocks. *Earth Planet. Sci. Lett.* **21**, 197-409.

Oskarsson, N., Steinþórsson, S., Sigvaldson, G.E., 1985. Iceland geochemical anomaly: origin, volcano tectonics, chemical fractionation and isotope evolution of the crust *J. Geophys. Res.* **90**, 10,011-10,025.

Oskarsson, N., Sigvaldson, G.E., Steinþórsson, S., 1982. A dynamic model of rift-zone petrogenesis and the regional petrology of Iceland. *J. Petrol.* **23**, 28-74.

Palmason, G., 1981. Crustal rifting and related thermomechanic processes in the lithosphere beneath Iceland. *Geolog. Rundsch.* **70**, 244-260.

Pedersen, A.K., Larsen, L.M., Riisager, P., Dueholm, K.S., 2002. Rates of volcanic deposition, facies changes and movements in a dynamic basin: Nuussuaq Basin, West Greenland, around the C27n-C26r transition. *In*: Jolley, D.W. & Bell, B.R. (eds). The North Atlantic Igenous Province: stratigraphy, tectonic, volcanic and magmatic processes. *Geol. Soc. London, Spec. Publ.* **197**, 157-181.

Persano, C., Stuart, F.M., Bishop, P., Barfod, D., 2002. Apatite (U-Th)/He age constraints on the development of the Great Escarpment, south east Australia. *Earth and Planet. Sci. Lett.* **200**, 79-90.

Porcelli, D., Wasserburg, G.J., 1995. Mass transfer of helium, neon, argon and xenon through a steady-state upper mantle. *Geochim. Cosmochim. Acta.* **59**, 4921-4937.

Porcelli, D., O'Nions, R.K., O'Reilly, S.Y., 1986. Helium and strontium isotopes in ultramafic xenoliths. *Chem. Geol.* **54**, 237 249.

Poreda, R., Schilling, J.-G., Craig, H., 1986. Helium and hydrogen isotopes in ocean-ridge basalts north and south of Iceland. *Earth Planet. Sci. Lett.* **78**, 1-17.

Prestvik, T., 1980. Petrology of hybrid intermediate and silicic rocks from Öræfajökull, southeast Iceland. *Geol. Föreningens i Stockholm Förhandlingar* **101**, 299-307.

Prestvik, T., 1985. Petrography, chemical characteristics and nomenclature of Öræfajökull rocks. *Jokull* **32**, 69-76.

Prestvik, T., Goldberg, S., Karlsson, H., Grönvold, K., 2001. Anomalous strontium and lead isotope signatures in the off-rift Öræfajökull central volcano in south-east Iceland. Evidence for enriched endmember(s) of the Iceland mantle plume? *Earth. Planet. Sci. Lett.* **190**, 211-220.

Richards, M.A., Duncan, R.A., Courtillot, V.E., 1989. Flood basalts and hot-spot tracks: plume heads and tails. *Science* **246,** 103-107.

Rudrick, R.L., Fountain, D.M., 1995. Nature and composition of the continental crust: a lower crustal perspective. *Reviews of Geophysics* **33,** 267-309.

Rollinson, H., 1993. *Using geochemical data: Evaluation, presentation, interpretation.* Prentice Hall, England.

Sæmundsson, K., 1974. Evolution if the axial rifting zone in northern Iceland and the Tjörnes fracture zone. *Geol. Soc. Am. Bull.* **85**, 495-504.

Sæmundsson, K., 1978. Fissure swarms and central volcanoes of the neovolcanic zones of Iceland. *Geol. J. Spec. Issue* **10**, 415-432.

Sæmundsson, K., 1979. Outline of the geology of Iceland. *Jokull* **29**, 7-28.

Saemundsson, K., Einarsson, S., 1980. Geological map of Iceland, sheet 3, south-west Iceland. *Icelandic Museum Nat. Hist. & Iceland Geodetic Surv., 1:250,000 geol. map.*

Sarda, P., Staudacher T., Allègre, C.J., 1988. Neon isotopes in submarine basalts. *Earth Planet. Sci. Lett.* **91**, 73-88.

Saunders, A.D., Fitton, J.G., Norry, M.J., Kent, R.W., 1997. The North Atlantic Igneous Province. *In*: Mahoney, J.J. and Coffin, M.F. (eds). Large Igneous Provinces. *Am. Geophys. Union Monogr.* **100**, 45-93.

Schilling, J.-G., 1973. Iceland mantle plume: geochemical evidence along the Reykjanes Ridge. *Nature* **242**, 565-571.

Schilling, J.-G., 1991. Fluxes and excess temperatures of mantle plumes inferred from their interaction with migrating mid- ocean ridges. *Nature* **352**, 397-403.

Schilling, J-G., Bergeron, M.B., Evans, R., 1980. Halogens in the mantle beneath the North Atlantic. *Phil. Trans. R. Soc. London* **A 297**, 147-178.

Schilling, J.-G., Meyer, P.S., Kingsley, R.H., 1982. Evolution of the Iceland hotspot. *Nature* **296**, 313-320.

Schilling, J.-G., Kingsley, R., Fontignie, D., Poreda, R., Xue, S., 1999. Dispersion of the Jan Mayen and Iceland mantle plumes in the Arctic: a He-Pb-Nd-Sr isotope tracer study of basalts from the Kolbeinsey, Mohns, and Knipovich Ridges. *J. Geophys. Res.* **104**(B5), 10,543-10,569.

Shaw, D.M. 1979. Trace element fractionation during anatexis. *Geochim. Cosmochim. Acta.* **34**, 237-243.

Shen, Y., Solomon, S.C., Bjarnason, I.T., Wolfe, C.J., 1998. Seismic evidence for a lower-mantle origin of the Iceland plume. *Nature* **395**, 62-65.

Shen, Y., Solomon, S.C., Bjarnason, I.T., Nolet, G., Morgan, W.J., Allen R.M., Vogfjörd, K., Jakobsdóttir, S., Stefansson, R., Julian, B.R., Fougler G.R., 2002. Seismic evidence for a tilted mantle plume and north-south mantle flow beneath Iceland. *Earth Planet. Sci. Lett.* **197**, 261-272.

Sigmarsson, O., Condomines, M., Fourcade, S., 1992. Mantle and crustal contribution in the genesis of recent basalts from off-rift zones in Iceland: constraints from Th, Sr and O isotopes. *Earth and Planet. Sci. Lett.* **110**, 149-162.

Sigurdsson, H., 1970 Structural origin and plate tectonics of the Snæfellsnes volcanic zone, western Iceland. *Earth Planet. Sci. Lett.* **10**, 129-135.

Sigvaldson, G.E., Annertz, K., Nilsson, M., 1992. Effect of glacier loading/deloading on volcanism: Postglacial volcanic eruption rate of the Dyngjufjoll area, central Iceland. *Bull. Volcanol.* **54**, 385 392.

Skovgaard, A., Storey, M., Baker, J., Blusztajn, J., Hart, S.R., 2001. Osmium-oxygen isotopic evidence for a recycled and strongly depleted component in the Iceland mantle plume. *Earth Planet. Sci. Lett.* **194**, 259-275.

Slater, R.A., Jull, M., McKenzie, D.M., Grönvold, K., 1998. Deglaciation effects on melting beneath Iceland. Results from the Northern Volcanic Zone. *Earth Planet. Sci. Lett.* **164**, 151-164.

Smit, Y., Parkinson., I.J., Hawkesworth, C.J., Peate, D.W., Cohen, A.S., 1999. Off-axis alkalic melt generation in Snæfellsnes peninsula, Iceland. *EOS Trans.* AGU **80**, F653.

Smit, Y., Parkinson., I.J., Hawkesworth, C.J., Peate, D.W., Cohen, A.S., 2000. Osmium isotope characteristics of the Iceland plume. *EOS Trans. AGU* **81**, F1344.

Stecher, O., Carlson, R.W., Gunnarsson, B., 1999. Torfajökull: a radiogenic end-member of the Iceland Pb-isotopic array. *Earth Planet Sci. Lett.* **165**, 117-127.

Steinþórsson, S., and Jacoby, W., 1985 Crustal accretion in and around Iceland. *J. Geophys. Res.* **90**, 9951-9952.

Steinthorsson, S., Oskarsson, N., Sigvaldason, G.E., 1985. Origin of alkali basalt in Iceland: a plate tectonic model. *J. Geophys. Res.* **90**, 10,027-10,042.

Steinþórsson, S., 1987. Rates of some geomorphological processes in Iceland (in Icelandic with an English summary). *Natturufraedingurinn* **57**, 81-95.

Storey, M., Duncan, R.A., Pedersen, A.K., Larsen, L.M., Larsen, H.C., 1998. $^{40}Ar/^{39}Ar$ geochronology of the West Greenland volcanic province. *Earth Planet Sci. Lett.* **160**, 569-586.

Stracke, A., Zindler, A., Salters, V.J.M., McKenzie, D., Blichert-Toft, J., Albarède, F., Grönvold, K., 2003. Theistareykir revisited. *Geochem. Geophys. Geosyst.* **4**, 2001GC000201.

Stuart, F.M., Ellam, R.M., Harrop. P.J., Fitton, J.G. and Bell, B.R. 2000. Constraints on mantle plumes from helium isotopic composition of basalts from the British Tertiary Igneous province. *Earth Planet. Sci. Lett.* **177**, 273-285.

Stuart, F.M., Lass-Evans, S., Fitton, J.G., Ellam, R.M., 2003. High $^{3}He/^{4}He$ ratios in picritic basalts from Baffin Island and the role of a mixed reservoir in mantle plumes. *Nature* **424**, 57-59.

Stuart, F.M., Ellam, R.M., Fitton, J.G., Kempton, P.D. Constraints on mantle enrichments in the North Atlantic Ocean from the geochemistry of basalts from Jan Mayen. *In preparation.*

Sun, S.-S., Jahn, B., 1975. Lead and strontium isotopes in post-glacial basalts from Iceland. *Nature* **255**, 527-530.

Sun, S.-S., Nesbitt, R.W., Sharaskin, A.Y., 1979. Geochemical characteristics of Mid-Ocean Ridge Basalts. *Earth Planet Sci Lett.* **44**, 119 - 138.

Sun, S.-S., McDonough, W.F., 1989. Chemical and isotopic systematics of ocean basalts: implications for mantle composition and processes. *In*: Saunders, A.D., & Norry, M.J. (eds). Magmatism in the ocean basins. *Geological Society Special Publication* **42**, 313-345.

Taylor, R.N., Thirlwall, M.F., Murton, B.J., Hilton, D.R., Gee, M.A.M., 1997. Isotopic constraints on the influence of the Icelandic plume. *Earth Planet. Sci. Lett.* **148**, E1-E8.

Thirlwall, M.F., 1995. Generation of the Pb isotopic characteristics of the Iceland plume. *J. Geol. Soc. London* **152**, 991-996.

Thirwall, M.F., 1997. Pb isotopic and elemental evidence for OIB derivation from young HIMU mantle. *Chem. Geol.* **139**, 51-74.

Thirlwall, M.F., Upton, B.G.J., Jenkins, C., 1994. Interaction between continental lithosphere and the Iceland plume - Sr-Nd-Pb isotope geochemistry of Tertiary basalts, NE Greenland. *J. Petrol.* **35**, 839-879.

Thirlwall, M.F., Gee, M.A.M., Taylor, R.N., Murton, B.J., 2004. Mantle components in Iceland and adjacent ridges investigated using double-spike Pb isotope ratios. *Geochim. Cosmochim. Acta* **68**, 361-386.

Thompson, A.B., 1992. Water in the earth's upper mantle. *Nature* **358**, 295-302.

Thy, P., Lofgren, G., Imsland, P., 1991. Melting relations and the evolution of the Jan Mayen magma system. *J. Petrol.* **32**, 303-322.

Thy, P., 1983. Phase relations in transitional and alkali basaltic glasses from Iceland. *Contrib. Mineral. Petrol.* **82**, 232-251.

Trønnes, R.G., Planke, S., Sundvoll, B., Imsland, P., 1999. Recent volcanic rocks from Jan Mayen: Low degree melt fractions of enriched northeast Atlantic mantle. *J. Geophys. Res.* **104**, 7153-7168.

Trull, T.W., Kurz, M.D., 1993. Experimental measurements of ^{3}He and ^{4}He mobility in olivine and clinopyroxene at magmatic temperatures. *Geochim. Cosmochim. Acta* **57**, 1313-1324.

Tryggvason, K., Husebye, E.S., Stefansson, R., 1983. Seismic image of the hypothesized Icelandic hotspot. *Tectonophysics* **100**, 97-118.

Van Soest, M.C., Hilton, D R., Macpherson, C.G., Mattey, D.P., 2002. Resolving sediment subduction and crustal contamination in the Lesser Antilles island arc: a combined He–O–Sr isotope approach. *J. Petrol.* **43**, 143-170.

Vink, G.E., 1984. A hotspot model for Iceland and the Vøring Plateau. *J. Geophys. Res.* **89**, 9949-9959.

Vogt, P.R., Avery, O.E., 1974. Detailed magnetic surveys in the northeast Atlantic and Labrador Sea. *Jour. Geophys. Res.* **79**, 363-388.

Walker, G.P.L., 1975. Excess spreading axes and spreading rate in Iceland. *Nature*, **255**, 468-471.

Weaver, B.L., 1991. The origin of ocean island basalt end-member compositions: trace element and isotopic constraints. *Earth Planet. Sci. Lett.* **104**, 381-397.

White, W. M., 1995. Geochemical tracers of mantle processes. In *U.S. National report to the IUGC: Properties of the solid earth,* pp. 19-24. *Rev. Geophys., Supplement.*

White, R.S., McKenzie, D., 1989. Magmatism at rift zones: the generation of volcanic continental margins and flood basalts. *J. Geophys. Res.* **94**, 7685-7729.

White, R.S., McKenzie, D., 1995. Mantle plumes and flood basalts. *J. Geophys. Res.* **100**, 17,543-17,585.

Williams, A.J., Stuart, F.M., Day, S.J., Phillips, W.M., 2005. Using pyroxene microphenocrysts to determine cosmogenic ^{3}He concentrations in old volcanic rocks: an example of landscape development in central Gran Canaria. *Quat. Sci. Rev.* **24/1-2,** 211-222.

Wolfe, C.J., Bjarnason, I.T., VanDecar, J.C., Solomon, S.C., 1997. Seismic structure of the Iceland mantle plume. *Nature* **385**, 247-247.

Woodhead, J.D., 1996. Extreme HIMU in an ocean setting – the geochemistry of Mangaia Island (Polynesia) and temporal evolution of the Cook-Austral hotspot. *J. Volc. Geotherm. Res.* **72**, 1-19.

Zindler, A., Hart, S., 1986. Chemical geodynamics. *Ann. Rev. of Earth Planet. Sci. Lett.* **14**, 493-571.

Zindler, A., Hart, S.R., Frey, F.A., 1979. Nd and Sr isotope ratios and rare element abundances in Reykjanes basalts: evidence for mantle heterogeneity beneath Iceland. *Earth. Planet. Sci. Lett.* **45**, 249-262.

APPENDIX

A1 Sample Details

A1.1 Sampling constraints

The diffusive loss of helium from magmatic minerals dictated that only samples containing fresh olivine and/or clinopyroxene phenocrysts were suitable for the study. Early He isotope results, demonstrated that the magmatic $^{3}He/^{4}He$ of many clinopyroxenes had been modified by pre-eruptive or post-eruptive processes (See Chapter 2), therefore subsequent sampling was restricted to rocks containing olivine phenocrysts. The size of phenocrysts was of less importance, though previous studies have demonstrated phenocrysts smaller than 125-250 μm contain negligible magmatic He (Williams *et al.*, 2005). Consequently, phenocryst separates were prepared from sieved fractions greater than 250 μm in size. Approximately 1-2 g of pure phenocryst separates are required in order to gain adequate helium abundances. Therefore, depending on phenocryst abundance, around 1 kg of basalt was needed for each sample. This meant that using samples from external collections was often limited by the lack of suitable material.

In addition to restricting sampling material to olivine-bearing rocks, helium isotope systematics also impose tight constraints on field sampling techniques. Post-eruptive production of cosmogenic ^{3}He in the crystal lattice of mafic minerals is greatest in high-latitude regions and at high-elevations (e.g., Lal, 1991). The crushing technique employed here to extract magmatic helium from inclusions in phenocrysts minimises the release of lattice-hosted helium (Williams et al., 2005) however, as an extra precaution samples were where possible collected from outcrops shielded from cosmic-rays by more than 2 metres of rock (e.g., the lower parts of lava-flows, cliff exposures, road-cuttings).

Finally, phenocrysts from evolved rocks have frequently been shown to yield anomalously low $^{3}He/^{4}He$, most likely as a result of the assimilation of ^{4}He-rich wall-rock or crustal material (e.g., Gasparon *et al.*, 1994). For this reason, sampling was restricted to primitive basalts with MgO concentrations greater than 8 wt. %. Additionally, this helps to eliminate magmatic differentiation as a cause of any observed variation in major and trace element geochemistry.

A1.2 Sample descriptions

Location	Sample Name	Mineralogy	Other comments
Snæfellsjökull	PSN1	**Phenocrysts:** 10% of rock total. Comprise olivine (40%), plagioclase (40%) and pyroxene (20%) **Groundmass:** plagioclase, augite, magnetite, olivine.	Basalt contains white veins of $CaCO_3$(?)
	PSN7	**Phenocrysts:** 40% by volume. Olivine (20%, 1-2mm, v.fresh); pyroxene (40%, v.fresh, euhedral >2mm); plagioclase (40%, >2mm). Some v.large crystals (>10mm) of plag and cpx.	Highly vesicular, pale grey basalt.
	PSN8	**Phenocrysts:** Fresh pyroxenes (40%), olivine (30%) and plagioclase (30%). Generally phenocrysts are 2-4mm size with occasional macrocrysts (>10mm) of cpx **Groundmass:** dark, fine-grained groundmass of ol, px, plag, Fe-Mg oxides.	Microvesicular in places
	PSN9	**Phenocrysts:** Pyroxene (80% - euhedral <30mm), olivine (10% - euhedral, fresh-oxidised) and plag. (10%, euhedral) phyric basalt. **Groundmass:** Pale grey groundmass containing plagioclase, augite, magnetite, olivine.	Low vesicularity
	PSN11	**Phenocrysts:** 15% by volume. Fresh, eubhedral olivines (50%, 1-2mm); fresh pyroxene (30%) and plagioclase (20%) **Groundmass:** pale grey containing plagioclase, augite, magnetite, olivine.	Medium vesicularity
	PSN13	**Phenocrysts:** 20% by volume comprising fresh, inclusion-rich olivines and (fewer) fresh augites. 1-2 mm	Light grey, non-vesicular basalt.
	PSN14	**Phenocrysts:** Pyroxene (50%, fresh, euhedral 5-10mm); olivine (15%, fresh, subhedral, 1-5mm), plagioclase (35%, fresh, euhedral, 1-5mm). **Groundmass:** plagioclase, augite, magnetite, olivine.	Contains some pyroxene-plagioclase glomerocrysts in equal abundance.
	GSN9	**Phenocrysts:** Abundant euhedral olivines and (fewer) augites. All > 2 mm **Groundmass:** plagioclase, augite,	Vesicular sample from a hyaloclastite/pillow

		magnetite, olivine.	breccia section, also containing abundant fresh glass.
	GSN11	**Phenocrysts:** Olivines (25% - 0.5-2mm, fresh), pyroxenes (10%, possibly altered i.e., oily appearance, 0.5-2mm) and plagioclase (65%, 1-2mm) **Groundmass:** plagioclase, augite, magnetite, olivine.	Dark grey microphyric basalt collected along with good quality hyaloclastite from same locality.
	SNB40	**Phenocrysts:** Abundant small euhedral olivines and (fewer) augites. All 0.5-1 mm.	
	SNS224	**Phenocrysts:** Euhedral olivines <2mm	
	SNS219	Only olivine mineral (0.5-2mm) concentrate sent by RGT.	
	SNS215	**Phenocrysts:** Few olivines, 1-2mm size	
	SNS214	**Phenocrysts:** Euhedral olivines (1-2mm)	
Lýsuskarð	LB298	**Phenocrysts:** Altered olivines (1-2mm) - significant iddingsite alteration and pyroxenes (0.5-1mm)	
	LB296	**Phenocrysts:** Large, fresh pyroxene phenocrysts (up to 5mm).	
	LB295	**Phenocrysts:** Olivine-pyroxene phyric basalt. Large, fresh olivines (1-5mm) and smaller euhedral pyroxenes (1-2mm). Plagioclase phenocrysts.	Some zeolite formation
	LB294	**Phenocrysts:** Abundant, euhedral olivines (1-2mm) and sparser pyroxenes. **Groundmass:** Plagioclase, augite, magnetite, olivine.	
	LB232	**Phenocrysts:** Few euhedral olivines (1-2mm)	
	LB230	**Phenocrysts:** Olivine and augite (> 2 mm) **Groundmass:** Plagioclase, augite, magnetite, olivine.	
	LB231	**Phenocrysts:** Olivine and augite	

		(> 2 mm) *Groundmass: plagioclase, augite, magnetite, olivine.	
	LB229	Phenocrysts: Euhedral olivines (1-2mm) and pyroxenes.	
Ljósufjöll	IC7	Phenocrysts: Phenocryst-poor basalt, containing sparse but large (1-8mm) fresh olivine crystals. Groundmass: Dark, fine-grained matrix consisting of plagioclase, Fe-Mg oxides, olivine and pyroxene.	Moderately vesicular, dark basalt.
	YS98-008	Phenocrysts: Euhedral fresh olivines (1-2 mm) and pyroxenes (0.5-1mm)	
	H105	Phenocrysts: 10% olivine, 13% cpx, <5% plagioclase.	Ankaramitic lava
	SNS-211	Phenocrysts: Large, fresh olivines 1-4mm	
	SNS-209	Phenocrysts: 1-2mm olivines, some iddingsite alteration on surface and along cracks in crystals	
	SNS-206	Phenocrysts: Olivine-phyric, up to 2mm in size	
	SNS-201	Phenocrysts: Small olivines <0.5mm in size.	
Öræfajökull	AW20	Phenocrysts: Large (10-20mm), fresh, euhedral olivine (10%), pyroxene (5-10%), and plagioclase (5%) phenocrysts Groundmass: Pale grey containing plagioclase, olivine, pyroxene and Fe-Mg oxides?	
	AW24	Phenocrysts: Three-phase basalt containing fresh olivine, pyroxene and plagioclase. Groundmass: Pale grey containing plagioclase, olivine, pyroxene and Fe-Mg oxides?	
	AW27	Phenocrysts: feldspar (10%, up to 10mm) and pyroxene (5% 1-5 mm). Sparse (<<2%), small olivine partly altered to iddingsite.	
	H52	Phenocrysts: feldspar (5-10%, up to 20mm) and olivine (1-5 mm)	Vesicular basalt

	H54	**Phenocrysts:** feldspar and fresh olivine	Non-vesicular basalt
Snæfell	H136	**Phenocrysts:** rare (<2%) olivine	Dark, vesicular lava
	H140	**Phenocrysts:** 3-5% fresh, olivine, up to 10mm	Basalt block
Vestmannaeyjar	AW31	**Phenocrysts:** Abundant olivine (30% total). Small phenocrysts (<0.5mm). **Groundmass:** plagioclase, Fe-Mg oxides, olivines	Light grey, olivine-phyric basalt
	H119	**Phenocrysts:** olivine-phyric comprising around 20% total volume. Olivines very fresh but small (<<0.5mm).	Light grey, olivine-rich basalt
	R23684	*Poorly-sorted sand collected from beach close to flows from 1967 eruption of Surtsey, containing dominantly glass fragments and olivine crystals, some altered to iddingsite on surface. Only fresh olivines used for helium determinations.*	
N-SFZ	H176	**Phenocrysts:** Up to 40% of volume, comprising fresh pyroxene (25%, up to 15mm) and olivine (15%; waxy appearance, 10-15mm).	Ankaramitic flow.
	H178	**Phenocrysts:** v. sparse euhedral olivines (<2%) and plagioclase (5%)	Highly vesicular, dark lava

A2 Analytical techniques

A2.1 Helium isotope analyses

All helium isotope analyses were performed in the Noble Gas Laboratory at SUERC. The helium isotope composition of the basalt source magma is contained within melt and fluid inclusions in olivine and pyroxene phenocrysts and was extracted by *in vacuo* crushing. Lattice-hosted He was released by melting the powders remaining from crushing. Helium isotope concentrations and ratios were determined by noble gas mass spectrometry.

A2.1.1 Sample preparation

Approximately 500 g of each sample was crushed in a stainless-steel jaw-crusher and manually sieved into size fractions of >2 mm, 1-2 mm, 0.5-1mm, 0.25-0.5 mm and <0.25 mm. Size-fractions greater than 0.5 mm were then washed in tap water in order to remove dust particles. Olivine and pyroxene phenocrysts were hand-picked under a binocular microscope from the size-fractions, starting with the largest size-fraction, until approximately 2 g of each mineral type had been separated. Phenocryst separates were ultrasonically cleaned in steps of 20% HNO_3 and rinsed in de-ionised (DI) water, in order to remove carbonate, adhering basalt and clay minerals. A second stage of hand-picking was necessary in order to remove phenocrysts with visible signs of alteration, adhering basalt or iron oxide. Finally, each pure phenocryst separate was cleaned in Analar acetone for 15 minutes in an ultrasonic bath prior to loading in the crushing apparatus.

A2.1.2 *In vacuo* crushing procedure

All samples for this study were crushed on-line in a multi-sample hydraulic crusher. Between 0.8 and 1.5 g of pure mineral separates were loaded into 25 mm diameter stainless steel pots, with each single layer of phenocrysts separated by a 2mm-thick stainless steel plate in order to maximise crushing efficiency. For each batch of crushing, ten sample pots were loaded into the crushing carousel, and sample pots numbered accordingly. After loading, the crushing equipment was baked at 100°C into a turbo-molecular pump. This was followed by pumping for 12-24 hours at room temperature overnight or until UHV was achieved. Samples were crushed using the hydraulic press at pressures of between 500 and 2000 p.s.i., until audible signs of mineral crushing had ceased. Active gases were removed by sequential exposure to two SAES GP50 getters at 500° C for 20 minutes. The heavy rare gases were subsequently adsorbed onto activated charcoal cooled at 77° K using liquid nitrogen for 20 minutes prior to introduction to the mass spectrometer for He isotope analysis. A cold GP50 getter and an additional liquid nitrogen cooled finger close to the mass spectrometer source were employed to minimise partial pressure of residual gases during analysis.

A2.1.3 Fusion procedure

Powders that remained after the *in vacuo* crushing were sieved, and the <100 μm fraction retained for determinations of lattice-hosted (non-magmatic) helium isotope concentrations and ratios. 50-100 mg of powder were wrapped in aluminium foil and heated in a double-walled resistance furnace using a two-step heating procedure, first at 900°C for 30 minutes, then at 1600°C for 15 minutes. Gases released were cleaned in the extraction line following the same procedures as for the crush extractions.

A2.1.4 Mass spectrometry

Helium isotope ratios and abundances were determined on an all-metal MAP 215-50 mass spectrometer. A conventional Nier-type source was operated at 500 A trap current in order to achieve a high sensitivity. The peaks HD^+ and ^3He, and backgrounds were measured by a Burle Channeltron 4869 electron multiplier operated in pulse-counting mode at 1.5 kV. A variable slit located in front of the multiplier was used to achieve a resolving power of 650, adequate for the resolution of $^3He^+$ from the H_3-HD^+ doublet (DM = 6.7×10^{-3} amu). $^4He^+$ and $^{20}Ne^+$ beam intensities were measured on a Faraday cup. Beam intensities were measured in ten cycles by peak jumping up-mass over a period of approximately 50 minutes.

^4He (V), ^3He (cps; counts per second) and ^{20}Ne (V) beam intensities were determined using in-house software. The uncertainties were derived by fitting regression lines to the data points, with the option of discarding anomalous measurements.

A2.1.5 Blank analyses

Procedural blank measurements were undertaken prior to the first crush analysis of each batch, and periodically during the analyses, in order to ascertain the contribution of non-sample-hosted helium released during the crushing. The blank component may consist of helium adhered to the sample and internal surfaces of the crushing equipment and released during the procedure or a minor amount of helium diffusing through the sapphire glass viewport of the crushing equipment. Additional blank analyses were performed immediately following the analyses of samples

A2.1.3 Fusion procedure

Powders that remained after the *in vacuo* crushing were sieved, and the <100 μm fraction retained for determinations of lattice-hosted (non-magmatic) helium isotope concentrations and ratios. 50-100 mg of powder were wrapped in aluminium foil and heated in a double-walled resistance furnace using a two-step heating procedure, first at 900°C for 30 minutes, then at 1600°C for 15 minutes. Gases released were cleaned in the extraction line following the same procedures as for the crush extractions.

A2.1.4 Mass spectrometry

Helium isotope ratios and abundances were determined on an all-metal MAP 215-50 mass spectrometer. A conventional Nier-type source was operated at 500 A trap current in order to achieve a high sensitivity. The peaks HD^+ and ^3He, and backgrounds were measured by a Burle Channeltron 4869 electron multiplier operated in pulse-counting mode at 1.5 kV. A variable slit located in front of the multiplier was used to achieve a resolving power of 650, adequate for the resolution of $^3He^+$ from the H_3-HD^+ doublet (DM = 6.7×10^{-3} amu). $^4He^+$ and $^{20}Ne^+$ beam intensities were measured on a Faraday cup. Beam intensities were measured in ten cycles by peak jumping up-mass over a period of approximately 50 minutes.

^4He (V), ^3He (cps; counts per second) and ^{20}Ne (V) beam intensities were determined using in-house software. The uncertainties were derived by fitting regression lines to the data points, with the option of discarding anomalous measurements.

A2.1.5 Blank analyses

Procedural blank measurements were undertaken prior to the first crush analysis of each batch, and periodically during the analyses, in order to ascertain the contribution of non-sample-hosted helium released during the crushing. The blank component may consist of helium adhered to the sample and internal surfaces of the crushing equipment and released during the procedure or a minor amount of helium diffusing through the sapphire glass viewport of the crushing equipment. Additional blank analyses were performed immediately following the analyses of samples

containing high concentrations of helium in order to constrain the potential for increased blank-levels due to inadequate lengths of pumping between analyses or a memory-effect in the mass spectrometer itself.

A2.1.6 Determining helium isotope concentrations and ratios

Helium abundances and isotope compositions were calculated by peak height comparison to pipettes of 2.9 $\times 10^{12}$ atoms He from an artificially prepared standard gas mixture ($^{3}He/^{4}He$ = 5.95 $\times$ 10^{-5}, $^{4}He/^{22}Ne$ > 6000), calibrated against a manometrically measured ^{4}He reservoir (Persano *et al.*, 2002). Standard He abundance determinations were made at the end of each day of analyses and the reproducibility over the period of analysis was 1% for ^{3}He and 0.5% for ^{4}He. Sample yields from crushing ranged from 0.03 $\times$ 10^{-9} to 37.9 $\times$ 10^{-9} cc STP of ^{4}He and 7.5 $\times$ 10^{-15} to 5.8 $\times$ 10^{-13} cc STP of ^{3}He. In order to calculate the weight of phenocryst separate crushed, and therefore the He concentration in cc STP/g, the powders remaining after the crush extractions were sieved into size fractions of <100, 100-250, 250-500 and >500 μm and the remaining <500um size fractions weighed.

Blank corrections were applied to both ^{3}He and ^{4}He, normally using the mean of the blanks measured during each day. Analytical uncertainties were almost twice more significant for ^{3}He blanks than for ^{4}He blanks due to smaller concentrations of ^{3}He in the samples. Crushing-blanks averaged 8.6 $\times$ 10^{-11} cc STP and 3.74 $\times$ 10^{-16} cc STP, for ^{3}He and ^{4}He respectively, over the 24 months during which the analyses took place.

A2.2 Strontium and neodymium isotope analyses

Sr and Nd isotope analyses were made on all samples for which $^{3}He/^{4}He$ had been determined. $^{87}Sr/^{86}Sr$ and $^{143}Nd/^{144}Nd$ measurements were made using thermal ionisation mass spectrometry (TIMS) at SUERC, East Kilbride.

A2.2.1 Sample preparation and chemical separation

For strontium and neodymium isotope measurements, whole-rock powder was prepared by grinding whole-rock chips for 2 to 3 minutes in a tungsten carbide Tema mill. Approximately 150 mg of powder were dissolved in Teflon beakers using successive HF/HNO_3-HNO_3-6M HCl treatment on a 150°C hotplate.

Strontium and rare earth elements (REEs) were separated using cation exchange chromatography. Dissolved samples were taken up in 2 ml 2.5M HCl and loaded onto pre-conditioned cation exchange columns containing Bio-Rad AG50W X8 200-400 mesh resin. Sr was washed and eluted in 2.5M HCl and evaporated to dryness under hot-lamps. Following extraction of Sr, the REE fraction was rinsed in 2.5M HCl and eluted in 3M HNO_3 and then dried-down under hot-lamps. The REE fractions were dissolved into a mixture of acetic acid, methanol and nitric acid, and loaded into anion exchange columns containing Bio-Rad AG1 X8 200-400 mesh resin. Nd was eluted in another mixture of acetic acid, methanol and nitric acid, and subsequently dried down under hot-lamps.

A2.2.2 Mass spectrometry

After chemical separation, Sr was loaded onto a single Ta filament using 1 M H_3PO_4 and Nd loaded onto the Ta side filament of a triple Ta-Re-Ta filament assembly using MQ H_2O. Both $^{87}Sr/^{86}Sr$ and $^{143}Nd/^{144}Nd$ were analysed on a VG Sector 54-30 multiple collector mass spectrometer, operated in peak-jumping mode. Sr isotope data was collected in fifteen blocks of ten ratios, and Nd in twelve blocks of ten ratios. Both $^{87}Sr/^{86}Sr$ and $^{143}Nd/^{144}Nd$ were corrected for mass fractionation using an exponential law with $^{87}Sr/^{86}Sr = 0.1194$ and $^{146}Nd/^{144}Nd = 0.7219$. Analyses of the NBS987 Sr standard and JM Nd standard were undertaken during each set of Sr or Nd isotope analyses.

A2.3 Lead isotope analyses

Pb isotope analyses were performed in the radiogenic isotope laboratory in SUERC over a period of several months. During this time it became apparent that the accuracy of the Pb isotope determinations was strongly dependent on the method of

sample preparation and on the cleanliness of chemistry, and developmental work was undertaken to optimise the sample preparation technique. As a consequence, determinations of Pb isotope ratios were made only on samples thought, on the basis of He-Sr-Nd chemistry, to represent compositional extremes.

A2.3.1 Sample preparation, Pb separation and mass spectrometry

Initially, Pb isotope determinations were made on 100mg splits of the same powders used for Sr and Nd isotope analyses. However, early results indicated that sample powders had been contaminated during their preparation (see below). For subsequent determinations, 100 mg of 1-2 mm whole-rock chips, prepared using a pestle and mortar, were used.

Powders and chips were dissolved in HF-HNO_3-HCl and after dissolution the residue was taken-up in 1 ml 1M HBr and loaded into pre-treated Teflon-pipette miniature columns. This was followed by cleaning and elution in 1M HBr and 1.5M HCl, and Pb was collected in 2ml of 6M HCl. The Pb aliquot was then evaporated to dryness on a 150°C hotplate. Blanks were undertaken for each set of samples, following the exact procedure (dissolution and column chemistry) as for samples.

$^{206}Pb/^{204}Pb$, $^{207}Pb/^{204}Pb$, and $^{208}Pb/^{204}Pb$ were initially determined on an IsoProbe multi-collector inductively coupled plasma mass spectrometer (MC-ICP-MS) at SUERC. After column chemistry, the Pb concentration of each sample was made up to a total of 50 ppb using a 5%HNO_3 solution containing 5 ppb of Tl to correct for instrumental mass bias. ^{204}Pb was corrected for ^{204}Hg isobaric interference.

For later analyses, $^{206}Pb/^{204}Pb$, $^{207}Pb/^{204}Pb$, and $^{208}Pb/^{204}Pb$ were determined on a VG Sector 54-30 multiple collector mass spectrometer, operated in peak-jumping mode. After chemical separation, Pb was loaded onto a Re filament using 0.1 M H_3PO_4. and silica gel. Pb isotope data was collected in five blocks of ten ratios.

A2.3.2 Eliminating environmental contamination in Pb analyses

Initial Pb isotope analyses on samples from Snaefellsjokull yielded highly variable $^{207}Pb/^{204}Pb$ and $^{208}Pb/^{204}Pb$ values which plotted outwith the Iceland array on Pb isotope diagrams. To eliminate sample contamination during dissolution or column chemistry in the laboratory as a cause of the variability, a suite of chemistry

blanks were undertaken for each step of the procedure. The resulting blanks had negligible Pb concentrations (<1ng, and typically 500 pg).

This indicated that the sample contamination was likely due to the method of sample preparation; a well-known difficulty in analysing Pb isotopic compositions of basalts (e.g. McDonough and Chauvel, 1991; Woodhead., 1995). Sample contamination could occur during initial crushing with a jaw-crusher, or during powder preparation in the TEMA mill. To investigate this, three samples were selected and separate aliquots prepared of agate-ground powders, tungsten-carbide ground powders, and hand-picked 1-2mm sized whole-rock chips (prepared with a pestle and mortar, and rinsed with DI water). The results demonstrated that the crushing and grinding equipment were significant sources of contamination. Sample powders prepared in an agate TEMA mill consistently yielded low $^{206}Pb/^{204}Pb$. Pb isotope ratios from powders prepared in a tungsten-carbide TEMA mill yielded variable $^{207}Pb/^{204}Pb$ and high $^{208}Pb/^{204}Pb$, as noted in the initial determinations. In contrast, Pb analyses performed on whole-rock chips yielded Pb isotope ratios generally in agreement with those previously determined for Snæfellsnes. To ensure intra-laboratory reproducibility of Pb isotope determinations, three splits of whole-rock chips from two of the three samples analysed in the earlier experiment were prepared and analysed. The results demonstrated good reproducibility, with Pb isotope ratios of all sample duplicates bar one in agreement.

A2.4. Major element and trace element analyses

Analyses of major and trace element concentrations were undertaken on all samples collected in order to identify primitive and incompatible-element-enriched basalts suitable for the study. For both major and trace elements, whole-rock powders of each sample were prepared in a tungsten-carbide TEMA mill. For the ten major element oxides (SiO_2, TiO_2, Al_2O_3, Fe_2O_3, MgO, Na_2O, K_2O, CaO and P_2O_5), approximately 1 g of whole-rock powder was fused using a lithium borate flux in a platinum capsule and then dried at 110°C in an oven. Samples were subsequently re-weighed in order to calculate percentage loss on ignition, then ignited in a furnace at 1100°C. Glass discs were prepared by re-melting the glass in the crucibles over a Bunsen burner, and pouring the melt into steel moulds. For the fifteen trace element

concentrations (Nb, Zr, Y, Sr, Rb, La, Ce, Nd, Zn, Cu, Ni, Cr, V, Ba and Sc), approximately 8 g of each of the whole-rock powders were made into pressed-powder pellets.

Major element and trace element determinations were made on a Phillips PW1480 X-Ray Fluorescence mass spectrometer at the University of Edinburgh. Analyses of the international standards, BHVO1, BCR1, BIR1 and BEN were performed during sample analyses and used for calibration.